

# **Studies on Development of Polymeric Nano-systems for Delivery of Anti-cancer Bioactive Molecules**

by

**Amarnath Singam  
10BB14A26041**

A thesis submitted to the  
Academy of Scientific & Innovative Research  
for the award of the degree of  
DOCTOR OF PHILOSOPHY  
in  
SCIENCE

Under the supervision of  
**Dr. GVN Rathna**



**CSIR- National Chemical Laboratory, Pune**



Academy of Scientific and Innovative Research  
AcSIR Headquarters, CSIR-HRDC campus  
Sector 19, Kamla Nehru Nagar,  
Ghaziabad, U.P. – 201 002, India

**January, 2022**

---

## Certificate

This is to certify that the work incorporated in this Ph.D. thesis entitled, "Studies on Development of Polymeric Nano-systems for Delivery of Anti-cancer Bioactive Molecules", submitted by Amarnath Singam to the Academy of Scientific and Innovative Research (AcSIR) in partial fulfillment of the requirements for the award of the Degree of Doctor of Philosophy in Science, embodies original research work carried-out by the student. We, further certify that this work has not been submitted to any other University or Institution in part or full for the award of any degree or diploma. Research material(s) obtained from other source(s) and used in this research work has/have been duly acknowledged in the thesis. Image(s), illustration(s), figure(s), table(s) etc., used in the thesis from other source(s), have also been duly cited and acknowledged.



Mr. Amarnath Singam

Research Scholar

Date: 05/01/2022



Dr. GVN Rathna

Research Supervisor

Date: 05/01/2022

---

---

## STATEMENTS OF ACADEMIC INTEGRITY

I Amarnath Singam, a Ph.D. student of the Academy of Scientific and Innovative Research (AcSIR) with Registration No. 10BB14A26041 hereby undertake that, the thesis entitled "*Studies on Development of Polymeric Nano-systems for Delivery of Anti-cancer Bioactive Molecules*" has been prepared by me and that the document reports original work carried out by me and is free of any plagiarism in compliance with the UGC Regulations on "*Promotion of Academic Integrity and Prevention of Plagiarism in Higher Educational Institutions (2018)*" and the CSIR Guidelines for "*Ethics in Research and in Governance (2020)*".




**Signature of the Student**

Date: 05/01/2022

Place: P u n e

---

It is hereby certified that the work done by the student, under my/our supervision, is plagiarism-free in accordance with the UGC Regulations on "*Promotion of Academic Integrity and Prevention of Plagiarism in Higher Educational Institutions (2018)*" and the CSIR Guidelines for "*Ethics in Research and in Governance (2020)*".



**Signature of the Supervisor**

Name: Dr. GVN Rathna

Date: 05/01/2022

Place: P u n e

---

## **ACKNOWLEDGEMENTS**

*The work presented in this thesis would not have been realized without my close association with many people who contributed in numerous ways to the success of this study. Herein, I take this opportunity to acknowledge and extend my heartfelt gratitude and appreciation to all those people who have been involved in making this thesis possible.*

*Foremost, I would like to express my sincere gratitude and respect to my research supervisor Dr. GVN Rathna, for giving me an opportunity to pursue research with her. I like to thank her for her dedicated help, thoughtful advice, constructive comments, and encouragement throughout my Ph.D. tenure. Her precious knowledge, wise advice regarding thinking about the long-term target of our projects, and being mindful of our planet earth's environment has significantly made me grow, not only as a researcher but also as a wise and responsible human being. Her enthusiasm, freedom to conduct research on topics of our choice has inspired me to become an independent researcher. I feel fortunate and privileged to be associated with her and part of her research group.*

*I would also like to thank my doctoral advisory committee members, Dr. Utpal Das, Dr. S. Kadhiravan, and Dr. Dhiman Sarkar, for their time, constructive suggestions, guidance, and support. I am grateful to Dr. M. V. Badiger, for always encouraging me and making me feel like part of a family in our group at lab 937.*

*I extend my sincere thanks to the present Director of CSIR-NCL Dr. Ashish Lele, Dr. Ashwini Kumar Nangia (former Director), and Dr. Sourav Pal (former Director) for allowing me to work in this prestigious institute and making the facilities available to carry out the research. I am also grateful to the Head of Polymer Science and Engineering Division, Dr. S. K. Asha, and Dr. U. Kharul (former HoD) for their kind help during my Ph.D. I wish to thank all the administrative and non-teaching staff of CSIR-NCL for their kind support and assistance over the years on various occasions.*

*I am also grateful to many people in the Center for Materials Characterization division, NCL, who have assisted me during my tenure. My sincere thanks to Mr. R. S. Gholap, Gaikwad Sir, Venkatesh, Sheetal, Medha, Chetan, Tushar, and Harsha for their timely help in TEM, and SEM measurements. I would also like to thank Sangeeta ma'am and Poorvi ma'am, for providing*

*access to TGA/DSC and FTIR analysis. My extended gratitude towards Dr. Bhat who gave me the access to DLS instrument. I would like to thank Dr. Sunita Barve and Gati Nayak Sir for the wonderful facility of our library and their assistance in publishing articles/plagiarism checks. I extend my deepest gratitude to Dr. Lekha Dinesh from CCMB, Hyderabad for the collaborative work which resulted in a publication in a reputed journal, also would like to thank her students Aviral and Guru. I learned a lot from this joint effort about teamwork and cooperation in the science fraternity. I am also grateful to the Department of Biotechnology (DBT), India, for providing me with the necessary funding and fellowship to pursue research as a career.*

*I also take an opportunity to thank my seniors from the lab, Dr. Suresha, Dr. Arun T, Dr. Anumon, Dr. Manjusha, Dr. Rajeshwari, Dr. Neha, Dr. Bhagyashri, Dr. Ashwini, and Dr. Naresh. I will always remember the knowledge they've shared, the discussion on various scientific topics and I hope to stay in touch with them. Nothing would have been possible without the instruments and equipment in our lab and for that, I thank Dr. Suresha and Dr. Arun for maintaining them and familiarizing me with them. Special thanks to our lab bearer Shivaji Ji who helped a lot in all administrative work and was of great help in the lab. I express my thanks to Nimisha ma'am for patiently teaching me the cell culture work. Her continuous cooperation and knowledge helped me understand many studies related to cell culture. I also thank all the colleagues who were part of the cell culture lab viz, Poulomi ma'am, Geetika, Isha, Kartiki, Shreya. I also thank Dr. Vishwanath M, Anuja, Jyothi, and Ritu who also helped a lot in cell culture work. I would also like to thank Prem, Bharat, and Shibam for the DSC measurements, Srijan and Nitin for IR measurements. My thanks to Swarali, Emmanuel, Bijosh, and Alaka for their help with the lyophilizer. I also thank Dr. Guruswamy, Dr. Sayam Sen, and Dr. Anuya for providing me the access to the cell lab facility.*

*I would also like to thank my colleagues and juniors Pratiksh (Pinka), Yogesh, Tripurari, Sravanya, Ajay, Loknatham, Rahul, Pranay, Sanoop, Raji, Jyothi, and Runali. Special mention for Pinka who is not only my junior but my dearest friend, together we have experienced innumerable moments of joy and sorrow at NCL. With all my labmates I attended many conferences and I will always cherish those moments. I thank my closest friends Dr. Arun, Dr. Ragini, Dr. Pragya, Dr. Indra, and Dr. Manjur for supporting and encouraging me throughout this Ph.D. journey. These were always in my close circle and always available for me. I also thank all my friends from Bio Division who were my first friends at NCL, Dr. Parag, Dr. Nirbhik, Dr. Debjyoti, Dr. Kushal, Dr. Sneha, Dr. Meghna, and Dr. Monika Mathur. Besides, I extend my affection to my other close*

*friends like Dr. Sameer, Sourosree, and Prachi. With all these close groups of friends, I have made many outdoor trips, parties, seen movies, and created memories. I will always remember late-night discussions and chitchats with Pinka and Arun over chai shai. I thank you all for your company, love, and care.*

*I stayed in the hostel from the first year and over these years I have made so many friends. I extend many thanks to my NCL seniors and friends Dr. Nidhi, Dr. Akshay Singan, Dr. Brijesh, Dr. Negi, Dr. Varchaswal, Dr. Kheria, Dr. Praveen Dwivedi, Shubhra, Sanjukta, Praveen Singh, Dr. Pravin Shinde, Dr. Arun Nikam, Dr. Rajan, Dr. Abhishek, Dr. Vinita, Dr. Manoj, Dr. Yachita, Dr. Nalini, Dr. Yashpal, Dr. Abhijit, Rahul, Dr. Siba, Dr. Debu, Subrashis, Dr. Arunava, Dr. Pronay, Dr. Deepak, Dr. Santigopal, Dr. Roby, Dr. Sayan, Dr. Gaurav, Dr. Swamy, Dr. Ramireddy, Dr. Chaitanya, Dr. Trinadh, Dr. Sagar, Vikas, Mahendra (Wagh & Pawar), Gopal, Himanshu, Anupam, Shrikanth, Pavan, Priya, and Monika Malik for being a valuable part of my life at NCL. How can I forget my football and basketball group, Dr. Vidyanand (fellow Gooner), Sandy, Rashid, Shebeeb, Fayis, Kiran, Ajmal, Ajit, Narugopal, Sarath, Dr. Pranav, Dr. Rajith, Prashant, Vasudev, Swapnil, and Dr. Amit.*

*I would also like to thank my M.Sc. friends Sachendra, Surendra, Ameya, and Vishram, my B.Sc. friends Roshan, Rashmi, Rakesh, my hometown friends Mohsin, Akshay, Anup, Rohan, Shashank, Padmanabhan, Vitesh, and Naveen who have constantly been in touch with me all these years and asked about my wellbeing. Despite only a few meetings past these years, the bond we share is remarkable.*

*I would like to express my heartfelt gratefulness to my parents, Mrs. Renuka Singam & Mr. Ram Singam, and my lovely sister Teju who provide me unconditional love and support. Their contribution is immense and cannot be stated in words, it is because of them I have come this far in life. Thank you for believing and keeping patience with me. I would also like to express my gratitude to Ikeda Sensei and all comrades of my Gakkai family. It would be incomplete without thanking my therapist Aishwarya who has helped me a lot to regulate my mental well being. It gives me immense pleasure to thank everyone who helped me write my thesis successfully (kindly excuse if I forgot to mention anyone).*

*Last but not least, I thank the Universe and Parmatma for everything.*

***Amarnath Singam***

*Amarnath Singam*



*Dedicated to  
My  
Mentors!*

## Abbreviations

---

DDS	Drug delivery system
NDDS	Nano drug delivery system
NP	Nanoparticle
PK	Pharmacokinetics
PM	Polymeric micelle
FDA	Food and drug administration
DLS	Dynamic light scattering
SEM	Scanning electron microscope
FE-SEM	Field emission scanning electron microscope
TEM	Transmission electron microscope
HRTEM	High resolution transmission electron microscope
FTIR	Fourier transform infrared spectroscopy
UV-Vis	Ultra violet visible spectrophotometry
DSC	Differential scanning calorimetry
MTT	3-(4,5-Dimethylthiazol-2-yl)-2,5-diphenyltetrazolium bromide
RT	Room temperature
Rpm	Revolutions per minute
DOX	Doxorubicin
EC	Ethyl cellulose
CEC	Carboxylated ethyl cellulose
mPEG	Methoxy polyethylene glycol
CS	Chitosan
CU	Curcumin
ES	Eudragit S100
shRNA	Short hairpin ribonucleic acid
DNA	Deoxyribonucleic acid
Eu	Eugenol
CMC	Carboxymethyl cellulose



PF127	Pluronic F127
Cet	Cetuximab
DAPI	4',6-diamidino-2-phenylindole
TEMPO	2,2,6,6-Tetramethylpiperidin-1-yl) oxyl or (2,2,6,6-tetramethylpiperidin-1-yl) oxidanyl
NaBr	Sodium bromide
NaClO	Sodium hypochlorite
EDC	1-Ethyl-3-(3-dimethylaminopropyl) carbodiimide
NHS	N-Hydroxysuccinimide
DCC	N, N'-Dicyclohexyl carbodiimide
DMAP	4-Dimethylaminopyridine
BCA	Bicinchoninic acid
DI	Deionized water
PBS	Phosphate buffer saline
EtOH	Ethanol
EGFR	Epithelial growth factor receptor
THF	Tetrahydrofuran
BSA	Bovine serum albumin
kDa	kilo Dalton
ppm	parts per million

# Table of Contents

---

## Chapter 1

### Introduction and Literature Review

1. Introduction	1
1.1. Drug delivery systems (DDS)	1
1.2. Polymers for NDDS	4
1.2.1. Biodegradable polymers	5
1.2.1.1. Synthetic polymers	5
1.2.1.2. Natural polymers	8
1.3. Preparation of nano drug delivery systems (NDDS)	10
1.3.1. Polymeric nanoparticles and their preparation	10
1.3.1.1. Methods of polymeric nanoparticle preparation	13
1.3.1.1.1. From preformed polymers	14
1.3.1.1.2. From monomers	17
1.3.2. Polymeric micelles and their preparation	18
1.3.2.1. Methods of micelles preparation	20
1.4. DDS for cancer	22
1.5. Routes of administration	25
1.5.1. Intravenous administration	25
1.5.2. Oral administration	27
1.6. Characterizations	29
1.6.1. Size and Shape	30
1.6.2. Stability	30
1.7. Conclusions	31
1.8. References	32

## Chapter 2

### Objectives and Scope of Work

2.1. Objectives and scope of work	43
2.2. References	45

# Table of Contents

---

## Chapter 3

### PEGylated Ethyl Cellulose Micelles as a Nanocarrier for Drug Delivery

3.1. Introduction	48
3.2. Experimental	51
3.2.1. Materials	51
3.2.2. Synthesis and characterization of EC-PEG graft polymer	51
3.2.2.1. TEMPO mediated oxidation of EC	51
3.2.2.2. Determination of carboxylate charge density of EC	52
3.2.2.3. PEGylation of carboxylated EC (CEC)	52
3.2.2.4. Critical micellar concentration (CMC) of EC-PEG	53
3.2.3. Preparation and characterization of micelles	54
3.2.3.1. Preparation of EC-PEG micelles	54
3.2.3.2. Preparation of DOX loaded EC-PEG micelles	54
3.2.4. Characterizations	54
3.2.4.1. NMR spectroscopy	54
3.2.4.2. Physicochemical characterization of micelles	55
3.2.4.3. <i>In vitro</i> DOX release	57
3.2.4.4. Hemolysis assay	57
3.2.4.5. Cell studies	58
3.3. Results and discussion	60
3.3.1. TEMPO mediated oxidation and determination of carboxylate charge density on EC	60
3.3.2. PEGylation of carboxylated EC (CEC)	63
3.3.3. Preparation and physicochemical characterization of micelles	68
3.3.4. <i>In vitro</i> DOX release	74
3.3.5. Hemolysis assay	75
3.3.6. Cell studies	76
3.4. Conclusions	80

## Table of Contents

---

3.5. References	80
-----------------	----

### Chapter 4

#### **Curcumin Loaded Polymeric Nano-encapsulates Complexed with Ephb4 shRNA as a Combinatorial Therapy for Colon Cancer**

4.1. Introduction	87
4.2. Experimental	89
4.2.1. Materials	89
4.2.2. Preparation of fluorescent nano-encapsulate of curcumin-chitosan (CU-CS)	90
4.2.2.1. Entrapment and loading efficiency	91
4.2.2.2. Complexation of shRNA to CU-CS NPs	91
4.2.2.3 Eudragit S-100 coated NPs	92
4.2.2.4. <i>In vitro</i> CU release studies	92
4.2.3. Characterizations of NPs	93
4.2.4. Cell studies	94
4.3. Results and discussion	96
4.3.1. Synthesis and characterization of curcumin-chitosan NPs	96
4.3.2. FTIR spectra and thermal analysis	98
4.3.3. Entrapment efficiency and drug release studies	101
4.3.4. Cell studies	103
4.4 Conclusions	106
4.5 References	107

### Chapter 5

#### **Cetuximab Conjugated Eugenol Loaded Carboxymethyl Cellulose Nanoparticles for Active Targeting Anti-cancer Therapy**

5.1. Introduction	112
5.2. Experimental	114

## Table of Contents

---

5.2.1. Materials	114
5.2.2. Preparation of eugenol loaded CMC nanoparticles	114
5.2.3. Physicochemical characterization of NPs	115
5.2.4. Drug encapsulation efficiency and <i>in vitro</i> release	116
5.2.5. Preparation of Cet-CMC NPs	117
5.2.6. Hemolysis assay	118
5.2.7. Cell studies	119
5.3. Results and discussion	120
5.3.1. Preparation and physicochemical characterization of NPs	121
5.3.2. Drug loading and <i>in vitro</i> release	125
5.3.3 Conjugation of Cet to NPs	126
5.3.4. Hemolysis assay	127
5.3.5. Cell studies	128
5.4. Conclusions	130
5.5. References	131

## Chapter 6

### Conclusions and Future Prospects

6.1. Conclusions and future prospects	137
---------------------------------------	-----

## Abstract

## Poster, oral presentations and Conferences attended

## List of publications

## List of Figures

<b>Figure No</b>	<b>Figure Caption</b>	<b>Page No</b>
<b>Figure 1.1</b>	Timeline of nanotechnology-based drug delivery.	4
<b>Figure 1.2</b>	Classification of biodegradable polymers.	5
<b>Figure 1.3</b>	Methods of NP preparation.	14
<b>Figure 1.4</b>	Passive and active targeting.	23
<b>Figure 1.5</b>	Routes of drug administration.	26
<b>Figure 3.1</b>	Scheme of oxidation of ethyl cellulose (EC) followed by reaction with mPEG by DCC/DMAP coupling.	53
<b>Figure 3.2</b>	Scheme of TEMPO mediated oxidation of EC.	61
<b>Figure 3.3</b>	Graph of conductometric titration of CEC-HCl dispersion with NaOH.	63
<b>Figure 3.4</b>	<sup>1</sup> H NMR spectrum of mPEG2000 in DMSO-d <sub>6</sub> , recorded on Bruker AV-200 NMR. $\delta$ 3.92 (-OCH <sub>2</sub> CH <sub>2</sub> O-) (m, 4 H), $\delta$ 3.65 (CH <sub>3</sub> OCH <sub>2</sub> CH <sub>2</sub> OH) (m, 3 H).	64
<b>Figure 3.5</b>	<sup>1</sup> H NMR spectrum of EC-PEG1 recorded on Bruker AV-200 NMR spectrometer operating at a frequency of 200 MHz with DMSO-d <sub>6</sub> as the solvent.	65
<b>Figure 3.6</b>	Solid state <sup>13</sup> C NMR spectrum of CEC recorded on Bruker NMR spectrometer. $\delta$ 15.75 (CH <sub>3</sub> CH <sub>2</sub> O-), $\delta$ 68.69 (CH <sub>3</sub> CH <sub>2</sub> O-), $\delta$ 103.84 (-OCHO-), $\delta$ 174.14 (OHCOCH-), $\delta$ 75.43 and 82.93 (C of the backbone of EC from C2 to C5).	65
<b>Figure 3.7</b>	<sup>13</sup> C NMR (125 MHz) of mPEG2000 in DMSO-d <sub>6</sub> , recorded on Bruker AV-500 NMR. $\delta$ 58.34 (CH <sub>3</sub> OCH <sub>2</sub> -), $\delta$ 60.49 (-OCH <sub>2</sub> CH <sub>2</sub> OH), $\delta$ 69.96 (-OCH <sub>2</sub> CH <sub>2</sub> OH), $\delta$ 70.16 (-OCH <sub>2</sub> CH <sub>2</sub> OCH <sub>2</sub> -), $\delta$ 71.66 (-OCH <sub>2</sub> CH <sub>2</sub> OCH <sub>2</sub> -), $\delta$ 72.67 (CH <sub>3</sub> OCH <sub>2</sub> CH <sub>2</sub> O).	66
<b>Figure 3.8</b>	<sup>13</sup> C NMR (125 MHz) spectrum of EC-PEG1 in DMSO-d <sub>6</sub> , recorded on Bruker AV-500 NMR. $\delta$ 15.75 (CH <sub>3</sub> CH <sub>2</sub> O-), $\delta$ 58.45 (CH <sub>3</sub> OCH <sub>2</sub> -), $\delta$ 69.98 (CH <sub>3</sub> CH <sub>2</sub> O-), from 60 ppm to 73	66

	ppm all peaks observed in the spectrum of mPEG merged into the peaks of CEC backbone with an intense peak at $\delta$ 70.18 (CH <sub>3</sub> OCH <sub>2</sub> CH <sub>2</sub> O-) due to the repeating unit of mPEG2000. [Note: The unassigned peaks are due to the traces of DCU (Dicyclohexylurea) formed during the DCC (N,N'-Dicyclohexylcarbodiimide) coupling].	
<b>Figure 3.9</b>	A) Critical micelle concentration (CMC) of EC-PEG1, derived from the plot of I338/I334 ratio vs copolymer concentration. B) CMC of EC-PEG2, derived from the plot of I338/I334 ratio vs copolymer concentration.	67
<b>Figure 3.10</b>	Graphical representation of preparation of DOX loaded micelles from PEGylated EC.	68
<b>Figure 3.11</b>	A) i) TEM image of B1 micelles (Scale bar 50 nm), ii) TEM image of B3 micelles (Scale bar 100 nm). B) i) TEM image of B4 micelles (Scale bar 50 nm), ii) TEM image of B6 micelles (Scale bar 100 nm).	70
<b>Figure 3.12</b>	FTIR spectrum of A) EC, mPEG, DOX, B) EC-PEG1 and EC-PEG2, C) B3 and B6 micelles.	72
<b>Figure 3.13</b>	DSC thermograms of A) EC, B) mPEG, C) CEC, D) B1 micelles, E) B4 micelles, F) B3 micelles, G) B6 micelles.	74
<b>Figure 3.14</b>	A) i) DOX release from B3 micelles in PBS at 5.5 and 7.4 pH for 72 h, ii) DOX release from B6 micelles in PBS at 5.5 and 7.4 pH for 72 h. B) % of Hemolysis on exposure to test samples, EC, CEC, B1, B3, B4, and B6 micelles.	75
<b>Figure 3.15</b>	A) i) Cytotoxicity of MDA-MB-231 and L929 cells treated by B1 micelles for 48 h, ii) Cytotoxicity of MDA-MB-231 and L929 cells treated by B4 micelles for 48 h. B) i) Cytotoxicity of MDA-MB-231 and MCF-7 cells treated by B3 micelles for 72 h, ii) Cytotoxicity of MDA-MB-231 and MCF-7 cells treated by B3 micelles for 72 h.	77
<b>Figure 3.16</b>	Fluorescent images of MDA-MB-231 cells treated with free DOX, B3 micelles, and B6 micelles for 4 h and 8 h. The right panels show the merged image of the nucleus stained with DAPI	79

	(blue), F-actin stained with Alexa fluor 488 phalloidin (green), and DOX fluorescence (red). Scale bar corresponds to 5 $\mu$ m.	
<b>Figure 4.1</b>	Graphical representation of preparation of CU nanoencapsulates.	92
<b>Figure 4.2</b>	A) TEM image of CU NPs, B) FE-SEM image of 1CU-2CS-Ephb4-ES, C) and D) TEM image of 1CU-2CS-Ephb4-ES.	97
<b>Figure 4.3</b>	A) Zeta potential measurements of CU formulations, B) Gel retardation assay of NPs bound with Ephb4 shRNA.	98
<b>Figure 4.4</b>	FTIR spectrum of A) bare CU, B) chitosan, C) Eudragit S100, D) CU coated with CS and ES (CU-CS-ES).	100
<b>Figure 4.5</b>	Differential scanning calorimetric (DSC) analysis of bare CU, CS, and ES with CU-CS-ES NPs.	101
<b>Figure 4.6</b>	A) Cumulative CU release at 1.2 pH from CU-CS and CU-CS-ES, and B) cumulative CU release at 6.8 and 7.4 pH from CU-CS and CU-CS-ES.	102
<b>Figure 4.7</b>	Cell viability assay results of HCT116 and MCF-7 (cancer cell lines) with L929 cells (control) after 48 h of CU-CS-Ephb4 shRNA-ES treatment.	103
<b>Figure 4.8</b>	Cellular uptake assay representing the L929 cells after 3 h involving CU (11 $\mu$ g/mL), CU-CS (50 $\mu$ g/mL), and CU-CS-ES (50 $\mu$ g/mL), Scale bar: 5 $\mu$ m.	105
<b>Figure 5.1</b>	Preparation of Eu loaded CMC NPs by emulsion-ionic gelation.	121
<b>Figure 5.2</b>	A) FE-SEM image of B3 NPs, B) HRTEM image of B3 NPs, C) FE-SEM image of B4 NPs, D) HRTEM image of B4 NPs. (Scale bar = 50 nm).	122
<b>Figure 5.3</b>	FTIR spectrum of A) CMC, B) PF127, C) Eu, D) B4 NP with components, E) B3 NP with components, F) B3 NP with and without Cet.	124
<b>Figure 5.4</b>	A) DSC thermograms of CMC and PF127, B) DSC thermograms of B3 and B4 NPs, C) <i>In vitro</i> release profile of Eu.	126
<b>Figure 5.5</b>	Graphical representation of Cet conjugation to NPs.	127



<b>Figure 5.6</b>	A) % of Hemolysis on exposure to pristine polymers (CMC and PF127) and their blank (B4) and Eu loaded (B3) NPs, B) Cell viability of L929 cells treated by B3 NPs for 48 h. C) Cell viability of A549 cells treated by B3 and B4 NPs for 24 h. D) Cell viability of A549 cells treated by Cet conjugated B3 and B4 NPs for 24 h.	128
<b>Figure 5.7</b>	Fluorescent images of A549 cells treated (for 2.5 h) with 200 µg/mL of i) A) B4 NPs without Cet, B) B4 NPs with Cet. ii) A) B3 NPs without Cet, B) B3 NPs with Cet. The right panels show the merged image of the nucleus stained with DAPI (blue), and NPs fluorescence red because of Rhodamine B staining. Scale bar corresponds to 20 µm.	130

### List of Tables

<b>Table No</b>	<b>Table Caption</b>	<b>Page No</b>
<b>Table 1.1</b>	Effect of DDS over non-ideal drugs	2
<b>Table 1.2</b>	A list of the pros and cons of synthetic versus natural polymers	7
<b>Table 1.3</b>	NPs approved for cancer therapy	13
<b>Table 3.1</b>	Formulations of EC-PEG with DOX	56
<b>Table 3.2</b>	Thermal properties of pure polymers and micelles with DOX	73
<b>Table 4.1</b>	Formulations of CU with CS coating	91
<b>Table 5.1</b>	Formulations of CMC NPs	115



---

# *CHAPTER 1*

---

Introduction and Literature Review



## 1. Introduction

This chapter provides an introduction to the scope and application of biodegradable polymers in the area of drug delivery. It includes a literature survey on drug delivery systems (DDS), various polymers/biopolymers used to prepare nano DDS (NDDS), and their characterization techniques. It also accentuates the potential of polymer-based NDDS in anti-cancer therapy.

### 1.1 Drug delivery systems (DDS)

DDS plays a vital role in regulating the pharmacokinetics (PK) of the drug. The rate of release of the drug depends on the composition of the delivery system. Conventional drug delivery systems are in the form of tablets, injections, suspensions, capsules, etc. Though these modes of delivery have been used in the treatment of various diseases they face limitations like poor biodistribution, low bioavailability, toxicity, burst release, low half-life, etc. DDS is different from the conventional method, where after administration they reside as designed at a particular location and deliver the drug for an extended period<sup>1,2</sup>. DDS deals with introducing foreign therapeutic agents into the body through different routes of administration like oral, buccal, transdermal, ocular, nasal, pulmonary, and parenteral<sup>3</sup>. It has several advantages like an ideal drug delivery system will give a high pharmacological effect in a controlled manner without any immune response<sup>4</sup>. It protects the drug or bioactive molecule from degradation and rapid clearance out of the body. At the beginning of the 19<sup>th</sup> century, to improve the pharmacological properties of DDS, studies on the development of micro and nanoformulations came into existence. Accordingly, several micro formulations were developed as DDS and are successfully being practiced<sup>5</sup>. The following Table 1.1 displays how DDS has overcome the barriers presented by conventional drugs.

**Table 1.1** Effect of DDS over non-ideal drugs<sup>1</sup>

Problem	Implication	Advantage of DDS
Poor solubility	A convenient pharmaceutical format is difficult to achieve, as hydrophobic drugs may precipitate in aqueous media. Toxicities are associated with the use of excipients such as Cremphor (the solubilizer for paclitaxel in Taxol).	DDS such as lipid micelles or liposomes provides both hydrophilic and hydrophobic environments, enhancing drug solubility.
Tissue damage on extravasation	Inadvertent extravasation of cytotoxic drugs leads to tissue damage, eg, tissue necrosis with free doxorubicin.	Regulated drug release from the DDS can reduce or eliminate tissue damage on accidental extravasation.
Rapid breakdown of the drug <i>in vivo</i>	Loss of activity of the drug follows administration, for example, loss of activity of camptothecins at physiological pH.	DDS protects the drug from premature degradation and functions as a sustained-release system. Lower doses of the drug are required.
Unfavorable pharmacokinetics (PK)	The drug is cleared too rapidly, by the kidney, for example, requiring high doses or continuous infusion.	DDS can substantially alter the PK of the drug and reduce clearance. Rapid renal clearance of small molecules is avoided.
Poor biodistribution	Drugs that have a widespread distribution in the body can affect normal tissues, resulting in dose-limiting side effects, such as the cardiotoxicity of doxorubicin.	The particulate nature of DDS lowers the volume of distribution and helps to reduce side effects in sensitive and non-targeted tissues.
Lack of selectivity for targeted tissues	Distribution of the drug to normal tissues leads to side effects that restrict the amount of administered drug. Low concentrations of drugs in targeted tissues will result in suboptimal therapeutic effects.	DDS can increase drug concentrations in diseased tissues such as tumors by the EPR effect. In addition, ligand-mediated targeting of the DDS can improve drug specificity.

Nanotechnology is a cutting-edge science where materials are manipulated at an atomic and molecular level. With the advent of nanotechnology, nanoparticle-based DDS has gained a lot of interest and is being studied extensively because of its unique physical and chemical properties. NDDS are being used to deliver bioactive polypeptides, proteins, vaccines, nucleic acids, genes, etc<sup>6</sup>. Among the various nanomaterials, such as nanotubes, nanofibers, nanoemulsions, etc the nanoparticles (NPs) in their solid form are being studied extensively as DDS. Generally, NPs are defined as particulate distribution or solid particles with a size in the range of 10-100 nm. Nano is submicron-

sized material that has a larger surface-to-volume ratio, with advantages over bulk or macro materials<sup>7</sup>. As a result, it provides several advantages like increased bioavailability, dose proportionality, less toxicity, smaller and stable dosage forms hence, less expensive and more effective in therapy. As per the literature<sup>8</sup>, in 1976 Jörg Kreuter was first to use the term “nanoparticle” in the context of drug delivery, and later to this, tremendous progress has been made in this domain with the progress of time, which is shown in Figure 1.1 Nanoparticulate drug delivery vehicles are advantages over the conventional forms methods. In addition, reduction in fed or fasted variability, improved half-life, ability to cross the blood-brain barrier (BBB), better interaction with cells, combinational therapy, transcytosis across tight gaps, etc. Therefore, NDDS is explored widely to develop a suitable nano system<sup>9</sup>. Nanocarriers for drug delivery can be formulated using inorganic materials (metals, semiconductors), lipids, polymers, and hybrid materials<sup>10</sup>. Among these liposomal and polymeric systems are being exploited, accordingly, many related systems are now in the market and are being lined up for clinical trials. The first reported nano-based drug delivery system was lipid-based vesicles known as liposomes reported in the 1960s. From there onwards tremendous progress has been achieved in the area of drug delivery, right from targeted delivery to stimuli response delivery with an increase in circulation time and biodegradability<sup>7</sup>. Currently, per year several articles related to nanosystems designed using polymers are being reported in the biomedical area<sup>11</sup>.

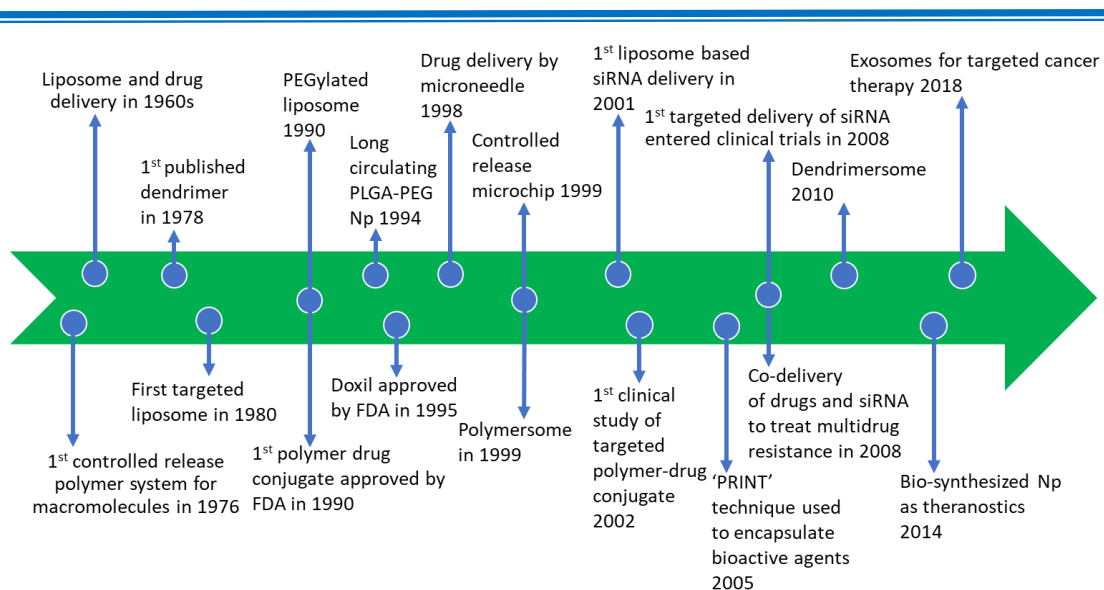


**Figure 1.1** Timeline of nanotechnology-based drug delivery<sup>12</sup>.

## 1.2 Polymers for NDDS

Polymers are large macromolecules made of repeating units of small chemical components called monomers. They can be classified as natural (DNA, cellulose) and synthetic (nylon, polyethylene) based on their source of origin. Since the acclaimed article of Folkman and Long in 1964 entitled “The use of silicone rubber as a carrier for prolonged drug therapy” the role of polymers in drug delivery has grown significantly<sup>11</sup>. Polymers are the most widely investigated materials for nano-based drug delivery because they can form various nano architectures like micelles, liposomes, solid lipid nanoparticles, dendrimers, core-shell particles, etc. The desired properties of a polymer to be used as DDS should be non-toxic, biocompatible, biodegradable with low immunogenicity. To sustain the ecological balance, the main focus over the past few decades is on biodegradable DDS. Because these polymers degrade safely in the body either by getting adsorbed or expelled so that the need for surgical extraction can be avoided and improve the biocompatibility of the DDS by resisting immune response<sup>3</sup>. Further, the process of polymer biodegradation is a slow process, the normal cellular functions are not disturbed<sup>13</sup>. Hence, these classes of

polymers have wide application from sutures in wound management to coatings on medical devices like stents. Dexon™ was the first biodegradable suture developed from synthetic polymer, polyglycolide in 1969<sup>3</sup>. Similarly, in 1989 Lupron® Depot microsphere was the first approved DDS fabricated from PLGA for delivery of leuprolide in the treatment of prostate cancer<sup>14</sup>. Currently, DDS are being tailored by modifying molecular weight, crystallinity, composition, backbone stability, hydrophobicity, and polydispersity of biodegradable polymers. Based on the source of origin the biodegradable polymers can be classified as natural and synthetic polymers (Figure 1.2)

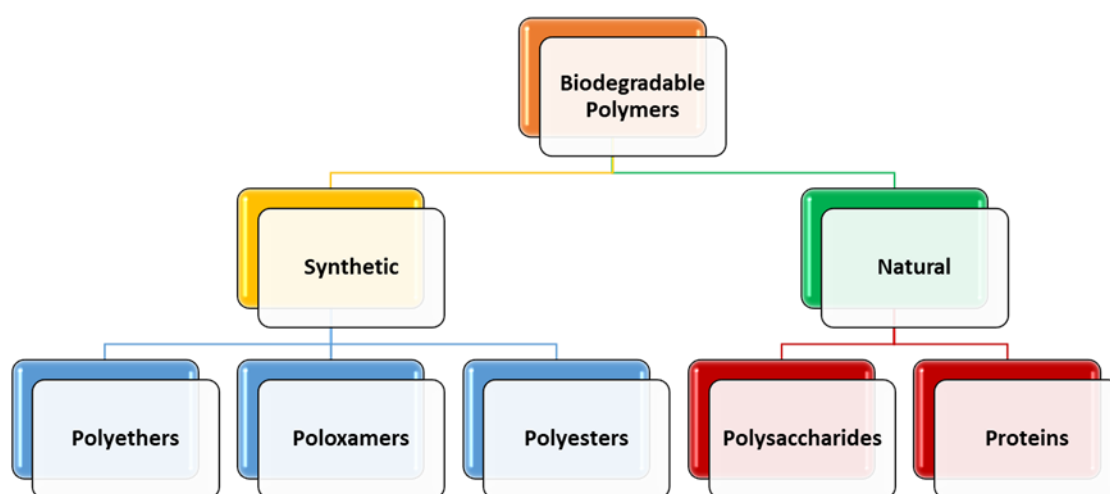


**Figure 1.2** Classification of biodegradable polymers<sup>15</sup>.

## 1.2.1 Biodegradable polymers

### 1.2.1.1 Synthetic polymers

As the name suggests these polymers are synthesized from monomers in a lab. Various biodegradable synthetic polymers are being studied and used for NDDS. Some of the common examples are polyethylene glycol, polylactic acid (PLA), polylactide-co-glycolide (PLGA), polycaprolactone (PCL), polyhydroxyalkanoates, etc. Drug

carriers designed by synthetic polymers provide passive function so they can be used for delivering charged bioactive peptides and proteins<sup>15</sup>. Synthetic polymers can be further classified as polyethers, polyesters, poloxamers, and recombinant protein-based polymers depending on the functional group present on the polymeric backbone. Polyethers, like PEG or PEO (polyethylene oxide), are used in the NDDS system, PEG has been the go-to polymer for all pharmaceutical experts. PEG is being used in combination with a variety of polymers to develop biodegradable NDDS. For instance, A Singam et al developed PEGylated ethyl cellulose nano-micelles as NDDS to deliver an anti-cancer drug like doxorubicin (DOX)<sup>16</sup>. PLA, PCL, and PLGA are a few well-known polyesters utilized in NDDS<sup>17, 18</sup>. In their reported work, Fessi et al demonstrated the application of PLA nanocapsules for the delivery of indomethacin<sup>19</sup>. PCL is a hydrophobic semicrystalline polymer that is usually used in combination with other hydrophilic polymers to form copolymers or block copolymers for drug delivery application. Accordingly, MPEG-PCL copolymeric NPs have been explored in drug delivery systems<sup>20</sup>. For example, hydroxy camptothecin an anti-cancer drug was reported to show efficacy in treating tumor-bearing mice when encapsulated in copolymeric micelles developed from MPEG-PCL. PLGA NPs as DDS were evaluated *in vivo* and these were found to be non-toxic and well biodistributed indicating their biocompatibility. Poloxamers are a combination of polymers (tri-block copolymers) that have hydrophobic and hydrophilic blocks. They are also called thermosensitive polymers owing to their temperature-responsive behavior. Commonly used poloxamer is pluronic which is inert and has good encapsulation property<sup>21</sup>. Pluronics and block copolymers of pluronics improve the pharmacokinetics of the drug by increasing the solubility of crystalline and polycyclic drugs. Likewise, Venne et al reported the advantages of drug encapsulates of pluronics. The DOX encapsulated pluronic was internalized in multi drug resistant cancer cells when compared with delivery of DOX alone<sup>22</sup>. Recombinant polymers are genetically engineered with amino acid sequences in the polymeric backbone. They have specific sequences to aid in absorption to the cellular receptors in the intestinal epithelium. The regularly used protein-based recombinant polymers are lectins, transferrin, silk-elastin-like proteins, and cell-

---



penetrating peptides (CPP)<sup>15</sup>. DDS of the conjugated HPMA (N-(2-Hydroxy-propyl) methacrylamide) with lectin aided in adhesion of DDS to the colon tissue and delivered aminocamptothecin specifically in the colon region<sup>23</sup>. In another report, CPP like penetratin was conjugated to elastin polypeptide and cyclin dependent kinase inhibitor p21 and was found to inhibit HeLa cancer cells<sup>24</sup>.

**Table 1.2** A list of the pros and cons of synthetic versus natural polymers<sup>3</sup>

Classification of polymer	Pros	Cons
Natural	Hydrophilic Biocompatible Cell/tissue-specific binding affinity Safe Readily available	Possible immunogenicity Require purification Lot-to-lot variation Less controlled raw material specifications Less controlled degradation Short release profile
Synthetic	Design desired physicochemical feature, such as a copolymer Easy to add functional groups to allow crosslinking and surface modification of chemical moieties to improve the functionality of polymer Precise controlled release profile No immunogenicity Control of mechanical and physical properties of polymer such as branching	Require ligands attached to achieve cell/tissue-specific binding affinity Require synthesis Scale-up challenges Hydrophobic

### 1.2.1.2 Natural polymers

Though biocompatible synthetic polymers are in practice for drug delivery, they suffer from drawbacks like depletion of resources, use of organic solvents, harsh and expensive formulation conditions<sup>3</sup>. Therefore, natural polymers are being preferred as they are renewable, biodegradable, biocompatible, non-toxic, economical, and are easily available. For example; monosaccharides and amino acids units of polysaccharides and proteins respectively have garnered attention to design as NDDS because they pose low immunogenicity and their units are well tolerated by the human body<sup>25</sup>. Some of the polymers extracted from plants, animals, microorganisms, insects, and fungi exhibit antibacterial activity due to their inherent nature. Likewise, Zhao R et al fabricated a nanocomposite fiber from natural biopolymers like chitosan and sericin which exhibited antibacterial properties against both Gram positive and negative bacteria<sup>26</sup>. Examples of plant polysaccharides are cellulose, starch, pectin, guar gum, inulin, gum acacia, agar, carrageenans, alginate, etc. Xanthan gum and dextran are isolated from microbes like fungi and bacteria respectively. Chitin a polysaccharide is extracted from the exoskeleton of crustaceans like crabs and insects. The polysaccharides are further classified as non-polyelectrolytes/neutral (cellulose, starch, etc) and polyelectrolytes/charged, where most of them are negatively charged owing to carboxylic or sulfate groups (alginate, hyaluronan, xanthan, pectin, etc), and some are positively charged (chitosan, dextran)<sup>6</sup>. Polysaccharides are used to coat drugs, in emulsions, as tablet coating matrix, and as gelling agents in NDDS<sup>5</sup>. Polysaccharides constitute a large number of materials as DDS because of their good bioadhesive property and the availability of the functional groups for modification as smart DDS. For instance, chitosan, starch, alginate, etc can form non-covalent bonds with mucous membrane and epithelium thus prolonging the residence time of the DDS thereby improving drug absorption<sup>27</sup>. Sarmiento et al developed alginate/chitosan NPs for effective delivery of insulin<sup>28</sup>. A. K. Jain et al in their work, fabricated starch-based mucoadhesive NPs for transnasal delivery of insulin<sup>29</sup>. Further, hyaluronic acid was modified with PLGA to form a nanosystem to deliver doxorubicin (DOX)<sup>30</sup>. In another

---

study, pullulan was derivatized with acetyl moieties and coated on Fe<sub>3</sub>O<sub>4</sub> magnetic NPs to develop an anticancer DDS<sup>31</sup>. Similarly, chitosan was covalently grafted with stearic acid to fabricate a pH-sensitive DDS for paclitaxel delivery<sup>32</sup>.

A large number of proteins such as collagen, gelatin, albumen (HSA, BSA, and EA) are also under practice for pharmaceutical applications<sup>33</sup>. Protein-based polymers are non-toxic, biodegradable, biocompatible, and generally water-soluble which makes them feasible to create NDDS without the use of any organic solvents<sup>34, 35</sup>. Some of the widely used protein polymers in NDDS are albumins (bovine serum albumin (BSA)/human serum albumin (HSA), keratin, soy, collagen, silk, zein, elastin, etc. Protein-based DDS have a high drug-binding capacity, low toxicity, and significant cellular internalization property<sup>25</sup>. The electrostatic charge, release behavior, mucoadhesive property, and degradation profile make protein-based materials attractive systems in drug delivery<sup>35</sup>. Proteins possess various functional groups on their backbone, hence chemical modifications can be done as desired. For example, BSA was conjugated with polycaprolactone (PCL) to assemble nano-micelles for targeted delivery of DOX using the thiol functional group of BSA<sup>36</sup>. Oleic acid was covalently bonded to the amine group of gelatin by EDC/NHS coupling to develop DDS for delivery of irinotecan HCl, as result, the drug loading was increased significantly<sup>37</sup>.

Although polysaccharides and proteins are inherently capable of forming a good DDS they face certain limitations, like low drug binding, uncontrolled rate of hydration, larger size distribution, and microbial contamination if not stored properly. They also exhibit batch-to-batch variations in terms of molecular weight and composition. Further, they can undergo enzymatic degradation *in vivo* and have low reproducibility in terms of drug release and fabrication as NDDS<sup>3</sup>. Hence, research on improving the properties is under progress.

### 1.3 Preparation of nano drug delivery systems (NDDS)

Polymers can be fabricated in various nanosize architectures such as micelles, dendrimers, liposomes, nanoparticles, nanogels, nanofibers, etc for DDS. This chapter mainly focuses on NPs and micelles as DDS because of their beneficial properties to treat chronic diseases.

#### 1.3.1 Polymeric nanoparticles and their preparation

Polymeric NPs (PNPs) can act as carrier vehicles for the targeted delivery of drugs for cancer treatment, vaccines, proteins, oligonucleotides, or nucleic acids for molecular medicine and gene therapy<sup>38</sup>. For intravenous and oral administration routes PNPs show good efficacy, stability, and bioavailability of volatile active molecules. They also enhance the bioavailability of water-insoluble drugs and carry large payloads by protecting the bioactive macromolecules (eg., DNA and siRNA) from physiological barriers<sup>39</sup>. In addition, they can easily get integrated into the other domains such as tissue engineering, regenerative medicine, implants, etc<sup>40,41</sup>. PNPs can be divided into nanocapsules and nanostructures (nanospheres/nanorods/nanodiscs). Nanocapsules are characterized by a polymer acting as an outer shell enclosing pharmaceutical active ingredients in the inner vesicle. Nanostructures are basically a solid matrix of polymer with a drug entrapped or adsorbed on the surface. Apart from size, the shape of the particle also plays a significant role in the entry of polymer-drug conjugates into the cells and helps in increasing circulation time in blood. Reports have established that non-spherical NPs such as rods, discs, and dendrimers have been proven better for improving circulation time in the blood thereby escaping phagocytosis paving to better organ distribution<sup>42</sup>. Gurny et al, (1985) were the pioneer in reporting nanoparticulate systems for ocular drug delivery. In their work, they prepared 300 nm-sized NPs of cellulose acetate hydrogen phthalate (CAP) latex, poly (methyl methacrylate) (PMMA), and lipophilic, butyl cyanoacrylate (BCA), or hexylcyanoacrylate (PHCA) to entrap pilocarpine drug for eye care<sup>43</sup>. Further, bio-active agents loaded in NPs were administered intravenously, which passed through the bloodstream breaching small

---

gaps and tight junctions, and were safely delivered to the tumors, brain, etc. These studies indicated that the drug delivery depends on dimensions of the NDDS to deliver the bioactive agent, where no targeting moiety is immobilized. In most of the studies, it was observed that the application of NPs faced rejection by the immune system and enzymatic degradation and was cleared from the body, which was a serious concern. Accordingly, in the late 1960s, the concept of PEGylation was brought up by Frank Davis for recombinant protein drugs. This idea was utilized by many researchers worldwide to prepare PEGylated nanoparticulate systems<sup>44</sup>. Further, Gref et al examined the efficacy of covalently attached PEG to alter the bio-distribution of NPs composed of poly lactide-co-glycolic acid (PLGA). Bio-distribution studies performed in mice resulted in increased blood circulation time of NPs as the molecular weight of PEG increased (from 5000 to 20000 Da). After 2 h of administration of with and without PEG-coated NPs, it was observed that 30% of coated NPs accumulated in the liver as compared to 66% accumulation of uncoated NPs<sup>45</sup>. Likewise, Perrachia et al reported PEGylation of polycyanoacrylates NPs for intravenous administration and splenic targeting. In his study, he proved that PEGylated NPs displayed extended blood circulation properties with minimal accumulation in the liver<sup>46</sup>. Other than PEG, poloxamer and poloxamines are also being studied to shield the NPs and to increase their blood circulation time. Illum et al reported polystyrene NPs coated with poloxamer-338 displayed prolonged circulation time in rabbits<sup>47</sup>. Likewise, Leu D et al studied the distribution and elimination of poloxamer coated polymethyl methacrylate NPs after injection in rats<sup>48</sup>. Troster et al studied the effect of the different classes of poloxamines coated on the polymethyl methacrylate NPs to understand the bio-distribution, where the *in vivo* studies on rats showed less content of coated nanosystem in the liver<sup>49</sup>. In the case of cancer and other diseases, passive targeting can have deleterious effects when the drug enters healthy cells leading to apoptosis. Passive targeting exploits the gaps in weak vasculature in certain diseases like cancer. The nanosized DDS enter these gaps owing to their size and release drug. To achieve specific targeted delivery of the drug, researchers have developed active targeting of NPs by attaching ligands to it like biotin, folic acid, transferrin, lectins, monoclonal

---

antibody, peptides, etc, so that healthy cells can be unaffected. Active targeting moiety is very specific towards the type of tissue or cell chosen for delivery. For example; In cancer, the receptors like biotin, transferrin, lectins, etc (ligands) are over expressed on the cell surface. So, treating these cancer cells with NPs decorated with these ligands will direct towards the over-expressed receptors of cancerous cells<sup>50</sup>. Chen et al reported PLGA NPs coated with biotinylated chitosan to deliver epirubicin, an anti-cancer drug. They observed that biotinylated PLGA particles showed better cellular uptake with sustained release of the drug and enhanced destruction of cancer cells as compared to unmodified PLGA particles<sup>51</sup>. In another study, Bu et al<sup>52</sup> investigated the use of biotin to deliver an anti-cancer drug, trans-resveratrol to specifically target hepatic carcinoma cells *via* chitosan NPs. The biotin-conjugated NDDS assisted in better uptake in the liver than plain chitosan NPs. To encounter cancer cells and to improve the efficacy, more advanced NDDS are being investigated, like gene therapy. Nucleic acids can be used as therapeutics to inhibit excessive expression of particular genes which lead to various abnormalities and diseases or they can replace defective genes to substitute them. They act by a phenomenon called gene silencing, where genes are prevented from translating into proteins in the case of overexpressed genes. Gene therapy is being studied for treating various diseases like cancer, AIDS, cardiovascular diseases, and other genetic diseases. siRNA, miRNA, shRNA, and plasmid DNA are some of the nucleic acids used in gene therapy. To protect these nucleic acids from enzymatic degradation, they are being encapsulated by polymers. Synthetic polymers such as polyethyleneimine (PEI) and dimethylaminoethyl methacrylate (DMAEMA) and natural polymers like chitosan, atelocollagen, and cyclodextrin were investigated by varying architecture, molecular weight (Mw), and charge density for siRNA delivery. Polyplexes (polymer immobilized nucleic acid) were frequently used as NPs to deliver genes briefly, they are formed by assembly of siRNA with cationic polymers<sup>53</sup>. There are several reports on nucleic acid delivery by encapsulated NPs. For example; H. Ragelle et al reported chitosan-based NPs for delivery of siRNA via intravenous route<sup>54</sup>. Likewise, Shinde RR et al reported PEG-PLA/PLGA NPs for *in vivo* RNAi delivery<sup>55</sup>. In recent studies, other than polymers, the cell-derived vesicles

---

like exosomes, erythrocytes, and stem cells, etc are being explored for drug delivery as they are of bio-origin and are in the micro to nano range with minimum toxicity<sup>56</sup>. For instance, Dong et al reported nano erythrocytes (RBCs) were used to deliver sodium tanshinone IIA sulfonate by intravenous route in rats to treat oxidative stress in endothelial cells<sup>57</sup>. Though there are extensive studies on development of advanced NDDS, very few systems are approved for application by the FDA. ABRAXANE<sup>®</sup> is one such commercial product fabricated from albumin NPs to transport paclitaxel for the treatment of breast, lung, and pancreatic cancers. PEGASYE<sup>®</sup> is PEGylated version of interferon approved for delivery of interferon alpha protein to treat hepatitis C and B. There are several other NPs developed for cancer drug delivery, which are approved by the FDA as shown in Table 1.3

**Table 1.3** NPs approved for cancer therapy<sup>58,59</sup>

Name	Material Description	Nanoparticle Advantage	Indication(s)	Year approved
Abraxane (Celgene)	Albumin particle bound paclitaxel	Improved dosage and reduced cytotoxicity of free drug	Various cancers including: solid malignancies, breast, lymphomas, bladder, lung, pancreatic, head and neck, prostate, melanoma, or liver	2005
Eligard <sup>®</sup> (Tolmar)	Leuprolide acetate and polymer (PLGH (poly (DL-Lactide-co-glycolide)))	Controlled delivery of payload with longer circulation time	Prostate Cancer	2002
Neulasta <sup>®</sup> /pegfilgrastim (Amgen)	PEGylated GCSF protein	Improved stability of protein through PEGylation	Neutropenia, Chemotherapy induced	2002
Oncaspar <sup>®</sup> /pegaspargase (Enzon Pharmaceuticals)	Polymer-protein conjugate (PEGylated L-asparaginase)	Improved stability of protein through PEGylation	Acute lymphoblastic leukemia	1994

### 1.3.1.1 Methods of polymeric nanoparticle preparation

Polymeric nanoparticles (PNP) can be prepared from preformed polymers or the polymerization of monomers depending on the polymer and the end application (Figure

1.3). PNP can be prepared from preformed polymers by using different methods namely solvent evaporation, salting-out, and dialysis. Another way of fabricating PNPs is by the polymerization of monomers using various techniques such as micro-emulsion, mini-emulsion, surfactant-free emulsion, and interfacial polymerization<sup>60</sup>.

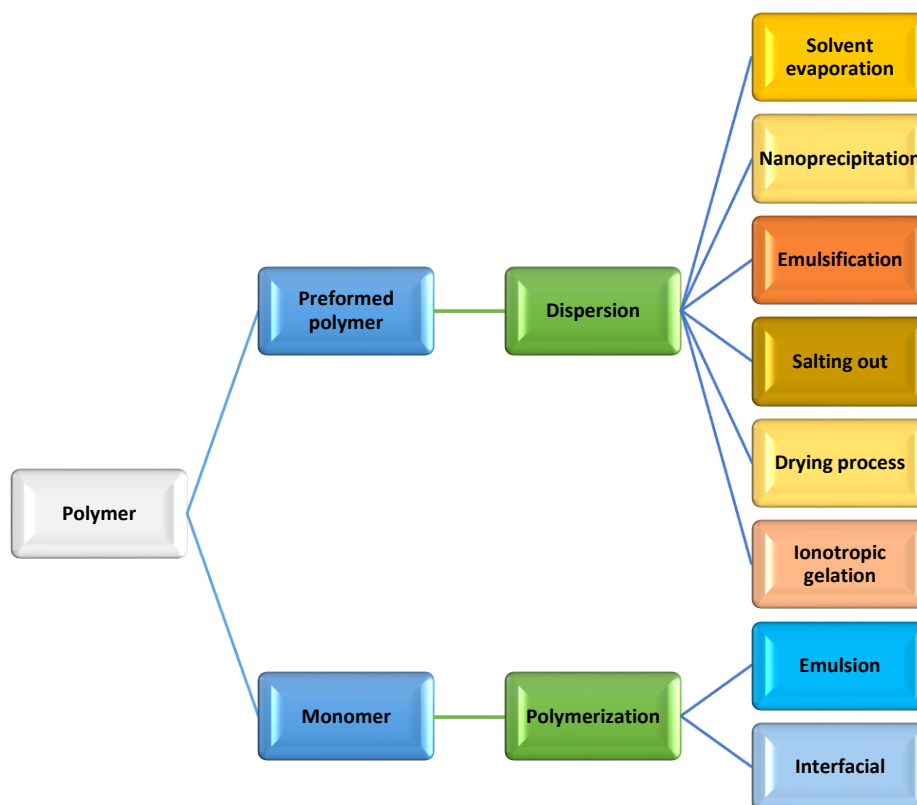


**Figure 1.3** Methods of NP preparation<sup>60</sup>.

### 1.3.1.1.1 From preformed polymers

*i) Desolvation:* This method is used for preparing nanosystems from preformed polymers. In this method, the polymer is precipitated in the presence of drugs. Polymers in the solution are precipitated by the addition of desolvating agents like ethanol,



inorganic salt solution, or by changing the pH of the solution. Generally, bio-polymeric NPs from proteins and polysaccharides are made by this method. Duclairoir C. et al reported gliadin NPs for all-trans-retinoic acid entrapment and release, by using this method. Weber C. et al reported HSA NPs by this desolvation method. Li F-Q et al accounted preparation and characterization of sodium ferulate entrapped bovine serum albumin NPs for liver targeting. After precipitation, the polymer was cross-linked to maintain its structural integrity and subsequently purified<sup>61,62</sup>.

*ii) Emulsification:* Preformed polymers are emulsified and after emulsification, the resultant NPs were harvested using either of these methods, solvent evaporation, solvent diffusion, and or salting out procedures. This method can be employed to a broader range of synthetic and natural polymers.

*a) Solvent evaporation:* It involves emulsification of polymer in an aqueous phase and dispersion in any of the volatile solvents like dichloromethane, chloroform, ethyl acetate. Then the solvent is evaporated using high temperature, vacuum, or by continuous stirring. The size of the particles can be controlled by adjusting parameters like manipulating evaporation temperature, controlling the rate of evaporation, manipulating stirring rate, etc. This method is being practiced for the development of NPs using respective polymers such as PLA, PLGA, PCL, polyhydroxybutyrate, etc, loaded with various drugs like tetanus toxoid, testosterone, loperamide, cyclosporin A, and indomethacin<sup>61</sup>. Song C. X. et al and Quellec P. et al reported a similar method to prepare various polymeric PLGA NPs for various drug loading<sup>63,64</sup>.

*b) Solvent diffusion:* Solvent diffusion is also known as the solvent displacement method. It constitutes a polymer dissolved in the organic phase, which is partially soluble in water. This organic phase diffuses into the aqueous phase and the polymer precipitates in the presence or absence of a surfactant. Briefly, the dissolved polymer in an intermediate polar organic solvent is injected into a stirred aqueous phase containing a surfactant as a stabilizer. As a result of quick diffusion of the solvent, the polymer gets deposited near the interface leading to the formation of colloidal

---

suspension. The poorly soluble antifungal drugs like, bifonazole and clotrimazole are reported to be encapsulated in cyclodextrins following this method<sup>61</sup>. Kwon H Y et al followed a similar method to prepare PLGA NPs containing estrogen. Also, Yan C. et al reported tumor-targeting 5-fluorouracil loaded N-succinyl-chitosan NPs using a similar method<sup>62</sup>.

*c) Salting out:* The salting out phenomenon is similar to the emulsification/solvent diffusion method. In this method, polymer and drug dissolved in an aqueous medium are desolvated in acetone (preferably water-miscible solvent with low boiling point) in the presence of salting out agents like magnesium chloride, calcium chloride, magnesium acetate, or non-electrolytes such as sucrose. Then this emulsion is diluted with enough amount of water to facilitate diffusion of acetone into an aqueous phase rendering polymers in nano form<sup>62</sup>. De Jaeghere et al reported the preparation of PLA-PEO copolymer NPs deploying salting out procedure. Perugini et al investigated the formation of (ethyl cellulose) EC-PLGA NPs embedded with sunscreen agent by using this method<sup>65</sup>.

*iii) Drying processes:* In the last few years, mechanical methods using nano spray dryer and electrospraying are being used to produce dry NPs from colloidal suspensions for pharmaceutical application. Briefly, the polymeric solution is sprayed into fine droplets and subsequently dried on contact with a hot surface to evaporate moisture to form solid particles. Lee et al reported bovine serum albumin NPs employing this method<sup>61</sup>. Li et al reported the preparation of various types of NPs from arabic gum, whey protein, polyvinyl alcohol, maltodextrin using nano spray dryer' developed by Buchi<sup>62</sup>.

*iv) Ionotropic gelation:* This method is generally used for producing NPs from charged polymers especially polysaccharides. Dilute solutions of polymers were stabilized using oppositely charged salts or polymers to form polyelectrolyte clusters or complexes. The charged polymer solution is stabilized by the addition of salts and then mixed with the oppositely charged polymer or mixed without the use of stabilizing salts. For example, in cationic polymer chitosan solution, anionic alginate solution is added

---

and stirred to achieve polyelectrolyte particles. Polysaccharides, such as chitosan, alginate, gelatin, agarose, etc are some of the charged polymeric NPs reported by this method<sup>66</sup>. M. L. Tsai et al reported the development of chitosan-sodium tripolyphosphate NPs by this method<sup>67</sup>.

#### 1.3.1.1.2 From monomers

*i) Emulsion polymerization:* An emulsion formed by a mixture of two or more totally or partially immiscible liquids containing monomers in the presence or absence of a surfactant, which may be polymerized. Depending on the type of dispersed phase and continuous phase, an emulsion can be a direct emulsion (oil in water) or inverse emulsion (water in oil). Emulsions can be further classified depending on their droplet sizes such as nanoemulsion (<100nm), microemulsion (100<1000nm), and macroemulsion (> 1 $\mu$ ). Emulsion polymerization is faster and readily scalable but there are concerns regarding the use of surfactants, toxic organic solvents, and initiators. There are several reports on the preparation of nano-emulsions. For instance; Chang Y-H et al reported particle nucleation mechanism by emulsion polymerization of styrene with a novel polyester emulsifier. Lu S. et al reported the preparation of magnetic polymeric composite NPs by emulsion polymerization. Likewise, Liu G. et al reported the synthesis of monodispersed crosslinked polystyrene NPs, which were decorated with carboxyl groups via emulsion polymerization. In another study, polyacrylamide and polymethyl methacrylate NPs prepared by emulsion polymerization were reported for drug delivery<sup>68,62</sup>.

*ii) Interfacial polymerization (condensation polymerization):* In this method, the monomers are dispersed in the aqueous phase and organic phase and are polymerized at the droplet interface. For the first time Al Khouri et al, (1986) reported the procedure for the preparation of nanocapsules of polyalkylcyanoacrylates by interfacial polymerization. Following a similar method, Lambert G. et al reported the preparation of polyisobutylcyanoacrylate nanocapsules containing an aqueous core as a novel colloidal carrier for the delivery of oligonucleotides. Jang J. et al accounted for selective

---

fabrication of poly(3,4-ethylenedioxythiophene) nanocapsules and mesocellular foams using surfactant mediated interfacial polymerization. This method generates nanocapsules that have good encapsulation efficiency. For instance; a similar procedure was carried for developing poly alkyl cyanoacrylates and polyurethane nanocapsules as drug delivery systems<sup>61,62</sup>.

### 1.3.2 Polymeric micelles and their preparation

Polymers can be assembled as three-dimensional micelles for the delivery of drugs and bioactive molecules. Polymers form micelles if the polymeric chain consists of hydrophilic and hydrophobic chains in the backbone. Such types of polymers are called amphiphilic block copolymers, which arrange themselves as core-shell architectures (micelles) depending on the nature of solvent media. In polar solvents, the hydrophobic chains of micelles arrange themselves on the inner side while the hydrophilic chains expose to the outside of the media and *vice versa* in the case of non-polar solvent<sup>69</sup>. Micelles are formed due to attractive and repulsive forces. Attractive force leads to the association of molecules while repulsive forces prevent unlimited growth of the micelles to a distinct macroscopic phase. Association occurs when the surfactants reach a threshold concentration in solution known as the critical micellization concentration (CMC). Below the CMC the molecules exist as a single chain in a molecular dispersion. The CMC is therefore defined as the concentration of surfactant/copolymer at a given temperature where the first micelle begins to form<sup>70</sup>. The small size, stability, and unique architecture of micelles make it a promising candidate as a good DDS. Polymeric micelles (PMs) are generally in the range of 10-100 nm and provide a very good platform for delivering hydrophobic drugs. In micelles, the hydrophobic core aids in encapsulating hydrophobic drugs which are otherwise difficult to inject as a free drug. Micelles improve the bioavailability, PKs, and biopharmaceutical properties of hydrophobic/lipophilic drugs. Micelles can be fabricated with large amounts of drug loading and can be targeted to specific sites by attaching ligands as targeting moieties<sup>71</sup>. PMs were first studied as DDS by the H. Ringsdorf group in 1984 and later in the 1990s,

---

Kataoka reported DOX conjugated micelles developed from copolymers<sup>72</sup>. The most widely studied hydrophobic block copolymer for micelles formation are poly(propylene oxide), poly(L-amino acid)s, and poly(ester)s<sup>70</sup>. Likewise, K. Kataoka et al<sup>73</sup> demonstrated the formation of polyion micellar complex using cationic poly(ethylene glycol)-poly(Lysine) and anionic oligonucleotides in an aqueous medium with narrow distribution (60 nm). In other studies, G. Kwon et al reported micelles encapsulating adriamycin, and in the year 1996 studied micelles encapsulating DOX, which remained in the blood for a longer duration and entered tumors compared to free DOX. The prepared micelles were composed of the block copolymer of poly(ethylene oxide)-poly(aspartate), PEO-PAsp<sup>70</sup>. Similarly, H K Nguyen et al reported the synthesis and characterization of a series of cationic copolymers derived by grafting polyethyleneimine (PEI) with non-ionic polyethers, poly (ethylene oxide) PEO, or pluronic 123 (P123) respectively. The micelles sized between 70-200 nm were complexed with DNA and administered in mice intravenously for gene therapy<sup>74</sup>. In another study, Kawano et al<sup>75</sup>, reported a new system in combination of synthetic and modified amino acid-based block-co-polymer, [poly(ethylene glycol)-poly(benzyl aspartate)]. These micelles showed enhanced bio-distribution and blood circulation of water-insoluble drug camptothecin. The *in vivo* studies showed significant inhibition of tumor growth. Further, a novel biodegradable conjugate system, (deoxycholic acid-O-carboxymethylated chitosan-folic acid) DOMC-FA was designed and developed as micelles by Wang et al and evaluated its tissue distribution and PKs to understand the delivery of paclitaxel intravenously. The micelles of 152 nm showed better bio-distribution and prolonged blood circulation time compared to taxol injection in bulk form<sup>76</sup>. Further, micelles are also being studied for gene delivery, for example; Hu et al designed and developed low mol wt. polyethyleneimine-conjugated stearic acid-g-chitosan oligosaccharide micelles which were complexed with plasmid DNA and these micelles showed improved localization in cancer tumour<sup>77</sup>. Likewise, Qian et al reported gene delivery in the brain via PEGylated poly(2-(dimethylamino)ethyl methacrylate) micelles attached with TGN phage peptide. The developed micelles were complexed with DNA to form polyplexes which yielded better gene expression after

---

injection in mice brain, these targeting micelles showed better cellular uptake and efficiency<sup>78</sup>. Advanced studies on micelles for delivery of nucleic acids in the combination of a pharmaceutically active agent were reported by Shi et al<sup>79</sup>, where they developed cationic methoxy poly(ethylene glycol)-poly( $\epsilon$  caprolactone)-g-poly(ethyleneimine) a triblock copolymer which could self assemble into micelles. To these micelles, they attached Msurvivin T3A gene and DOX for effective treatment of cancer since these micelles have a good ability to translocate into tumor tissues. Similarly, Pittella et al, reported a hybrid kind of micellar system using poly(ethylene glycol)-block-charge-conversional-calcium phosphate to deliver siRNA in cancer treatment. The siRNA once injected, down-regulated the cancerous gene in pancreatic tumor of mice<sup>80</sup>. In another study Long et al<sup>81</sup>, synthesized advanced polymer, star branched polylactic acid-poly(2-methacryloylethyl phosphorylcholine) copolymer which was self-assembled into micelles and used as vectors for delivery of paclitaxel drug. The mean diameter of these micelles was 65 nm with an ultra-hydrophilic surface to suppress the adhesion of serum proteins which in turn increased the blood circulation duration. These star branched micelles showed better tumor accumulation compared to PLA-PEG micelles after injection in mice, thus opening new paths for intravenous drug delivery.

### 1.3.2.1 Methods of micelles preparation

PMs are prepared mainly by three different methods viz, direct dissolution, solvent evaporation, and dialysis.

*i) Direct dissolution:* This method is commonly used for copolymers with hydrophobic segments like poloxamers or block copolymers. The drug and copolymer are dissolved separately in an aqueous solvent and then mixed. Later, the mixture is heated to cause dehydration, which allows hydrophobic interactions of polymer to assemble as micelles. Z. Tuzar et al, reported micelles assemblies using PDMAEMA-PMMA, [poly(2-(dimethylamino)ethyl methacrylate) Poly (methyl methacrylate)] block copolymers following the direct dissolution method<sup>82</sup>. X. Wu et al and L. Yang et al

---

reported the formation of micelles using PLA-PEG block copolymer using the direct dissolution method<sup>83</sup> for immobilization of drug and their delivery<sup>84</sup>.

**ii) Solvent evaporation:** This method is suitable to prepare micelles when both the drug and copolymer are soluble in a common volatile organic solvent. After the proper dissolution of drug and copolymer in the solvent, the solvent is evaporated which leads to the formation of a thin film of the drug-copolymer complex. To this complex water is added slowly to obtain drug-loaded PMs. For example, A. Lavasanifar et al<sup>85</sup> developed micelles of PEO-b-PHSA [poly(ethylene oxide)-block-poly(N-hexyl stearate-L-aspartamide)] by solvent evaporation method for encapsulation of antifungal drug amphotericin B. Likewise, M. Su et al studied the effect of the rate of solvent evaporation on the shape of PEO-b-PS [poly(ethylene oxide)-block-polystyrene] copolymer micelles<sup>86</sup>. In another report, Y. Liu et al prepared resveratrol-loaded F127-SS-TOC (pluronic F127-SS- $\alpha$ -tocopherol) micelles *via* solvent evaporation method for breast cancer therapy<sup>87</sup>.

**iii) Dialysis:** This is a simple and efficient method to prepare micelles loaded with poorly soluble drugs. Briefly, drug and copolymer are mixed in an organic solvent and then enclosed in a dialysis bag, which is later placed in a beaker containing water. The attractive and repulsive forces between the polymer chains during the movement of water and solvent lead to the formation of micelles. For example, S. B. La et al (1996) developed indomethacin-loaded PEO-PBLA [poly(ethylene oxide)-poly(beta-benzyl L-aspartate)] nano micelles by dialyzing against water<sup>88</sup>. Similarly, W. Lin et al<sup>89</sup> documented a detailed study related to the formation of micelles using various PEGylated copolymers like PCL, PLA, and PVL [poly  $\delta$  -valero lactone ( $\delta$ -VL)]. Likewise, Z. Song et al fabricated curcumin-loaded PLGA-PEG-PLGA nano micelles by dialysis method and studied the PKs and tissue distribution of curcumin *in vivo*<sup>90</sup>.

#### 1.4 DDS for cancer

Cancer is a deadly disease affecting millions of people worldwide. It is characterized by the uncontrolled division of cells leading to tumor formation, which metastasizes to different parts of the body. The conventional method for the treatment of this disease is chemotherapy and radiotherapy both have lots of side effects like nausea, weight loss, loss of appetite, hair loss, body pains, etc. These side effects are due to high doses of potent drugs which affect even normal cells. To avoid all these ill-effects and improve patient's life conditions NDDS are studied and applied in present times. NDDS can be targeted to the tumors by passive and active targeting. The size and shape of NDDS have a huge role in passing vascular junctions and tight cell junctions to deliver the drug/bioactive compound into the desired cells. Maeda et al explained in their concept the movement of NDDS into the tumor by enhanced permeation and retention effect (EPR)<sup>91</sup>. Owing to the poor vasculature of tumor tissues the NDDS enters the site of the tumor, retains at the site, and slowly releases the drug. This is known as passive targeting as the dimensions of the particle control the entry into the tissue. In the active targeting, the NDDS is conjugated with a targeting moiety that is specific to cancerous cells present in tumor tissue, thus bypassing the healthy cells. The active targeting moieties are biotin, folic acid, transferrin, lectins, monoclonal antibody, peptides, etc. Active targeting is preferred over passive targeting due to its advantages<sup>7</sup>.



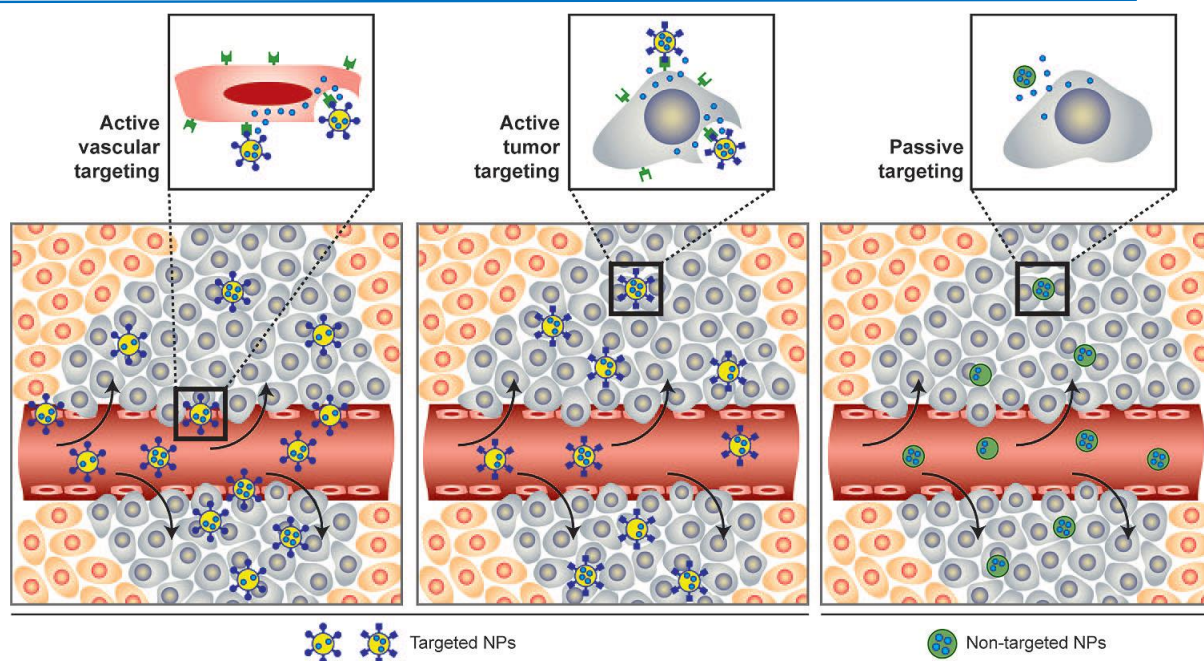


**Figure 1.4** Passive and active targeting<sup>7</sup>.

The different NDDS that are reported for cancer treatment are liposomal, micellar, and polymer conjugate assemblies. The following Table 1.4 enumerates the status of all such formulations in terms of approval by the FDA.

**Table 1.4** NDDS for cancer that are in clinical trials or have been approved<sup>59</sup>

Brand name	Composition	Indication	Status
Doxil/Caelyx	PEGylated liposomal doxorubicin	Ovarian cancer, Kaposi's sarcoma	Approved
DaunoXome (Galen)	Liposomal daunorubicin	Kaposi's sarcoma	Approved

Myocet (Sopherion)	Non-PEGylated liposomal doxorubicin	Breast cancer	Approved
Genexol-PM	Paclitaxel-loaded PEG-PLA micelle	Breast cancer, lung cancer	Approved
NK911	Doxorubicin-loaded PEG-pAsp micelle	Various cancers	Phase 2
NK012	SN-38-loaded PEG-PGlu(SN-38) micelle	Breast cancer	Phase 2
NC-6004	Cisplatin-loaded PEG-PGlu micelle	Various cancers	Phase 1
SP1049C	Doxorubicin-loaded pluronic micelle	Gastric cancer	Phase 3
NK105	Paclitaxel-loaded PEG-PAA micelle	Breast cancer	Phase 3
OPAXIO (Cell Therapeutics)	Paclitaxel combined with a polyglutamate polymer	Ovarian cancer	Phase 3

IT-101	Camptothecin conjugated to cyclodextrin-based polymer	Various cancers	Phase 1/2
HPMA-DOX (PK1)	Doxorubicin bound to HPMA	Lung cancer, breast cancer	Phase 2
HPMA-DOX-galactosamine (PK2)	Doxorubicin linked to HPMA bearing galactosamine	Hepatocellular carcinoma	Phase 1/2
CT-2106	Camptothecin poly-L-glutamate conjugate	Various cancers	Phase 1/2
Abraxane	Albumin-bound paclitaxel nanoparticles	Metastatic breast cancer	Approved

### 1.5 Routes of administration

There are various routes to administer the DDS like oral, buccal, transdermal, ocular, nasal, pulmonary, and parenteral<sup>3</sup>. The NDDS developed in this thesis are mainly designed for intravenous and oral administration, hence the illustrations are limited to those routes.

#### 1.5.1 Intravenous administration

In this mode, the drug bypasses the gastrointestinal tract and enters the blood. It is the preferred route for drug delivery as it has rapid action, higher bioavailability, and lower drug metabolism. Injections can be intramuscular, intravascular, or subcutaneous. This

route is advantageous because it is precise, accurate, the quantities can be regulated and it is easy to administer to unconscious patients, further the unpleasant taste of the drug can be avoided <sup>92</sup>.

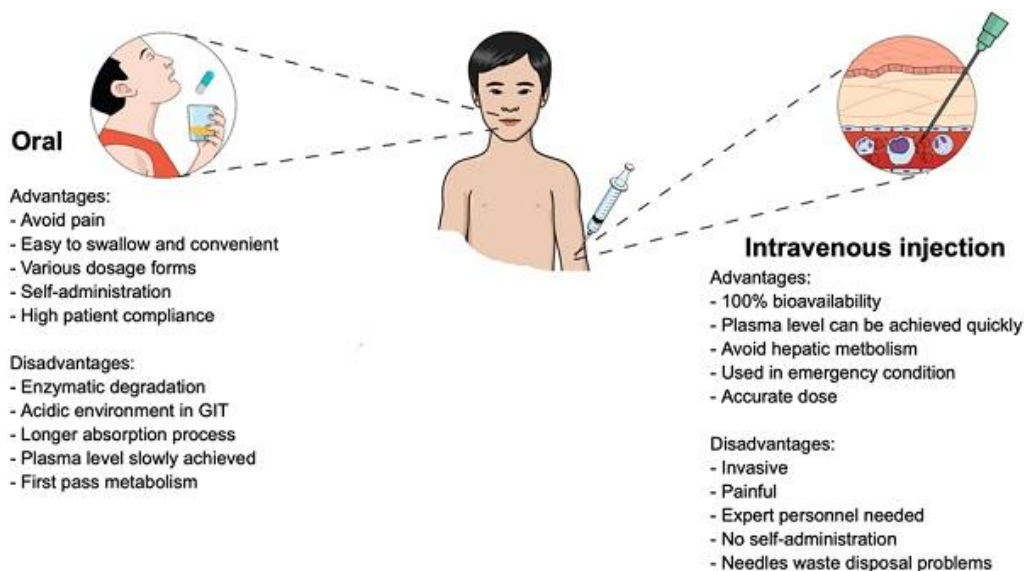


**Figure 1.5** Routes of drug administration<sup>93</sup>.

Most DDS get opsonized by phagocytic cells after being detected as foreign particles; they get cleared from the blood within minutes and end up in the liver and spleen. To overcome this problem, various types of chemical modifications with PEG, poloxamers, albumins, etc. Further, to increase the circulation time and evade the immune system, the DDS are being PEGylated. For example, biodegradable polymer, poly ethylene glycol is coated onto the surface of NPs<sup>94</sup>.

For NDDS to be effective after intravenous injection it has to avoid the immune systems' macrophages and reticular endothelial system (RES)<sup>95</sup>. In intravenous DDS the shape, size, and surface charge of the particles determine their fate. To pass through tight gaps and small capillaries the particles need to be less than 5 $\mu$ m and a dimension of less than 200 nm is required to avoid RES. The hydrophobic and negatively charged surface is not desired when it comes to NPs since they are readily taken up by immune systems macrophages. A completely hydrophilic surface attracts adsorption of albumin

proteins present in the blood hence making the NPs unsuitable for targeted cellular uptake. It is important to strike a proper balance of hydrophobicity and hydrophilicity for an increased blood circulation time of the NPs<sup>94</sup>. Hence polymers of those properties were chosen for the development of NPs for intravenous administration. For instance; the anticancer drug, paclitaxel is a highly hydrophobic and potent molecule that can cause severe hypersensitive reactions, neuro and nephron toxicities when administered in the free bulk form. To avoid these effects, C. Liang et al developed a NP formulation, where paclitaxel was coated with folate receptor conjugated with PEG-PLA copolymer. This drug when administered in mice *via* intravenous route, minimum damage to the liver and kidneys was observed. In another study, doxorubicin-loaded folate-conjugated methyl- $\beta$ -cyclodextrin (FA-M-b-CyD) NPs were prepared by R. Onodera et al to demonstrate as antitumor NDDS. These NDDS were administered via intravenous route into tumor-bearing mice and these mice survived for more than 140 days in comparison to the untreated mice<sup>96</sup>. DDS are also stimuli-responsive which release payload with the change in pH, temperature, pressure or presence of enzymes, ultrasound, magnetic field, etc. In their work, Y. Bae et al displayed pH-triggered release of anti-tumor drug adriamycin from PEG-Asp polypeptide (aspartic acid) NPs. In the acidic microenvironment of the tumor, these nanocarriers degraded and released the drug without any hypertoxicity. These studies were confirmed from *in-vivo* studies of tumor-bearing mice<sup>97</sup>. Abraxane is one such famous DDS approved by the US FDA, it is an albumin-based NPs of size 130 nm loaded with paclitaxel for anticancer therapy<sup>39</sup>. Nevertheless, there is a need for advanced NDDS for effective cancer therapy. Hence, research in this direction is progressing.

### 1.5.2 Oral administration

Administration of the drug through the mouth is known as the oral route. It is an easy method for the delivery of drugs as it is convenient for patients to self-administer without any pain<sup>92</sup>. In this method, the absorption of the drug takes place along the entire gastrointestinal (GI) tract. The villi present on the epithelial cells of the intestine

---

make the human GI tract highly absorptive<sup>98</sup>. There are limitations associated with the oral route as the gastric pH influences the properties of the drug. Therapeutic bioactive molecules like peptides and nucleic acids are unstable in gastric juices of the gut, drugs with low solubility and bioavailability are not absorbed and mucus acts as a barrier for penetration of drugs. The majority of anti-cancer drugs are of the class IV category in the biopharmaceutical classification system (BCS), which have low permeability and solubility in aqueous fluids<sup>99</sup>. To overcome these limitations, bio-adhesive polymeric nanomaterials were developed that can adhere to mucous and release the drugs without being metabolized. The phenomenon of adhesion between mucus and synthetic or biomacromolecule via interfacial forces is known as mucoadhesion. The mucoadhesive polymers are chitosan, carboxymethyl cellulose, poly acrylic acid (PAA), polyvinyl alcohol (PVA), polyvinyl pyrrolidone (PVP), methyl cellulose, hyaluronic acid, gellan gum, alginates, lectins, etc. These polymers provide mucoadhesive property and confers the DDS with prolonged residence and enhances absorption of the drug<sup>100</sup>.

H. Hosseinzadeh et al prepared chitosan-pluronic NPs as oral delivery vehicles of anti-cancer drug gemcitabine. They showed that these 80-170 nm particles were mucoadhesive in nature and had better cytotoxicity to cancer compared to the free drug<sup>101</sup>. Y.M. Tsai et al demonstrated increased bioavailability of hydrophobic curcumin when encapsulated in PLGA as NDDS. As a result, the bioavailability of curcumin is enhanced due to an increase in solubility, which is otherwise insoluble<sup>67</sup>. Polymers are modified to improve their properties to hold drugs and interact with the M-cells present in the intestinal epithelium and evade the efflux of the drug. Common methods of modifications are PEGylation, thiolation, polyelectrolyte coating, and ligand anchoring. PEGylation is the most favored modification as they improve bio-adhesion and impart stealth characteristics to NPs. V. Zabaleta et al studied the potential of PEGylated poly(anhydride) NPs for the delivery of paclitaxel orally. The intestinal permeability of this anti-cancer drug increased 3-7 times because of PEGylation. Also, PEG groups conferred polyanhydride with bio-adhesiveness and inhibitory activity to protect the drug from efflux by the glycoprotein P-gp on the mucus layer<sup>102</sup>. S. Saremi

---

et al in their study used thiolated chitosan NPs for the delivery of anti-cancer drug docetaxel. The modified polymer enhanced bioavailability and absorption of docetaxel *in vitro* and *ex vivo*<sup>103,104</sup>. Iqbal et al prepared and studied NDDS of poly(acrylic acid)-cysteine at different molecular weights for oral administration of paclitaxel. The polymeric particles could successfully inhibit the P-gp efflux pumps and cytochrome P450 metabolism thus, increasing the plasma concentration and bioavailability of the drug<sup>105</sup>.

The pH throughout the GI tract is not the same, it varies from highly acidic in the gut to neutral and slight alkaline in the colon region. This has been of particular interest for researchers to develop DDS from polymers that are pH-responsive. Acrylic-based polymers such as poly(methacrylic acid) (PMAA) along with its blends with poly(ethyl acrylate) (PEA) and poly(methacrylate) (PMA) are stable in a collapsed state in the low pH of the stomach and start swelling along the GI tract as pH increases<sup>98</sup>. R. Khatik et al reported delivery of curcumin to the colon region by using eudragit coated chitosan NPs *in vitro* and *in vivo*. The eudragit (PMAA-PMA) coating on NPs protected the drug curcumin from metabolizing in the acidic gut pH and released in higher pH of the colonic region<sup>106</sup>. Alginate salts are another such natural biopolymers that are pH-responsive, which are used for coating drugs to deliver those in the colon region. P. Sinha et al encapsulated capecitabine an anti-cancer drug with chitosan succinate-sodium alginate for targeted delivery to colon cancer. Sodium alginate protects the drug from the acidic pH of the gut, as it doesn't swell at low pH<sup>107</sup>. T. Agarwal et al reported calcium alginate-carboxymethyl cellulose beads for colon-targeted drug delivery of anti-cancer drug 5-fluorouracil. They elaborated on pH-responsive swelling, mucoadhesivity, and biodegradability of beads due to the colonic microflora for colon-specific drug delivery<sup>108</sup>.

## 1.6 Characterizations

Nanomaterials need to be characterized to understand the physical or chemical changes before and after the fabrication of nanomaterials. This is important in order to

---

manipulate and make them useable for biomedical applications. The properties of the nanomaterial are influenced by its size, shape, surface modification, composition, purity, and stability. Some of the instruments used for the nanomaterial characterization and analysis are optical spectroscopy, electron microscopy, light scattering, circular dichroism, mass spectroscopy, magnetic resonance, X-ray scattering, thermal techniques, and zeta potential measurements.

### **1.6.1 Size and shape**

Size plays a crucial role in deciding the fate of DDS, if too small they are cleared by the kidney, if too big RES clears it. In addition to size, shape also determines the potency of DDS for cellular internalization<sup>109</sup>. For example, Ispas et al established higher toxicity of dendrimer-shaped nickel NPs compared to that of the spherical ones towards zebrafish embryos<sup>110</sup>. For determining the size and shape of nanomaterials several standard instruments are used such as scanning electron microscope (SEM), transmission electron microscope (TEM), scanning tunneling microscope (STM), atomic force microscope (AFM), dynamic light scattering (DLS), fluorescence correlation spectroscopy (FCS), small-angle X-ray scattering (SAXS), etc<sup>12</sup>.

### **1.6.2 Stability**

Chemical composition of nanomaterials decides their stability and biocompatibility. Zeta potential measurements provide the charge density on NPs in suspension form<sup>111</sup>. Infrared spectroscopy (IR), X-ray diffraction (XRD), Raman spectroscopy are utilized to determine the chemical composition and crystalline properties of materials. In the case of protein-based systems, circular dichroism (CD) technique is used for determining their structural integrity and stability. The thermal properties of nanosystems are characterized by thermal gravimetric analysis (TGA) and differential scanning calorimetry (DSC)<sup>112</sup>.



## 1.7 Conclusions

NDDS have shown a lot of promise and potential over the last few years in overcoming challenges present in therapeutics. NDDS come to the rescue when most of the chemotherapeutics fail due to their toxic side effects and non-specific targeting. The dimensions of NPs and PMs make them wonderful vehicles to deliver different kinds of soluble/insoluble drugs, peptides, and nucleic acids. Polymers in general have a lot of advantages in developing DDS as they can be modified and tailored according to the drug and the target organs. Natural and synthetic polymers have been explored for their biocompatibility and biodegradability. Many polymers have been tuned and manipulated to make them more compatible for drug delivery *in vivo*. Encapsulating drugs in polymers improves physicochemical properties such as their bioavailability, blood circulation duration, and absorption. The drug dumping shall be reduced, if NDDS are used, especially in the case of potent anti-cancer drugs which can be highly toxic at higher concentrations. The half-life and plasma concentration are also elevated for certain drugs when introduced into the blood by NDDS. Certain drugs have an unpleasant bitter taste which can be surpassed by using polymeric coating for oral administration. The first pass effect wherein, the drug is metabolized in the liver after being absorbed through the gut is also avoided by NDDS.

Many new methods are explored to increase the efficiency of these NDDS using a combination of polymers. The suitable NDDS can be designed using different combinations of hydrophobic and hydrophilic polymers which can carry drugs/peptides/nucleic acids across the tumors. The major focus is now given to the specificity of NDDS by attaching ligands and antibodies which release the drug in targeted cells and conditions (stimuli) thus eliminating the risk of side effects. The synergistic effect is the phenomenon exploited wherein a combination of drugs, drug/peptide, drug/nucleic acid is used. This is being more investigated due to its potential in treating chronic diseases. The future of polymer therapeutics will result in

---

the development of various NDDS using hybrid systems, following clinical trials, through the combined efforts of medicinal chemists, researchers, pharmaceutical scientists, and clinicians. Synergistic collaborations will certainly favor the development of novel carrier technologies with increased pharmacological effects.

### 1.8 References

- (1) Allen, T. M.; Cullis, P. R. Drug delivery systems: entering the mainstream. *Science* **2004**, *303* (5665), 1818-1822.
  - (2) Buckles, R. G. Biomaterials for drug delivery systems. *Journal of biomedical materials research* **1983**, *17* (1), 109-128.
  - (3) Tsung, J.; Burgess, D. J. Biodegradable polymers in drug delivery systems. In *Fundamentals and Applications of Controlled Release Drug Delivery*, Springer, 2012; pp 107-123.
  - (4) Dhand, C.; Prabhakaran, M. P.; Beuerman, R. W.; Lakshminarayanan, R.; Dwivedi, N.; Ramakrishna, S. Role of size of drug delivery carriers for pulmonary and intravenous administration with emphasis on cancer therapeutics and lung-targeted drug delivery. *Rsc advances* **2014**, *4* (62), 32673-32689.
  - (5) Kharkwal, H.; Janaswamy, S. *Natural Polymers for Drug Delivery*; CABI, 2016.
  - (6) Liu, Z.; Jiao, Y.; Wang, Y.; Zhou, C.; Zhang, Z. Polysaccharides-based nanoparticles as drug delivery systems. *Advanced drug delivery reviews* **2008**, *60* (15), 1650-1662.
  - (7) Farokhzad, O. C.; Langer, R. Impact of nanotechnology on drug delivery. *ACS nano* **2009**, *3* (1), 16-20.
  - (8) Kreuter, J.; Speiser, P. P. In vitro studies of poly (methyl methacrylate) adjuvants. *Journal of pharmaceutical sciences* **1976**, *65* (11), 1624-1627.
  - (9) Gundloori, R. V. N.; Singam, A.; Killi, N. Nanobased intravenous and transdermal drug delivery systems. In *Applications of Targeted Nano Drugs and Delivery Systems*, Elsevier, 2019; pp 551-594.
  - (10) Joo, J.; Kwon, E. J.; Kang, J.; Skalak, M.; Anglin, E. J.; Mann, A. P.; Ruoslahti, E.; Bhatia, S. N.; Sailor, M. J. Porous silicon–graphene oxide core–shell nanoparticles for targeted delivery of siRNA to the injured brain. *Nanoscale horizons* **2016**, *1* (5), 407-414.
-

- (11) Merkle, H. P. Drug delivery's quest for polymers: Where are the frontiers? *European Journal of Pharmaceutics and Biopharmaceutics* **2015**, *97*, 293-303.
- (12) Shi, J.; Votruba, A. R.; Farokhzad, O. C.; Langer, R. Nanotechnology in drug delivery and tissue engineering: from discovery to applications. *Nano letters* **2010**, *10* (9), 3223-3230.
- (13) Panyam, J.; Labhasetwar, V. Biodegradable nanoparticles for drug and gene delivery to cells and tissue. *Advanced drug delivery reviews* **2003**, *55* (3), 329-347.
- (14) Anderson, J. M.; Shive, M. S. Biodegradation and biocompatibility of PLA and PLGA microspheres. *Advanced drug delivery reviews* **1997**, *28* (1), 5-24.
- (15) Hamid Akash, M. S.; Rehman, K.; Chen, S. Natural and synthetic polymers as drug carriers for delivery of therapeutic proteins. *Polymer Reviews* **2015**, *55* (3), 371-406.
- (16) Singam, A.; Killi, N.; Patel, P. R.; Gundloori, R. V. N. PEGylated ethyl cellulose micelles as a nanocarrier for drug delivery. *RSC Advances* **2021**, *11* (49), 30532-30543.
- (17) Lee, B. K.; Yun, Y.; Park, K. PLA micro-and nano-particles. *Advanced drug delivery reviews* **2016**, *107*, 176-191.
- (18) Bala, I.; Hariharan, S.; Kumar, M. N. V. R. PLGA nanoparticles in drug delivery: the state of the art. *Critical Reviews™ in Therapeutic Drug Carrier Systems* **2004**, *21* (5). Pohlmann, A. R.; Fonseca, F. N.; Paese, K.; Detoni, C. B.; Coradini, K.; Beck, R. C. R.; Guterres, S. S. Poly ( $\epsilon$ -caprolactone) microcapsules and nanocapsules in drug delivery. *Expert opinion on drug delivery* **2013**, *10* (5), 623-638.
- (19) Fessi, H.; Puisieux, F.; Devissaguet, J. P.; Ammoury, N.; Benita, S. Nanocapsule formation by interfacial polymer deposition following solvent displacement. *International journal of pharmaceutics* **1989**, *55* (1), R1-R4.
- (20) Danafar, H. MPEG–PCL copolymeric nanoparticles in drug delivery systems. *Cogent Medicine* **2016**, *3* (1), 1142411.
- (21) Bodratti, A. M.; Alexandridis, P. Formulation of poloxamers for drug delivery. *Journal of functional biomaterials* **2018**, *9* (1), 11.
- (22) Venne, A.; Li, S.; Mandeville, R.; Kabanov, A.; Alakhov, V. Hypersensitizing effect of pluronic L61 on cytotoxic activity, transport, and subcellular distribution of doxorubicin in multiple drug-resistant cells. *Cancer research* **1996**, *56* (16), 3626-3629.
-

- (23) Lu, Z.-R.; Shiah, J.-G.; Sakuma, S.; Kopečková, P.; Kopeček, J. Design of novel bioconjugates for targeted drug delivery. *Journal of controlled release* **2002**, *78* (1-3), 165-173.
- (24) Massodi, I.; Bidwell, G. L.; Raucher, D. Evaluation of cell penetrating peptides fused to elastin-like polypeptide for drug delivery. *Journal of controlled release* **2005**, *108* (2-3), 396-408.
- (25) Sabra, S.; Abdelmoneem, M.; Abdelwakil, M.; Mabrouk, M. T.; Anwar, D.; Mohamed, R.; Khattab, S.; Bekhit, A.; Elkhodairy, K.; Freag, M. Self-assembled nanocarriers based on amphiphilic natural polymers for anti-cancer drug delivery applications. *Current pharmaceutical design* **2017**, *23* (35), 5213-5229.
- (26) Zhao, R.; Li, X.; Sun, B.; Zhang, Y.; Zhang, D.; Tang, Z.; Chen, X.; Wang, C. Electrospun chitosan/sericin composite nanofibers with antibacterial property as potential wound dressings. *International journal of biological macromolecules* **2014**, *68*, 92-97.
- (27) Lee, J. W.; Park, J. H.; Robinson, J. R. Bioadhesive-based dosage forms: The next generation. *Journal of pharmaceutical sciences* **2000**, *89* (7), 850-866.
- (28) Sarmiento, B.; Ribeiro, A.; Veiga, F.; Sampaio, P.; Neufeld, R.; Ferreira, D. Alginate/chitosan nanoparticles are effective for oral insulin delivery. *Pharmaceutical research* **2007**, *24* (12), 2198-2206.
- (29) Jain, A. K.; Khar, R. K.; Ahmed, F. J.; Diwan, P. V. Effective insulin delivery using starch nanoparticles as a potential trans-nasal mucoadhesive carrier. *European journal of pharmaceuticals and biopharmaceutics* **2008**, *69* (2), 426-435.
- (30) Kang, D. H.; Jeong, Y.-I. L.; Chung, C.-W. Self-organized polymeric micelles of hyaluronic acid-b-poly (DL-lactide-co-glycolide) block copolymer for targeted delivery of anticancer agent.
- (31) Saranya, D.; Rajan, R.; Suganthan, V.; Murugeswari, A.; Raj, N. A. N. Synthesis and characterization of pullulan acetate coated magnetic nanoparticle for hyperthermic therapy. *Procedia materials science* **2015**, *10*, 2-9.
- (32) You, J.; Hu, F.-Q.; Du, Y.-Z.; Yuan, H. Polymeric micelles with glycolipid-like structure and multiple hydrophobic domains for mediating molecular target delivery of paclitaxel. *Biomacromolecules* **2007**, *8* (8), 2450-2456.
- (33) Tiwari, P.; Panthari, P.; Katare, D. P.; Kharkwal, H. Natural polymers in drug delivery. *World J. Pharm. Pharm. Sci* **2014**, *3* (9), 1395-1409.
-

- (34) Garrait, G.; Beyssac, E.; Subirade, M. Development of a novel drug delivery system: chitosan nanoparticles entrapped in alginate microparticles. *Journal of microencapsulation* **2014**, *31* (4), 363-372.
- (35) Jao, D.; Xue, Y.; Medina, J.; Hu, X. Protein-based drug-delivery materials. *Materials* **2017**, *10* (5), 517.
- (36) Liu, Z.; Dong, C.; Wang, X.; Wang, H.; Li, W.; Tan, J.; Chang, J. Self-assembled biodegradable protein–polymer vesicle as a tumor-targeted nanocarrier. *ACS applied materials & interfaces* **2014**, *6* (4), 2393-2400.
- (37) Park, C.; Vo, C. L.-N.; Kang, T.; Oh, E.; Lee, B.-J. New method and characterization of self-assembled gelatin–oleic nanoparticles using a desolvation method via carbodiimide/N-hydroxysuccinimide (EDC/NHS) reaction. *European Journal of Pharmaceutics and Biopharmaceutics* **2015**, *89*, 365-373.
- (38) Mogoşanu, G. D.; Grumezescu, A. M.; Bejenaru, C.; Bejenaru, L. E. Polymeric protective agents for nanoparticles in drug delivery and targeting. *International journal of pharmaceutics* **2016**, *510* (2), 419-429.
- (39) Kumar, B.; Jalodia, K.; Kumar, P.; Gautam, H. K. Recent advances in nanoparticle-mediated drug delivery. *Journal of Drug Delivery Science and Technology* **2017**, *41*, 260-268.
- (40) Yang, Y.; Chawla, A.; Zhang, J.; Esa, A.; Jang, H. L.; Khademhosseini, A. Applications of nanotechnology for regenerative medicine; healing tissues at the nanoscale. In *Principles of regenerative medicine*, Elsevier, 2019; pp 485-504.
- (41) Sharma, S.; Malik, A.; Gupta, P. Bionanocomposites in tissue engineering and regenerative medicine. In *Bionanocomposites in Tissue Engineering and Regenerative Medicine*, Elsevier, 2021; pp 507-532.
- (42) Venkataraman, S.; Hedrick, J. L.; Ong, Z. Y.; Yang, C.; Ee, P. L. R.; Hammond, P. T.; Yang, Y. Y. The effects of polymeric nanostructure shape on drug delivery. *Advanced drug delivery reviews* **2011**, *63* (14-15), 1228-1246.
- (43) Gurny, R.; Boye, T.; Ibrahim, H. Ocular therapy with nanoparticulate systems for controlled drug delivery. *Journal of Controlled Release* **1985**, *2*, 353-361.
- (44) Hoffman, A. S. The origins and evolution of “controlled” drug delivery systems. *Journal of controlled release* **2008**, *132* (3), 153-163.
-

- (45) Gref, R.; Minamitake, Y.; Peracchia, M. T.; Trubetskoy, V.; Torchilin, V.; Langer, R. Biodegradable long-circulating polymeric nanospheres. *Science* **1994**, *263* (5153), 1600-1603.
- (46) Peracchia, M. T.; Fattal, E.; Desmaele, D.; Besnard, M.; Noel, J. P.; Gomis, J. M.; Appel, M.; d'Angelo, J.; Couvreur, P. Stealth® PEGylated polycyanoacrylate nanoparticles for intravenous administration and splenic targeting. *Journal of Controlled Release* **1999**, *60* (1), 121-128.
- (47) Illum, L.; Davis, S. S. The organ uptake of intravenously administered colloidal particles can be altered using a non-ionic surfactant (Poloxamer 338). *FEBS letters* **1984**, *167* (1), 79-82.
- (48) Leu, D.; Manthey, B.; Kreuter, J.; Speiser, P.; Delucax, P. P. Distribution and elimination of coated polymethyl [2-14C] methacrylate nanoparticles after intravenous injection in rats. *Journal of pharmaceutical sciences* **1984**, *73* (10), 1433-1437.
- (49) Tröster, S. D.; Müller, U.; Kreuter, J. Modification of the body distribution of poly (methyl methacrylate) nanoparticles in rats by coating with surfactants. *International Journal of Pharmaceutics* **1990**, *61* (1-2), 85-100.
- (50) Sinha, R.; Kim, G. J.; Nie, S.; Shin, D. M. Nanotechnology in cancer therapeutics: bioconjugated nanoparticles for drug delivery. *Molecular cancer therapeutics* **2006**, *5* (8), 1909-1917.
- (51) Chen, H.; Xie, L. Q.; Qin, J.; Jia, Y.; Cai, X.; Nan, W.; Yang, W.; Lv, F.; Zhang, Q. Q. Surface modification of PLGA nanoparticles with biotinylated chitosan for the sustained in vitro release and the enhanced cytotoxicity of epirubicin. *Colloids and Surfaces B: Biointerfaces* **2016**, *138*, 1-9.
- (52) Bu, L.; Gan, L.-C.; Guo, X.-Q.; Chen, F.-Z.; Song, Q.; Gou, X.-J.; Hou, S.-X.; Yao, Q. Trans-resveratrol loaded chitosan nanoparticles modified with biotin and avidin to target hepatic carcinoma. *International journal of pharmaceutics* **2013**, *452* (1-2), 355-362.
- (53) Dahlman, J. E.; Barnes, C.; Khan, O. F.; Thiriot, A.; Jhunjunwala, S.; Shaw, T. E.; Xing, Y.; Sager, H. B.; Sahay, G.; Speciner, L. In vivo endothelial siRNA delivery using polymeric nanoparticles with low molecular weight. *Nature nanotechnology* **2014**, *9* (8), 648.
- (54) Ragelle, H.; Riva, R.; Vandermeulen, G.; Naeye, B.; Pourcelle, V.; Le Duff, C. S.; D'Haese, C.; Nysten, B.; Braeckmans, K.; De Smedt, S. C. Chitosan nanoparticles for siRNA delivery: optimizing formulation to increase stability and efficiency. *Journal of Controlled Release* **2014**, *176*, 54-63.
-

(55) Suri, S. S.; Fenniri, H.; Singh, B. Nanotechnology-based drug delivery systems. *Journal of occupational medicine and toxicology* **2007**, *2* (1), 1-6.

(56) Lakhal, S.; Wood, M. J. A. Exosome nanotechnology: an emerging paradigm shift in drug delivery: exploitation of exosome nanovesicles for systemic in vivo delivery of RNAi heralds new horizons for drug delivery across biological barriers. *Bioessays* **2011**, *33* (10), 737-741.

(57) Dong, X.; Niu, Y.; Ding, Y.; Wang, Y.; Zhao, J.; Leng, W.; Qin, L. Formulation and drug loading features of nano-erythrocytes. *Nanoscale research letters* **2017**, *12* (1), 1-13.

(58) Anselmo, A. C.; Mitragotri, S. Nanoparticles in the clinic. *Bioengineering & translational medicine* **2016**, *1* (1), 10-29.

(59) Cheng, Z.; Al Zaki, A.; Hui, J. Z.; Muzykantov, V. R.; Tsourkas, A. Multifunctional nanoparticles: cost versus benefit of adding targeting and imaging capabilities. *Science* **2012**, *338* (6109), 903-910.

(60) Rao, J. P.; Geckeler, K. E. Polymer nanoparticles: preparation techniques and size-control parameters. *Progress in polymer science* **2011**, *36* (7), 887-913.

(61) Reis, C. P.; Neufeld, R. J.; Veiga, F.; Balogh, L. P. Preparation of drug-loaded polymeric nanoparticles. **2017**.

(62) Allouche, J. Synthesis of organic and bioorganic nanoparticles: an overview of the preparation methods. *Nanomaterials: a danger or a promise?* **2013**, 27-74.

(63) Song, C. X.; Labhasetwar, V.; Murphy, H.; Qu, X.; Humphrey, W. R.; Shebuski, R. J.; Levy, R. J. Formulation and characterization of biodegradable nanoparticles for intravascular local drug delivery. *Journal of Controlled Release* **1997**, *43* (2-3), 197-212.

(64) Quellec, P.; Gref, R.; Dellacherie, E.; Sommer, F.; Tran, M. D.; Alonso, M. J. Protein encapsulation within poly (ethylene glycol)-coated nanospheres. II. Controlled release properties. *Journal of Biomedical Materials Research: An Official Journal of The Society for Biomaterials, The Japanese Society for Biomaterials, and The Australian Society for Biomaterials and the Korean Society for Biomaterials* **1999**, *47* (3), 388-395.

(65) Perugini, P.; Simeoni, S.; Scalia, S.; Genta, I.; Modena, T.; Conti, B.; Pavanetto, F. Effect of nanoparticle encapsulation on the photostability of the sunscreen agent, 2-ethylhexyl-p-methoxycinnamate. *International journal of pharmaceutics* **2002**, *246* (1-2), 37-45.

---

(66) Sailaja, A. K.; Amareshwar, P.; Chakravarty, P. Different techniques used for the preparation of nanoparticles using natural polymers and their application. *Int J Pharm Pharm Sci* **2011**, *3* (2), 45-50.

(67) Tsai, M. L.; Bai, S. W.; Chen, R. H. Cavitation effects versus stretch effects resulted in different size and polydispersity of ionotropic gelation chitosan–sodium tripolyphosphate nanoparticle. *Carbohydrate Polymers* **2008**, *71* (3), 448-457.

(68) Liu, G.; Liu, P. Synthesis of monodispersed crosslinked nanoparticles decorated with surface carboxyl groups via soapless emulsion polymerization. *Colloids and Surfaces A: Physicochemical and Engineering Aspects* **2010**, *354* (1-3), 377-381.

(69) Nasongkla, N.; Bey, E.; Ren, J.; Ai, H.; Khemtong, C.; Guthi, J. S.; Chin, S.-F.; Sherry, A. D.; Boothman, D. A.; Gao, J. Multifunctional polymeric micelles as cancer-targeted, MRI-ultrasensitive drug delivery systems. *Nano letters* **2006**, *6* (11), 2427-2430.

(70) Croy, S. R.; Kwon, G. S. Polymeric micelles for drug delivery. *Current pharmaceutical design* **2006**, *12* (36), 4669-4684.

(71) Xu, W.; Ling, P.; Zhang, T. Polymeric micelles, a promising drug delivery system to enhance bioavailability of poorly water-soluble drugs. *Journal of drug delivery* **2013**, *2013*.

(72) Yokoyama, M.; Kwon, G. S.; Okano, T.; Sakurai, Y.; Seto, T.; Kataoka, K. Preparation of micelle-forming polymer-drug conjugates. *Bioconjugate chemistry* **1992**, *3* (4), 295-301.

(73) Kataoka, K.; Togawa, H.; Harada, A.; Yasugi, K.; Matsumoto, T.; Katayose, S. Spontaneous formation of polyion complex micelles with narrow distribution from antisense oligonucleotide and cationic block copolymer in physiological saline. *Macromolecules* **1996**, *29* (26), 8556-8557.

(74) Nguyen, H. K.; Lemieux, P.; Vinogradov, S. V.; Gebhart, C. L.; Guerin, N.; Paradis, G.; Bronich, T. K.; Alakhov, V. Y.; Kabanov, A. V. Evaluation of polyether-polyethyleneimine graft copolymers as gene transfer agents. *Gene Therapy* **2000**, *7* (2), 126-138.

(75) Kawano, K.; Watanabe, M.; Yamamoto, T.; Yokoyama, M.; Opanasopit, P.; Okano, T.; Maitani, Y. Enhanced antitumor effect of camptothecin loaded in long-circulating polymeric micelles. *Journal of controlled release* **2006**, *112* (3), 329-332.



(76) Wang, F.; Zhang, D.; Zhang, Q.; Guo, S.; Zheng, D.; Hao, L.; Guo, H.; Li, C. Tissue distribution and pharmacokinetics evaluation of DOMC-FA micelles for intravenous delivery of PTX. *Journal of drug targeting* **2013**, *21* (2), 137-145.

(77) Hu, F. Q.; Chen, W. W.; Zhao, M. D.; Yuan, H.; Du, Y. Z. Effective antitumor gene therapy delivered by polyethylenimine-conjugated stearic acid-g-chitosan oligosaccharide micelles. *Gene Therapy* **2013**, *20* (6), 597-606.

(78) Qian, Y.; Zha, Y.; Feng, B.; Pang, Z.; Zhang, B.; Sun, X.; Ren, J.; Zhang, C.; Shao, X.; Zhang, Q. PEGylated poly (2-(dimethylamino) ethyl methacrylate)/DNA polyplex micelles decorated with phage-displayed TGN peptide for brain-targeted gene delivery. *Biomaterials* **2013**, *34* (8), 2117-2129.

(79) Shi, S.; Shi, K.; Tan, L.; Qu, Y.; Shen, G.; Chu, B.; Zhang, S.; Su, X.; Li, X.; Wei, Y. The use of cationic MPEG-PCL-g-PEI micelles for co-delivery of Msurvivin T34A gene and doxorubicin. *Biomaterials* **2014**, *35* (15), 4536-4547.

(80) Pittella, F.; Cabral, H.; Maeda, Y.; Mi, P.; Watanabe, S.; Takemoto, H.; Kim, H. J.; Nishiyama, N.; Miyata, K.; Kataoka, K. Systemic siRNA delivery to a spontaneous pancreatic tumor model in transgenic mice by PEGylated calcium phosphate hybrid micelles. *Journal of controlled release* **2014**, *178*, 18-24.

(81) Long, L.-x.; Zhao, J.; Li, K.; He, L.-g.; Qian, X.-m.; Liu, C.-y.; Wang, L.-m.; Yang, X.-q.; Sun, J.; Ren, Y. Synthesis of star-branched PLA-b-PMPC copolymer micelles as long blood circulation vectors to enhance tumor-targeted delivery of hydrophobic drugs in vivo. *Materials Chemistry and Physics* **2016**, *180*, 184-194.

(82) Tuzar, Z.; Pospisil, H.; Plestil, J.; Lowe, A. B.; Baines, F. L.; Billingham, N. C.; Armes, S. P. Micelles of hydrophilic– hydrophobic poly (sulfobetaine)-based block copolymers. *Macromolecules* **1997**, *30* (8), 2509-2512.

(83) Wu, X.; El Ghzaoui, A.; Li, S. Anisotropic self-assembling micelles prepared by the direct dissolution of PLA/PEG block copolymers with a high PEG fraction. *Langmuir* **2011**, *27* (13), 8000-8008.

(84) Yang, L.; Wu, X.; Liu, F.; Duan, Y.; Li, S. Novel biodegradable polylactide/poly (ethylene glycol) micelles prepared by direct dissolution method for controlled delivery of anticancer drugs. *Pharmaceutical research* **2009**, *26* (10), 2332-2342.

(85) Lavasanifar, A.; Samuel, J.; Sattari, S.; Kwon, G. S. Block copolymer micelles for the encapsulation and delivery of amphotericin B. *Pharmaceutical research* **2002**, *19* (4), 418-422.

- (86) Su, M.; Su, Z. Effects of Solvent Evaporation Rate and Poly (acrylic acid) on Formation of Poly (ethylene oxide)-block-polystyrene Micelles from Emulsion. *Macromolecules* **2014**, *47* (4), 1428-1432.
- (87) Liu, Y.; Lin, L.; Song, J.; Zhao, Y.; Chao, Z.; Li, H. Preparation, characterization and anticancer activities of resveratrol loaded redox-sensitive F127-SS-TOC micelles. *RSC advances* **2017**, *7* (74), 47091-47098.
- (88) La, S. B.; Okano, T.; Kataoka, K. Preparation and characterization of the micelle-forming polymeric drug indomethacin-incorporated poly (ethylene oxide)-poly ( $\beta$ -benzyl L-aspartate) block copolymer micelles. *Journal of pharmaceutical sciences* **1996**, *85* (1), 85-90.
- (89) Lin, W.-J.; Juang, L.-W.; Lin, C.-C. Stability and release performance of a series of pegylated copolymeric micelles. *Pharmaceutical research* **2003**, *20* (4), 668-673.
- (90) Song, Z.; Feng, R.; Sun, M.; Guo, C.; Gao, Y.; Li, L.; Zhai, G. Curcumin-loaded PLGA-PEG-PLGA triblock copolymeric micelles: Preparation, pharmacokinetics and distribution in vivo. *Journal of colloid and interface science* **2011**, *354* (1), 116-123.
- (91) Maeda, H.; Wu, J.; Sawa, T.; Matsumura, Y.; Hori, K. Tumor vascular permeability and the EPR effect in macromolecular therapeutics: a review. *Journal of controlled release* **2000**, *65* (1-2), 271-284.
- (92) Verma, P.; Thakur, A. S.; Deshmukh, K.; Jha, A. K.; Verma, S. Routes of drug administration. *International Journal of Pharmaceutical Studies and Research* **2010**, *1* (1), 54-59.
- (93) Ramadon, D.; McCrudden, M. T. C.; Courtenay, A. J.; Donnelly, R. F. Enhancement strategies for transdermal drug delivery systems: Current trends and applications. *Drug Delivery and Translational Research* **2021**, 1-34.
- (94) Gref, R.; Domb, A.; Quellec, P.; Blunk, T.; Müller, R. H.; Verbavatz, J. M.; Langer, R. The controlled intravenous delivery of drugs using PEG-coated sterically stabilized nanospheres. *Advanced drug delivery reviews* **2012**, *64*, 316-326.
- (95) Yoon, I.-S.; Park, J.-H.; Kang, H. J.; Choe, J. H.; Goh, M. S.; Kim, D.-D.; Cho, H.-J. Poly (D, L-lactic acid)-glycerol-based nanoparticles for curcumin delivery. *International journal of pharmaceutics* **2015**, *488* (1-2), 70-77.
- (96) Masood, F. Polymeric nanoparticles for targeted drug delivery system for cancer therapy. *Materials Science and Engineering: C* **2016**, *60*, 569-578.
-

(97) Ross, K. A.; Brenza, T. M.; Binnebose, A. M.; Phanse, Y.; Kanthasamy, A. G.; Gendelman, H. E.; Salem, A. K.; Bartholomay, L. C.; Bellaire, B. H.; Narasimhan, B. Nano-enabled delivery of diverse payloads across complex biological barriers. *Journal of Controlled Release* **2015**, *219*, 548-559.

(98) Ensign, L. M.; Cone, R.; Hanes, J. Oral drug delivery with polymeric nanoparticles: the gastrointestinal mucus barriers. *Advanced drug delivery reviews* **2012**, *64* (6), 557-570.

(99) Mazzaferro, S.; Bouchemal, K.; Ponchel, G. Oral delivery of anticancer drugs III: formulation using drug delivery systems. *Drug discovery today* **2013**, *18* (1-2), 99-104.

(100) Mansuri, S.; Kesharwani, P.; Jain, K.; Tekade, R. K.; Jain, N. K. Mucoadhesion: A promising approach in drug delivery system. *Reactive and functional polymers* **2016**, *100*, 151-172.

(101) Hosseinzadeh, H.; Atyabi, F.; Dinarvand, R.; Ostad, S. N. Chitosan–Pluronic nanoparticles as oral delivery of anticancer gemcitabine: preparation and in vitro study. *International journal of nanomedicine* **2012**, *7*, 1851.

(102) Zabaleta, V.; Ponchel, G.; Salman, H.; Agüeros, M.; Vauthier, C.; Irache, J. M. Oral administration of paclitaxel with pegylated poly (anhydride) nanoparticles: permeability and pharmacokinetic study. *European Journal of Pharmaceutics and Biopharmaceutics* **2012**, *81* (3), 514-523.

(103) Saremi, S.; Dinarvand, R.; Kebriaeezadeh, A.; Ostad, S. N.; Atyabi, F. Enhanced oral delivery of docetaxel using thiolated chitosan nanoparticles: preparation, in vitro and in vivo studies. *BioMed research international* **2013**, *2013*.

(104) Thanki, K.; Gangwal, R. P.; Sangamwar, A. T.; Jain, S. Oral delivery of anticancer drugs: challenges and opportunities. *Journal of controlled release* **2013**, *170* (1), 15-40.

(105) Iqbal, J.; Sarti, F.; Perera, G.; Bernkop-Schnürch, A. Development and in vivo evaluation of an oral drug delivery system for paclitaxel. *Biomaterials* **2011**, *32* (1), 170-175.

(106) Khatik, R.; Mishra, R.; Verma, A.; Dwivedi, P.; Kumar, V.; Gupta, V.; Paliwal, S. K.; Mishra, P. R.; Dwivedi, A. K. Colon-specific delivery of curcumin by exploiting Eudragit-decorated chitosan nanoparticles in vitro and in vivo. *Journal of nanoparticle research* **2013**, *15* (9), 1-15.

(107) Sinha, P.; Udhumasha, U.; Rathnam, G.; Ganesh, M.; Jang, H. T. Capecitabine encapsulated chitosan succinate-sodium alginate macromolecular complex beads for

---

colon cancer targeted delivery: In vitro evaluation. *International journal of biological macromolecules* **2018**, *117*, 840-850.

(108) Agarwal, T.; Narayana, S. N. G. H.; Pal, K.; Pramanik, K.; Giri, S.; Banerjee, I. Calcium alginate-carboxymethyl cellulose beads for colon-targeted drug delivery. *International journal of biological macromolecules* **2015**, *75*, 409-417.

(109) Champion, J. A.; Katare, Y. K.; Mitragotri, S. Particle shape: a new design parameter for micro-and nanoscale drug delivery carriers. *Journal of controlled release* **2007**, *121* (1-2), 3-9.

(110) Ispas, C.; Andreescu, D.; Patel, A.; Goia, D. V.; Andreescu, S.; Wallace, K. N. Toxicity and developmental defects of different sizes and shape nickel nanoparticles in zebrafish. *Environmental science & technology* **2009**, *43* (16), 6349-6356.

(111) Lin, P.-C.; Lin, S.; Wang, P. C.; Sridhar, R. Techniques for physicochemical characterization of nanomaterials. *Biotechnology advances* **2014**, *32* (4), 711-726.

(112) Li, X.; Anton, N.; Arpagaus, C.; Belleteix, F.; Vandamme, T. F. Nanoparticles by spray drying using innovative new technology: The Büchi Nano Spray Dryer B-90. *Journal of Controlled Release* **2010**, *147* (2), 304-310.





---

# *Chapter 2*

---

Objectives and Scope of Work



## 2.1 Objectives and scope of work

Cancer, a sequential process of genetic alterations, is counted as the most menacing health-related problem worldwide. According to the GLOBOCAN, cancer-related mortality surged to 10 million deaths, with 19.3 million new incidences reported in 2020<sup>1</sup>. There are different treatment modalities like surgery, radiotherapy, and chemotherapy to treat cancer. among those chemotherapy was preferred because highly potent drugs were used for faster therapy. Nevertheless, the drugs are nonspecific to cancer cells, hence this therapy is related to debilitating side effects, remission, with lower patient survival<sup>2</sup>. To overcome these shortcomings, controlled drug delivery systems (DDS) are being explored for cancer therapy, so that administering low doses of potent drugs in carriers will reduce the off-target toxicity. The delivery of the potent drugs in the bulk form is less effective when compared with drugs in the nanoform. Because the surface-to-volume ratio of the bulk drugs is less and therefore less available to the cancer cells, which are in the micron size. Further, the solubility of the drug in the nanoform is more when compared to its bulk counterparts. Hence, the nano DDS systems have become more popular and are being extensively explored. The studies on NDDS also reported that the healthy cells are also being affected leading to significant side effects, so as to avoid this the targeted NDDS are being investigated. Generally, polymers are being used as drug carriers because of their inertness, high molecular weight to regulate the pharmacokinetics, pharmacodynamics, and half-life of the drugs. To sustain the ecological balance, biodegradable DDS gained importance. Because these polymers degrade safely in the body either by getting adsorbed or expelled so that the need for surgical extraction can be avoided and as well improve the biocompatibility of the DDS by resisting immune response<sup>3</sup>. Further, the process of polymer biodegradation being a slow process, the normal cellular functions are not disturbed<sup>4</sup>. Accordingly, in this thesis, we have designed and developed NDDS from various biocompatible and biodegradable polymers. We fabricated those polymers as micelles or nanoparticles to deliver anti-cancer bioactive molecules to enhance bioavailability and efficacy.

---

Cancer tumor tissue and its extracellular matrix are characterized by loosely formed blood vessels and sluggish blood flow thus generating the enhanced permeability and retention (EPR) effect<sup>5</sup>. This unique architecture of tumors can be exploited by NDDS by the virtue of their size and surface chemistry. The NDDS can accumulate and deliver the bioactive molecules at a controlled rate once they enter the tumor environment thereby decreasing drug resistance of cancer cells<sup>6</sup>. NDDS also influence the toxicity of the cyclic cytotoxic drugs due to their controlled drug release ability. In general, the drugs which are killing the healthy cells of the body during chemotherapy due to their high volume of doses can be released in a controlled and sustained manner once entrapped in polymeric NDDS<sup>7,8</sup>. Natural plant extracts or phytochemicals are reported to possess anti-cancer properties and are being investigated extensively<sup>9,10</sup>. But they suffer from drawbacks like sensitivity to light, air, different pH, and insolubility in aqueous media leading to low bioavailability. For example, curcumin and eugenol having therapeutic properties (anti-cancer, anti-inflammatory, anti-oxidant, anti-bacterial, etc) show more bioavailability when encapsulated in polymers<sup>11,12</sup>. Likewise, we have developed polymeric micelles (PMs) and nanoparticles (NPs) from biocompatible polymers to entrap cytotoxic chemotherapeutic drug doxorubicin or phytochemicals like curcumin and eugenol. Biocompatible charged polymers like chitosan, Eudragit S100, carboxymethyl cellulose, ethyl cellulose, and PEG were chosen to functionalize as these polymers are non-immunogenic and non-toxic at an optimum concentration to formulate NDDS.

Apart from the nanosize feature of NDDS, the cancer cell's surface chemistry is also being utilized for therapy. Cancer cells overexpress particular antigens or proteins like folic acid, biotin, transferrin, epithelial growth factor (EGF), etc. making them a target for NDDS equipped with molecules that identify these antigens<sup>13,14</sup>. With this strategy, we have developed NPs decorated with EGFR monoclonal antibodies. This novel system will be specific to EGFR overexpressing neck and colorectal cancer cells<sup>15,16</sup>. In addition to these factors, the next generation of cancer therapy involves the use of nanohybrids a combination of synthetic drugs or herbal bioactive

---



molecules, and the utilization of a phenomenon called gene silencing by RNA interference (RNAi). RNAi is gaining immense clinical attention regarding its use as a potential weapon against solid tumors. RNAi could target multiple genes in different pathways that account for tumor progression leading to cancer suppression without any side effects. Nucleic acids used in RNAi need to be delivered to the site of cancer for therapy, but they are susceptible to enzymes in the biosystem. Hence, polymer-based NDDS became forefront in resolving this problem by protecting the nucleic acid cargo till their release. Charged biodegradable polymers are one of the preferred choices to deliver these therapeutic nucleic acids. The studies of this thesis work revealed the design, development of *in vitro* and *in vivo* studies of targeted NDDS using biodegradable polymers.

The objectives and scope of the research work have been summarized below:

1. To develop nano DDS from preformed or functionalized biodegradable polymers using various techniques.
2. To develop polymeric encapsulates/complexes as NDDS to deliver anti-cancer drugs like doxorubicin, curcumin, or bioactive gene silencing plasmid DNA.
3. To develop EGFR conjugated carboxymethyl NPs loaded with eugenol for active targeting.
4. To evaluate the physicochemical properties of the developed NDDS by different physicochemical characterization techniques.
5. To understand the drug delivery and cell cytotoxicity potential of developed NDDS by conducting *in vitro* drug release and cellular studies.

## 2.2 References

(1) Xi, Y.; Xu, P. Global colorectal cancer burden in 2020 and projections to 2040. *Translational Oncology* **2021**, *14* (10), 101174.

---

- (2) Kumar, A.; Golani, A.; Kumar, L. D. EMT in breast cancer metastasis: an interplay of microRNAs, signaling pathways and circulating tumor cells. *Front. Biosci* **2020**, *25*, 979-1010. Crawford, S. Is it time for a new paradigm for systemic cancer treatment? Lessons from a century of cancer chemotherapy. *Frontiers in pharmacology* **2013**, *4*, 68.
- (3) Tsung, J.; Burgess, D. J. Biodegradable polymers in drug delivery systems. In *Fundamentals and Applications of Controlled Release Drug Delivery*, Springer, 2012; pp 107-123.
- (4) Panyam, J.; Labhasetwar, V. Biodegradable nanoparticles for drug and gene delivery to cells and tissue. *Advanced drug delivery reviews* **2003**, *55* (3), 329-347.
- (5) Fang, J.; Nakamura, H.; Maeda, H. The EPR effect: unique features of tumor blood vessels for drug delivery, factors involved, and limitations and augmentation of the effect. *Advanced drug delivery reviews* **2011**, *63* (3), 136-151. Wilhelm, S.; Tavares, A. J.; Dai, Q.; Ohta, S.; Audet, J.; Dvorak, H. F.; Chan, W. C. W. Analysis of nanoparticle delivery to tumours. *Nature reviews materials* **2016**, *1* (5), 1-12.
- (6) Kang, H.; Rho, S.; Stiles, W. R.; Hu, S.; Baek, Y.; Hwang, D. W.; Kashiwagi, S.; Kim, M. S.; Choi, H. S. Size-dependent EPR effect of polymeric nanoparticles on tumor targeting. *Advanced healthcare materials* **2020**, *9* (1), 1901223.
- (7) Sawyer, A. J.; Saucier-Sawyer, J. K.; Booth, C. J.; Liu, J.; Patel, T.; Piepmeier, J. M.; Saltzman, W. M. Convection-enhanced delivery of camptothecin-loaded polymer nanoparticles for treatment of intracranial tumors. *Drug delivery and translational research* **2011**, *1* (1), 34-42.
- (8) Jain, S.; Spandana, G.; Agrawal, A. K.; Kushwah, V.; Thanki, K. Enhanced antitumor efficacy and reduced toxicity of docetaxel loaded estradiol functionalized stealth polymeric nanoparticles. *Molecular pharmaceutics* **2015**, *12* (11), 3871-3884.
- (9) Xie, J.; Yang, Z.; Zhou, C.; Zhu, J.; Lee, R. J.; Teng, L. Nanotechnology for the delivery of phytochemicals in cancer therapy. *Biotechnology advances* **2016**, *34* (4), 343-353.
- (10) Hosseini, A.; Ghorbani, A. Cancer therapy with phytochemicals: evidence from clinical studies. *Avicenna journal of phytomedicine* **2015**, *5* (2), 84.
- (11) Li, Z.; Veeraraghavan, V. P.; Mohan, S. K.; Bolla, S. R.; Lakshmanan, H.; Kumaran, S.; Aruni, W.; Aladresi, A. A. M.; Shair, O. H. M.; Alharbi, S. A. Apoptotic induction and anti-metastatic activity of eugenol encapsulated chitosan nanopolymer on rat glioma C6 cells via alleviating the MMP signaling pathway. *Journal of Photochemistry and Photobiology B: Biology* **2020**, *203*, 111773.
-

(12) Bisht, S.; Feldmann, G.; Soni, S.; Ravi, R.; Karikar, C.; Maitra, A.; Maitra, A. Polymeric nanoparticle-encapsulated curcumin ("nanocurcumin"): a novel strategy for human cancer therapy. *Journal of nanobiotechnology* **2007**, *5* (1), 1-18.

(13) Brannon-Peppas, L.; Blanchette, J. O. Nanoparticle and targeted systems for cancer therapy. *Advanced drug delivery reviews* **2004**, *56* (11), 1649-1659.

(14) Park, J. H.; Saravanakumar, G.; Kim, K.; Kwon, I. C. Targeted delivery of low molecular drugs using chitosan and its derivatives. *Advanced drug delivery reviews* **2010**, *62* (1), 28-41.

(15) Master, A. M.; Sen Gupta, A. EGF receptor-targeted nanocarriers for enhanced cancer treatment. *Nanomedicine* **2012**, *7* (12), 1895-1906.

(16) Maya, S.; Kumar, L. G.; Sarmiento, B.; Rejinold, N. S.; Menon, D.; Nair, S. V.; Jayakumar, R. Cetuximab conjugated O-carboxymethyl chitosan nanoparticles for targeting EGFR overexpressing cancer cells. *Carbohydrate polymers* **2013**, *93* (2), 661-669.



---

# *Chapter 3*

---

PEGylated Ethyl Cellulose Micelles as a Nanocarrier for Drug  
Delivery



### 3.1 Introduction

Amphiphilic polymers are being explored as micelles for several decades and are extensively studied for various applications<sup>1</sup>. In pharmaceuticals, polymeric micelles (PMs) gained attention as DDS because of their nano size, ability to solubilize the hydrophobic molecules, and shield until the molecules are being used. The *in vivo* studies documented that these micelles have higher drug loading capacity with enhanced stability in comparison to the other nanosystems like liposomes, nanoparticles, and dendrimers<sup>2, 3</sup>. They demonstrate prolonged circulation time in the bloodstream by avoiding rapid clearance by the renal and reticuloendothelial systems (RES)<sup>4</sup>. Micelles in an aqueous medium expose the hydrophilic corona, which is responsible for the protection of the system from the RES, enhances the permeability of PMs, and regulates the pharmacokinetic behavior, whereas, the inner hydrophobic domain supports and stabilizes the hydrophobic drugs for slow and sustained release<sup>2</sup>. It is well documented that the nanosized PMs can extravasate and penetrate tumors and its extracellular matrix due to the loosely formed blood vessels and sluggish blood flow, thus making way for the enhanced permeability and retention (EPR) effect<sup>5,6</sup>. As a result, PMs get accumulated and deliver the drug at a controlled rate for a sustainable period thereby decreasing the drug resistance and increasing the effectiveness of therapy. Accordingly, anti-cancer formulations like Genexol-PM® and Nanoxel® were developed and approved by FDA for human treatment. In line with these studies the advanced PM formulations (NK105, NK911, NC-6004) are being studied, which are in clinical trial for anti-cancer therapy<sup>7</sup>.

Generally, the PMs are being designed using synthetic block co-polymers and triblock copolymers and are extensively being studied for drug delivery application<sup>1</sup>. However, synthetic PMs are less compatible with high immunogenicity, as their cell interactions with the anatomy of humans are less favorable. Further, to produce these PMs, complex protocols are involved, and the cost to manufacture is exorbitant, therefore the application of those would limit for the wide range of the population. Currently, PM formulations designed from natural and renewable polymers are attracting much attention because they are highly biocompatible with low immunogenicity. The proteins and polysaccharides being an integral part of humans,

---

they are well tolerated, and further to develop these as a nano assembly may not be expensive as the protocols to design would be less expensive, easily available from a renewable resource, and are safe to use. Accordingly, micelles are being investigated using, proteins (albumin, gelatin, zein, etc) and polysaccharides (hyaluronic acid, chitosan, pullulan, dextran, alginate, xyloglucan, inulin, etc) by functional modification to attain self-assembled nanocarriers<sup>8</sup>.

Polysaccharide-based DDS are reported to form nano-micelles at very low concentrations in an aqueous medium, which demonstrated the ability to enter cells and improved the pharmacokinetics of the drug, and provided a platform for sustained and controlled release of the drug<sup>8</sup>. Ethyl cellulose (EC), a derivative of polysaccharide cellulose, is being explored in the fields of cosmetics, food additives, adhesives, and medicine owing to its chemically inert nature, stability, sustained drug release ability, and good biocompatibility<sup>9,10</sup>. In a report by Balzus et al, EC displayed extended-release behavior in comparison to polymers like Eudragit RS 100 and other lipids<sup>11</sup>. However, there are very few reports about the application of EC in drug delivery systems other than oral or topical administration. Nevertheless, S. Leitner et al reported the development of EC nanoparticles as a new transfection tool for antisense oligonucleotide delivery<sup>12</sup>. The hydrophobic nature of EC, has benefits in terms of sustained release for oral administration however, its hydrophobicity proves to be a hurdle for it to be used in parenteral administration as the hydrophobicity activates the macrophages of the immune system. To overcome this, the structure of EC needs to be modified without sacrificing its desirable properties. Therefore, the synthesis of EC-grafted polymers has attracted significant attention in recent years. For instance, Yuan et al reported synthesis, characterization, and *in vitro* degradation of EC-graft-poly( $\epsilon$ -caprolactone)-block-poly(l-lactide) copolymers by sequential ring-opening polymerization<sup>13</sup>. One of the best choices in pharmaceuticals of drug delivery is the FDA-approved PEG, because of its tuneable properties and well-established safety profile in terms of biocompatibility and non-immunogenicity. Several polymers of different properties are PEGylated to prolong their duration in blood circulation to shield them from the immune system and to complete their targeted function<sup>14</sup>. For example; PEGylation of cellulose or its derivatives is explored to improve its

---

dispersibility and colloidal stability. For instance, Lasseguette grafted PEG to microfibrillated cellulose by EDC-coupling<sup>15</sup>. T. Kaldeus et al reported PEGylation of TEMPO-oxidized cellulose and studied its colloidal stability<sup>16</sup>. EC is well established for oral delivery however, there are seldom reports on EC for systemic application due to its drawbacks as explained above. The properties of EC being favorable for drug delivery, its potential application for invasive delivery is being explored by addressing the incompatibility and immunogenicity by grafting it with PEG. For example, Huang et al synthesized thermosensitive micelles from the amphiphilic graft copolymer of EC-poly(PEG methyl methacrylate), EC-PMMA for systemic drug delivery applications<sup>17</sup>. In their studies, they have designed and developed EC-PMMA as nano self-assemblies and characterized their thermosensitive behavior. However, a detailed study of EC-PMMA nano-assembly for drug delivery, cytotoxicity, and hemocompatibility studies were not reported to support their utility for systemic application. In accordance with these studies, we aimed to develop EC-PEG nanomicelles by simple methods and evaluate their physicochemical properties and *in vitro* studies such as cytotoxicity, drug delivery, cell interaction, and hemolysis so as to understand their potential for systemic application. We have chosen doxorubicin (DOX) as a model drug to load in EC-PEG micelles for anti-cancer therapy in the form of CDDS (controlled drug delivery system). DOX is a potent anti-cancer drug used in chemotherapy to treat solid tumors, lymphoma, soft tissue sarcoma, etc. However, its application at higher doses is limited because of its off-target effects like cardiotoxicity and its role in the development of tumor cells' resistance<sup>18</sup>. To mitigate these limitations, our amphiphilic copolymer based micelles are designed.

In this chapter, EC was converted to carboxylated EC (CEC) by TEMPO mediated oxidation and subsequently grafted with mPEG<sub>(2000)</sub> by N, N'-dicyclohexylcarbodiimide (DCC) coupling. This mPEG grafted EC (EC-PEG) was developed as micelles in an aqueous medium and loaded with hydrophobic DOX. The release pattern of the drug showed a sustained release profile. The *in vitro* effectivity of the system was also investigated in breast cancer cell lines MDA-MB-231 and MCF-7. Herein, the use of EC in the form of micelles as a DDS to deliver DOX is reported for the first time.

---

## 3.2 Experimental

### 3.2.1 Materials

Ethyl cellulose (Ethoxy content 44-51%, 18-24 mPas) was procured from S.D. Fine Chemicals, India. Doxorubicin HCl (hydrochloride) and 4-dimethylaminopyridine (DMAP) were obtained from Himedia Laboratories, India. Poly (ethylene glycol) methyl ether, Mw 2000 (mPEG) and (2,2,6,6-tetramethylpiperidin-1-yl)oxidanyl (TEMPO) were procured from Aldrich, USA. N, N'-dicyclohexylcarbodiimide (DCC) was procured from Spectrochem Pvt. Ltd, India. DMEM (Dulbecco's modified Eagle's medium), MEM (Minimal essential medium), MTT (3-(4, 5-dimethylthiazol-2-yl)-2, 5-diphenyltetrazolium bromide) were purchased from Invitrogen, India. All the solvents and salts were of analytical grade and used without any further purification. Cell lines were procured from National Centre for Cell Science (NCCS) Pune.

### 3.2.2 Synthesis and characterization of EC-PEG graft polymer

#### 3.2.2.1 TEMPO mediated oxidation of EC

Oxidation of hydroxy groups of EC (-CH<sub>2</sub>OH) was done according to the reported literature by J Araki et al<sup>19</sup>, as shown in Figure 1. Briefly, to 400 mL aqueous suspension of EC (10 mg/mL, 4 g), TEMPO (0.4 g), sodium bromide (4 g) were added and stirred at room temperature (RT) for 15 min. The oxidation was initiated with the addition of 60 mL of NaClO (sodium hypochlorite) solution, where the concentration of NaClO was maintained at 25 wt% with respect to EC (1.25 g NaClO for 5 g EC). The solution pH was maintained between 10-11 while stirring at RT for 4 h. After 4 h, NaCl (30 g) was added to the reaction mixture and the EC suspension was precipitated. The product was filtered through a pore fritted glass filter and washed with 0.5-1.0 M NaCl. The product was dispersed in NaCl of the same concentration and centrifuged at 12000 rpm for 30 min at 25 °C. This washing procedure was repeated 3 times to remove the unused NaClO. The sodium salt of EC was converted to free acid form by washing it twice with 0.1 N HCl. The obtained product was dialyzed against deionized water for 3 days with frequent change of

---



water. The colloidal carboxylic EC obtained was dried, quantified, and characterized to confirm the product (yield 2.32 g, 58%).

### 3.2.2.2 Determination of carboxylate charge density of EC

The carboxylate charge density on EC after oxidation reaction was estimated via the conductometric titration method. Briefly, TEMPO-oxidized EC (240 mg) was dispersed in 30 mL of de-ionized (DI) water. This dispersion was stirred and sonicated for 30 min in a bath sonicator (Bio-technics, India) and left standing overnight. Later, 10 mL of the dispersion was added to 80 mL of DI water. Subsequently, 50  $\mu$ L of concentrated HCl was added to carboxylated EC (CEC) dispersion and titrated against 0.5 M NaOH. The conductivity of the solution was measured (Orion Star, Thermo Scientific Conductometer, India) with every addition of 20  $\mu$ L of 0.5M NaOH to the CEC-HCl dispersion. The degree of carboxylated EC was estimated using the graph plotted for the conductivity of CEC-HCl dispersion against the volume of NaOH.

### 3.2.2.3 PEGylation of carboxylated EC (CEC)

mPEG (Mw 2000) was grafted to CEC using DCC reagent and a catalyst DMAP. For example; In a two necked RB, CEC [400 mg, (0.33 mmol (calculated from the titration equation S1))] was dispersed in 10 mL of dry tetrahydrofuran (THF) and stirred for 45 min under N<sub>2</sub> atmosphere at R.T. To the CEC solution, a solution of DCC (0.99 mmol) and DMAP (0.165 mmol) prepared in dry THF was added and stirred for 2 h at RT. Later, to the solution mixture, mPEG (0.33 mmol) dissolved in 5 mL of dry THF was added dropwise using a syringe. Following this, this reaction mixture was stirred under nitrogen atmosphere at 40 °C for 48 h. After 48 h, the reaction was stopped and filtered through Whatman's filter paper to collect the filtrate. This filtrate was concentrated using a rota evaporator at 50 °C and then precipitated in diethyl ether. The diethyl ether was evaporated and the precipitate was dispersed in DI water and dialyzed (10 kDa cut off) against DI water for 48 h to remove the unreacted mPEG and reagents to obtain EC-PEG of 1:1. Similarly, in another set of reaction, mPEG (0.66 mmol) was reacted with EC following the same procedure and reaction

---

conditions to obtain EC-PEG of 1:2. The final compound EC-PEG (1:1 and 1:2) labeled as EC-PEG1 and EC-PEG2 respectively were characterized by  $^1\text{H}$  NMR,  $^{13}\text{C}$  NMR, and FTIR. The yield of this reaction was 320 mg, 80%.

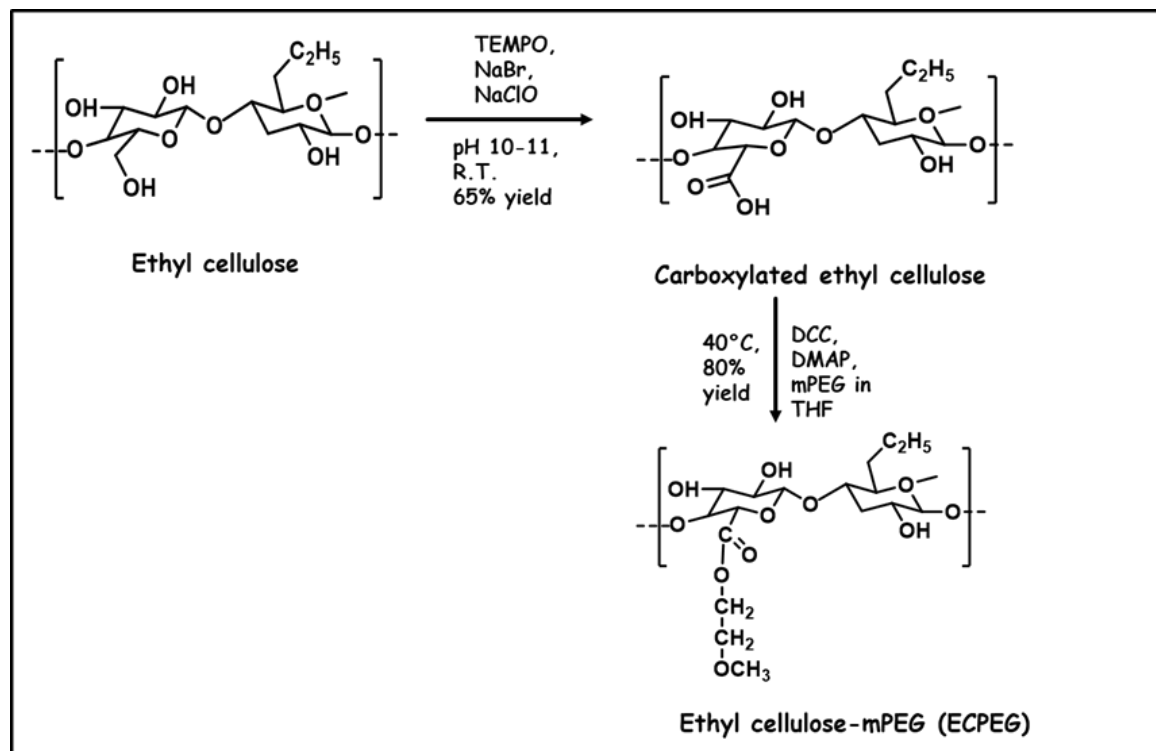


**Figure 3.1** Scheme of oxidation of ethyl cellulose (EC) followed by reaction with mPEG by DCC/DMAP coupling.

#### 3.2.2.4 Critical micellar concentration (CMC) of EC-PEG

Following a reported protocol by J. Chen et al<sup>20</sup>, the CMC of the EC-PEG1 and EC-PEG2 was determined. Hydrophobic probe pyrene was used for estimating the CMC of the respective EC-PEG in water by fluorescence spectroscopy. To individual 5 mL vials, a total of 25  $\mu\text{L}$  of pyrene in acetone solvent (20  $\mu\text{g}/\text{mL}$ ) was added and allowed the acetone to evaporate to obtain dry pyrene. To these respective vials, 5 mL of the aqueous solution of EC-PEG copolymers were added with varying series of concentrations from 0.00025 to 0.09 mg/mL. The final concentration of pyrene in each sample solution was 0.1  $\mu\text{g}/\text{mL}$ . The excitation spectra (300-360 nm) of the solutions were recorded at an emission wavelength of 395 nm. The ratio of the peak

intensities at 338 nm over 334 nm ( $I_{338}/I_{334}$ ) of the excitation spectra were recorded and plotted as a function of polymer concentration, Log C (mg/mL).

### 3.2.3 Preparation and characterization of micelles

#### 3.2.3.1 Preparation of EC-PEG micelles

The dialysis method was used for fabricating micelles of EC-PEG (1:1 and 1:2). Briefly, EC-PEG1 (20 mg) was dissolved in 2 mL DMF, and 10 mL PBS buffer (pH 7.4) was added drop-wise to it while sonicating at 20% amplitude (Vibracell, VCX 500, USA). Later this solution was dialyzed against DI water for 24 h using a dialysis membrane of 10 kDa cut-off to obtain micelles. These micelles were lyophilized to obtain the dry powder, which was used for characterization. Similarly, EC-PEG2 micelles were also prepared and characterized.

#### 3.2.3.2 Preparation of DOX loaded EC-PEG micelles

The EC-PEG micelles loaded with DOX were prepared at 0.1 % (w/v), following the procedure as described: briefly, DOX (1 mg) was dissolved in 1 mL DMF, to this added 1.5 eq of triethylamine and stirred at RT. Later, 20 mg of EC-PEG1 was added to this DOX solution and stirred for 1 h while maintaining the conditions at RT. To this, PBS buffer (10 mL) was added dropwise under sonication at 20% amplitude. Further, this solution was dialyzed against DI water for 24 h using a 10 kDa cut-off membrane. After dialysis, the obtained DOX-loaded micelles were lyophilized to give DOX-EC-PEG1 powder, which was red in color. The same protocol was followed to obtain DOX-loaded micelles of EC-PEG2. The developed formulations are shown in Table 1. The micelles with and without DOX were characterized by various physicochemical characterization methods.

### 3.2.4 Characterizations

#### 3.2.4.1 NMR spectroscopy

$^1\text{H}$  NMR spectra for characterization of mPEG and EC-PEG were recorded on Bruker AV-200 NMR spectrometers operating at a  $^1\text{H}$  frequency of 200 MHz.  $^1\text{H}$  spectra of

---

all the compounds were recorded in DMSO-d<sub>6</sub> (polymer concentration: 50 mg/mL). The samples were homogenized before recording the NMR spectra. Similarly, <sup>13</sup>C NMR spectra of mPEG and EC-PEG were also recorded on Bruker AV-500 NMR spectrometers operating at a <sup>13</sup>C frequency of 125 MHz.

### 3.2.4.2 Physicochemical characterization of micelles

The size distribution, hydrodynamic diameter and charge density for the blank and DOX loaded micelles were determined by DLS (90 Plus Brookhaven Instruments Corp, PALS zeta potential analyzer, USA). The morphology of the micelles was investigated by TEM (FEI Tecnai TF20, 200kV FEG high-resolution Transmission Electron Microscope, USA). For TEM analysis, the samples were diluted (5X) in Millipore water, stained with 1% (w/v) uranyl acetate dye, and drop casted on copper grid mesh.

The percent of drug loading efficiency and content was determined using a UV-Vis spectrophotometer (UV 1601PC UV spectrophotometer, Shimadzu, Japan). For instance, 1.5 mg of DOX loaded micelles were dissolved in 1 mL DMF, filtered, and estimated the content of DOX using the standard DOX calibration curve recorded at 480 nm. The percent of drug loading efficiency and loading content were calculated using the following equations:

$$\text{Drug loading efficiency (DLE) (\%)} = \frac{\text{wt of loaded DOX}}{\text{wt of feeding DOX}} \times 100 \dots\dots (1)$$

$$\text{Drug loading content (DLC) (\%)} = \frac{\text{wt of loaded DOX}}{\text{wt of DOX loaded polymer}} \times 100 \dots\dots (2)$$

**Table 3.1** Formulations of EC-PEG with DOX

<b>Batch No.</b>	<b>EC-PEG1 % (w/v)</b>	<b>DOX % (w/v)</b>	<b>Hydrodynamic diameter (nm)</b>	<b>PDI</b>	<b>DLE (%)</b>	<b>DLC (%)</b>
B1.	2	-	153.5	0.293	-	-
B2.	2	0.1	204.9	0.122	36.73	1.73
B3.	2	0.15	257.7	0.297	52.73	4.11
<b>Batch No.</b>	<b>EC-PEG2 % (w/v)</b>	<b>DOX % (w/v)</b>	<b>Hydrodynamic diameter (nm)</b>	<b>PDI</b>	<b>DLE (%)</b>	<b>DLC (%)</b>
B4.	2	-	249.9	0.191	-	-
B5.	2	0.1	338.6	0.18	32.93	1.55
B6.	2	0.15	350.5	0.357	52.51	3.66

FTIR spectroscopy analysis was conducted for DOX, bare polymers (EC and mPEG), grafted copolymers (EC-PEG1 and EC-PEG2), and DOX loaded micelles (Batch 3 and 6) to confirm the grafting of mPEG with EC and their functional interactions with DOX. For FTIR, the samples (2-3 mg) were ground with anhydrous potassium bromide KBr (97 mg) to form a pellet, which was used for analyzing (PerkinElmer spectrometer I, FT-IR diffused reflectance (DRIFT) mode, USA). The scans were recorded at 400  $\text{cm}^{-1}$  to 4000  $\text{cm}^{-1}$  with an average of 10 scans per sample.

Thermal analysis was carried out using DSC (Model Q100 DSC, TA instrument, Newcastle, DE, USA) to investigate the thermal properties of EC in its pristine form, after grafting, and after DOX loading (Batch 3 and 6). The samples were crimped in aluminum pans and the thermal properties were analyzed in cycles. In the first heating cycles, the ramp was subjected to temperature from -70  $^{\circ}\text{C}$  to 250  $^{\circ}\text{C}$  at a rate of 10

°C/min. The sample was cooled up to -70 °C in 2<sup>nd</sup> cycle at a rate of 10 °C/min and in the third heating cycle, the ramp temperature was set from -70 °C to 250 °C at a rate of 10 °C/min. The entire experiment was done under nitrogen gas (50 mL/min). An empty cubicle of the aluminum pan was used as a reference pan.

#### 3.2.4.3 *In vitro* DOX release

The release of DOX from the micelles was studied by dispersing 5 mg DOX loaded micelles (B3, B6) in 10 mL buffer and enclosing them in a dialysis membrane tube (Mw cut off 12 kDa). This dialysis bag was kept in 20 mL phosphate buffer (100 mM, pH 7.4), and incubated at 37 °C in a shaker bath (Julabo SW23) with 100 rpm. At regular intervals of time, 1 mL was withdrawn from the buffer and 1 mL fresh buffer was added to maintain the sink conditions. The withdrawn buffer was estimated for the amount of DOX released using a UV-Vis spectrophotometer recorded at 480 nm. Similarly, the release studies were performed in a phosphate buffer of pH 5.5. The cumulative release of DOX was calculated using the following equation:

$$\text{Cumulative drug release (\%)} = \frac{\text{wt of DOX released}}{\text{wt of DOX in PMS}} \times 100 \dots\dots (3)$$

#### 3.2.4.4 Hemolysis assay

To study the biocompatibility of the developed graft polymer on RBCs (red blood cells), hemolysis assay was conducted. Briefly, blood was collected in tubes containing EDTA from healthy volunteers at National Chemical Laboratory, Pune, India. The RBCs were separated from the whole blood by density gradient centrifugation. For instance, 5 mL whole blood was added slowly in 5 mL of PBS and centrifuged at 2000 rpm for 30 min. The supernatant devoid of RBCs was discarded and the pellet was washed thrice with PBS and centrifuged again for 30 min at 2000 rpm. Later, the cells were dispersed in PBS to prepare a stock dispersion of 2% (v/v). Further, 2 mL of this stock dispersion was dispensed in 2 mL vials in duplicates, to the respective vials, test samples such as EC, CEC, B1, B3, B4, and B6 at a concentration of 0.5 mg/mL and 1 mg/mL were added. The respective controls like RBC suspension in PBS (negative) and RBC suspension in DI water (positive) were

---

prepared. All the respective test samples and controls were incubated at 37 °C for 2 h with gentle shaking for every 30 min to re-suspend the precipitated RBCs. After the incubation period, the suspensions were centrifuged at 1500 g for 10 min at RT. The supernatant obtained was dispensed in a 96 well plate and the hemoglobin (Hb) release was read in a microtiter plate reader spectrophotometrically at 540 nm (Multiskan Ex, (51118170(200–240 V) Thermo Scientific, Finland)). Considering 100% lysis of cells in DI water and 0% lysis in PBS, the percentage of hemolysis for test samples was calculated using the following equation.

$$\text{Hemolysis (\%)} = \frac{\text{Abs.test} - \text{Abs.negative control}}{\text{Abs.positive control} - \text{Abs.negative control}} \times 100 \dots\dots (4)$$

#### 3.2.4.5 Cell studies

Fibroblast cell line L929 and breast cancer cell line MDA-MB-231 were maintained in DMEM supplemented with 10% FBS under standard conditions at 37 °C, in a humidified CO<sub>2</sub> incubator. Under similar incubation conditions, breast cancer cell line MCF-7 was also cultured in MEM supplemented with 10% FBS. The cells were routinely grown as monolayer cultures in a 25cm<sup>2</sup> flask and passaged once a week using trypsin/EDTA at 80% confluence.

**Cytotoxicity assay:** Blank micelles, B1 and B4 were investigated for their cellular toxicity in L929 fibroblast cells by MTT assay. A confluent flask of L929 cells was trypsinized to harvest cells which were further seeded in a 96 well plate at 10,000 cells/well. The plate was incubated at 37°C, in a 5% CO<sub>2</sub> humidified atmosphere for 16 h to allow cells to attach and form a monolayer. Later, the media from the wells was flicked off, and added B1 and B4 micelles respectively. The stock concentration of micelles at 1 mg/mL was prepared in serum-free media. From these, a series of concentrations ranging from 0 to 400 µg/mL was added to the respective wells and incubated for 48 h. Post incubation, the media was tipped off from the wells and the MTT solution prepared in DMEM-FBS media was added to the wells. Following, the plate was incubated in dark at 37 °C, in a humidified CO<sub>2</sub> incubator for 4 h. Finally,

---

the MTT media in the wells was replaced with 100  $\mu$ L DMSO and the plate was read at 550 nm in a plate reader (Multiskan Ex, (51118170(200–240 V) Thermo Scientific, Finland)). Cells grown in the wells devoid of any test sample were considered as positive control and the cells incubated in the media with 30% DMSO (v/v) were the negative control. The relative cell viability was calculated by comparing the absorbance read in test samples to positive control [(Abs.sample/Abs.positive control) x 100]. Data are presented as average  $\pm$  SD (n=3). The cytotoxicity of B1 and B4 micelles was also evaluated in MDA-MB-231 cells by this assay under the same parameters. Similarly, the MTT assay was also carried out for DOX-loaded micelles (B3, B6), in MDA-MB-231 and MCF-7 cells for 72 h.

***In vitro cellular uptake:*** The uptake of the B3 and B6 micelles was studied in MDA-MB-231 cells. A count of  $5 \times 10^4$  cells was seeded on sterile 12 mm round coverslips placed in a 24 well plate and incubated for 24 h at 37 °C in a 5% CO<sub>2</sub> atmosphere. After incubation, the media were aspirated from the wells and washed thrice with PBS. Free DOX at a concentration of 4  $\mu$ g/mL and DOX loaded micelles (B3 and B6) of 100  $\mu$ g/mL containing an equivalent amount of DOX (calculated by loading efficiency) were dispersed in the serum-free media and incubated for 4 and 8 h separately. Later, the cells were washed thrice with PBS and fixed by adding 300  $\mu$ L of 4% paraformaldehyde and incubating for 15 min at RT. Post fixing step, the cells were washed extensively with PBS and incubated with Alexa fluor 488 phalloidin (60 nM) for 30 min in dark to colorize the actin filaments, to identify the cytoplasm and cell boundary. The nucleus was stained with DAPI (300 nM) for 15 min in dark and washed off with PBS. Finally, the coverslips were mounted on a clean slide with the application of mounting media (fluoroshield). Excess mounting media was dabbed with tissue and the cells were visualized using an epifluorescence microscope by Carl Zeiss (Model: Axio Observer.Z1, Oil emersion objective, 63X). The nucleus stained with DAPI was observed under the blue channel, the cytoskeleton stained with Alexa fluor 488 under the green channel, and DOX under the red channel.



### 3.3 Results and discussion

EC, a natural polymer derivative was grafted covalently with mPEG to develop an amphiphilic copolymer that assembles into a micellar structure in an aqueous medium. The EC core of the micellar architecture was used for loading anti-cancer drug DOX. The purpose of mPEG grafts on the outer layer is to protect the drug carrier from being recognized by the immune system as well facilitate the duration of micelles to circulate in the blood for effective therapy.

#### 3.3.1 TEMPO mediated oxidation and determination of carboxylate charge density on EC

**Mechanism of oxidation:** TEMPO-mediated oxidation has been explored over the last few decades in the conversion of alcoholic hydroxyls of polysaccharides to carboxyls under aqueous alkaline conditions<sup>21</sup>. In the TEMPO ((2,2,6,6-tetramethylpiperidin-1-yl)oxidanyl) oxidation system, NaClO (sodium hypochlorite) and NaBr (sodium bromide) act as a primary and secondary oxidant respectively. The mechanism proceeds in two steps as shown in Figure 3.2. In the first step TEMPO selectively attacks the primary C6 hydroxyl group and converts it into an aldehyde group. In the second step, the aldehyde group converts to a carboxylic acid group by NaClO. The reaction is performed in alkaline conditions since TEMPO decomposes in acidic media to hydrogenated derivative TEMPO-H, rather than its nitronium ion form. At higher pH > 10.5, the secondary oxidant used in the reaction starts consumption of OH<sup>-</sup> ion to generate NaOH and  $\dot{O}Cl$  radical, which retards the reaction. In some cases, the use of buffer solutions was reported to maintain the pH of reaction media<sup>22</sup>.

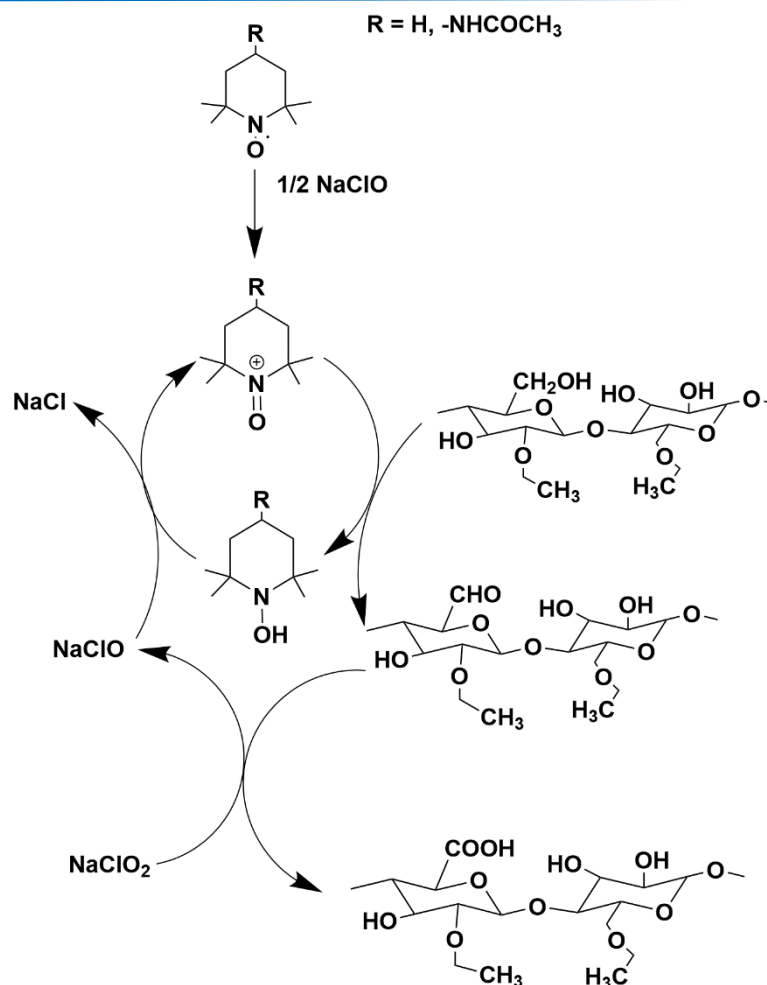


**Figure 3.2** Scheme of TEMPO mediated oxidation of EC.

It is a highly selective reaction and oxidizes only the primary hydroxyl group at carbon (C-6) on the EC backbone. TEMPO in combination with NaBr and NaClO efficiently converts the hydroxyl groups to carboxylates via aldehydes. At alkaline conditions, the selectivity of TEMPO is further enhanced, hence the oxidation of EC was performed at the pH 10-11<sup>23</sup>. The degree of substitution of primary hydroxyl groups of EC with carboxylate groups after TEMPO oxidation was calculated by conductometric titration.

**Conductometric titration and charge density estimation:** Briefly, carboxylated EC (CEC) was dispersed in 10 mL DI water at a concentration of 8 mg/mL by bath sonication and diluted to 80 mL DI water. The dispersion was properly stirred and a calibrated conductivity probe was dipped into the dispersion. 50  $\mu$ L of 12N HCl was

added to this CEC dispersion which precipitated the CEC whiskers. To neutralize the acid groups, 20  $\mu\text{L}$  (0.5M) NaOH solution was added to this dispersion in a stepwise manner and the conductivity of the solution was noted till the endpoint reached and the conductivity raised again. From the values of conductivity measured after the subsequent addition of NaOH in a stepwise fashion, a titration graph was plotted. From the titration graph, as represented in Figure 3.3, it is noted that there are two equivalence points (EP). The first EP is observed when the anions of the HCL are neutralized by the addition of NaOH. The next EP denotes the point where the carboxyl groups present on the oxidized EC were neutralized by the NaOH. The curve begins to rise again because of the conductivity of the excess  $\text{OH}^-$  ions of NaOH. The difference between the two EP's corresponds to the volume of NaOH needed to neutralize the accessible carboxylate groups on EC. This volume can be used to determine the charge density on EC as shown in the following equations.

From the graph we calculated the carboxylate charge density on EC

$$\text{Volume of NaOH } (\mu\text{L}) = \Delta x - x$$

$$\text{For } x: -1.564x + 2152 = 0.1185x + 534.24$$

$$\text{For } \Delta x: 0.1185x + 534.24 = 1.385x - 810.01$$

Solving the above equations, we got 100  $\mu\text{L}$

Charge density (mmol/kg)

$$= (\text{Vol. of NaOH (mL)} * 0.5) / (1000 * \text{mg of whiskers} * 10^{-6}) \dots\dots (5)$$

$$= (0.100 * 0.5) / (1000 * 80 * 10^{-6}) = \sim 625 \text{ mmol/kg.}$$

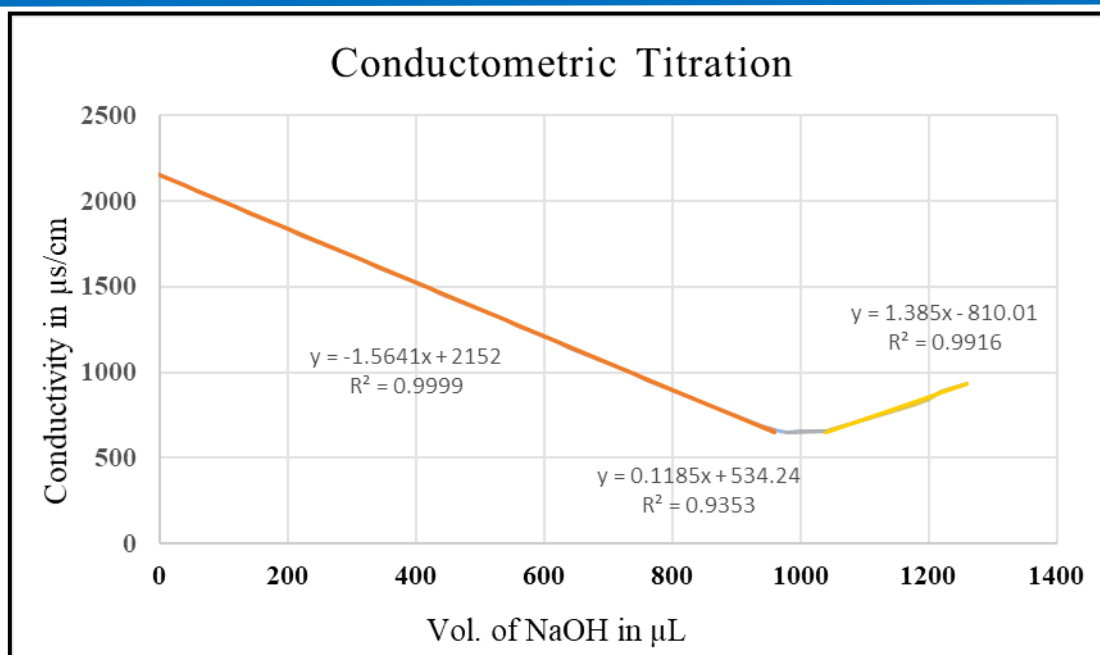


**Figure 3.3** Graph of conductometric titration of CEC-HCl dispersion with NaOH.

From the graph in Figure 3.3 and equation 5, the density of carboxylate groups of EC was calculated to be 625 mmol/kg. It was observed that with the increase in the volume of NaClO, the degree of carboxylation was increased, which is similar to the reported literature<sup>19</sup>. The concentration of NaClO was optimized at 25% to the dry weight of EC to obtain ~600 mmol/kg of carboxylate content on EC. The reproducible yield of this reaction was 58%. The carboxylate groups will be available for further modification with mPEG so as to increase the hydrophilicity of the EC.

### 3.3.2 PEGylation of carboxylated EC (CEC)

After the confirmation of oxidation of EC by conductometric titration, the product, CEC was used for synthesizing graft copolymer of EC-PEG by esterification. The reaction was carried out in THF, carboxylic acid of CEC was deprotonated by DMAP which nucleophilically added to DCC to give an intermediate O-acylisourea, a good leaving group. The hydroxyl groups of mPEG were nucleophilically reacted to this intermediate to form the desired ester bond between the carboxyl group of CEC and the hydroxyl group of mPEG<sup>24</sup>. Along with the grafted copolymer a side product dicyclohexyl urea (DCU) was obtained which was removed by the filtration steps.

The grafting of mPEG onto CEC was performed at 1 and 2 equivalents and the product was labelled as EC-PEG1 and EC-PEG2 respectively. The final product was dialyzed against DI water to remove unreacted mPEG, reagents and finally confirmed by  $^1\text{H}$  NMR,  $^{13}\text{C}$  NMR in DMSO- $d_6$ . The yield of this reaction was optimized up to 80%. Figure 3.5 shows the  $^1\text{H}$  NMR (DMSO- $d_6$ ) of EC-PEG1 copolymer:  $\delta$  3.92 (-OCH<sub>2</sub>CH<sub>2</sub>O-),  $\delta$  3.65 (CH<sub>3</sub>OCH<sub>2</sub>CH<sub>2</sub>OH),  $\delta$  1.51 (-CH<sub>2</sub>CH<sub>3</sub> of ethyl group),  $\delta$  2.92 (CH<sub>3</sub>CH<sub>2</sub>OCH-, CH<sub>3</sub>CH<sub>2</sub>OCH<sub>2</sub>CH). The integration of the peaks corresponding to the terminal methyl (-CH<sub>3</sub>) of mPEG at 3.65 ppm and methylene (-CH<sub>2</sub>CH<sub>2</sub>-) group of ethylene glycol at 3.92 ppm, suggest 46 repeating units corresponding to mPEG<sub>2000</sub>. From, the reported literature<sup>24, 25</sup>, in the  $^1\text{H}$  NMR spectra of ethyl cellulose (EC), the protons of the EC backbone appear between 3.4 to 4.5 ppm. The peaks of mPEG also appeared at a similar region, which resulted in the merging of the peaks of protons of EC with the protons of mPEG.

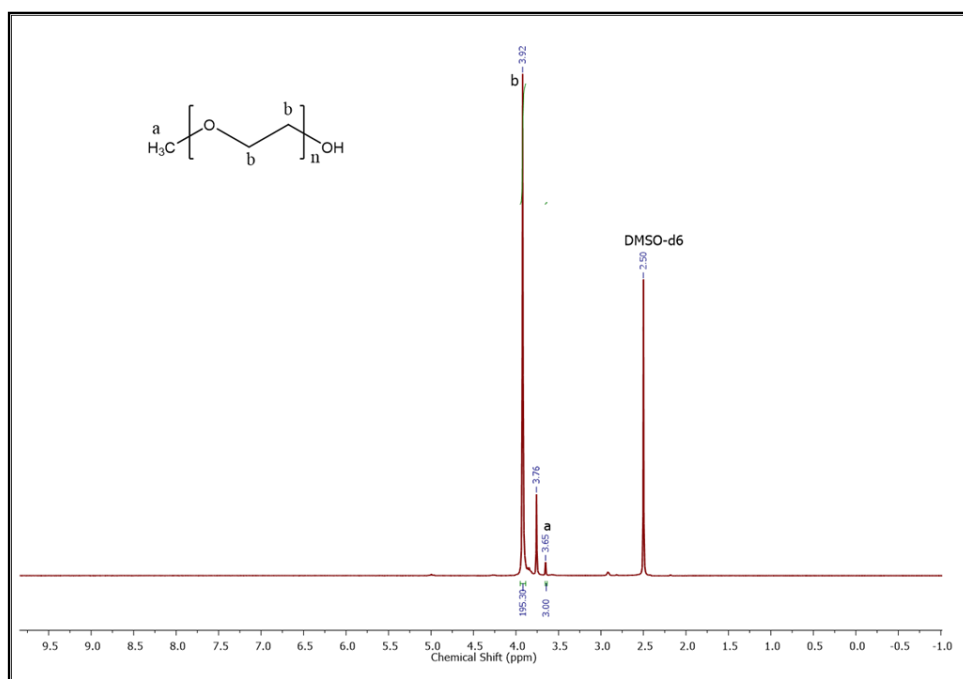


**Figure 3.4**  $^1\text{H}$  NMR spectrum of mPEG<sub>2000</sub> in DMSO- $d_6$ , recorded on Bruker AV-200 NMR.  $\delta$  3.92 (-OCH<sub>2</sub>CH<sub>2</sub>O-) (m, 4 H),  $\delta$  3.65 (CH<sub>3</sub>OCH<sub>2</sub>CH<sub>2</sub>OH) (m, 3 H).

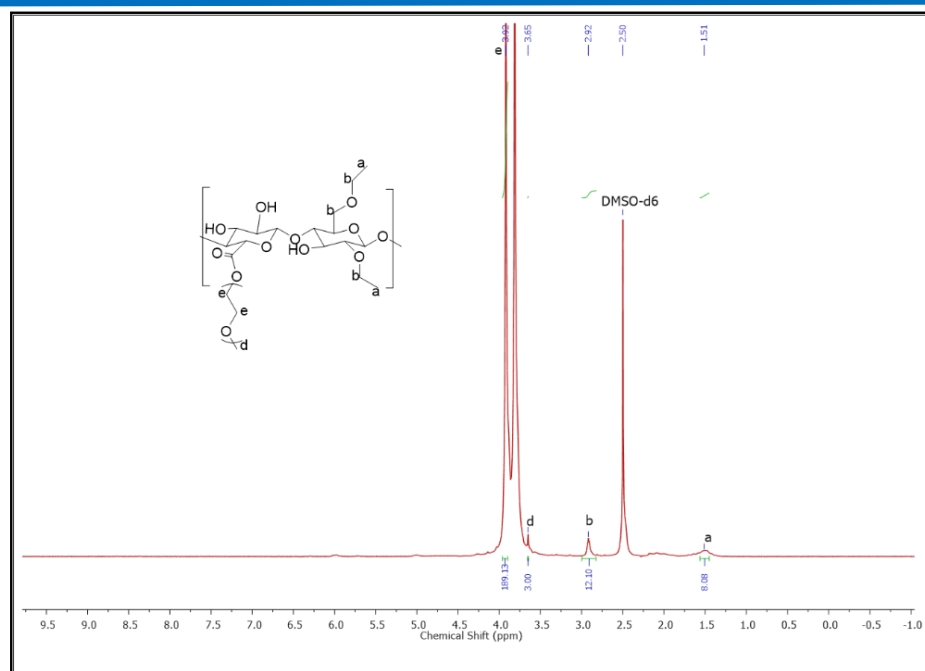


**Figure 3.5**  $^1\text{H}$  NMR spectrum of EC-PEG1 recorded on Bruker AV-200 NMR spectrometer operating at a frequency of 200 MHz with DMSO-d6 as the solvent.

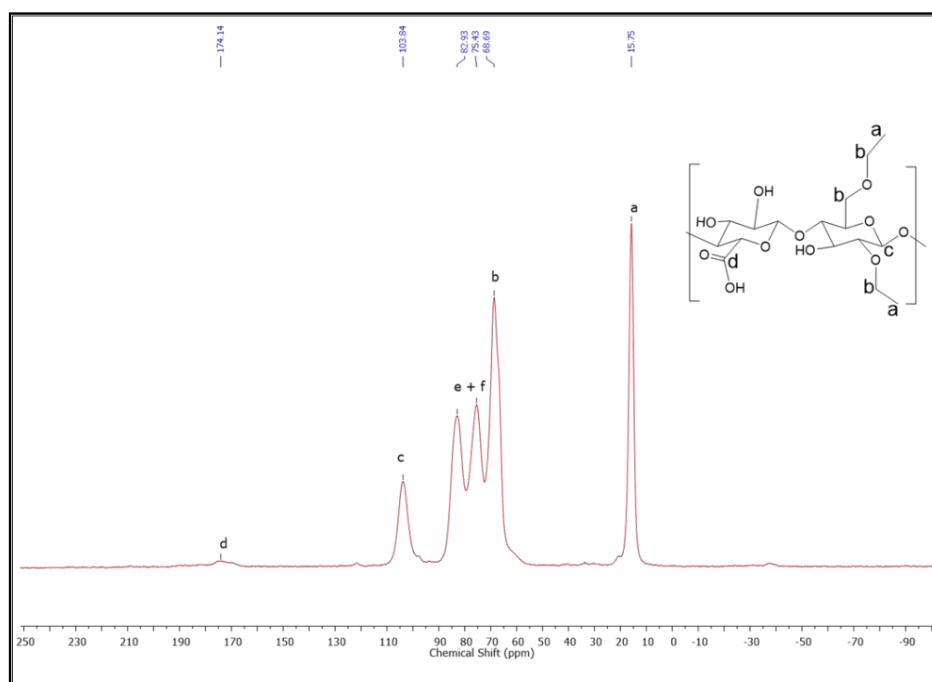


**Figure 3.6** Solid state  $^{13}\text{C}$  NMR spectrum of CEC recorded on Bruker NMR spectrometer.  $\delta$  15.75 ( $\text{CH}_3\text{CH}_2\text{O}-$ ),  $\delta$  68.69 ( $\text{CH}_3\text{CH}_2\text{O}-$ ),  $\delta$ 103.84 ( $-\text{OCHO}-$ ),  $\delta$ 174.14 ( $\text{OHCOCH}-$ ),  $\delta$  75.43 and 82.93 (C of the backbone of EC from C2 to C5).

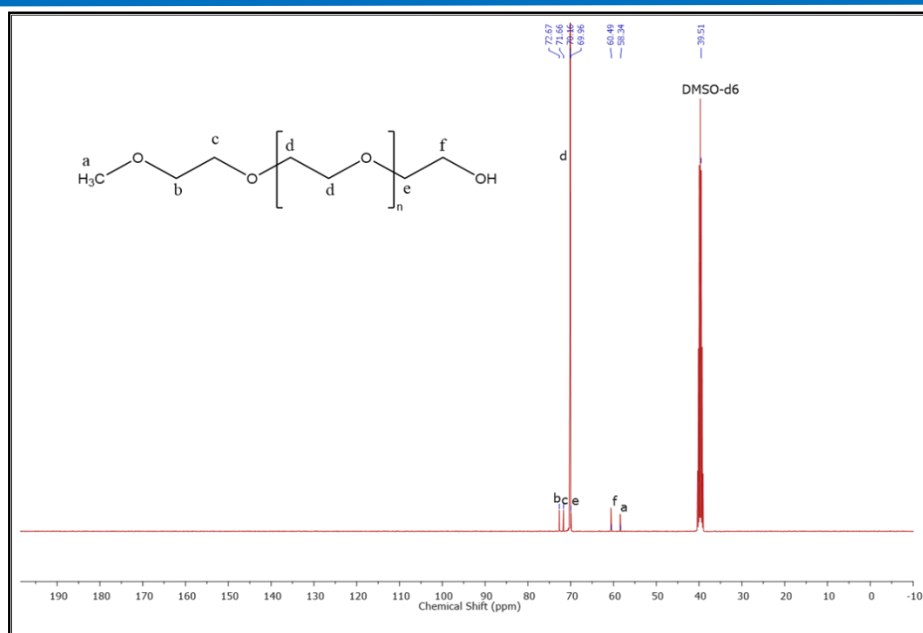


**Figure 3.7**  $^{13}\text{C}$  NMR (125 MHz) of mPEG<sub>2000</sub> in DMSO-d<sub>6</sub>, recorded on Bruker AV-500 NMR.  $\delta$  58.34 ( $\text{CH}_3\text{OCH}_2-$ ),  $\delta$  60.49 ( $-\text{OCH}_2\text{CH}_2\text{OH}$ ),  $\delta$  69.96 ( $-\text{OCH}_2\text{CH}_2\text{OH}$ ),  $\delta$  70.16 ( $-\text{OCH}_2\text{CH}_2\text{OCH}_2-$ ),  $\delta$  71.66 ( $-\text{OCH}_2\text{CH}_2\text{OCH}_2-$ ),  $\delta$  72.67 ( $\text{CH}_3\text{OCH}_2\text{CH}_2\text{O}$ ).

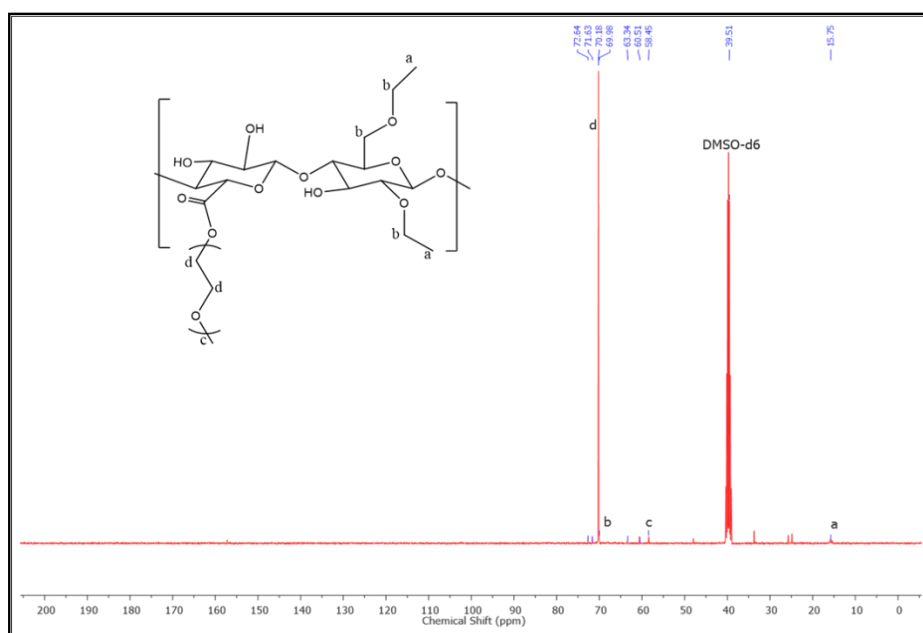


**Figure 3.8**  $^{13}\text{C}$  NMR (125 MHz) spectrum of EC-PEG1 in DMSO-d<sub>6</sub>, recorded on Bruker AV-500 NMR.  $\delta$  15.75 ( $\text{CH}_3\text{CH}_2\text{O}-$ ),  $\delta$  58.45 ( $\text{CH}_3\text{OCH}_2-$ ),  $\delta$  69.98 ( $\text{CH}_3\text{CH}_2\text{O}-$ ), from 60 ppm to 73 ppm all peaks observed in the spectrum of mPEG merged into the peaks of CEC backbone with an intense peak at  $\delta$  70.18

( $\text{CH}_3\text{OCH}_2\text{CH}_2\text{O}-$ ) due to the repeating unit of mPEG<sub>2000</sub>. [Note: The unassigned peaks are due to the traces of DCU (Dicyclohexylurea) formed during the DCC (N,N'-Dicyclohexylcarbodiimide) coupling].

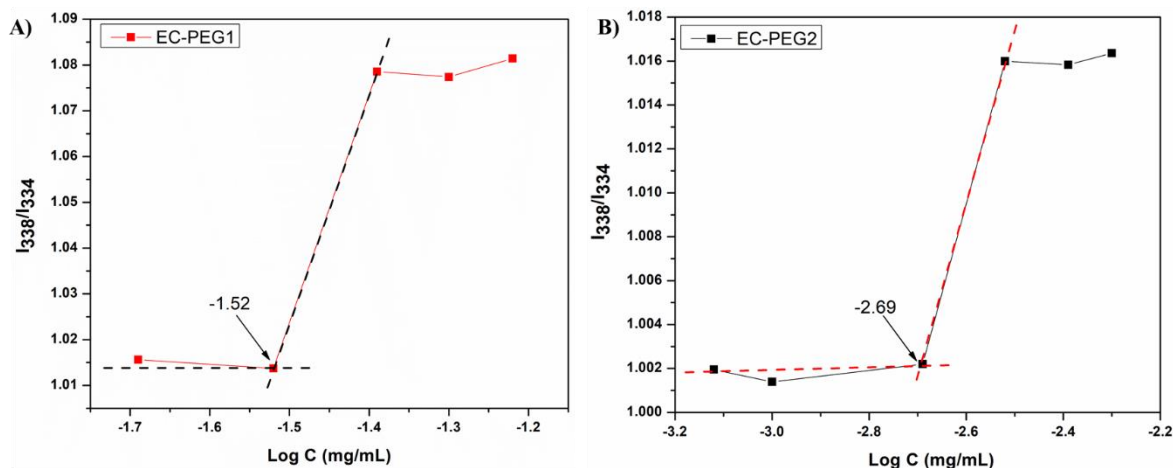


**Figure 3.9 A)** Critical micelle concentration (CMC) of EC-PEG1, derived from the plot of  $I_{338}/I_{334}$  ratio vs copolymer concentration. **B)** CMC of EC-PEG2, derived from the plot of  $I_{338}/I_{334}$  ratio vs copolymer concentration.

CMC is an important factor in deciding the micelle formation capacity of any amphiphilic polymer. To determine the CMC of the developed graft copolymer of EC-PEG, a well-documented method of fluorometry using a hydrophobic probe pyrene was used. The excitation spectrum of the probe with increasing concentration of polymer was monitored at an emission wavelength of 395 nm. Figure 3.9, shows the intensity ratio of  $I_{338}/I_{334}$  plotted against the log of concentration, varying from 0.00025 mg/mL to 0.09 mg/mL. The CMC value was taken from the intersection points of the tangent to the curve at the high concentrations with a horizontal line passing through the point at the low concentrations. From the graph, the CMC of EC-PEG1 (Figure 3.9A) and EC-PEG2 (Figure 3.9B) was observed at 0.03 mg/mL and 0.00193 mg/mL respectively. So, with the increase in grafting of mPEG to EC, the CMC value dropped. This suggested that in an aqueous medium, EC-PEG2 formed micelles at a much lower concentration as compared to EC-PEG1. The grafting of 2 equivalent mPEG to EC made the molecule more amphiphilic compared to 1 equivalent mPEG. This observation was similar to the reported literature by Chen et



al, where polymer modified with 5000 Mw PEG had a lower CMC value than 2000 Mw PEG<sup>20</sup>. A lower CMC value signifies the ability of the polymer to maintain a stable micellar structure at diluted conditions like the bloodstream<sup>26</sup>.

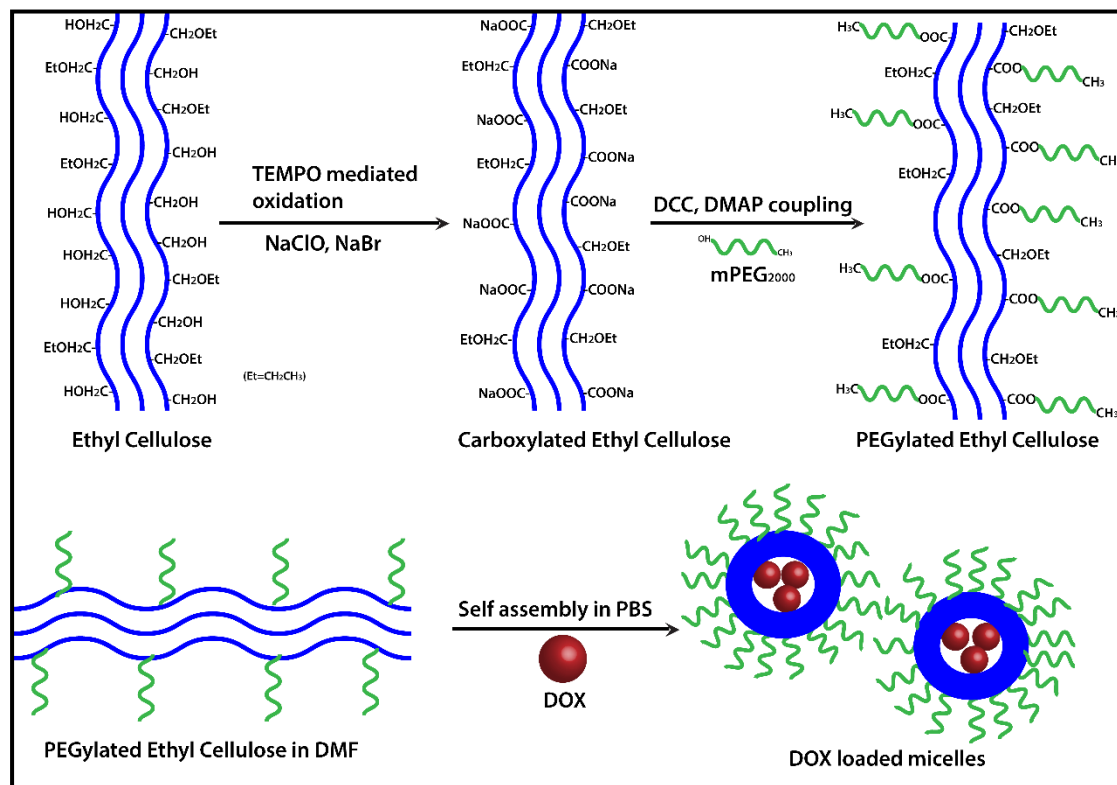


**Figure 3.10** Graphical representation of preparation of DOX loaded micelles from PEGylated EC.

### 3.3.3 Preparation and physicochemical characterization of micelles

Table 3.1 shows the various formulations of EC-PEG with and without DOX at various concentrations, which were abbreviated as B1, B2, B3, B4, B5, and B6. The micelles of EC-PEG (B1, B4) were prepared by dissolving the polymer in DMF and dialyzing against DI water. Similarly, DOX-loaded micelles were also fabricated by dissolving copolymer along with DOX in DMF and dialyzed against DI water (Figure 3.10). Figure 3.11, shows the morphology, and size distribution of the prepared micelles, which were analyzed by DLS and TEM. From the DLS measurement, as shown in Table 1, the size (B1=153.5 and B4=249.9 nm) of the micelles increased

with the addition of DOX, this validated the interaction and entrapment of DOX within the hydrophobic core of the micelles. The TEM images of blank and DOX loaded micelles shown in Figure 3.11 presents the average size of micelles below 150 nm, which is lower than the mean diameter measured by the DLS method. It should be noted that the mean diameter of the micelles determined by the DLS method is dependent on the size of the biggest micelle. Further, DLS measures the hydrodynamic diameter of the solvated micelles whereas, TEM measures dried micelles<sup>12</sup>. The PEG chains on the outer domain of the micelles are hydrophilic and hold water molecules which is reflected in the DLS measurements hence, formulations with more content of mPEG grafted (B4, B5, and B6) are larger in size. All these formulations possessed a net negative charge on their surface (-15 mV to -42 mV) which was due to the OH<sup>-</sup> groups on PEG chains of the micelles. The formulations prepared from EC-PEG2 had slightly more negative charge than formulations prepared from EC-PEG1 which could be explained by the additional mPEG grafting. The drug loading efficiency was determined by UV-Vis spectrophotometric analysis and the values obtained are shown in Table 3.1 The formulations with higher drug loading efficiency (52.73% and 52.51%) namely B3 and B6 were chosen for further studies.

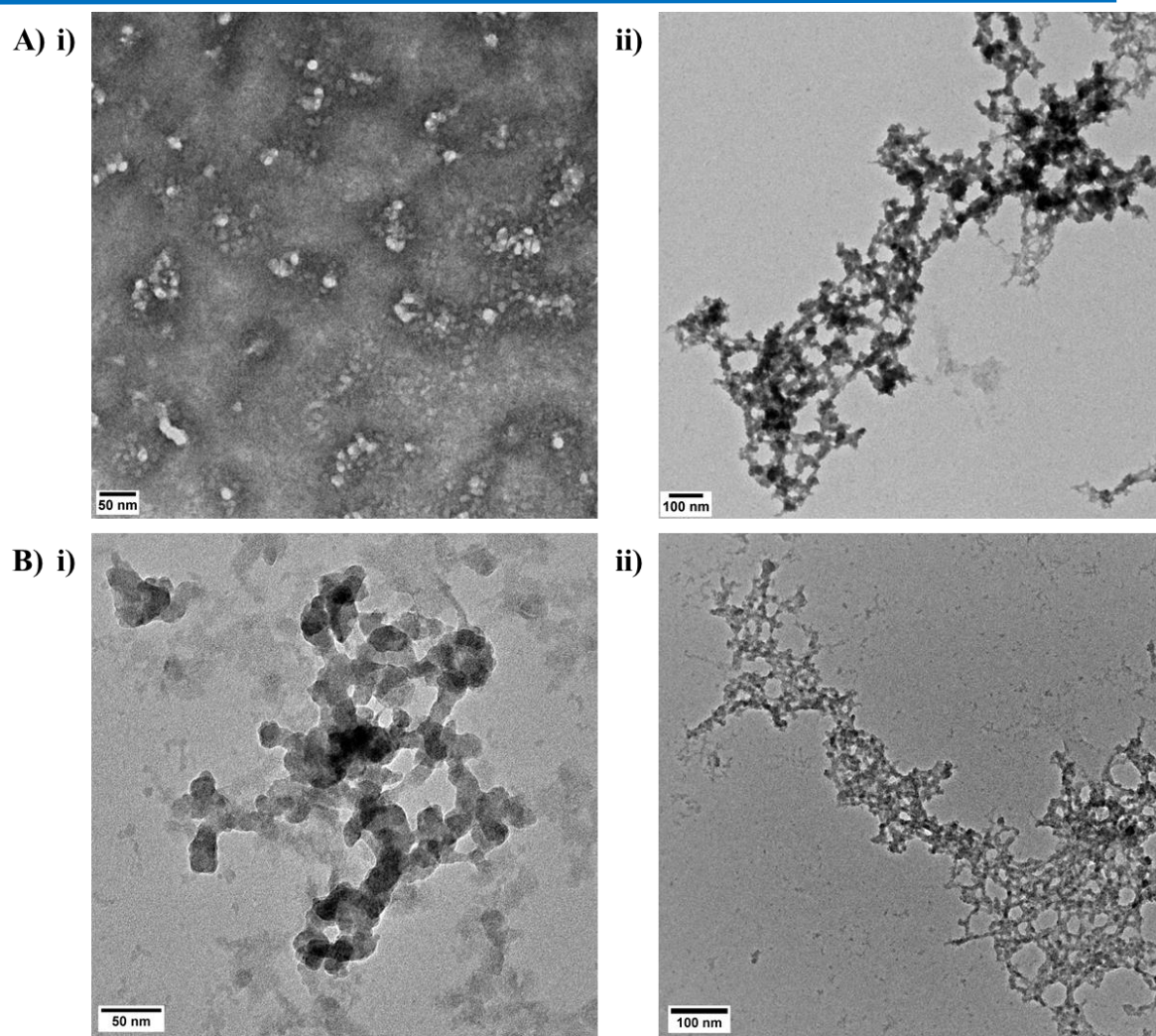


**Figure 3.11** A) i) TEM image of B1 micelles (Scale bar 50 nm), ii) TEM image of B3 micelles (Scale bar 100 nm). B) i) TEM image of B4 micelles (Scale bar 50 nm), ii) TEM image of B6 micelles (Scale bar 100 nm).

The functional group interaction between polymers and their formulations in the form of micelles was characterized by FTIR spectroscopy. FTIR spectrum of EC (Figure 3.12A) showed characteristic peaks at  $3485\text{ cm}^{-1}$  due to O–H stretching,  $2974\text{ cm}^{-1}$ ,  $2872\text{ cm}^{-1}$ , and  $1376\text{ cm}^{-1}$  due to the C–H stretching and bending respectively. The peak noticed at  $1060\text{ cm}^{-1}$  corresponds to the C–O–C group while the one at  $1120\text{ cm}^{-1}$  is peculiar to the C–C stretching<sup>27</sup>. The bare mPEG recorded a broad absorption peak of the terminal O–H that appeared around  $3421\text{ cm}^{-1}$ . Characteristic bands of the C–H bend were observed at  $2880\text{ cm}^{-1}$ ,  $1475\text{ cm}^{-1}$ ,  $948\text{ cm}^{-1}$ , and  $842\text{ cm}^{-1}$ . The peaks were visible at  $1150\text{ cm}^{-1}$  and  $1060\text{ cm}^{-1}$  were due to the ether linkage of the C–O–C

group (Figure 3.12A)<sup>28,29,30</sup>. The spectrum of EC-PEG1 as shown in Figure 3.12B, showed peaks at 3465 cm<sup>-1</sup>, 2972 cm<sup>-1</sup>, 2879 cm<sup>-1</sup> which is represented by both EC and mPEG, in the fingerprint region characteristic peaks of mPEG at 1112 cm<sup>-1</sup>, 948 cm<sup>-1</sup>, and 842 cm<sup>-1</sup> are evident<sup>28</sup>. A peak at 1745 cm<sup>-1</sup> was observed due to the formation of ester C=O between CEC and mPEG. Further, similar peaks were observed in the EC-PEG2 (Figure 3.12B) at 3465 cm<sup>-1</sup>, 2972 cm<sup>-1</sup>, 2879 cm<sup>-1</sup>, 1745 cm<sup>-1</sup>, 1112 cm<sup>-1</sup>, 948 cm<sup>-1</sup>, and 842 cm<sup>-1</sup>. The FTIR spectrum of DOX (Figure 3.12A), possessed characteristic peaks: N–H stretching at 3527 cm<sup>-1</sup>, carbonyl C=O peaks at 1730 cm<sup>-1</sup>, aromatic C=C stretching at 1620 cm<sup>-1</sup>, aromatic C–H stretching at 2930 cm<sup>-1</sup>, and O–H stretching at 3334 cm<sup>-1</sup><sup>31</sup>. The FTIR spectra of DOX-EC-PEG micelles, B3 and B6 are shown in Figure 3.12C. The spectra displayed a broad peak at 3464 cm<sup>-1</sup> due to the N–H and O–H functional groups present in the compositions (B3 and B6). The C–H stretching present in EC and mPEG was observed in the spectra at 2880 cm<sup>-1</sup> and 2974 cm<sup>-1</sup>. A broad peak at 1740 cm<sup>-1</sup> was attributed to the characteristic C=O group of DOX and CEC. The sharp peak of C–C stretching at 1120 cm<sup>-1</sup> which is characteristic of EC was also observed, the C–O–C peak at 1060 cm<sup>-1</sup> of mPEG merged in this sharp broad peak. The characteristic C–H bend of mPEG at 948 cm<sup>-1</sup> and 842 cm<sup>-1</sup> was also observed in B3 and B6. The observations from the FTIR spectra of B3 and B6 suggested the prepared micelles were a combination of the copolymer, EC-PEG with DOX. Moreover, the peaks of DOX were merged with the copolymer of EC-PEG due to its interaction and well distribution in the micelle.

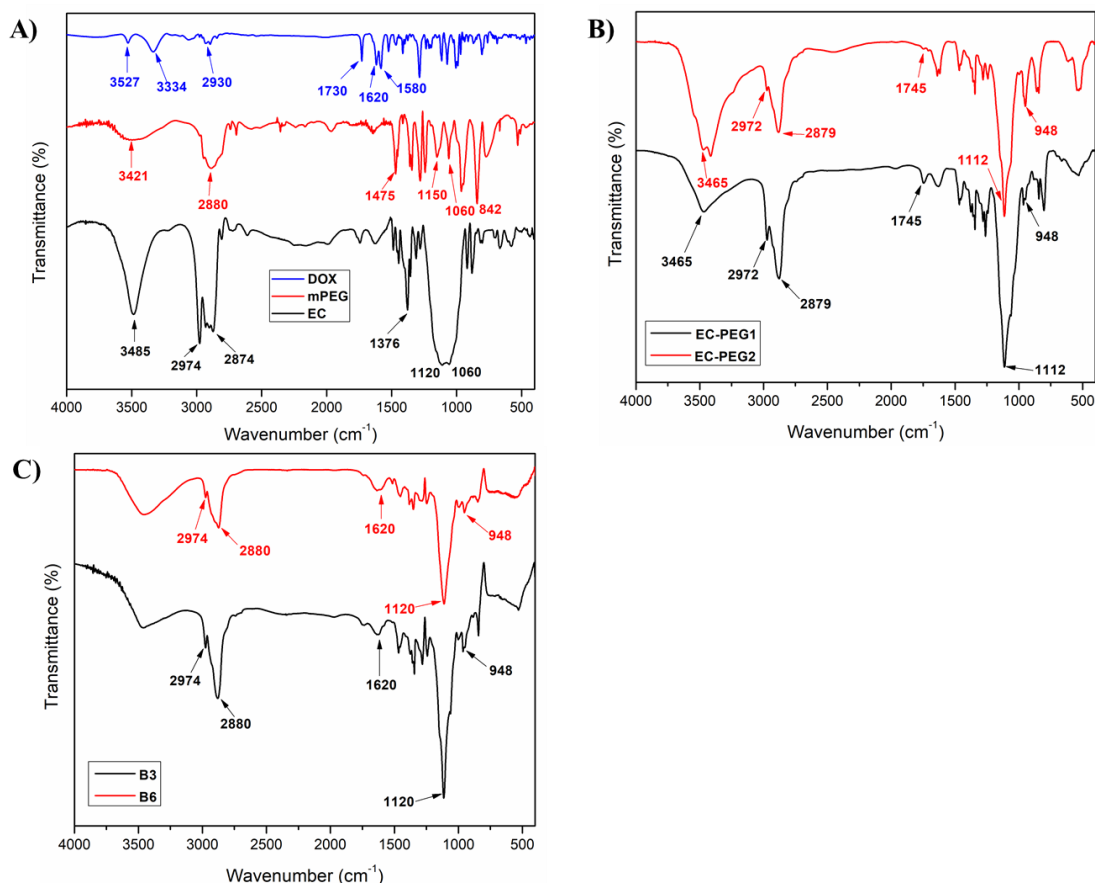


**Figure 3.12** FTIR spectrum of **A)** EC, mPEG, DOX, **B)** EC-PEG1 and EC-PEG2, **C)** B3 and B6 micelles.

Thermal properties of the pure polymers (EC, mPEG, CEC) and formulations with (B3, B6) and without DOX (B1, B4) are shown in Table 3.2, Figure 3.13. Glass transition temperature ( $T_g$ ) of the pure EC was recorded at 115 °C and melting temperature ( $T_m$ ) at 233 °C. Similarly, the CEC recorded  $T_g$  and  $T_m$  at 116 °C and 233 °C respectively. Further,  $T_g$ , crystallization temperature ( $T_c$ ), and  $T_m$  of mPEG were obtained at -66 °C, 29 °C, and 56 °C respectively. The thermogram of B4 recorded  $T_g$ ,  $T_c$ , and  $T_m$  at -29 °C, 21 °C, and 53/176 °C respectively, which indicated the semi-crystalline nature of EC-PEG. Further, the  $T_g$  of EC disappeared after grafting mPEG to the CEC. These results suggested that the grafting of the PEG to the CEC was done successfully. The thermal properties of the B6 micelles were recorded, where the  $T_g$ ,  $T_c$ , and  $T_m$  appeared at -26 °C, 24 °C, and 53/175 °C respectively. The changes in  $T_g$ ,  $T_c$  indicated the loading of DOX in the micelles. According to the reported

literature<sup>32</sup>, DOX has a  $T_m$  at 218 °C. The  $T_m$  of DOX disappeared in the thermogram of DOX-loaded micelles B3 and B6, which indicated that the drug was molecularly dispersed and bound to the polymer<sup>14</sup>. This also suggests an improved solubility of crystalline DOX in an aqueous medium when entrapped in a polymeric system.

**Table 3.2** Thermal properties of pure polymers and micelles with DOX

<b>Chemical composition name</b>	<b>Glass transition temperature (<math>T_g</math>) (°C)</b>	<b>Crystallization temperature (<math>T_c</math>) (°C)</b>	<b>Melting temperature (<math>T_m</math>) (°C)</b>
EC	115	-	233
mPEG	-66	29	56
CEC	116	-	233
B1	-24	24	53.17
B4	-29	21	53.17
B3	-29	25	53.17
B6	-26	24	53.17

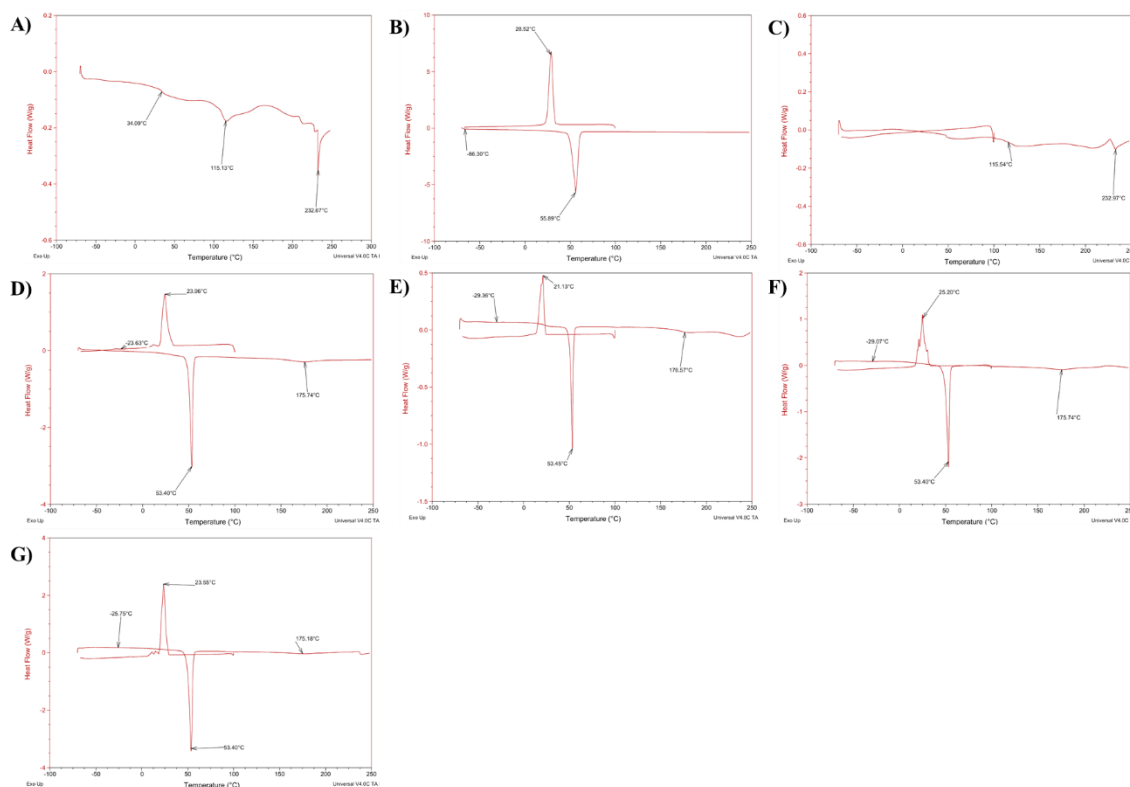


**Figure 3.13** DSC thermograms of **A)** EC, **B)** mPEG, **C)** CEC, **D)** B1 micelles, **E)** B4 micelles, **F)** B3 micelles, **G)** B6 micelles.

### 3.3.4 *In vitro* DOX release

The release of DOX from EC-PEG micelles (B3 and B6) was studied for 72 h by dialysis method at 37 °C using phosphate buffer of pH 5.5 and 7.4 respectively. The release of DOX was faster in pH 5.5 as compared to the release of DOX in pH 7.4 because the ester bond formed between CEC and mPEG was susceptible to the acidic pH<sup>33</sup>. Figure 3.14A shows the release profile of DOX at various pH. In pH 5.5, B3 micelles recorded 100% of release of DOX within 35 h and in pH 7.4, 96% of DOX was released within 72 h. Whereas, the release of DOX from B6 micelles was slow in both the pH as compared to B3 micelles. For instance, 99% of DOX was released in pH 5.5 within 48 h and 72% of DOX was released in pH 7.4 within 72 h. This trend of slow-release from B6 micelles compared to B3 micelles suggested that increased grafting of mPEG increased the molecular weight of the copolymer thus the rate of

release was slow<sup>34</sup>. Overall, the sustained release of DOX can be attributed to the encapsulating property of EC and hydrophobic interactions between DOX and EC<sup>26, 35</sup>. The pH-dependent release from the micelles can be utilized to deliver DOX at the tumor pH because the tumor extracellular environment is slightly acidic (pH 6.8) and after endocytosis by cancer cells, the pH of lysosomes/endosomes is also acidic (pH 5.5), thus minimizing the release of DOX in the normal tissue pH (pH 7.4)<sup>36, 37</sup>.

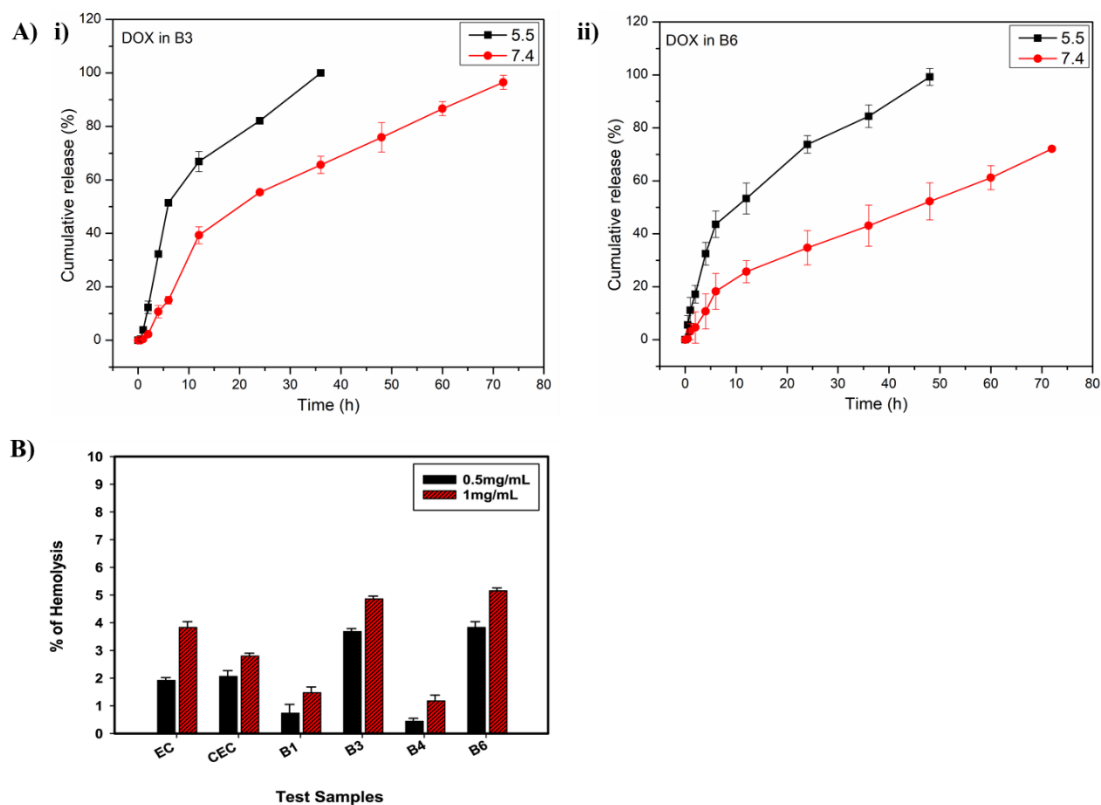


**Figure 3.14** A) i) DOX release from B3 micelles in PBS at 5.5 and 7.4 pH for 72 h, ii) DOX release from B6 micelles in PBS at 5.5 and 7.4 pH for 72 h. B) % of Hemolysis on exposure to test samples, EC, CEC, B1, B3, B4, and B6 micelles.

### 3.3.5 Hemolysis assay

Hemolysis assay is demonstrated to validate the biocompatibility of biomaterial or polymer. According to the ASTM standards (E2524-08), hemolysis for the test samples above 5% indicates toxicity to the RBCs<sup>38</sup>. Likewise, the test samples EC, CEC, B1, B3, B4, and B6 were assessed for their biocompatibility in human blood at a concentration of 0.5 and 1 mg/mL. The % of hemolysis was calculated from



---

equation 3, considering 100% lysis in DI water and 0% lysis in PBS. In Figure 3.14B histogram, EC displayed less than 5% hemolysis hence, it can be termed as non-hemolytic material, and after modification and formation of micelles (B1, B3, B4, and B6), the material maintained its hemocompatibility. As observed, CEC had slightly better hemocompatibility than EC which could be due to the addition of negatively charged carboxylic groups. In the case of B1 and B4, even at a higher concentration of 1 mg/mL, the observed hemolysis % was  $1.47 \pm 0.2$  and  $1.17 \pm 0.2$  respectively. The improved hemocompatibility in micelles in comparison to EC and CEC can be attributed to the mPEG grafting<sup>39</sup>. These results consolidate the advantages of PEGylation of polymers, with the grafting of mPEG the ability of test materials to induce RBC lysis decreased significantly. In B3 and B6, at 0.5 mg/mL the observed hemolysis % was  $3.68 \pm 0.1$  and  $3.82 \pm 0.2$  respectively, which is within the permissible limit of 5%, whereas at 1 mg/mL the hemolysis is close to 5%. The toxicity to RBCs in presence of B3 and B6 samples at higher concentrations was due to DOX. DOX is known to enter the RBCs and cause their swelling and lysis by building up the osmotic pressure<sup>40</sup>. As per the report of Shuai et al<sup>41</sup>, free DOX induces 11% hemolysis at 200  $\mu\text{g/mL}$ , but when loaded in micelles its toxicity largely diminished. The reason for the lower hemotoxicity of DOX in EC-PEG micelles in comparison to that of reported free DOX is the entrapment of DOX in the hydrophobic core thus, reducing the amount of DOX available on the surface for interaction with RBCs. As mentioned earlier the hydrophilic mPEG chains formed a protective cover and therefore, the RBCs were inhibited from being lysed. In line with these findings, we consider that the developed copolymer EC-PEG is biocompatible and can be used as a potential nanocarrier for DD.

### 3.3.6 Cell studies

**Cytotoxicity assay:** The cytotoxicity of blank and DOX loaded EC-PEG micelles was determined by the MTT assay. The cytotoxic effects of B1 and B4 micelles were investigated in fibroblast L929 and breast cancer MDA-MB-231 cell lines. DMSO solubilized the formazan crystals formed after the addition of the MTT reagent which indicated cellular respiratory activity. As shown in Figure 3.15, B1 (Figure 3.15A i) and B4 (Figure 3.15A ii) micelles exhibited no cellular cytotoxicity for up to 48 h of

---

incubation with varying concentrations. The relative cell viability was above 80% even at the higher concentration of micelles at 400  $\mu\text{g/mL}$ . Thus, demonstrating the non-cytotoxic nature of the mPEG grafted EC micelles and establishing them as promising drug delivery vehicle. The cytotoxic ability of B3 and B6 micelles was investigated in breast cancer cell lines, MDA-MB-231 and MCF-7 for 72 h. From the histogram, as shown in Figure 3.14B, the DOX loaded micelles, B3 (Figure 3.15B i), and B6 (Figure 3.15B ii) recorded a decrease in cell viability as a function of DOX dose concentration. The concentration of the micelles was varied from 0  $\mu\text{g/mL}$  to 500  $\mu\text{g/mL}$ , and the  $\text{IC}_{50}$  (the dose inducing 50% cell inhibition) value noted for B3 and B6 in both the cell lines was  $\sim 100$   $\mu\text{g/mL}$ . These results proved the competence of EC-PEG micelles as biocompatible and non-toxic DDS to deliver DOX at a controlled rate over an extended period.

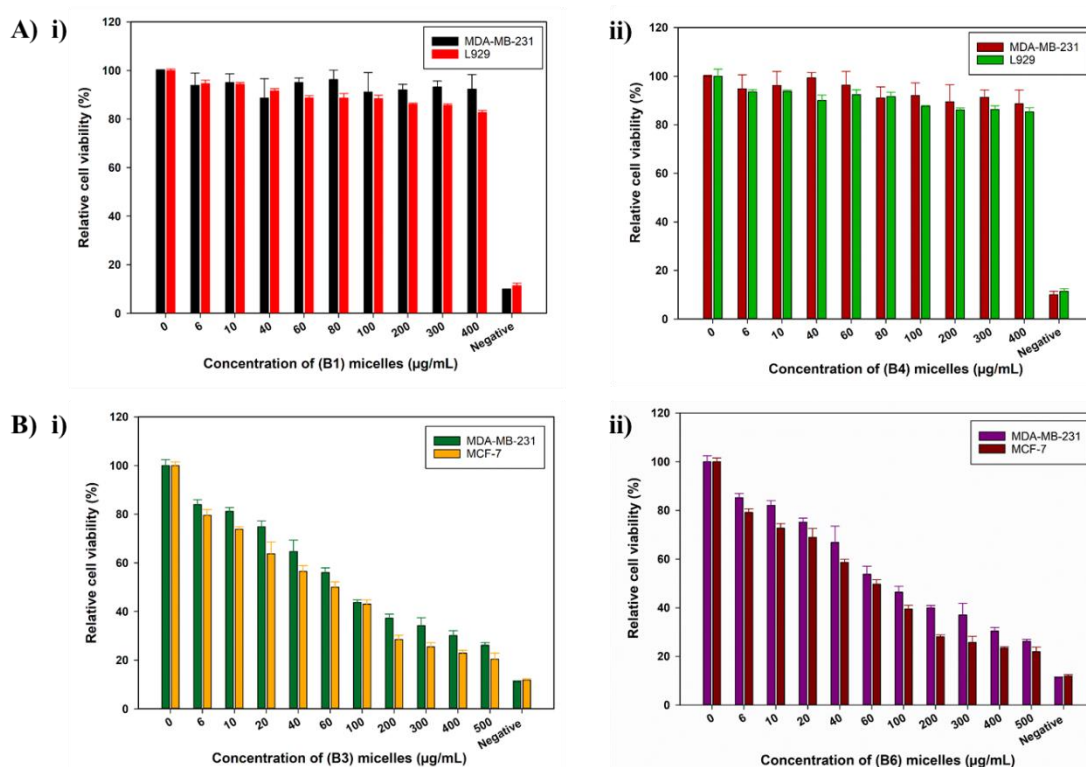


**Figure 3.15** A) i) Cytotoxicity of MDA-MB-231 and L929 cells treated by B1 micelles for 48 h, ii) Cytotoxicity of MDA-MB-231 and L929 cells treated by B4 micelles for 48 h. B) i) Cytotoxicity of MDA-MB-231 and MCF-7 cells treated by B3 micelles for 72 h, ii) Cytotoxicity of MDA-MB-231 and MCF-7 cells treated by B6 micelles for 72 h.

***In vitro cellular uptake:*** The cellular uptake of free DOX and DOX-EC-PEG (B3, B6) micelles was studied in breast cancer cells MDA-MB-231 by incubating them with the samples in the media at 37 °C for 4 h and 8 h respectively, and later analyzed using epifluorescence microscopy. The nuclei of cells were stained with DAPI, the actin filaments of cytoskeleton were stained by Alexa Fluor 488 phalloidin, and DOX emitted red fluorescence. In the cells treated with free DOX, as shown in Figure 3.16, it was observed that the DOX was exclusively present in the nucleus. This can be explained by the fact that DOX can be readily transported into the cells by the mechanism of passive diffusion which is energy independent and binds to the DNA in the nucleus by intercalation<sup>42,43</sup>. In the cells treated with B3 and B6 micelles at 100 µg/mL, it was observed that the red fluorescence of DOX was located in the cytoplasm and nuclear region (Figure 3.16, row B3 and B6). This observation leads to an inference that the DOX-loaded micelles were taken up by the cells via the endocytosis pathway and were located in the intracellular compartment (endosomes and lysosomes), which is supported by the reported literature<sup>36,44</sup>.

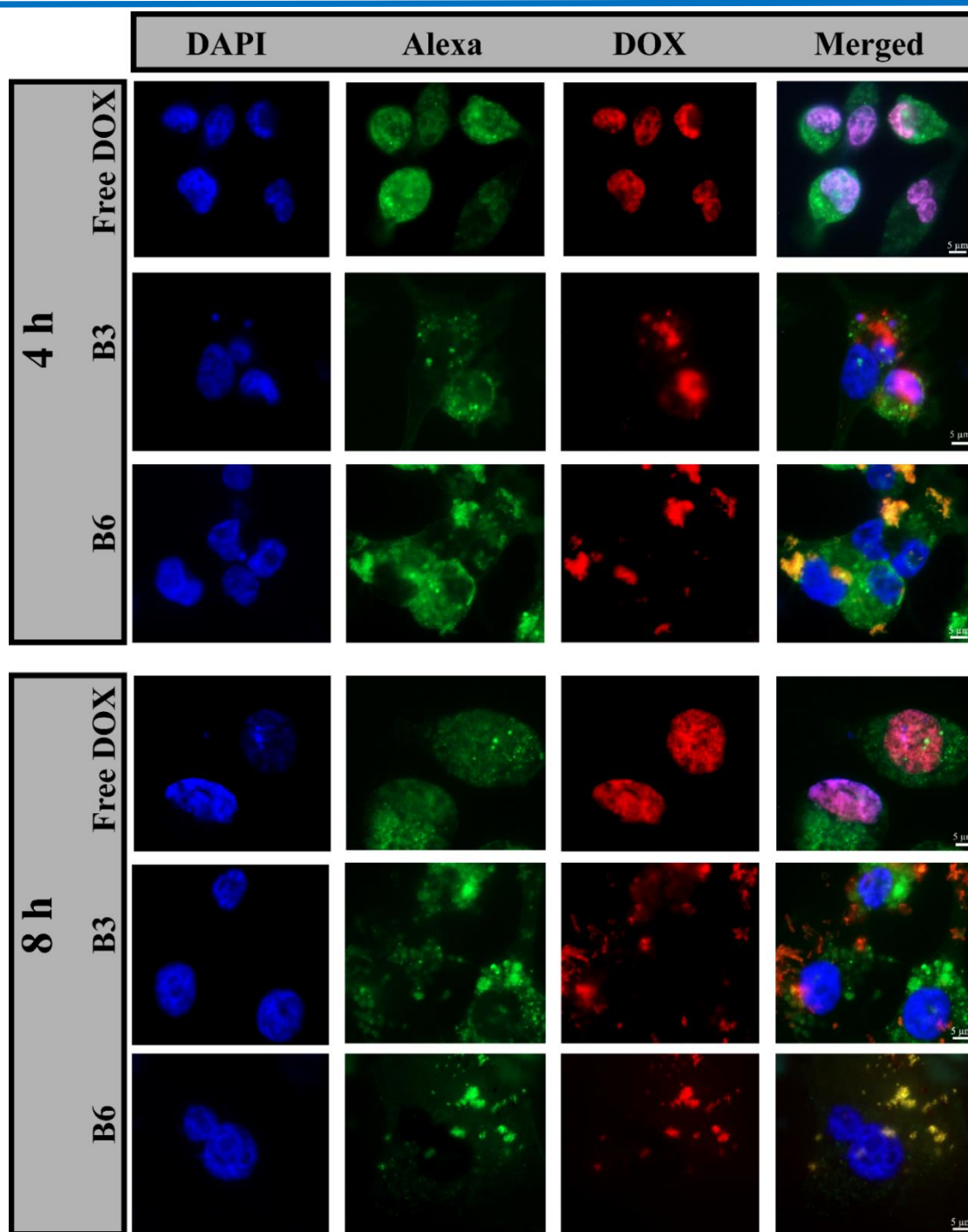


**Figure 3.16** Fluorescent images of MDA-MB-231 cells treated with free DOX, B3 micelles, and B6 micelles for 4 h and 8 h. The right panels show the merged image of the nucleus stained with DAPI (blue), F-actin stained with Alexa fluor 488 phalloidin (green), and DOX fluorescence (red). Scale bar corresponds to 5  $\mu$ m.

### 3.4 Conclusions

In this study, we synthesized a new amphiphilic copolymer by grafting PEG to EC. The developed copolymer was self-assembled into micelles in the aqueous system by dialysis method and were confirmed by DLS, TEM, and fluorescence spectroscopy, and the CMC of the copolymers, EC-PEG1 and EC-PEG2 were recorded at 0.03 mg/mL and 0.00193 g/mL respectively. The size of the DOX encapsulated EC-PEG nano-micelles was greater than the size of the blank micelles which was confirmed by DLS. The DOX-loaded micelles demonstrated faster release in acidic pH, 5.5 whereas, slow release of DOX was observed at physiological pH, 7.4. The hemolysis assay and MTT assay studies confirmed the micelles were biocompatible and non-toxic to the normal cells. Further, the DOX-loaded micelles showed toxicity to the cancerous cells, MDA-MB-231 and MCF-7 and the fluorescence microscopy images exhibited internalization of the DOX-loaded micelles in MDA-MB-231 cells. According to the above observations, we concluded that the developed micelles can be used as potential DDS for cancer therapy. In the future scope of this work, the micelles can be tailored with various targeting moieties to achieve site-specific targeted delivery.

### 3.5 References

- (1) Hwang, D.; Ramsey, J. D.; Kabanov, A. V. Polymeric micelles for the delivery of poorly soluble drugs: from nanoformulation to clinical approval. *Advanced Drug Delivery Reviews* **2020**.
- (2) Gong, J.; Chen, M.; Zheng, Y.; Wang, S.; Wang, Y. Polymeric micelles drug delivery system in oncology. *Journal of Controlled Release* **2012**, *159* (3), 312-323.
- (3) Ahmad, Z.; Shah, A.; Siddiq, M.; Kraatz, H.-B. Polymeric micelles as drug delivery vehicles. *Rsc Advances* **2014**, *4* (33), 17028-17038.
- (4) Cabral, H.; Kataoka, K. Progress of drug-loaded polymeric micelles into clinical studies. *Journal of Controlled Release* **2014**, *190*, 465-476.

- (5) Fang, J.; Nakamura, H.; Maeda, H. The EPR effect: unique features of tumor blood vessels for drug delivery, factors involved, and limitations and augmentation of the effect. *Advanced drug delivery reviews* **2011**, *63* (3), 136-151.
- (6) Wilhelm, S.; Tavares, A. J.; Dai, Q.; Ohta, S.; Audet, J.; Dvorak, H. F.; Chan, W. C. W. Analysis of nanoparticle delivery to tumours. *Nature reviews materials* **2016**, *1* (5), 1-12.
- (7) Biswas, S.; Kumari, P.; Lakhani, P. M.; Ghosh, B. Recent advances in polymeric micelles for anti-cancer drug delivery. *European Journal of Pharmaceutical Sciences* **2016**, *83*, 184-202.
- (8) Sabra, S.; Abdelmoneem, M.; Abdelwakil, M.; Mabrouk, M. T.; Anwar, D.; Mohamed, R.; Khattab, S.; Bekhit, A.; Elkhodairy, K.; Freag, M. Self-assembled nanocarriers based on amphiphilic natural polymers for anti-cancer drug delivery applications. *Current pharmaceutical design* **2017**, *23* (35), 5213-5229.
- (9) Su, X.; Yang, Z.; Tan, K. B.; Chen, J.; Huang, J.; Li, Q. Preparation and characterization of ethyl cellulose film modified with capsaicin. *Carbohydrate Polymers* **2020**, *241*, 116259.
- (10) Muschert, S.; Siepmann, F.; Leclercq, B.; Carlin, B.; Siepmann, J. Prediction of drug release from ethylcellulose coated pellets. *Journal of controlled release* **2009**, *135* (1), 71-79.
- (11) Balzus, B.; Colombo, M.; Sahle, F. F.; Zoubari, G.; Staufenbiel, S.; Bodmeier, R. Comparison of different in vitro release methods used to investigate nanocarriers intended for dermal application. *International journal of pharmaceutics* **2016**, *513* (1-2), 247-254.
- (12) Leitner, S.; Grijalvo, S.; Solans, C.; Eritja, R.; García-Celma, M. J.; Calderó, G. Ethylcellulose nanoparticles as a new “in vitro” transfection tool for antisense oligonucleotide delivery. *Carbohydrate polymers* **2020**, *229*, 115451.
-

- (13) Yuan, W.; Yuan, J.; Zhang, F.; Xie, X. Syntheses, characterization, and in vitro degradation of ethyl cellulose-graft-poly ( $\epsilon$ -caprolactone)-block-poly (l-lactide) copolymers by sequential ring-opening polymerization. *Biomacromolecules* **2007**, *8* (4), 1101-1108.
- (14) Gref, R.; Domb, A.; Quellec, P.; Blunk, T.; Müller, R. H.; Verbavatz, J. M.; Langer, R. The controlled intravenous delivery of drugs using PEG-coated sterically stabilized nanospheres. *Advanced drug delivery reviews* **2012**, *64*, 316-326.
- (15) Lasseguette, E. Grafting onto microfibrils of native cellulose. *Cellulose* **2008**, *15* (4), 571-580.
- (16) Kaldéus, T.; Nordenström, M.; Carlmark, A.; Wågberg, L.; Malmström, E. Insights into the EDC-mediated PEGylation of cellulose nanofibrils and their colloidal stability. *Carbohydrate polymers* **2018**, *181*, 871-878.
- (17) Shen, D.; Huang, Y. The synthesis of CDA-g-PMMA copolymers through atom transfer radical polymerization. *Polymer* **2004**, *45* (21), 7091-7097.
- (18) Zhao, Q.; Han, B.; Wang, Z.; Gao, C.; Peng, C.; Shen, J. Hollow chitosan-alginate multilayer microcapsules as drug delivery vehicle: doxorubicin loading and in vitro and in vivo studies. *Nanomedicine: Nanotechnology, Biology and Medicine* **2007**, *3* (1), 63-74.
- (19) Araki, J.; Wada, M.; Kuga, S. Steric stabilization of a cellulose microcrystal suspension by poly (ethylene glycol) grafting. *Langmuir* **2001**, *17* (1), 21-27.
- (20) Chen, J.; Qiu, X.; Ouyang, J.; Kong, J.; Zhong, W.; Xing, M. M. Q. pH and reduction dual-sensitive copolymeric micelles for intracellular doxorubicin delivery. *Biomacromolecules* **2011**, *12* (10), 3601-3611.
- (21) Hirota, M.; Tamura, N.; Saito, T.; Isogai, A. Oxidation of regenerated cellulose with NaClO<sub>2</sub> catalyzed by TEMPO and NaClO under acid-neutral conditions. *Carbohydrate polymers* **2009**, *78* (2), 330-335.
-

(22) Arends, I. W. C. E.; Li, Y.-X.; Sheldon, R. A. Stabilities and rates in the laccase/TEMPO-catalyzed oxidation of alcohols. *Biocatalysis and Biotransformation* **2006**, *24* (6), 443-448.

(23) De Nooy, A. E. J.; Besemer, A. C.; Van Bekkum, H. Highly selective TEMPO mediated oxidation of primary alcohol groups in polysaccharides. *Recueil des Travaux Chimiques des Pays-Bas* **1994**, *113* (3), 165-166. Ding, B.; qing Ye, Y.; Cheng, J.; Wang, K.; Luo, J.; Jiang, B. TEMPO-mediated selective oxidation of substituted polysaccharides—an efficient approach for the determination of the degree of substitution at C-6. *Carbohydrate Research* **2008**, *343* (18), 3112-3116. Isogai, A.; Saito, T.; Fukuzumi, H. TEMPO-oxidized cellulose nanofibers. *nanoscale* **2011**, *3* (1), 71-85.

(24) Heinze, T.; Liebert, T.; Koschella, A. *Esterification of polysaccharides*; Springer Science & Business Media, 2006.

(25) Shen, D.; Yu, H.; Huang, Y. Densely grafting copolymers of ethyl cellulose through atom transfer radical polymerization. *Journal of Polymer Science Part A: Polymer Chemistry* **2005**, *43* (18), 4099-4108. Li, Y.; Liu, R.; Liu, W.; Kang, H.; Wu, M.; Huang, Y. Synthesis, self-assembly, and thermosensitive properties of ethyl cellulose-g-P (PEGMA) amphiphilic copolymers. *Journal of Polymer Science Part A: Polymer Chemistry* **2008**, *46* (20), 6907-6915. Zhu, J.; Dong, X.-T.; Wang, X.-L.; Wang, Y.-Z. Preparation and properties of a novel biodegradable ethyl cellulose grafting copolymer with poly (p-dioxanone) side-chains. *Carbohydrate Polymers* **2010**, *80* (2), 350-359. Dong, Y.; Edgar, K. J. Imparting functional variety to cellulose ethers via olefin cross-metathesis. *Polymer Chemistry* **2015**, *6* (20), 3816-3827.

(26) Lv, S.; Tang, Z.; Li, M.; Lin, J.; Song, W.; Liu, H.; Huang, Y.; Zhang, Y.; Chen, X. Co-delivery of doxorubicin and paclitaxel by PEG-polypeptide nanovehicle for the treatment of non-small cell lung cancer. *Biomaterials* **2014**, *35* (23), 6118-6129.

(27) Suthar, V.; Pratap, A.; Raval, H. Studies on poly (hydroxy alkanoates)/(ethylcellulose) blends. *Bulletin of Materials Science* **2000**, *23* (3), 215-219.

---



(28) Li, Y.; Liu, R.; Huang, Y. Synthesis and phase transition of cellulose-graft-poly (ethylene glycol) copolymers. *Journal of applied polymer science* **2008**, *110* (3), 1797-1803.

(29) Shoaefifar, P.; Abbasian, M.; Entezami, A. A. A convenient method for preparation of amphiphilic monomethoxypoly (ethylene glycol)–polystyrene diblock copolymer by NMRP technique. *Journal of Polymer Research* **2007**, *14* (1), 45-52.

(30) Asadi, H.; Rostamizadeh, K.; Salari, D.; Hamidi, M. Preparation of biodegradable nanoparticles of tri-block PLA–PEG–PLA copolymer and determination of factors controlling the particle size using artificial neural network. *Journal of microencapsulation* **2011**, *28* (5), 406-416.

(31) Depan, D.; Shah, J.; Misra, R. D. K. Controlled release of drug from folate-decorated and graphene mediated drug delivery system: synthesis, loading efficiency, and drug release response. *Materials Science and Engineering: C* **2011**, *31* (7), 1305-1312. Neacșu, A. Physicochemical investigation of the complexation between  $\gamma$ -cyclodextrin and doxorubicin in solution and in solid state. *Thermochimica Acta* **2018**, *661*, 51-58.

(32) Missirlis, D.; Kawamura, R.; Tirelli, N.; Hubbell, J. A. Doxorubicin encapsulation and diffusional release from stable, polymeric, hydrogel nanoparticles. *European journal of pharmaceutical sciences* **2006**, *29* (2), 120-129.

(33) Rostamizadeh, K.; Manafi, M.; Nosrati, H.; Manjili, H. K.; Danafar, H. Methotrexate-conjugated mPEG–PCL copolymers: a novel approach for dual triggered drug delivery. *New Journal of Chemistry* **2018**, *42* (8), 5937-5945. Carrillo-Castillo, T. D.; Castro-Carmona, J. S.; Luna-Velasco, A.; Zaragoza-Contreras, E. A. pH-responsive polymer micelles for methotrexate delivery at tumor microenvironments. *e-Polymers* **2020**, *20* (1), 624-635.

(34) Du, Y.-Z.; Weng, Q.; Yuan, H.; Hu, F.-Q. Synthesis and antitumor activity of stearate-g-dextran micelles for intracellular doxorubicin delivery. *Acs Nano* **2010**, *4* (11), 6894-6902.

---

(35) Wasilewska, K.; Winnicka, K. Ethylcellulose—a pharmaceutical excipient with multidirectional application in drug dosage forms development. *Materials* **2019**, *12* (20), 3386.

(36) Lv, S.; Li, M.; Tang, Z.; Song, W.; Sun, H.; Liu, H.; Chen, X. Doxorubicin-loaded amphiphilic polypeptide-based nanoparticles as an efficient drug delivery system for cancer therapy. *Acta biomaterialia* **2013**, *9* (12), 9330-9342.

(37) Wang, Z.; Deng, X.; Ding, J.; Zhou, W.; Zheng, X.; Tang, G. Mechanisms of drug release in pH-sensitive micelles for tumour targeted drug delivery system: A review. *International journal of pharmaceutics* **2018**, *535* (1-2), 253-260. Justus, C. R.; Dong, L.; Yang, L. V. Acidic tumor microenvironment and pH-sensing G protein-coupled receptors. *Frontiers in physiology* **2013**, *4*, 354.

(38) Choi, J.; Reipa, V.; Hitchins, V. M.; Goering, P. L.; Malinauskas, R. A. Physicochemical characterization and in V itro hemolysis evaluation of silver nanoparticles. *Toxicological Sciences* **2011**, *123* (1), 133-143.

(39) Lale, S. V.; Kumar, A.; Naz, F.; Bharti, A. C.; Koul, V. Multifunctional ATRP based pH responsive polymeric nanoparticles for improved doxorubicin chemotherapy in breast cancer by proton sponge effect/endo-lysosomal escape. *Polymer Chemistry* **2015**, *6* (11), 2115-2132.

(40) Lu, D.; Liang, J.; Fan, Y.; Gu, Z.; Zhang, X. In Vivo Evaluation of a pH-Sensitive Pullulan–Doxorubicin Conjugate. *Advanced Engineering Materials* **2010**, *12* (9), B496-B503.

(41) Shuai, X.; Ai, H.; Nasongkla, N.; Kim, S.; Gao, J. Micellar carriers based on block copolymers of poly ( $\epsilon$ -caprolactone) and poly (ethylene glycol) for doxorubicin delivery. *Journal of Controlled Release* **2004**, *98* (3), 415-426.

(42) Cao, Y.; Gu, Y.; Ma, H.; Bai, J.; Liu, L.; Zhao, P.; He, H. Self-assembled nanoparticle drug delivery systems from galactosylated polysaccharide–doxorubicin

conjugate loaded doxorubicin. *International journal of biological macromolecules* **2010**, 46 (2), 245-249.

(43) Wang, H.; Zhao, Y.; Wu, Y.; Hu, Y.-l.; Nan, K.; Nie, G.; Chen, H. Enhanced anti-tumor efficacy by co-delivery of doxorubicin and paclitaxel with amphiphilic methoxy PEG-PLGA copolymer nanoparticles. *Biomaterials* **2011**, 32 (32), 8281-8290.

(44) Arora, H. C.; Jensen, M. P.; Yuan, Y.; Wu, A.; Vogt, S.; Paunesku, T.; Woloschak, G. E. Nanocarriers enhance doxorubicin uptake in drug-resistant ovarian cancer cells. *Cancer research* **2012**, 72 (3), 769-778.



---

# *Chapter 4*

---

Curcumin Loaded Polymeric Nano-encapsulates Complexed  
with Ephb4 shRNA as a Combinatorial Therapy for Colon  
Cancer



## 4.1 Introduction

Globally, cancer disease is affecting millions due to the mutations leading to uncontrolled cell division and its metastasis. Among various cancers, colorectal cancer is the second leading cause of death and the third most cancer diagnosed globally<sup>1</sup>. Therefore, to improve the therapeutic strategy new combinations of drugs and natural bioactive agents are explored. In the advent of natural compounds to treat cancer due to their least side effects, natural herbal medicines are given preference. Curcumin (CU) is a natural polyphenol compound extracted from turmeric (*Curcuma longa*) and has been reported to possess anti-inflammatory, antioxidant, anticarcinogenic properties. Furthermore, it is reported to be antidiabetic and anti-HIV<sup>2,3</sup>. CU is reported to be an antiproliferative agent in cancer treatment, it downregulates the COX-2 enzyme which thereby decreases the levels of DNA adducts responsible for cancer. Chin-Cheng et al, in their study, reported that CU was able to inhibit colon cancer cell division and induce apoptosis of cancer cells *via* caspase 3 activity<sup>4</sup>. In another report by Aggarwal et al, CU is established as a chemopreventive agent for colorectal cancer by inhibiting carcinogens that initiate cancer<sup>5</sup>. Though CU is bioactive, it has limitations to be used as a therapeutic agent because it is hydrophobic and less bioavailable for efficient therapeutic action. To overcome these limitations, various strategies are being deployed like using nano-curcumin or encapsulating it in drug delivery systems made of polymers or other inorganic materials<sup>6,7</sup>. There is remarkable research done with bulk materials like films, scaffolds, hydrogels as carriers<sup>8</sup>. For example, CU was loaded in PVA/chitosan blend films for developing a transdermal drug delivery system with controlled release of CU as reported by K. Vidyalakshmi et al<sup>9</sup>. Apart from films, CU has also been entrapped in microcapsules, liposomes, and micelles according to literature. Shahani et al reported PLGA based CU microparticles for breast cancer treatment<sup>10</sup>. A. Altunbas et al had conducted successful entrapment of CU in peptide-based hydrogels as injectable drug delivery systems<sup>11</sup>. However, the current advanced research is focusing on the development of nanomaterials systems for the delivery of CU for improved therapy.

---

With the advent of next-generation technologies and high-throughput analysis, the innovative and personalized biological anticancer treatment is expected to find its way from bench to bedside<sup>12</sup>. RNA interference (RNAi), a post-transcriptional gene silencing, is gaining immense clinical attention regarding its usage as a potential weapon against solid tumors<sup>13</sup>. RNAi could target multiple genes in different pathways that account for tumor progression, making them more effective and without any side effects<sup>14</sup>. Most of the existing chemotherapeutic agents are directed towards tyrosine kinases to suppress cancer<sup>15</sup>. One of the significant tyrosine kinase receptors overexpressed in various cancers is Ephb4 receptors which are associated with tumor angiogenesis, growth, and metastasis<sup>16</sup>. In the present study, we aimed to silence this Ephb4 receptor using the RNAi approach in different cancer models. The lack of safe and effective delivery methods for RNAi molecules remains the primary challenge that prevents full utilization of the potential of RNAi-based therapy in biological systems<sup>17</sup>. A plethora of literature demystifies the promising potential of nanoparticles in delivering RNA-based therapeutics because of their surface modifications, site targeted delivery, enhanced permeability and retention effect, and accumulation at pharmacological levels<sup>18</sup>.

Polymers are being used for delivering bioactive agents and therapeutic molecules to the colon region. Polycationic polymers are promising candidates for gene delivery as they constitute amine groups for interactions with nucleic acids. They also possess a high degree of molecular diversity thus, available for modifications and tailoring to overcome the extracellular and intracellular obstacles<sup>19</sup>. CS is one such polycationic biodegradable polymer that can be readily prepared, non-toxic without any biological threat, and is non-immunogenic. It is a mucoadhesive polymer, obtained from natural sources like shells of insects and crustaceans (crabs, shrimps, etc). Its mucoadhesive property helps in adhering to the mucosal wall of the gastrointestinal tract so it is explored as a drug delivery system. It forms a polyelectrolyte complex with nucleic acids and protects them from DNases, RNases, and other enzymes<sup>20</sup>. Katas et al were one of the pioneering groups to develop and characterize chitosan nanoparticles for siRNA delivery *in vitro*<sup>21</sup>. L. Chuah et al demonstrated this mucoadhesive property of chitosan nanoparticles loaded with CU, in colorectal cancer cells *ex vivo* and *in*

---

*vitro*<sup>22</sup>. K. Mladenovska et al also reported colon-specific delivery of 5-aminosalicylic acid from chitosan-Ca-alginate microparticles<sup>23</sup>.

Furthermore, targeting the Nano-RNAi complexes in the colon through the oral route requires bypassing the formulation from the harsh conditions of the stomach<sup>24-26</sup>. Eudragit S-100, an anionic pH-sensitive polymer, has been used as a protective coating to protect the drugs from degradation in the stomach and release the therapeutic molecules targeting the colon region where the pH is 7.5, low alkaline to neutral<sup>3, 27, 28</sup>. Khan et al, utilized this pH-sensitive property of ES to release model drug mesalazine in the colonic region of the gastrointestinal tract<sup>29</sup>. In another study, Mehta et al reported formulation and *in vitro* evaluation of ES coated naproxen matrix tablets for colon-targeted drug delivery system<sup>30</sup>. So, ES is one of the tried and tested polymers used to deliver the drug or bioactive payload in the colon because of its pH sensitivity and biocompatibility.

Since cancer is a complex disease an individual drug or gene may not be sufficient to arrest its growth, so a combination of drug and therapeutic genes is being explored. As reported in the literature by Babu et al, chitosan-coated polylactic acid nanoparticle-mediated combinatorial delivery of cisplatin and siRNA/plasmid DNA chemosensitized cisplatin-resistant human ovarian cancer cells<sup>31</sup>. R.Khatik et al have explored and reported colon-specific delivery of curcumin coated with eudragit-chitosan nanoparticles *in vitro* and *in vivo*<sup>3</sup>. To this end, we designed a combinatorial approach of using nano-curcumin to encapsulate Ephb4 shRNA along with other bioactive agents for its increased uptake and targeting to the tumor site. Therefore, the objectives of this work include, preparation of CU loaded polymeric NPs decorated with Ephb4 shRNA, its morphological, and physicochemical characterization. After characterization, study their biocompatibility and toxicity both *in vitro* and *in vivo*.

## 4.2 Experimental

### 4.2.1 Materials

Curcumin crystalline was purchased from S. D. Fine, India. Chitosan (medium mol. wt.) was procured from Aldrich (medium mol. wt), eudragit S-100 was a gift sample

---

from Evonik, calcium chloride from Spectrochem, India. Cyanine 7.5 NHS dye was procured from Lumiprobe, USA. FBS (fetal bovine serum), DMEM (Dulbecco's modified Eagle's medium), MTT (3-(4, 5-dimethylthiazol-2-yl)-2, 5-diphenyltetrazolium bromide) were obtained from Invitrogen, India. L929, HCT116, and MCF-7 cell lines were acquired from the cell repository of the National Centre for Cell Science (NCCS), Pune. All analytical reagents used were of laboratory grade obtained from local vendors.

#### **4.2.2 Preparation of fluorescent nano-encapsulate of curcumin-chitosan (CU-CS)**

Curcumin (CU) (1 g/100 mL) was dispersed in 60% ethanol, and it was subjected to sonication by an ultra-probe sonicator (VCX 500, Vibra-Cell, Sonics, USA) at 40% amplitude for 1 h with a sonication time of 5 seconds in an ice bath. After sonication, cyanine 7.5 NHS dye (10 µg/mL) was dissolved in DMSO and was added to the dispersed CU solution. The solution mixture was stirred for 30 min at ambient temperature. Further, the respective 1 and 2 wt% of chitosan (CS) solutions of pH 5.0 were prepared in 2% (v/v) acetic acid solution by stirring for 6 h. Equal volume of CS and CU-cyanine-7.5 NHS dye dispersion was added slowly drop wise under high-speed stirring to make CU-CS suspension. The CU nanoparticles concentration was fixed at 1 wt%, and the CS concentration was varied to attain various formulations. To crosslink, the individual formulations were electrosprayed vertically in 100 mL calcium chloride (5 wt%) solution using an electrospinning unit (ESPIN Nano, PECO, India). Parameters for electrospraying were optimized at a voltage of 24 kV, with a flow rate of 0.5 mL/h, and the distance between the tip of the needle and the collector was maintained at a distance of 15 cm. The electrosprayed dispersion was centrifuged at 16,000 rpm for 24 min at 12 °C to pelletize the NPs. The obtained pellet was dispersed in 20 mL of deionized water (DI) and washed twice, followed with repeated centrifugations. Further, the pellet of the NPs was dried by lyophilization and characterized to analyze the Ephb4-shRNA (plasmid DNA) complexation and Eudragit S-100 (ES) coating.



**Table 4.1** Formulations of CU with CS coating

Sr. No.	Formulation		Batch name	Zeta Potential (mV)	Hydrodynamic diameter (nm)	PDI
	CU% (w/v)	CS% (w/v)				
1.	1	-	1CU	-31.66	129.8	0.247
2.	1	1	1CU-1CS	+51.52	348.5	0.216
3.	-	1	1CS	+29.77	361.6	0.288
4.	1	2	1CU-2CS	+55.51	402.4	0.169
5.	-	2	2CS	+33.54	295.3	0.282

#### 4.2.2.1 Entrapment and loading efficiency

The entrapment and loading efficiency of NPs were calculated according to the reported literature<sup>25, 32</sup>. Briefly, 2 mg of 1:1 ratio of CU-CS NPs was dispersed in 2 mL of methanol by sonication for 2 min. The resulting dispersion was centrifuged at 16,500 rpm for 35 min at 12°C and collected from the supernatant. The untrapped CU concentration present in the supernatant was calculated using a standard calibration curve of CU at  $\lambda_{\text{max}}$  of 423 nm, which was analyzed using a UV-Vis spectrophotometer (UV 1601PC UV spectrophotometer, Shimadzu, Japan). The percent of entrapment efficiency (EE) was estimated using Equation 1. The percent of loading efficiency was estimated using Equation 2. Similarly, the percent of entrapment and loading efficiency were calculated for other formulations.

$$\text{Encapsulation Efficiency (\%)} = \frac{(\text{wt. of CU used} - \text{wt. of untrapped CU})}{\text{wt. of CU used}} \times 100 \dots (1)$$

$$\text{Loading Efficiency (\%)} = \frac{\text{entrapped CU in NP}}{\text{wt. of NP}} \times 100 \dots (2)$$

#### 4.2.2.2 Complexation of shRNA to CU-CS NPs

Complexes of Ephb4-shRNA with the respective ratios of CU-CS NPs were carried out at two different weight ratios, 25:0.8 and 25:1.0 [(CU-CS) and shRNA]. The

respective NPs with different ratios of Ephb4-shRNA were heated separately for 12 min at 55 °C and later mixed and vortexed the solutions for 30 seconds to obtain the respective complexes of CU-CS-shRNA NPs. The respective complexed NPs were loaded in the wells of an agarose gel (1 wt%) and confirmed complexation by agarose gel retardation assay.

#### 4.2.2.3 Eudragit S-100 coated NPs

CU-CS-shRNA NPs were coated with eudragit (ES) using 1 wt% of ES solution of pH 5, which was prepared using a solvent mixture of ethanol and acetone at a 2:1 ratio. From this solution, 200  $\mu$ L was added dropwise to the dispersion of 800  $\mu$ L of CU-CS-shRNA NPs to form ES coated CU-CS- shRNA (CU-CS-shRNA-ES) NPs (Figure 4.1).

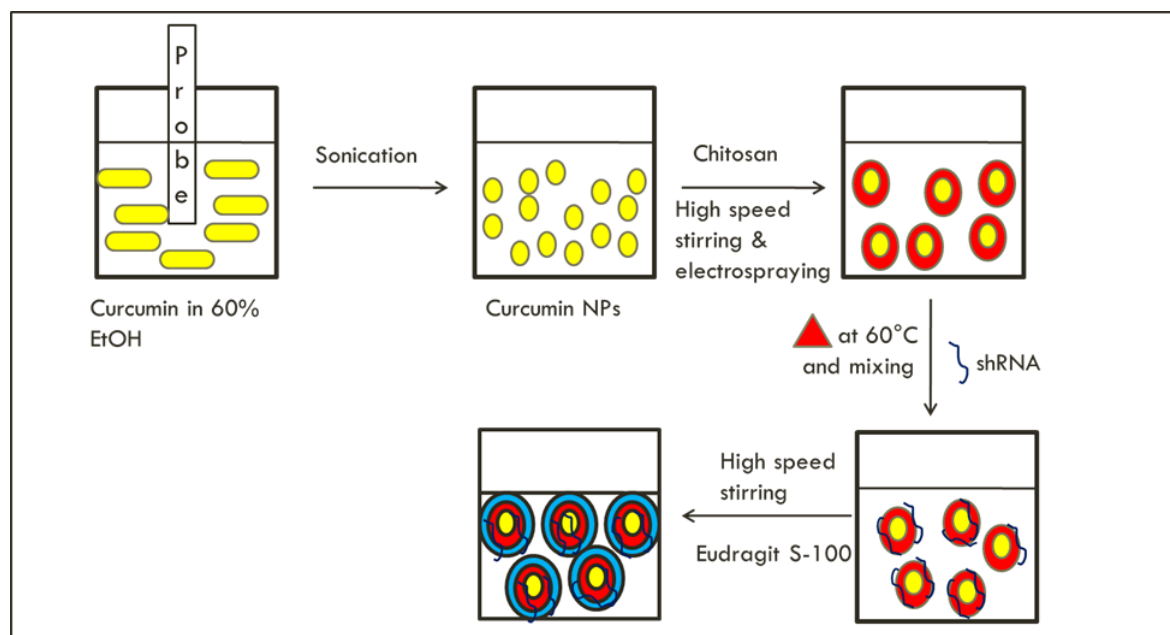


**Figure 4.1** Graphical representation of preparation of CU nanoencapsulates.

#### 4.2.2.4 *In vitro* CU release studies

The drug release studies for the developed formulations were performed by direct dispersion method in different buffers, HCl-KCl (hydrochloric acid-potassium

chloride 0.1 M, pH 1.2), and PBS (phosphate buffer solution, 0.1 M, pH 6.8), and (phosphate buffer solution, 0.1 M, pH 7.4)<sup>33</sup>. The release of CU from CU-CS NPs and CU-CS-ES NPs was determined according to the reported protocol<sup>26</sup>. For example, 5 mg of the respective lyophilized NPs were dispersed separately in 20 mL of different buffers as mentioned above. A duplicate set of 1 mL each were aliquoted from the above respective dispersions. Release kinetics was monitored at 37 °C in a water bath shaker (50 rpm) for a period of 4 h in the buffer of pH 1.2. Similarly, the release studies were done in the respective buffers of pH 6.8 and 7.4 for up to 72 h. After the designated time intervals, the sample tubes were taken out and centrifuged at 1200 rpm for 3 min to collect the pellet of released CU. Later, the collected CU pellet was dissolved in 1 mL of methanol and the amount of CU was quantified by a UV-Vis spectrophotometer (UV 1601PC UV spectrophotometer, Shimadzu, Japan) at a wavelength of 423 nm. The cumulative % of CU released was calculated using the following equation:

$$\text{Cumulative drug release (\%)} = \frac{\text{wt of CU released}}{\text{wt of CU in NPs}} \times 100 \dots\dots (3)$$

#### 4.2.3 Characterizations of NPs

The zeta potential and particle size distribution of CU NP, CU-CS NPs, CU-CS-shRNA NPs, and CU-CS-shRNA-ES NPs were analyzed using 90 Plus Brookhaven Instruments Corp, PALS zeta potential analyzer, USA. Morphological characterizations of CU-CS-shRNA-ES NPs were done using SEM (Quanta 200 3D, FEI, USA). The lyophilized NPs were dispersed and diluted (10X) in millipore water to form a suspension which was later casted on a silicon wafer and sputter-coated with gold for ESEM analysis. Similarly, the NP dispersions were prepared, drop casted on a copper grid, and stained with 1 wt% uranyl acetate dye for Transmission Electron Microscope (TEM) analysis (FEI Tecnai TF20 200kV FEG high-resolution Transmission Electron Microscope, USA). Pure polymers, curcumin encapsulates and polymeric interactions with CU were analyzed by FTIR (PerkinElmer spectrometer I, FT-IR diffused reflectance (DRIFT) mode, USA). The spectra recorded were in the range of 400 to 4000 cm<sup>-1</sup> with an average of 10 scans per sample. The thermal behavior of pure polymers (CS, ES), CU, and NPs (CU-CS, CU-CS-ES) was recorded

---

using differential scanning calorimetry (DSC) instrument (Model Q10 DSC, TA instrument, USA). The respective sample of ~5 mg was used for recording the thermogram. Each sample was crimped in an aluminum pan and was placed in the sample chamber of DSC which was equilibrated to  $-80\text{ }^{\circ}\text{C}$  for 2 min and exposed to the heating and cooling cycles. In the first cycle, the sample was heated to  $200\text{ }^{\circ}\text{C}$  at a rate of  $10\text{ }^{\circ}\text{C min}^{-1}$ . In the second cycle, the sample was quenched to  $-80\text{ }^{\circ}\text{C}$  at a rate of  $100\text{ }^{\circ}\text{C min}^{-1}$ . In the third cycle, the sample was heated from 0 to  $200\text{ }^{\circ}\text{C}$  at a rate of  $10\text{ }^{\circ}\text{C/min}$ . The DSC studies were done under dry nitrogen atmosphere at a purging rate of 50 mL/min.

#### **4.2.4 Cell studies**

Mouse fibroblast L929 cell line as control was grown as monolayer cultures under standard cell culture conditions in DMEM media supplemented with 10% FBS and incubated at  $37\text{ }^{\circ}\text{C}$ , humidified with 5%  $\text{CO}_2$  atmosphere. Similarly, human colorectal carcinoma HCT116 and breast adenocarcinoma cell line MCF-7 were cultured in DMEM and MEM media respectively. The respective media were supplemented with 10% FBS, and incubated while maintaining similar conditions.

**Cytotoxicity assay:** The cytotoxicity assay, MTT for CU-CS-Ephb4 shRNA-ES NPs was done in HCT116 and MCF-7 cell lines for 48 hrs. Briefly, a confluent flask of cells was harvested by trypsinization and to each well of a 96 well plate,  $100\text{ }\mu\text{L}$  cell suspension (~10,000 cells) was introduced. The plate was incubated at  $37^{\circ}\text{C}$ , in a 5%  $\text{CO}_2$  humidified atmosphere for 16 h to allow cells to attach and form a monolayer. Thereafter, the media from the wells was flicked off and NPs were added. The NPs dispersed in serum-free media at 1 mg/mL stock concentration were sterilized for 30 min under UV light and different concentrations ranging from  $2\text{ }\mu\text{g/mL}$  to  $500\text{ }\mu\text{g/mL}$  were added. These cells were incubated at  $37\text{ }^{\circ}\text{C}$  in 5%  $\text{CO}_2$  conditions for 48 h and then the media from the wells was replaced with MTT reagent. After 4 h of the incubation period, the media was siphoned off and added  $100\text{ }\mu\text{L}$  of DMSO in the wells to solubilize formazan crystals to develop color and the readings were recorded at 550 nm using a UV plate reader (Multiskan, Thermo Scientific, Finland).

***In vitro cellular uptake:*** Cellular uptake behavior of the NPs was evaluated in L929 fibroblast cells using fluorescence microscopy. For instance, L929 fibroblast cells were seeded on the top of glass coverslips in a 24 well plate and incubated for 24 h at 37 °C in a 5% CO<sub>2</sub> atmosphere. After incubation, the media was aspirated from the wells and washed thrice with phosphate buffer (PBS). CU alone, CU-CS NPs, and CU-CS-ES NPs were added to the individual wells at different concentrations and incubated for 3 h at 37 °C. Later the media was aspirated off, washed the cells with PBS, and 300 µL of 4% paraformaldehyde was added to the respective wells and incubated for 15 min at ambient temperature to fix the cells. Later to this, paraformaldehyde was washed off using PBS and given 0.1% (v/v) Triton X-100 wash for 8 min. Then stained with DAPI-PBS (1 µg/mL) solution for 05 min. Subsequently, coverslips were washed with PBS solution and placed on a clean glass slide with mounting media (Fluoroshield). Excess media was wiped off with tissue and the cells were observed using an epi-fluorescence microscope (Carl Zeiss, Model: Axio Observer.Z1, Oil immersion objective, 60X). The nucleus of the cells was observed using the blue filter of DAPI and CU being fluorescent was visualized using the green filter of FITC (535-600 nm).

***Hemolysis assay:*** To examine the hemolytic capacity of developed nanocarrier i.e., CU-CS-shRNA, the Hemolytic assay was performed on fresh rodent red blood cells (RBCs). 2% v/v suspension of RBCs was prepared. Then dispersion of CU-CS-Ephb4 shRNA-ES NPs at concentrations from 0, 2, 4, 6, 8, 20, 40, 60, 80, 100, 150, 200, 300, 400, and 500 µg/mL were incubated with suspension of RBCs at 37°C for 1 h. The positive and negative controls were Milli-Q water (100% hemolysis) and normal saline (0% hemolysis), respectively. After 1 h of incubation at room temperature, nanoparticles treated RBCs were spun at 4000 rpm at 4°C for 10 min and the supernatant was separated. The absorbance was measured at 540 nm using a Microplate Reader (Thermo Scientific, USA). The percent hemolysis was calculated as follows:

$$\text{Hemolysis (\%)} = \frac{\text{Abs.test} - \text{Abs.negative control}}{\text{Abs.positive control} - \text{Abs.negative control}} \times 100 \dots (4)$$

### 4.3 Results and discussion

A nano-system was developed from pH-sensitive biodegradable polymers chitosan and Eudragit to encapsulate CU and complex Ephb4 shRNA. The polymers will protect the cargo and release the bioactive molecules at the site of the tumor in the colon region. The *in vitro* studies were carried out to evaluate the toxicity of the developed nanoencapsulates, the work was translated to *in vivo* study in knockout mouse models at CSIR-CCMB, Hyderabad.

#### 4.3.1 Synthesis and characterization of curcumin-chitosan NPs

The hydrophobic curcumin (CU) was sized down to nano-CU by sonication. CU nanoparticles being negatively charged interacts with positively charged polymers<sup>34</sup>. The desolvation approach is usually used for encapsulation of CU with polymers. However, following this method, the yield of the NPs was low. Therefore, several alternative methods were tried for the fabrication of the nanoparticles. Electro spraying is one of the simple and powerful methods that is being used for the production of NPs at high yield and reproducibility<sup>35</sup>. Accordingly, electro spraying method was successfully employed for fabricating the nanoparticulate system and the nanoparticles were obtained in sufficient quantities.

The morphology of fabricated NPs was examined by SEM and TEM. The size, shape, and distribution of the formulated CU, CU-CS NPs and CU-CS-shRNA-ES NPs were in the range of 100-200 and 110-230 nm diameter respectively with spherical morphology as shown in Figure 4.2. Coatings of polymers on CU NPs were observed in TEM images where coating with ES changed the surface morphology of CU with a thickness of the polymer coating between 20-30 nm. Nanoencapsulation of negatively charged CU was carried out using the individual polymer, chitosan (CS), followed by Eudragit S-100 (ES). The charge of the CU particles before and after coating with polymers was confirmed by zeta ( $\zeta$ ) potential measurements. CU possessed a net negative charge of -24.78 mV, which on interaction with a cationic polymer, CS (+29.1 mV) yielded positively charged particles of +51.52 mV.

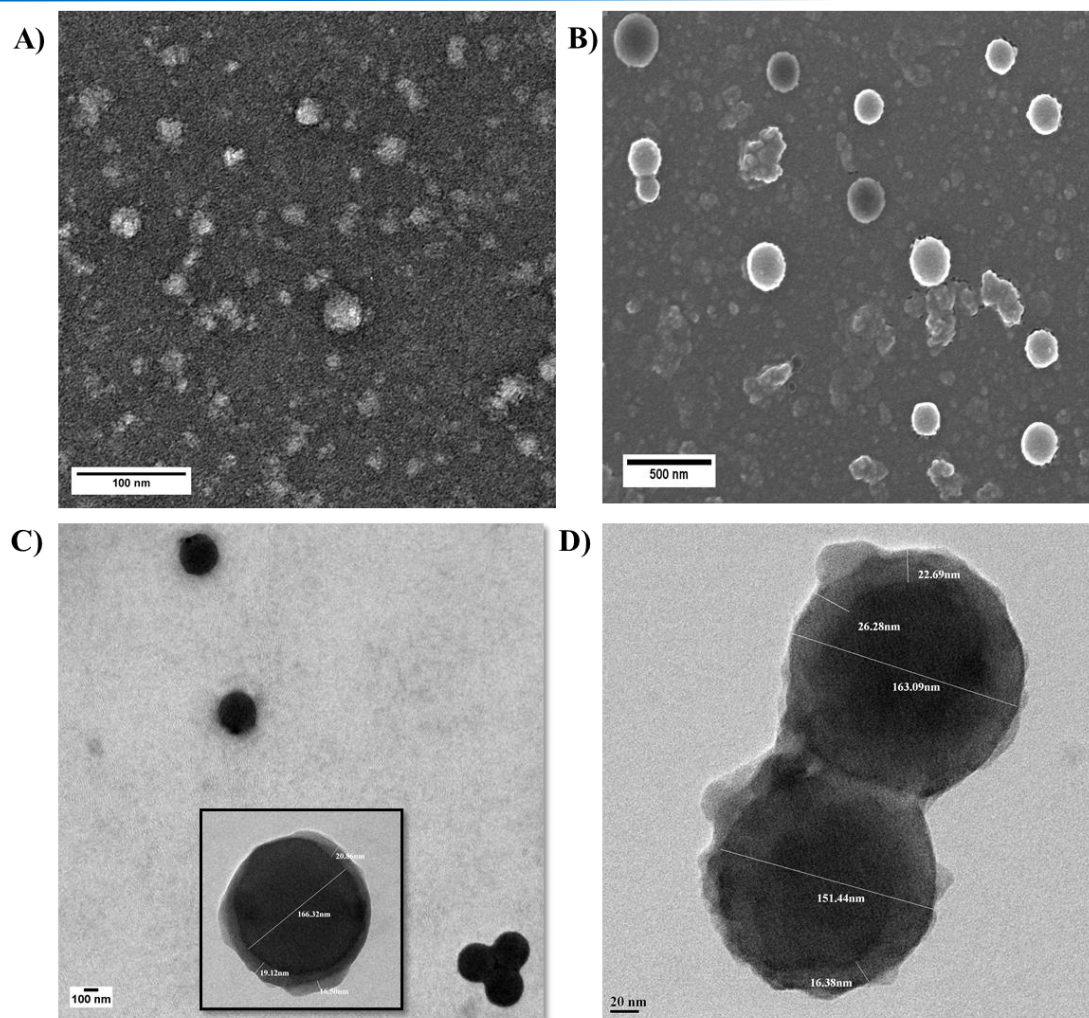


**Figure 4.2** A) TEM image of CU NPs, B) SEM image of 1CU-2CS-Ephb4-ES, C) and D) TEM image of 1CU-2CS-Ephb4-ES.

The increase in positive charge was attributed due to the crosslinking of NPs with  $\text{Ca}^{++}$  ions. With an increase in the ratio of CS, the positive charge of the NPs increased in a concentration-dependent manner. Table 4.1 shows the different formulations and their PDI with varying concentrations of CS. With the progress of Ephb4, shRNA plasmid conjugation, the net positive charge on NPs decreased to 24.83 mV. This complex formation of CU-CS-shRNA NPs was aided due to the positively charged amine groups of CS. Further, the complexed NPs recorded a decrease in net positive charge when coated with anionic ES (Figure 4.3A). Different ratios of CU-CS NPs were formulated and checked for their charge and shRNA plasmid retention, based on the suitability, 1:2 ratio of CU-CS NPs was taken for pre-

clinical evaluation. Further, the gel retardation assay was used to validate the conjugation of Ephb4 shRNA plasmid to the CU-CS NP system. Two different ratios of NPs to Ephb4 shRNA plasmid were prepared (25:0.8 and 25:1.0), loaded in 1 % of agarose gel. It was observed that the control lane containing free nucleic acids migrated down the gel without hindrance, while the lane with the Ephb4 conjugated NPs did not show the migration of Ephb4 (Figure 4.3B). Moreover, the 25:0.8 ratio exhibited better conjugation efficiency than the 25:1.0 ratio.

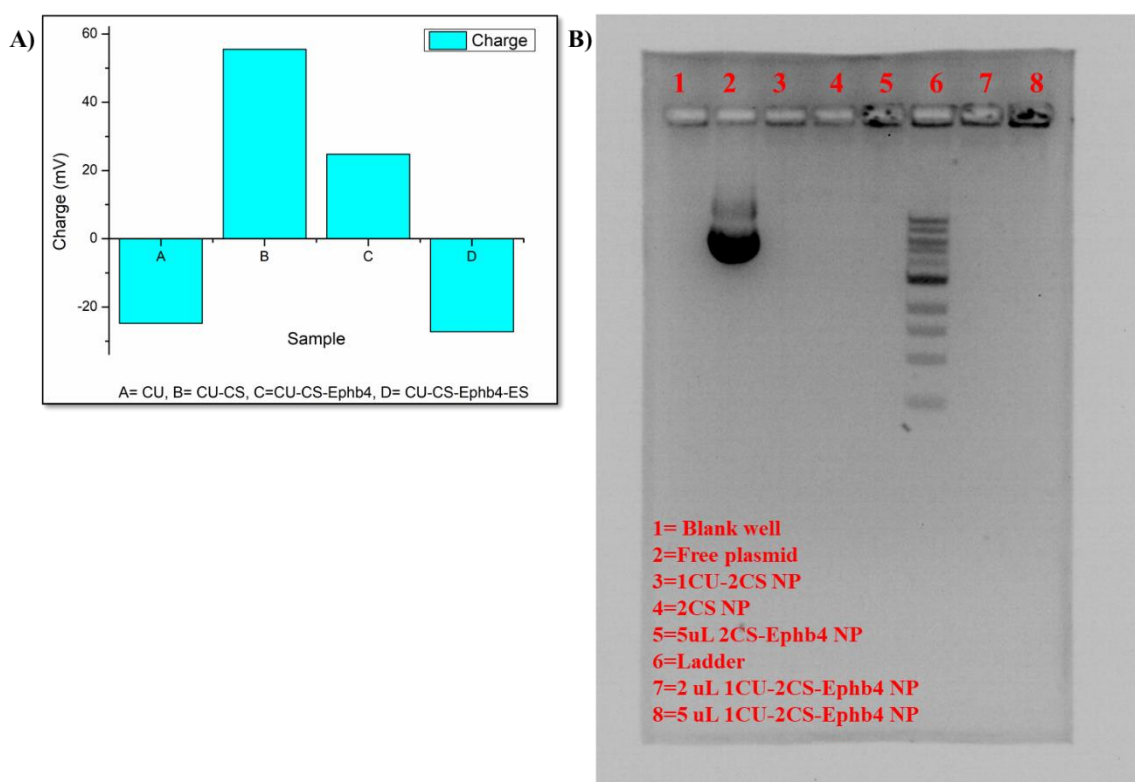


**Figure 4.3** A) Zeta potential measurements of CU formulations, B) Gel retardation assay of NPs bound with Ephb4 shRNA.

#### 4.3.2 FTIR spectra and thermal analysis

The nanoparticulate system consisted of the respective components CU, CS, and ES possessing the characteristic functional groups, and their sequential additions were confirmed by FTIR. Individual peaks of the respective components were first observed to understand the functional changes before and after the fabrication of NPs. In the CU spectrum, the characteristic peaks such as phenolic O–H peak was observed



at  $3500\text{ cm}^{-1}$ , carboxylic C=O stretching at  $1628\text{ cm}^{-1}$ , C=C stretching at  $1512\text{ cm}^{-1}$  and C-H stretching at  $1430\text{ cm}^{-1}$  (Figure 4.4A)<sup>36</sup>. For the CS spectrum (Figure 4.4B), a characteristic broad peak at  $3400\text{ cm}^{-1}$  was observed due to the merging of N-H and O-H functional groups. Other characteristics peak included C-H stretching at  $2961\text{ cm}^{-1}$  and  $2921\text{ cm}^{-1}$ , carboxylic C=O peak at  $1655\text{ cm}^{-1}$  and bending peak for N-H peak at  $1590\text{ cm}^{-1}$ <sup>37</sup>. In the ES spectrum (Figure 4.4C), the characteristic broad O-H absorption band at  $3100\text{--}3500\text{ cm}^{-1}$  was noticed along with C-H stretching vibrations at  $2998$  and  $2954\text{ cm}^{-1}$ , C=O stretching at  $1730\text{ cm}^{-1}$ , and C-O-C stretching vibration at  $1150\text{ cm}^{-1}$ <sup>28</sup>. In Figure 4.4D, the IR spectrum of CU-CS exhibited C=C peaks of curcumin at  $1512\text{ cm}^{-1}$  and  $1430\text{ cm}^{-1}$ , downshift of C=O peak from  $1655\text{ cm}^{-1}$  to  $1635\text{ cm}^{-1}$  and N-H peak of CS merged into this C=O peak, which suggested strong interaction of CU with CS. In the same figure, the IR spectrum of CU-CS-ES reported the changed peak at  $1640\text{ cm}^{-1}$  that could be attributed to the formation of a carboxylate bond between the  $\text{-NH}^+$  groups of CS and  $\text{COO}^-$  groups of ES which are as per the earlier literature<sup>38</sup>. These findings confirmed the encapsulation of CU- CS NPs with ES.

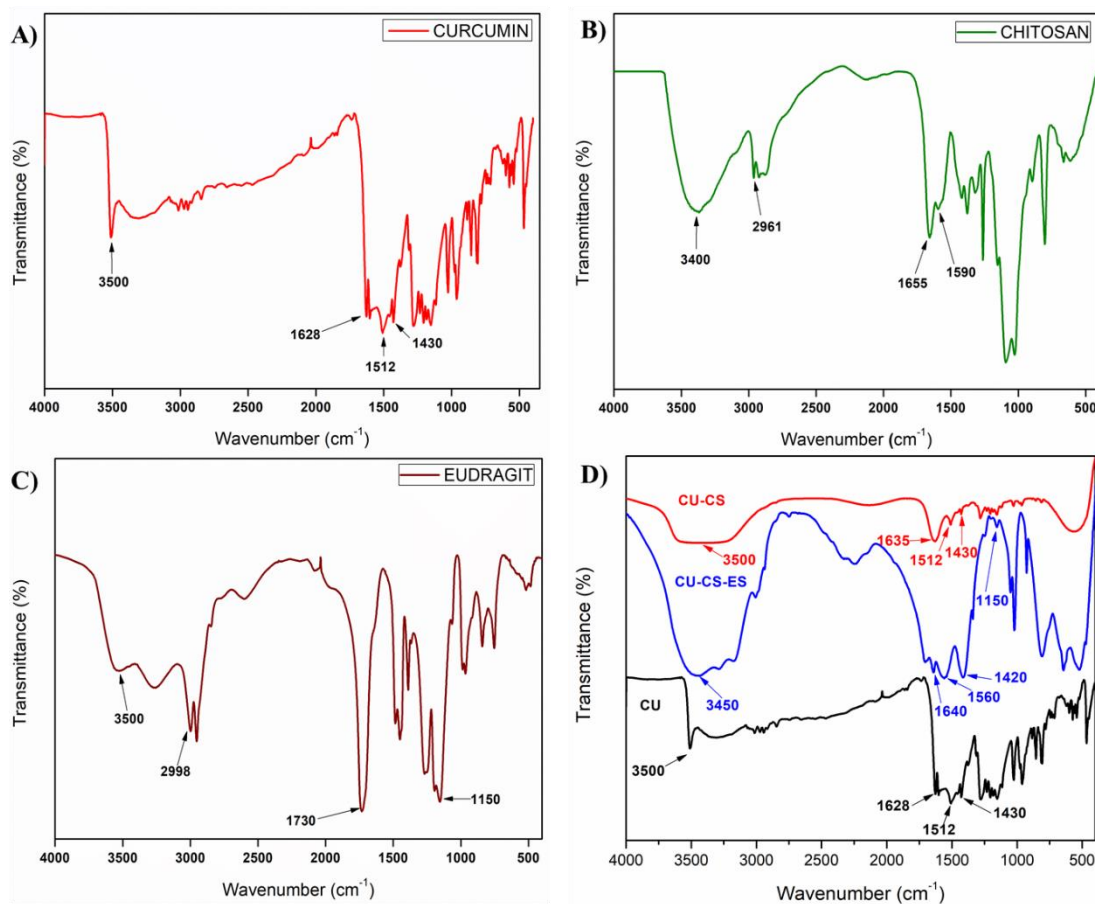


**Figure 4.4** FTIR spectrum of **A)** bare CU, **B)** chitosan, **C)** Eudragit S100, **D)** CU coated with CS and ES (CU-CS-ES).

To understand the coating strength of ES on the CU-CS NP system, thermal analysis by DSC was performed for CU, CS and ES, and CU-CS-ES NPs as shown in Figure 4.5. Glass transition temperature ( $T_g$ ) was observed at 95 °C for CS and 71 °C for ES, which was in accordance with reported literature<sup>28, 39</sup>. Likewise, a sharp endothermic peak due to the melting temperature ( $T_m$ ) for CU was observed at 177 °C. In CU-CS-ES NPs, two broad endothermic peaks were observed at 110 °C and 150 °C. The  $T_m$  of CU decreased because of the interactions between the CS and CU. The crosslinking of CU-CS with CaCl<sub>2</sub> resulted in a shift of endothermic peak ( $T_g$ ), from 95°C to 110°C which could be attributed due to an increase in the rigidity of the nanoparticle system. As reported in the earlier studies, the shift in the peak of CU to a lower temperature indicated the disordered crystalline phase in the final preparation<sup>40</sup>.

Finally, we could conclude that the shifting and broadening of CU peak supported and validated the encapsulation of CU by CS and ES polymers.

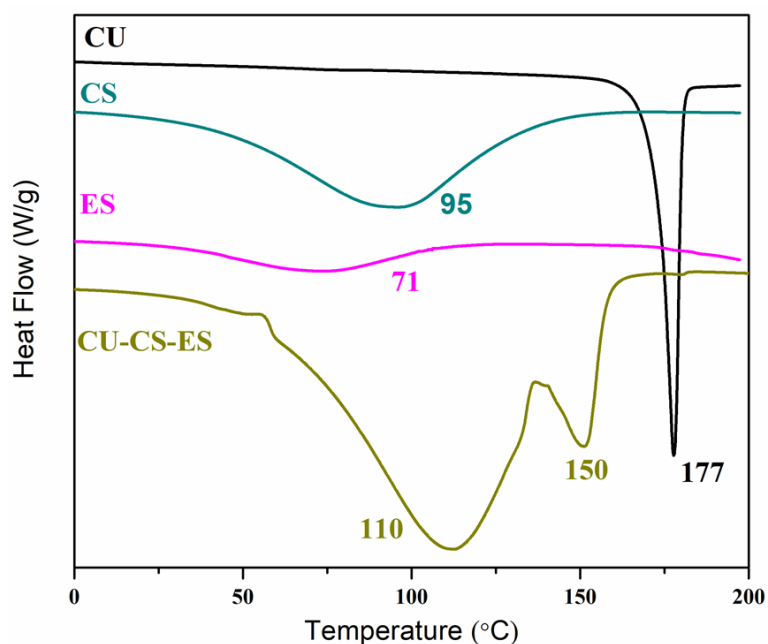


**Figure 4.5** Differential scanning calorimetric (DSC) analysis of bare CU, CS, and ES with CU-CS–ES NPs.

### 4.3.3 Entrapment efficiency and drug release studies

The entrapment and loading efficiency of CU was determined using equations 1 and 2 as given in the experimental section. The CU-CS-NPs were sonicated, centrifuged and the unentrapped CU was extracted into methanol and quantified using a calibration curve recorded at  $\lambda_{\max}$  423. Later the percent of CU concentration was estimated using equation 1. The entrapment efficiency for different compositions of CU-CS (1:1 and 1:2) was 76.67 and 68.21% respectively. The loading efficiency was calculated using equation 2, which was 38.3 and 22.85% for the respective compositions, 1CU-1CS, and 1CU-2CS. We observed that with the increase in chitosan concentration, the entrapment and loading efficiency of CU was reduced, which could be attributed to the hindrance of CU entrapment as a result of an increase in the viscosity of CS solution.

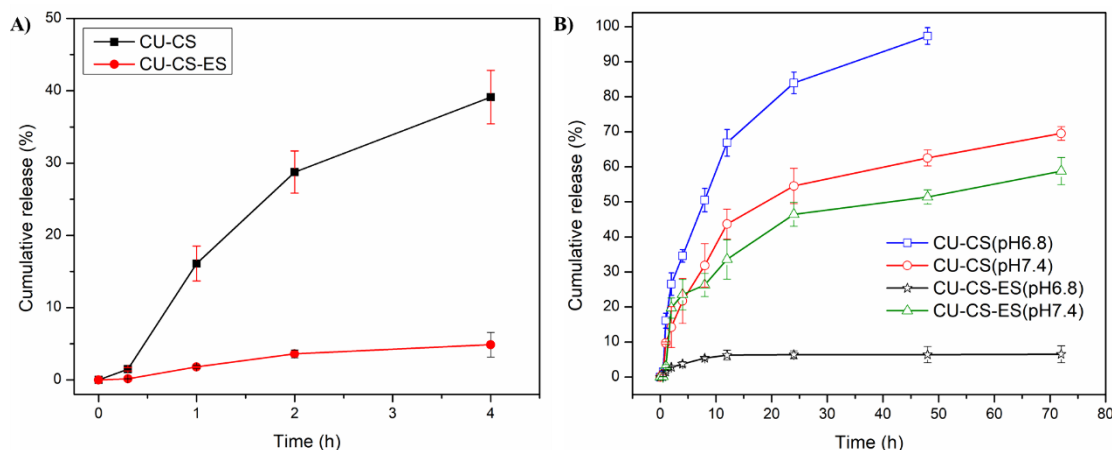


**Figure 4.6** A) Cumulative CU release at 1.2 pH from CU-CS and CU-CS-ES, and B) cumulative CU release at 6.8 and 7.4 pH from CU-CS and CU-CS-ES.

CU-CS NPs coated with and without ES were studied for their release of CU at three different pH values. The physiological pH of the stomach is 1.2 (acidic) whereas the pH of the gut ranges from 6.8 to 7.5. Different pH like 1.2, 6.8, and 7.4 were taken into consideration for mimicking the pH in gastrointestinal track to understand the reaching and release of biodrug at the targeted site in a non-degradable form. It was observed (Figure 4.6A) that at 1.2 pH after 4 h of release studies, the amount of CU released from the nanoparticle system without ES coating was 39%, which is considered as burst release, whereas the NPs of CU-CS-ES recorded ~ 5% of CU release. The decrease in the quantity of CU release is due to the ES coating as a result of the protonation of COO<sup>-</sup> groups of ES that enabled the protection of chitosan from degradation in the acidic pH of 1.2. CU release at pH 7.4 for NPs of CU-CS and CU-CS-ES after 8 h, was 32 and 26% respectively (Figure 4.6B), which followed a sustained release mechanism. Further, a continuation of CU release for 72 h at the same pH, recorded, 70 and 59% from CU-CS and CU-CS-ES respectively. At this pH, the carboxyl groups of ES were ionized leading to the dissolution of ES thereby exposing CS coated CU NPs<sup>35, 47</sup>. At 6.8 pH (Figure 4.6B), the entire CU was released from CU-CS alone within 48 h, whereas only 7% was released from CU-CS-ES, though the release studies were extended up to 72 h. The diffusion of CU and swelling of chitosan at 6.8 pH, resulted in high CU release from CU-CS, while the stability of ES at 6.8 pH did not lead to any CU release from CU-CS-ES NPs.

#### 4.3.4 Cell studies

**Cytotoxicity assay:** To demonstrate the cytotoxic effects of the biodrug (CU-CS-Ephb4 shRNA-ES), MTT assay was performed in normal L929, colon cancer HCT116 and breast cancer MCF-7 cell lines for 48 h. MTT reagent solubilized the formazan crystals which indicated cellular respiratory activity in live cells. Figure 4.7 displays the viability of L929, HCT116 and MCF-7 cells after incubation with varying concentrations of NPs. The CU-based NPs were observed to inhibit the proliferation of both cancer cell lines in a concentration dependent manner as compared with the controls. We observed the highest toxicity in cancer cell lines (HCT116 and MCF-7) where the cell viability was reduced to more than 50%. Furthermore, there was no toxicity observed in normal L929 cell lines exhibiting its activity against only cancer cell lines. So, the results clearly indicated that the developed CU-CS-Ephb4 shRNA-ES biodrug is potent in reducing colon and breast cancer cell proliferation *in vitro*.

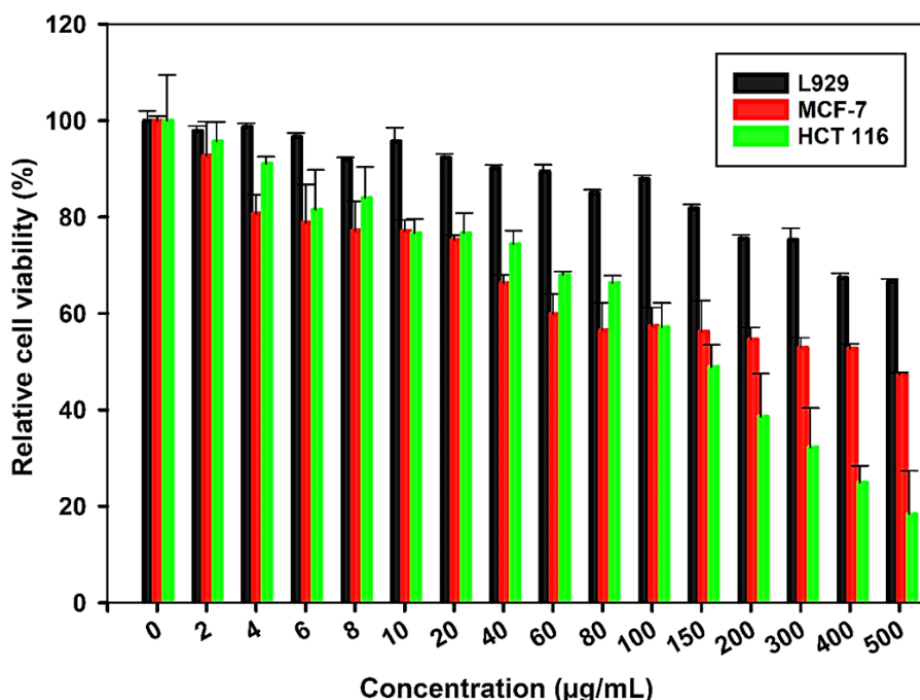


**Figure 4.7** Cell viability assay results of HCT116 and MCF-7 (cancer cell lines) with L929 cells (control) after 48 h of CU-CS-Ephb4 shRNA-ES treatment.

***In vitro cellular uptake:*** The cellular uptake and intracellular trafficking of CU NP and CU based NP (CU-CS and CUCS-ES NPs) formulations were investigated in L929 fibroblast cells at a concentration of 50 µg/mL for CU loaded NPs and 11 µg/mL for CU NPs (calculated from the loading %). The NPs were incubated for 3 h with the cells for assessing their internalization. Nuclei were visualized by DAPI and intrinsic green fluorescence from CU was detected using FITC filter. Control cells that were not exposed to CU did not display any green fluorescence. As seen in Figure 4.8, after 3 h incubation, CU appeared to enter the cells and green fluorescence was observed in the cytoplasmic region of the cells. Moreover, the positive charge on CS is reported to be beneficial in interacting with the cells having an intrinsic negative charge and able to loosen the tight junction of cells to facilitate uptake of the particles<sup>41</sup>. This also suggested that after the pH-responsive release of ES, the CU-CS-Ephb4 shRNA had a better cellular uptake, thus increasing the efficacy of the biodrug.

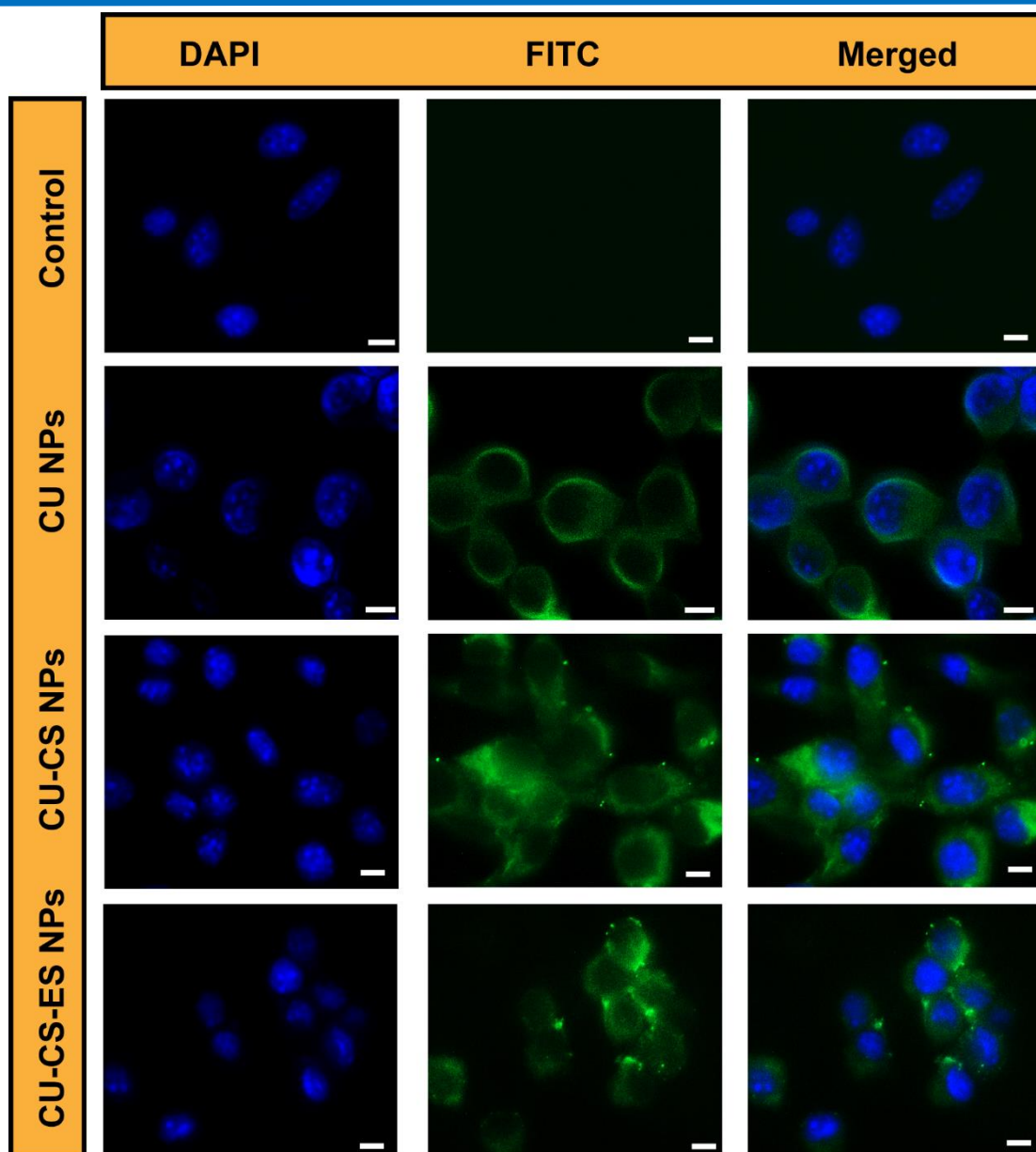


**Figure 4.8** Cellular uptake assay representing the L929 cells after 3 h involving CU (11  $\mu\text{g}/\text{mL}$ ), CU-CS (50  $\mu\text{g}/\text{mL}$ ), and CU-CS-ES (50  $\mu\text{g}/\text{mL}$ ), Scale bar: 5  $\mu\text{m}$ .

**Hemolysis assay:** The hemolysis brought about by altered concentrations of polymeric nanocomposites was measured after incubating the drug with 2% v/v suspension of red blood cells. A concentration of 100  $\mu\text{g}/\text{mL}$  induced the maximum hemolysis among all the concentrations of NPs.

**In vivo studies:** The NPs were tested at CSIR-CCMB and were found to be safe and effective in the *in vivo* mouse models. The oral administration of NPs increased the

survivability of tumor-bearing mice. For further details, kindly refer to our paper accepted in RSC Nanoscale (<https://doi.org/10.1039/D1NR04411G>)

#### **4.4 Conclusions**

The emergence of gene-based therapies in the clinical realm has enabled the use of nucleic acids in therapeutic approaches, opening infinite possibilities for the treatment of a wide range of genetic, innate, and acquired diseases, including cancers. Nano-formulations, with their unique characteristics, have been positively established as competent carriers for delivering RNAi molecules. In addition, it has been suggested that the shRNA-based approach could be better than siRNA-based RNAi approach as shRNAs is known to be more stable compared to siRNAs which are degraded rapidly under in vivo conditions. Also, it has been opined that natural therapeutic compounds as carrier molecules enable biocompatible, nontoxic, targeted delivery with prolonged survival. To this end, we have demonstrated the development and applicability of a combinatorial approach involving the nano-RNAi biodrug formulation for successful site-specific delivery in both breast and colon cancer knockout mice models. In the current study, we have used nanoformulations of curcumin (CU), a well-known anticancer nutraceutical agent, with chitosan (CS) for an enhanced permeation effect. The CU-CS NPs were conjugated with Ephb4 shRNA and then coated with Eudragit S100 for specific delivery to the site of action. Our study showed that the nano-RNAi biodrug was stable, biocompatible and non-toxic, and possessed pH-specific attributes. Moreover, the uptake in the colon models was found to be efficient, with the distribution of NPs localized mostly to the intestinal tract. The efficient and site-specific knockdown of Ephb4 resulted in attenuated tumor growth leading to increased survival in mice models. Oral delivery of this bio-formulation permitted the drug to be precisely delivered to the tumor micro-environment, therein, guarding it against degradation under harsh conditions of the stomach. Though the NPs alone cohorts showed the animals survived up to 37 days, the Apc-deficient mice treated with the combination (NPs and EphB4 shRNA) showed a remarkable survival of more than 6 months as compared to controls where the median survival was 10 days, thus affirming the synergistic effect and potential of this bio-formulation for efficient colon cancer treatment. To the best of our knowledge, we are the first to demonstrate

---



the combination of CU NPs with RNA interference in a pre-clinical setting for cancer therapeutics. Our bio-drug formulation, a combination of RNAi and nanotechnology, illustrated the high therapeutic efficacy with biocompatibility and no toxicity of our novel nano-based formulation in a solid tumor model of the colon. Thus, this demonstration of a proof of concept has paved the way for a promising alliance of RNA interference and nanotechnology as next-generation cancer therapeutics.

#### 4.5 References

- (1) Xi, Y.; Xu, P. Global colorectal cancer burden in 2020 and projections to 2040. *Translational Oncology* **2021**, *14* (10), 101174.
- (2) Tong, W.; Wang, Q.; Sun, D.; Suo, J. Curcumin suppresses colon cancer cell invasion via AMPK-induced inhibition of NF- $\kappa$ B, uPA activator and MMP9. *Oncology letters* **2016**, *12* (5), 4139-4146.
- (3) Khatik, R.; Mishra, R.; Verma, A.; Dwivedi, P.; Kumar, V.; Gupta, V.; Paliwal, S. K.; Mishra, P. R.; Dwivedi, A. K. Colon-specific delivery of curcumin by exploiting Eudragit-decorated chitosan nanoparticles in vitro and in vivo. *Journal of nanoparticle research* **2013**, *15* (9), 1-15.
- (4) Su, C.-C.; Lin, J.-G.; Li, T.-M.; Chung, J.-G.; Yang, J.-S.; Ip, S.-W.; Lin, W.-C.; Chen, G.-W. Curcumin-induced apoptosis of human colon cancer colo 205 cells through the production of ROS, Ca<sup>2+</sup> and the activation of caspase-3. *Anticancer research* **2006**, *26* (6B), 4379-4389.
- (5) Aggarwal, B. B.; Kumar, A.; Bharti, A. C. Anticancer potential of curcumin: preclinical and clinical studies. *Anticancer research* **2003**, *23* (1/A), 363-398.
- (6) Gou, M.; Men, K.; Shi, H.; Xiang, M.; Zhang, J.; Song, J.; Long, J.; Wan, Y.; Luo, F.; Zhao, X. Curcumin-loaded biodegradable polymeric micelles for colon cancer therapy in vitro and in vivo. *Nanoscale* **2011**, *3* (4), 1558-1567.
- (7) Sindhu, K.; Rajaram, A.; Sreeram, K. J.; Rajaram, R. Curcumin conjugated gold nanoparticle synthesis and its biocompatibility. *Rsc Advances* **2014**, *4* (4), 1808-1818.
- (8) Gundloori, R. V. N.; Singam, A.; Killi, N. Nanobased intravenous and transdermal drug delivery systems. In *Applications of Targeted Nano Drugs and Delivery Systems*, Elsevier, 2019; pp 551-594.
- (9) Vidyalakshmi, K.; Rashmi, K. N.; Pramod Kumar, T. M.; Siddaramaiah. Studies on formulation and in vitro evaluation of PVA/chitosan blend films for drug delivery. *Journal of Macromolecular Science, Part A* **2004**, *41* (10), 1115-1122.

(10) Shahani, K.; Panyam, J. Highly loaded, sustained-release microparticles of curcumin for chemoprevention. *Journal of pharmaceutical sciences* **2011**, *100* (7), 2599-2609.

(11) Altunbas, A.; Lee, S. J.; Rajasekaran, S. A.; Schneider, J. P.; Pochan, D. J. Encapsulation of curcumin in self-assembling peptide hydrogels as injectable drug delivery vehicles. *Biomaterials* **2011**, *32* (25), 5906-5914.

(12) Rawoof, A.; Swaminathan, G.; Tiwari, S.; Nair, R. A.; Dinesh Kumar, L. LeukmiR: a database for miRNAs and their targets in acute lymphoblastic leukemia. *Database (Oxford)* **2020**, *2020*. DOI: 10.1093/database/baz151. Rishabh, K.; Khadilkar, S.; Kumar, A.; Kalra, I.; Kumar, A. P.; Kunnumakkara, A. B. MicroRNAs as Modulators of Oral Tumorigenesis-A Focused Review. *Int J Mol Sci* **2021**, *22* (5). DOI: 10.3390/ijms22052561. Kumar, M. D.; Dravid, A.; Kumar, A.; Sen, D. Gene therapy as a potential tool for treating neuroblastoma-a focused review. *Cancer Gene Ther* **2016**, *23* (5), 115-124. DOI: 10.1038/cgt.2016.16. Swaminathan, G.; Shigna, A.; Kumar, A.; Byroju, V. V.; Durgempudi, V. R.; Dinesh Kumar, L. RNA interference and Nanotechnology: A promising alliance for next generation cancer therapeutics. *Frontiers in Nanotechnology* **2021**, *3*, 42.

(13) Wang, P.; Zhou, Y.; Richards, A. M. Effective tools for RNA-derived therapeutics: siRNA interference or miRNA mimicry. *Theranostics* **2021**, *11* (18), 8771-8796. DOI: 10.7150/thno.62642.

(14) Tangudu, N. K.; Verma, V. K.; Clemons, T. D.; Beevi, S. S.; Hay, T.; Mahidhara, G.; Raja, M.; Nair, R. A.; Alexander, L. E.; Patel, A. B.; et al. RNA Interference Using c-Myc-Conjugated Nanoparticles Suppresses Breast and Colorectal Cancer Models. *Mol Cancer Ther* **2015**, *14* (5), 1259-1269. DOI: 10.1158/1535-7163.MCT-14-0970.

(15) Chen, J. Regulation of tumor initiation and metastatic progression by Eph receptor tyrosine kinases. *Adv Cancer Res* **2012**, *114*, 1-20. DOI: 10.1016/B978-0-12-386503-8.00001-6.

(16) Huang, X.; Yamada, Y.; Kidoya, H.; Naito, H.; Nagahama, Y.; Kong, L.; Katoh, S. Y.; Li, W. L.; Ueno, M.; Takakura, N. EphB4 overexpression in B16 melanoma cells affects arterial-venous patterning in tumor angiogenesis. *Cancer Res* **2007**, *67* (20), 9800-9808. DOI: 10.1158/0008-5472.CAN-07-0531. Stephenson, S. A.; Slomka, S.; Douglas, E. L.; Hewett, P. J.; Hardingham, J. E. Receptor protein tyrosine kinase EphB4 is up-regulated in colon cancer. *BMC Mol Biol* **2001**, *2*, 15. DOI: 10.1186/1471-2199-2-15. Xia, G.; Kumar, S. R.; Masood, R.; Zhu, S.; Reddy, R.; Krasnoperov, V.; Quinn, D. I.; Henshall, S. M.; Sutherland, R. L.; Pinski, J. K.; et al. EphB4 expression and biological significance in prostate cancer. *Cancer Res* **2005**, *65* (11), 4623-4632. DOI: 10.1158/0008-5472.CAN-04-2667. Yang, N. Y.; Lopez-Bergami, P.; Goydos, J. S.; Yip, D.; Walker, A. M.; Pasquale, E. B.; Ethell, I. M. The EphB4 receptor promotes the growth of melanoma cells expressing the ephrin-B2 ligand. *Pigment Cell Melanoma Res* **2010**, *23* (5), 684-687. DOI: 10.1111/j.1755-148X.2010.00745.x.

---

(17) Hattab, D.; Gazzali, A. M.; Bakhtiar, A. Clinical Advances of siRNA-Based Nanotherapeutics for Cancer Treatment. *Pharmaceutics* **2021**, *13* (7). DOI: 10.3390/pharmaceutics13071009. Li, D.; Gao, C.; Kuang, M.; Xu, M.; Wang, B.; Luo, Y.; Teng, L.; Xie, J. Nanoparticles as Drug Delivery Systems of RNAi in Cancer Therapy. *Molecules* **2021**, *26* (8). DOI: 10.3390/molecules26082380.

(18) Conde, J.; Bao, C.; Tan, Y.; Cui, D.; Edelman, E. R.; Azevedo, H. S.; Byrne, H. J.; Artzi, N.; Tian, F. Dual targeted immunotherapy via in vivo delivery of biohybrid RNAi-peptide nanoparticles to tumour-associated macrophages and cancer cells. *Adv Funct Mater* **2015**, *25* (27), 4183-4194. DOI: 10.1002/adfm.201501283. Conde, J.; Tian, F.; Hernandez, Y.; Bao, C.; Baptista, P. V.; Cui, D.; Stoeger, T.; de la Fuente, J. M. RNAi-based glyconanoparticles trigger apoptotic pathways for in vitro and in vivo enhanced cancer-cell killing. *Nanoscale* **2015**, *7* (19), 9083-9091. DOI: 10.1039/c4nr05742b. Cui, D.; Zhang, C.; Liu, B.; Shu, Y.; Du, T.; Shu, D.; Wang, K.; Dai, F.; Liu, Y.; Li, C.; et al. Regression of Gastric Cancer by Systemic Injection of RNA Nanoparticles Carrying both Ligand and siRNA. *Sci Rep* **2015**, *5*, 10726. DOI: 10.1038/srep10726. Liu, B.; Cao, W.; Qiao, G.; Yao, S.; Pan, S.; Wang, L.; Yue, C.; Ma, L.; Liu, Y.; Cui, D. Effects of gold nanoprism-assisted human PD-L1 siRNA on both gene down-regulation and photothermal therapy on lung cancer. *Acta Biomater* **2019**, *99*, 307-319. DOI: 10.1016/j.actbio.2019.08.046. Sun, X.; Chen, Y.; Zhao, H.; Qiao, G.; Liu, M.; Zhang, C.; Cui, D.; Ma, L. Dual-modified cationic liposomes loaded with paclitaxel and survivin siRNA for targeted imaging and therapy of cancer stem cells in brain glioma. *Drug Deliv* **2018**, *25* (1), 1718-1727. DOI: 10.1080/10717544.2018.1494225.

(19) Mansouri, S.; Lavigne, P.; Corsi, K.; Benderdour, M.; Beaumont, E.; Fernandes, J. C. Chitosan-DNA nanoparticles as non-viral vectors in gene therapy: strategies to improve transfection efficacy. *European journal of pharmaceutics and biopharmaceutics* **2004**, *57* (1), 1-8.

(20) Hejazi, R.; Amiji, M. Chitosan-based gastrointestinal delivery systems. *Journal of controlled release* **2003**, *89* (2), 151-165.

(21) Mao, S.; Sun, W.; Kissel, T. Chitosan-based formulations for delivery of DNA and siRNA. *Advanced drug delivery reviews* **2010**, *62* (1), 12-27.

(22) Chuah, L. H.; Roberts, C. J.; Billa, N.; Abdullah, S.; Rosli, R. Cellular uptake and anticancer effects of mucoadhesive curcumin-containing chitosan nanoparticles. *Colloids and Surfaces B: Biointerfaces* **2014**, *116*, 228-236.

(23) Mladenovska, K.; Raicki, R. S.; Janevik, E. I.; Ristoski, T.; Pavlova, M. J.; Kavrakovski, Z.; Dodov, M. G.; Goracinova, K. Colon-specific delivery of 5-aminosalicylic acid from chitosan-Ca-alginate microparticles. *International Journal of Pharmaceutics* **2007**, *342* (1-2), 124-136.

(24) Wathoni, N.; Nguyen, A. N.; Rusdin, A.; Umar, A. K.; Mohammed, A. F. A.; Motoyama, K.; Joni, I. M.; Muchtaridi, M. Enteric-Coated Strategies in Colorectal

Cancer Nanoparticle Drug Delivery System. *Drug Des Devel Ther* **2020**, *14*, 4387-4405. DOI: 10.2147/DDDT.S273612.

(25) Chishti, N.; Jagwani, S.; Dhamecha, D.; Jalalpure, S.; Dehghan, M. H. Preparation, Optimization, and In Vivo Evaluation of Nanoparticle-Based Formulation for Pulmonary Delivery of Anticancer Drug. *Medicina (Kaunas)* **2019**, *55* (6). DOI: 10.3390/medicina55060294.

(26) Hales, D.; Tefas, L. R.; Tomuta, I.; Moldovan, C.; Gulei, D.; Munteanu, R.; Porfire, A. Development of a Curcumin-Loaded Polymeric Microparticulate Oral Drug Delivery System for Colon Targeting by Quality-by-Design Approach. *Pharmaceutics* **2020**, *12* (11). DOI: 10.3390/pharmaceutics12111027.

(27) Philip, A. K.; Philip, B. Colon targeted drug delivery systems: a review on primary and novel approaches. *Oman Med J* **2010**, *25* (2), 79-87. DOI: 10.5001/omj.2010.24. Yoshida, T.; Lai, T. C.; Kwon, G. S.; Sako, K. pH- and ion-sensitive polymers for drug delivery. *Expert Opin Drug Deliv* **2013**, *10* (11), 1497-1513. DOI: 10.1517/17425247.2013.821978.

(28) Vlachou, M.; Kikionis, S.; Siamidi, A.; Kyriakou, S.; Tsotinis, A.; Ioannou, E.; Roussis, V. Development and Characterization of Eudragit((R))-Based Electrospun Nanofibrous Mats and Their Formulation into Nanofiber Tablets for the Modified Release of Furosemide. *Pharmaceutics* **2019**, *11* (9). DOI: 10.3390/pharmaceutics11090480.

(29) Khan, M. Z. I.; Prebeg, Ž.; Kurjaković, N. A pH-dependent colon targeted oral drug delivery system using methacrylic acid copolymers: I. Manipulation of drug release using Eudragit® L100-55 and Eudragit® S100 combinations. *Journal of Controlled Release* **1999**, *58* (2), 215-222.

(30) Mehta, R.; Chawla, A.; Sharma, P.; Pawar, P. Formulation and in vitro evaluation of Eudragit S-100 coated naproxen matrix tablets for colon-targeted drug delivery system. *Journal of advanced pharmaceutical technology & research* **2013**, *4* (1), 31.

(31) Babu, A.; Wang, Q.; Muralidharan, R.; Shanker, M.; Munshi, A.; Ramesh, R. Chitosan coated polylactic acid nanoparticle-mediated combinatorial delivery of cisplatin and siRNA/plasmid DNA chemosensitizes cisplatin-resistant human ovarian cancer cells. *Molecular pharmaceutics* **2014**, *11* (8), 2720-2733.

(32) Sun, S. B.; Liu, P.; Shao, F. M.; Miao, Q. L. Formulation and evaluation of PLGA nanoparticles loaded capecitabine for prostate cancer. *Int J Clin Exp Med* **2015**, *8* (10), 19670-19681.

(33) D'Souza, S. A review of in vitro drug release test methods for nano-sized dosage forms. *Advances in Pharmaceutics* **2014**, 2014.

(34) Fu, D.; Okimoto, H.; Lee, C. W.; Takenobu, T.; Iwasa, Y.; Kataura, H.; Li, L. J. Ultrasensitive Detection of DNA Molecules with High On/Off Single-Walled Carbon Nanotube Network. *Advanced Materials* **2010**, *22* (43), 4867-4871.

(35) Sridhar, R.; Ramakrishna, S. Electrospayed nanoparticles for drug delivery and pharmaceutical applications. *Biomatter* **2013**, *3* (3). DOI: 10.4161/biom.24281.

(36) Pan Ch, J.; Tang, J. J.; Weng, Y. J.; Wang, J.; Huang, N. Preparation, characterization and anticoagulation of curcumin-eluting controlled biodegradable coating stents. *J Control Release* **2006**, *116* (1), 42-49. DOI: 10.1016/j.jconrel.2006.08.023.

(37) Fernandes Queiroz, M.; Melo, K. R.; Sabry, D. A.; Sasaki, G. L.; Rocha, H. A. Does the use of chitosan contribute to oxalate kidney stone formation? *Mar Drugs* **2014**, *13* (1), 141-158. DOI: 10.3390/md13010141.

(38) Lorenzo-Lamosa, M. L.; Remunan-Lopez, C.; Vila-Jato, J. L.; Alonso, M. J. Design of microencapsulated chitosan microspheres for colonic drug delivery. *J Control Release* **1998**, *52* (1-2), 109-118. DOI: 10.1016/s0168-3659(97)00203-4.

(39) Nair, R. S.; Morris, A.; Billa, N.; Leong, C. O. An Evaluation of Curcumin-Encapsulated Chitosan Nanoparticles for Transdermal Delivery. *AAPS PharmSciTech* **2019**, *20* (2), 69. DOI: 10.1208/s12249-018-1279-6.

(40) Sabra, R.; Billa, N.; Roberts, C. J. An augmented delivery of the anticancer agent, curcumin, to the colon. *Reactive and Functional Polymers* **2018**, *123*, 54-60.

(41) Vllasaliu, D.; Exposito-Harris, R.; Heras, A.; Casettari, L.; Garnett, M.; Illum, L.; Stolnik, S. Tight junction modulation by chitosan nanoparticles: comparison with chitosan solution. *Int J Pharm* **2010**, *400* (1-2), 183-193. DOI: 10.1016/j.ijpharm.2010.08.020.



---

# *CHAPTER 5*

---

Cetuximab Conjugated Eugenol Loaded Carboxymethyl  
Cellulose Nanoparticles for Active Targeting Anti-cancer  
Therapy



## **5.1 Introduction**

Current cancer therapies are focusing on the specific delivery of the drugs or bioactive molecules to the tumor site. Application of NDDS can provide two alternates for drug targeting viz, passive and active. In our thesis work, we have investigated the passive targeting ability of polymeric NDDS as an anti-cancer system. However, in the current chapter, we have researched the potential of active targeting of NDDS using a monoclonal antibody, for cancer therapy. Active targeting or tumor-activated prodrug therapy is based on the activation of the NDDS upon reaching the tumor site<sup>1</sup>. They depend on the interactions with the molecules present on the surface of cancerous cells and not the healthy cells. Tumor cells upregulate certain kinds of receptors that promote tumor growth, proliferation, angiogenesis, survival in low oxygen levels, and pH conditions<sup>2</sup>. Among them, epidermal growth factor receptor (EGFR) is one such moiety that is overexpressed in glioma, colorectal, head, neck, non-small cell lung, ovarian, breast, and prostate cancers<sup>3,4</sup>. Therefore, EGFR has become a strategy for active targeting by attaching anti-EGFR molecules like peptides, oligonucleotides, and antibodies to NDDS<sup>5</sup>. Recent research is inclined towards antibody immunotherapy for the treatment of cancer. For this purpose, FDA-approved antibodies like cetuximab and trastuzumab are being suggested<sup>5</sup>. Herein, we have selected cetuximab (Cet) a monoclonal antibody (mAb) approved for colorectal carcinoma, head and neck cancers, gastric adenocarcinoma treatment in combination with chemotherapeutic agents<sup>6,7</sup>. Accordingly, Cet has been utilized to conjugate to polymeric nanoparticles (NPs) as anti-cancer NDDS<sup>8</sup>. For example; Liu et al conjugated Cet to poly (lactic acid-co-l-lysine) NPs for effective uptake of (PLA-PLL-EGFRmAb) NPs in hepatocellular carcinoma<sup>9</sup>. Likewise, Maya et al, reported Cet conjugated O-carboxymethyl chitosan (O-CMC) NPS, for targeted delivery of paclitaxel (PTXL) to EGFR over-expressing cancer cells<sup>10</sup>. Similarly, Deepagan et al investigated Cet conjugated PLGA-ZnS NPs for targeted imaging and delivery of camptothecin, their studies demonstrated higher uptake and cytotoxicity of camptothecin in cell lines that overexpress the EGFR<sup>11</sup>.

Eugenol (Eu) is phytochemical known to have anti-inflammatory, antiviral, antibacterial, antioxidant, anticancer properties<sup>12,13,14</sup>. It has been reported to arrest the

---

cells in S-phase and induce apoptosis in cancer cells like melanoma, leukemia, and colon cancer<sup>15</sup>. Like other active phytochemicals, it is highly volatile, unstable, and sensitive to oxygen, light, and heat during processing, utilization, and storage<sup>16,17</sup>. One of the preferred mechanisms to overcome the shortcomings of such phytochemicals is nanoencapsulation in biodegradable polymers. Likewise, Eu has been reported to be encapsulated in lipids and polymers<sup>18,19</sup>. In our investigations, we are focusing on the use of natural polysaccharides and their derivatives. Accordingly, sodium carboxymethyl cellulose (CMC) was chosen to investigate its potential as a nanocarrier. It is a water-soluble versatile polymer and is being used extensively in the food industry and pharmaceuticals for encapsulation and delivery of bioactive molecules as its functional groups make it attractive for modifications<sup>20,21,22</sup>. Further, CMC being biocompatible, biodegradable, and bio-eliminable, has been approved by the FDA for parenteral application in pharmaceutical formulations such as Sandostatin, Sandolog, and Vivitrol<sup>23</sup>. CMC and its conjugates have been reported to increase the bioavailability and pharmacokinetics of hydrophobic anti-cancer agents like docetaxel and doxorubicin<sup>20,24</sup>. Therefore, we have hypothesized the entrapment of eugenol in the matrix of CMC using a non-ionic surfactant like pluronic F127 (PF127). PF127 is a biocompatible triblock copolymer of poly(ethylene oxide) (PEO) and poly(propylene oxide) (PPO) with a PEO-PPO-PEO structure<sup>25</sup>. In an aqueous medium above the critical concentration PF127 forms micelles with the PPO segment forming the inner core accumulating the hydrophobic drugs. While the PEO segments form outer hydrated corona which is non-toxic and improves the PKs of the drug. Hence, the bioavailability and solubility of hydrophobic drugs are enhanced on encapsulation within PF127<sup>26,27</sup>. For example; Nguyen et al improved the loading efficiency and bioavailability of curcumin on entrapment in PF127-gelatin which led to better cytotoxicity against cancer cells in comparison to free curcumin<sup>28</sup>. Similarly, Manaspon et al, reported high drug loading and sustained release of DOX in a folate conjugated PF127/chitosan nanosystem leading to better efficiency than free DOX<sup>25</sup>. Nevertheless, the PF127 and CMC nanosystem for encapsulation of Eu with targeting moiety is yet to be studied.

---



Accordingly, in this study, we have attempted to develop NDDS by encapsulating Eu by PF127 and CMC, which is conjugated with Cet for targeted delivery to improve cancer therapy. The augmentation of NDDS was attained by conjugating Cet and increasing the bioavailability of hydrophobic, Eu by encapsulating with PF127 and CMC. The design and development of the targeted CMC NPs to deliver Eu and their physicochemical characterization, uptake, pharmacological efficacy in cultured cells are detailed in this chapter.

## **5.2 Experimental**

### **5.2.1 Materials**

Eugenol (Eu), pluronic F127 (PF127), 1-ethyl-3-(3-dimethylaminopropyl) carbodiimide (EDC), and rhodamine B were purchased from Sigma Aldrich, USA. Na-carboxymethyl cellulose (CMC) (2.5 lakhs mol wt) was procured from Fluka, Switzerland. Sulfo-NHS sodium salt was purchased BLDPharmatech, India. Cetuximab (5mg/mL) was procured from Merck, Germany. All salts and solvents were of analytical grade. Cell lines were obtained from the cell repository at National Centre for Cell Science (NCCS), Pune.

### **5.2.2 Preparation of Eu loaded CMC NPs**

Five weight percent of PF127 was dissolved in 50% aqueous ethanol solvent and stirred at room temperature for 2 h. In 20 mL of the above PF127 solution, 100  $\mu$ L of Eu was slowly added while sonicating in an ultra-probe sonicator (VCX 500, Vibra-Cell, Sonics, USA) at 40% amplitude with a sonication time of 5 seconds on and 5 seconds off to obtain 0.5% (v/v) Eu-PF127 emulsion. Similarly, 200 and 400  $\mu$ L Eu was also added to another 20 mL batches of PF127 solutions to achieve 1 and 2% (v/v) Eu-PF127 emulsions respectively. CMC solution were prepared by dissolving NaCMC in DI water at 0.5 and 1.0 wt% at RT. To this CMC solution, the respective Eu-PF127 emulsion was slowly added dropwise while stirring on a magnetic stirrer at a constant rate. The prepared mixture was left open in a hood to evaporate the ethanol from the solution. Thereafter, while stirring vigorously, 1 wt% CaCl<sub>2</sub> solution was added

---

dropwise slowly until the solution turned opalescent. Likewise, the various formulations of CMC NP with and without Eu were prepared. The respective opalescent formulations were centrifuged at 17,000 rpm for 30 min at 16 °C and the pellet was freeze-dried for further characterization, while the supernatant was used for estimation of encapsulation efficiency. The different formulations that were prepared are shown in Table 5.1

**Table 5.1** Formulations of CMC NPs

Batch No.	Eu% (v/v)	PF127% (w/v)	CMC% (w/v)	Hydrodynamic diameter (nm)	PDI	Drug encapsulation efficiency (%)
A1.	0.5	5	0.5	243.7	0.369	70.12
A2.	1	5	0.5	402.4	0.470	73.43
A3.	2	5	0.5	445.5	0.418	79.12
A4.	-	5	0.5	496.2	0.404	
B1.	2	5	1	302.8	0.350	71.33
B2.	2	5	1	260.7	0.434	75.46
B3.	2	5	1	342.7	0.407	83.33
B4.		5	1	472.2	0.309	

### 5.2.3 Physicochemical characterization of NPs

Among the various formulations that were prepared (Table 1), B3 and B4 were selected for further studies as they were more suitable (more groups available for Cet conjugation). These NPs were characterized by various techniques like DLS, FE-SEM, HRTEM, FTIR, DSC, etc to determine their morphology and evaluate their chemical components. The drug encapsulation efficiency and *in vitro* drug release were also performed to study the drug delivery ability of the developed NPs. The NPs were dispersed in DI water (0.22 µm syringe filtered) and their hydrodynamic diameter was measured using the DLS instrument (90 Plus Brookhaven Instruments Corp, PALS zeta potential analyzer, USA). The morphology and size of the prepared NPs were evaluated by electron microscopy like FE-SEM (FEI NOVA NANOSEM 450, 30kV field emission scanning electron microscope, USA) and HRTEM (JEOL JEM F200, 200kV

---

FEG high-resolution transmission electron microscope, Japan). Briefly, NPs diluted (5X) in Millipore water were drop-cast on a silicon wafer and allowed to dry followed by gold coating for FE-SEM analysis. For HRTEM analysis, diluted NPs were stained with 1% (w/v) uranyl acetate dye and drop-cast on copper grid mesh before imaging. FTIR spectroscopy analysis was conducted on Eu, bare polymers (CMC and PF127), and Eu-loaded NPs (B1 to B4) to confirm the functional interactions with Eu. For FTIR, samples (2–3 mg) were ground with anhydrous potassium bromide, KBr, (97 mg) to form a pellet, which was used for analysis (PerkinElmer spectrometer I, FT-IR diffuse reflectance (DRIFT) mode, USA). The scans were recorded from 400 cm<sup>-1</sup> to 4000 cm<sup>-1</sup> with an average of 32 scans per sample. Thermal analysis was carried out using DSC (Model Q100 DSC, TA instruments, Newcastle, DE, USA) to investigate the thermal properties of CMC and PF127 in their pristine form, and their NPs before (B4) and after Eu loading (B3). The samples were crimped in aluminum pans and the thermal properties were analyzed in cycles. In the first heating cycle, the temperature was ramped from -60 °C to 300 °C at a rate of 10 °C min<sup>-1</sup>. The sample was then cooled to -60 °C in the 2nd cycle at a rate of 10 °C min<sup>-1</sup>, and in the third heating cycle, the temperature was ramped from -60 °C to 300 °C at a rate of 10 °C min<sup>-1</sup>. The entire experiment was done under nitrogen gas (50 mL min<sup>-1</sup>). An empty aluminum pan was used as a reference pan.

#### 5.2.4 Drug encapsulation efficiency and *in vitro* release

The drug encapsulation efficiency percentage was determined using a UV-vis spectrophotometer (UV 1601 PC UV spectrophotometer, Shimadzu, Japan). Briefly, after the formation of opalescent solution on addition of CaCl<sub>2</sub>, the resultant solution was centrifuged at 17,000 rpm for 30 min at 16 °C. The supernatant obtained after the centrifugation was analyzed using a UV-Vis spectrophotometer at λ<sub>max</sub> of 282 nm the concentration was determined by a standard curve of known concentrations of the drug. The drug encapsulation efficiency percentage was calculated using the following equation:

$$\text{Drug encapsulation efficiency (\%)} = \frac{\text{wt of loaded Eu}}{\text{wt of feeding Eu}} \times 100 \quad \dots\dots(1)$$

---

For *in vitro* drug release, Eu loaded A3 and B3 NPs were weighed at 20 mg and dispersed in 10 mL of 5.5 and 7.4 pH buffer each (in duplicates). This dispersion was then packed in an activated dialysis bag (12 KDa) and later immersed in a container containing 40 mL of dissolution media (5.5 or 7.4 pH). The container was thereafter placed in a water bath shaker maintained at 37±5 °C at 100 rpm. After regular set intervals, 2 mL was withdrawn from the dissolution media and 2 mL of fresh buffer was replaced to maintain sink conditions. The withdrawn solution was analyzed in a UV-Vis spectrophotometer like the method used for the encapsulation study to calculate cumulative Eu release.

$$\text{Cumulative drug release (\%)} = \frac{\text{wt of Eu released}}{\text{wt of Eu in NPs}} \times 100 \quad \dots\dots\dots(2)$$

### 5.2.5 Preparation of Cet-CMC NPs

To conjugate Cet to the surface of Eu loaded B3 and blank B4 NPs, EDC/sulfo-NHS cross-linking chemistry was implemented<sup>29,11</sup>. Briefly, 20 mg of B3 NPs were dispersed in 10 mL MES buffer (0.1 M, 0.5 M NaCl, pH 6.5) and treated with 10 mg (2 mM) EDC.HCl by stirring at RT for 15 min to activate the carboxyl groups of CMC NPs. Later, 6 mg (5 mM) of sulfo NHS was added to the reaction mixture and stirred for 15 min at RT to stabilize the activated carboxyl groups of the NPs. Later, the stirring was stopped and the reaction mixture was stored at 4 °C for 2.5 h, followed by centrifugation at 18,000 rpm for 25 min at 14 °C. The obtained pellet was dispersed in MES buffer (pH 6.5) and repeated centrifugation to wash off the unreacted EDC and sulfo NHS. Further, the pellet was resuspended in buffer and added 200 µL of Cet (5 mg/mL stock in PBS) to the dispersion and stirred for 2.5 h at RT. Later this dispersed mixture was stored overnight at 4 °C. The subsequent day, the reaction mixture was centrifuged at 18,000 rpm for 32 min, the obtained pellet was dispersed in buffer, and collected the supernatant to determine the unreacted Cet concentration. A similar reaction procedure was followed for the formulation of B4 NPs.

The conjugation of Cet on the surface of the compositions B3 and B4 NPs was confirmed by BCA (Bicinchoninic acid) colorimetric assay. Briefly, a known amount of NPs reacted with Cet was mixed with the reaction mixture (BCA:CuSO<sub>4</sub> in 49:1

---

---

ratio) in the ratio of 1:10. This mixture was mixed homogeneously and incubated in dark for 30 min at 37 °C. The supernatant obtained after centrifugation of the Cet conjugated dispersion was mixed with the BCA reaction mixture and incubated at similar conditions to determine the unreacted Cet. After incubation, the OD was recorded at 550 nm in a microplate reader (Multiskan Ex, (51118170(200–240 V) Thermo Scientific, Finland)) and the unknown concentration of Cet was estimated from a standard curve of Cet (concentrations ranged 50 µg/mL to 250 µg/mL).

### 5.2.6 Hemolysis assay

To study the biocompatibility of the B3 and B4 NPs on RBCs (red blood cells), hemolysis assay was conducted. Briefly, blood was collected in tubes containing EDTA from healthy volunteers at National Chemical Laboratory, Pune, India. The RBCs were separated from the whole blood by density gradient centrifugation. For instance, 5 mL whole blood was added slowly in 5 mL of PBS and centrifuged at 2000 rpm for 30 min. The supernatant devoid of RBCs was discarded and the pellet was washed thrice with PBS and centrifuged again for 30 min at 2000 rpm. Later, the cells were dispersed in PBS to prepare a stock dispersion of 2% (v/v). Further, 2 mL of this stock dispersion was dispensed in 2 mL vials in duplicates, to the respective vials, test samples such as CMC, PF127, B3, and B4 at a concentration of 0.5 mg/mL and 1 mg/mL were added. The respective controls like RBC suspension in PBS (negative) and RBC suspension in DI water (positive) were prepared. All the respective test samples and controls were incubated at 37 °C for 2 h with gentle shaking for every 30 min to re-suspend the precipitated RBCs. After the incubation period, the suspensions were centrifuged at 1500 g for 10 min at RT. The supernatant obtained was dispensed in a 96 well plate and the hemoglobin (Hb) release was read in a microtiter plate reader spectrophotometrically at 550 nm (Multiskan Ex, (51118170(200–240 V) Thermo Scientific, Finland)). Considering 100% lysis of cells in DI water and 0% lysis in PBS, the percentage of hemolysis for test samples was calculated using the following equation.

$$\text{Hemolysis (\%)} = \frac{\text{Abs.test} - \text{Abs.negative control}}{\text{Abs.positive control} - \text{Abs.negative control}} \times 100 \dots\dots(3)$$

### 5.2.7 Cell studies

Fibroblast cell line L929 and lung cancer cell line A549 were maintained in DMEM supplemented with 10% FBS under standard conditions at 37 °C, in a humidified CO<sub>2</sub> incubator. The cells were routinely grown as monolayer cultures in a 25cm<sup>2</sup> flask and passaged once a week using trypsin/EDTA at 80% confluence.

**Cytotoxicity assay:** Eu loaded NPs were investigated for their cellular toxicity in L929 fibroblast cells by MTT assay. A confluent flask of L929 cells was trypsinized to harvest cells which were further seeded in a 96 well plate at 10,000 cells/well. The plate was incubated at 37°C, in a 5% CO<sub>2</sub> humidified atmosphere for 16 h to allow cells to attach and form a monolayer. Later, the media from the wells was flicked off and added B3 NPs. The stock concentration of NPs at 1 mg/mL was prepared in serum-free media. From these, a series of concentrations ranging from 0 to 500 µg/mL was added to the respective wells and incubated for 48 h. Post incubation, the media was tipped off from the wells and the MTT solution prepared in DMEM-FBS media was added to the wells. Following, the plate was incubated in dark at 37 °C, in a humidified CO<sub>2</sub> incubator for 4 h. Finally, the MTT media in the wells was replaced with 100 µL DMSO and the plate was read at 550 nm in a plate reader (Multiskan Ex, (51118170(200–240 V) Thermo Scientific, Finland)). Cells grown in the wells devoid of any test sample were considered as positive control and the cells incubated in the media with 30% DMSO (v/v) were the negative control. The relative cell viability was calculated by comparing the absorbance read in test samples to positive control [(Abs.sample/Abs.positive control) x 100]. The data were presented as average ± SD (n=3). Similarly, the MTT assay was also carried out for B3 and B4 NPs with and without Cet conjugation, in A549 cells for 24 h.

**In vitro cellular uptake:** The uptake of the B3 and B4 NPs with and without Cet was studied in A549 cells. The NPs were stained with rhodamine B (5 mg/mL) overnight in dark and washed with PBS. A count of 5x10<sup>4</sup> cells was seeded on sterile 12 mm round coverslips placed in a 24 well plate and incubated for 24 h at 37 °C in a 5% CO<sub>2</sub> atmosphere. After incubation, the media were aspirated from the wells and washed thrice with PBS. Rhodamine-stained B3 and B4 NPs with and without Cet at a

---

concentration of 200 µg/mL were dispersed in the serum-free media and incubated for 2.5 h. Later, the cells were washed thrice with PBS and fixed by adding 300 µL of 4% paraformaldehyde and incubating for 15 min at RT. Post fixing step, the cells were washed extensively with PBS and stained with DAPI (300 nM) for 05 min in dark and washed off with PBS. Finally, the coverslips were mounted on a clean slide with the application of Fluoroshield mounting media. Excess mounting media was dabbed with tissue and the cells were visualized using an epifluorescence microscope by Carl Zeiss (Model: Axio Observer.Z1, Oil emersion objective, 63X). The nucleus stained with DAPI was observed under the blue channel and rhodamine B under the red channel.

### **5.3 Results and discussion**

A biodegradable nanosystem was prepared using biopolymer cellulose derivative, CMC to load an anti-cancer phytochemical, Eu. This entrapment of Eu in hydrophilic polymer CMC was facilitated by a non-ionic biocompatible surfactant PF127. To this nanoparticulate system, an active targeting monoclonal antibody Cet was conjugated *via* EDC/sulfoNHS coupling. The conjugation of Cet imparted specific targeting to the Eu-CMC NPs by directing those to cancer cells that have overexpressed EGFR receptors (like the A549 cell line).

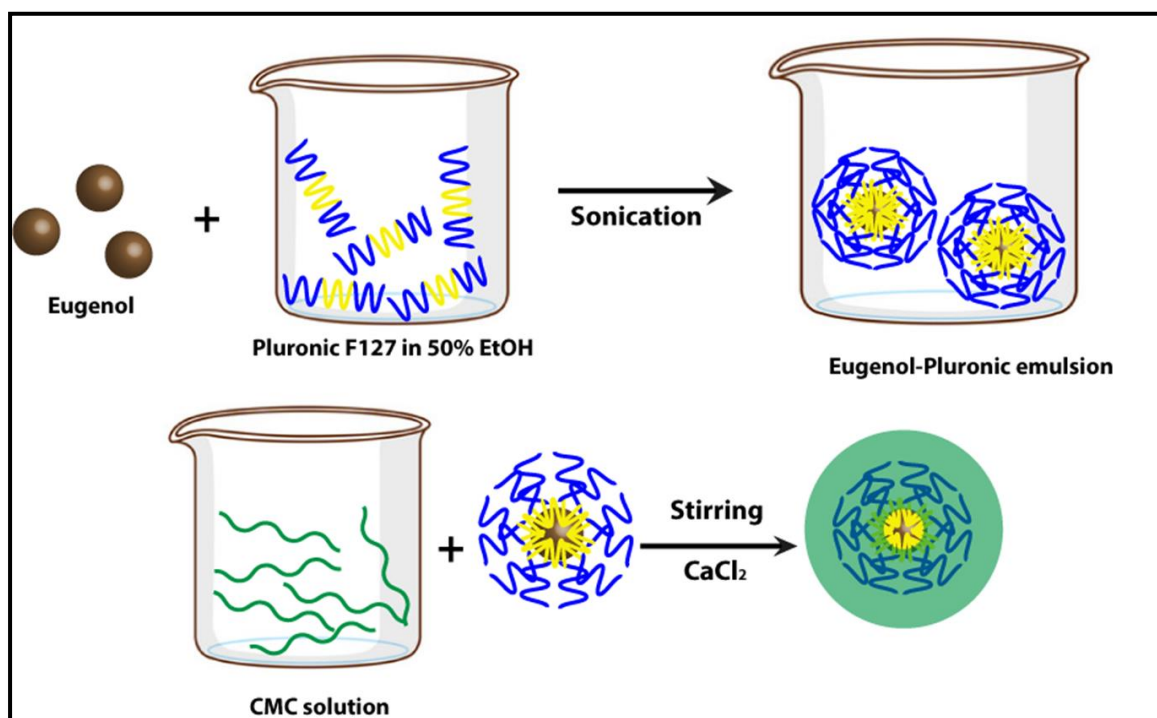


**Figure 5.1** Preparation of Eu loaded CMC NPs by emulsion-ionic gelation.

### 5.3.1 Preparation and physicochemical characterization of NPs

Eu loaded NPs were prepared by the formation of Eu-PF127 nanoemulsion followed by the coating with CMC *via* ionic gelation on the addition of CaCl<sub>2</sub> as shown in Figure 5.1. This process of emulsion-ionic crosslinking is non-toxic and an easy technique to encapsulate hydrophobic bioactive molecules as the crosslinker used is non-toxic. Similar studies are reported based on this technique to develop NPs<sup>30,31</sup>. Figure 5.2 shows the morphology, size of the prepared NPs, which were analyzed by FE-SEM, and HRTEM. The FE-SEM and HRTEM images of Eu loaded (B3) and blank (B4) NPs showed spherical NPs with an average size below 100 nm, which is lower than the mean diameter measured by the DLS method. It should be noted that the mean diameter of the NPs determined by the DLS method is dependent on the size of the biggest NP. Further, DLS measures the hydrodynamic diameter of the solvated NPs whereas, TEM measures dried NPs<sup>32,33</sup>. The CMC chains on the outer domain of the NPs are hydrophilic and hold water molecules which is reflected in the DLS measurements. The



net charge on all the formulations was between -10 to -20 mV, due to the carboxyl groups of CMC<sup>34</sup>.

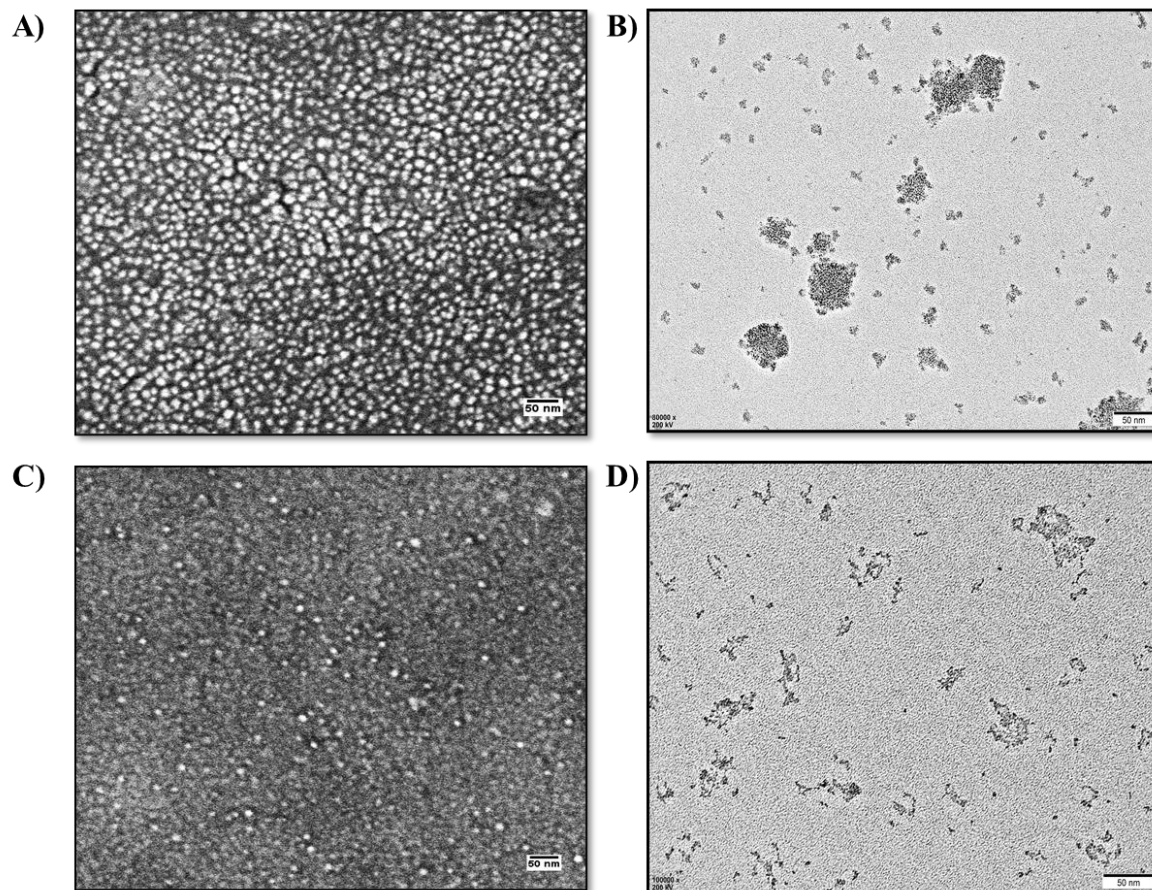


**Figure 5.2** A) FE-SEM image of B3 NPs, B) HRTEM image of B3 NPs, C) FE-SEM image of B4 NPs, D) HRTEM image of B4 NPs. (Scale bar = 50 nm).

The functional group interaction between polymers and their formulations of NPs was characterized by FTIR spectroscopy. FTIR spectrum of CMC (Figure 5.3A) showed characteristic peaks at  $3400\text{ cm}^{-1}$  due to O–H stretching,  $2920\text{ cm}^{-1}$  due to the asymmetric C–H stretching. The peak noticed at  $1060\text{ cm}^{-1}$  corresponds to the C–O–C group while the peaks at  $1602\text{ cm}^{-1}$  and  $1418\text{ cm}^{-1}$  were peculiar to asymmetric and stretching vibrations of the –COO group<sup>35,36</sup>. The bare PF127 (Figure 5.3B) recorded a broad absorption peak of the terminal O–H that appeared around  $3500\text{ cm}^{-1}$ . The characteristic band of the C–H bend was observed at  $2882\text{ cm}^{-1}$  and O–H bend at  $1343\text{ cm}^{-1}$ . The peak visible at  $1112\text{ cm}^{-1}$  was due to the C–O stretching<sup>37,38</sup>. The spectrum

of Eu as shown in Figure 5.3C, indicated a strong peak at  $3522\text{ cm}^{-1}$  corresponding to the O–H stretching. Multiple peaks are observed between  $2841$  to  $3076\text{ cm}^{-1}$  due to the C–H stretching. The peaks visible at  $1515\text{ cm}^{-1}$ ,  $1611\text{ cm}^{-1}$ , and  $1638\text{ cm}^{-1}$  were due to the aromatic C=C stretching. In addition, signature peaks in the  $720$ – $1270\text{ cm}^{-1}$  region corresponding to the C=C region were evident in the spectrum of Eu<sup>30,39</sup>. The FTIR spectrum of blank NPs (B4) (Figure 5.3D), possessed characteristic peaks: O–H stretching at  $3400\text{ cm}^{-1}$ , C–H stretching at  $1468\text{ cm}^{-1}$  and  $2882\text{ cm}^{-1}$ , asymmetric vibrations of –COO at  $1620\text{ cm}^{-1}$ , C–O stretching at  $1112\text{ cm}^{-1}$ . The FTIR spectrum of B3 NPs is shown in Figure 5.3E, the spectrum displayed the signature peak of  $1515\text{ cm}^{-1}$  belonging to aromatic C=C stretching of Eu along with the peaks that were present in the blank NPs spectrum. In the spectrum of Cet conjugated B3 NPs (Figure 5.3F), a peak at  $1635\text{ cm}^{-1}$  was recorded, which was attributed to the amide bond formed between the amino group of Cet and the acid group of CMC<sup>11,40</sup>. The observations from the FTIR spectra suggested encapsulation of Eu in the CMC-PF127 matrix and conjugation of Cet to the NPs.

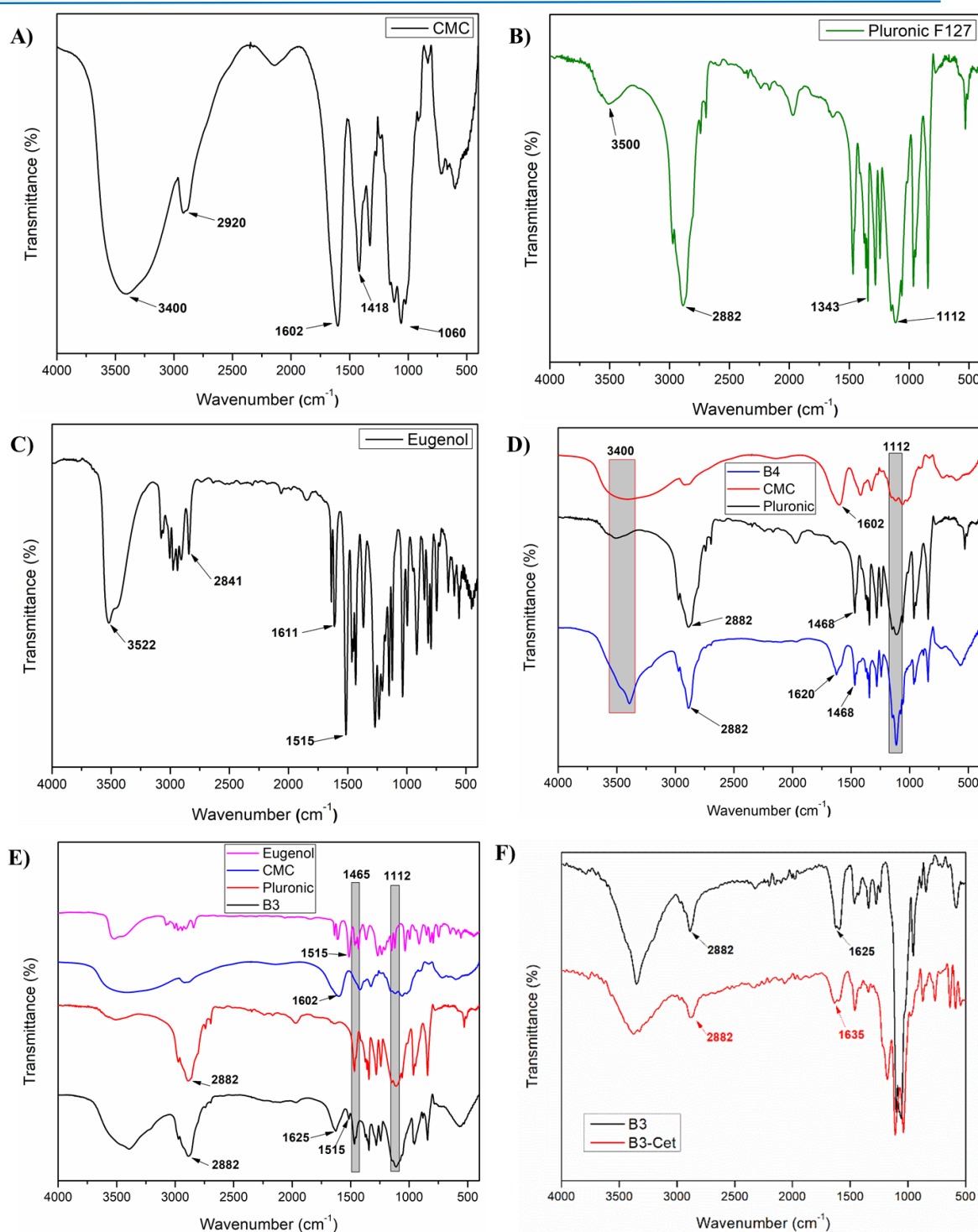


**Figure 5.3** FTIR spectrum of **A)** CMC, **B)** PF127, **C)** Eu, **D)** B4 NP with components, **E)** B3 NP with components, **F)** B3 NP with and without Cet.

Thermal properties of the pure polymers (CMC, PF127) and formulations with (B3) and without Eu (B4) are shown in Figures 5.4A and 5.4B. PF127 is a semi-crystalline

polymer and it displayed an endothermic peak at 55 °C, associated with its melting point ( $T_m$ )<sup>41,42</sup>. As reported the glass transition temperatures ( $T_g$ ) of the pure CMC were recorded at 90 °C (during the first heating cycle) which was due to the loss of water molecules and at 253 °C, which was due to partial oxidation of the sugar ring<sup>43,44</sup>. Also, with CMC being amorphous, the melting temperature was not recorded. The thermogram of Eu encapsulated B3 NPs (Figure 5.4B) did not record  $T_g$  of CMC as the CMC was crosslinked with  $CaCl_2$ . Further, there is a minor change in the  $T_m$  of PF127 in the thermogram of NPs which suggested the presence and interaction of PF127 with CMC and Eu. Eu being liquid the thermogram was not recorded. According to the reported literature, Eu displays a sharp endothermic peak at 258 °C which is due to its volatilization<sup>39,45</sup>. This peak did not appear in the thermogram of B3 NPs because of hydrophobic interactions between Eu and PF127. Similar studies were reported on the absence of endothermic peak of Eu<sup>46,39</sup>. Therefore, the thermal studies by DSC suggested the presence of Eu in well dispersed form within the matrix of PF127 and crosslinked CMC.

### 5.3.2 Drug loading and *in vitro* release

The entrapment efficiency for the various formulations is given in Table 5.1. From the experiments, we have noticed a higher drug entrapment efficiency of Eu with an increase in the drug concentration. But when the Eu concentration was increased above 2% (v/v), a viscous solution was formed, which could be due to the over-saturation of Eu in PF127. Therefore, 2% (v/v) is the ideal concentration of Eu which was present in batch A3 and B3 and these were selected for *in vitro* drug release studies. Accordingly, the release of Eu from the respective CMC NPs (A3 and B3) was studied *via* dialysis method at 37 °C using phosphate buffer of pH 5.5 and 7.4 respectively. As denoted in Figure 5.4C, A3 NPs (0.5 wt% CMC) recorded a faster release of Eu than B3 NPs (1 wt% CMC). After 36 h of release studies, it was observed that A3 NPs, recorded 98 and 94 % of Eu release at 5.5 and 7.4 pH respectively. Whereas, B3 NPs, recorded 78 and 72% of Eu release at 5.5 and 7.4 pH respectively. The difference in the release was due to the density of the CMC coating. B3 NPs being densely coated released less Eu as compared to A3 NPs. The slow and sustained release of Eu could be attributed to the

---

crosslinking between  $\text{CaCl}_2$  and CMC through electrostatic interactions and the swelling of water-soluble CMC in aqueous media<sup>47,48</sup>. Further, the equilibrium swelling of the NPs due to a prolonged incubation time led to a slow release of  $\text{Eu}^{36}$ . As the NPs followed the sustained release of EU molecules for a longer duration, this system can be suggested as a desirable candidate for drug delivery application.

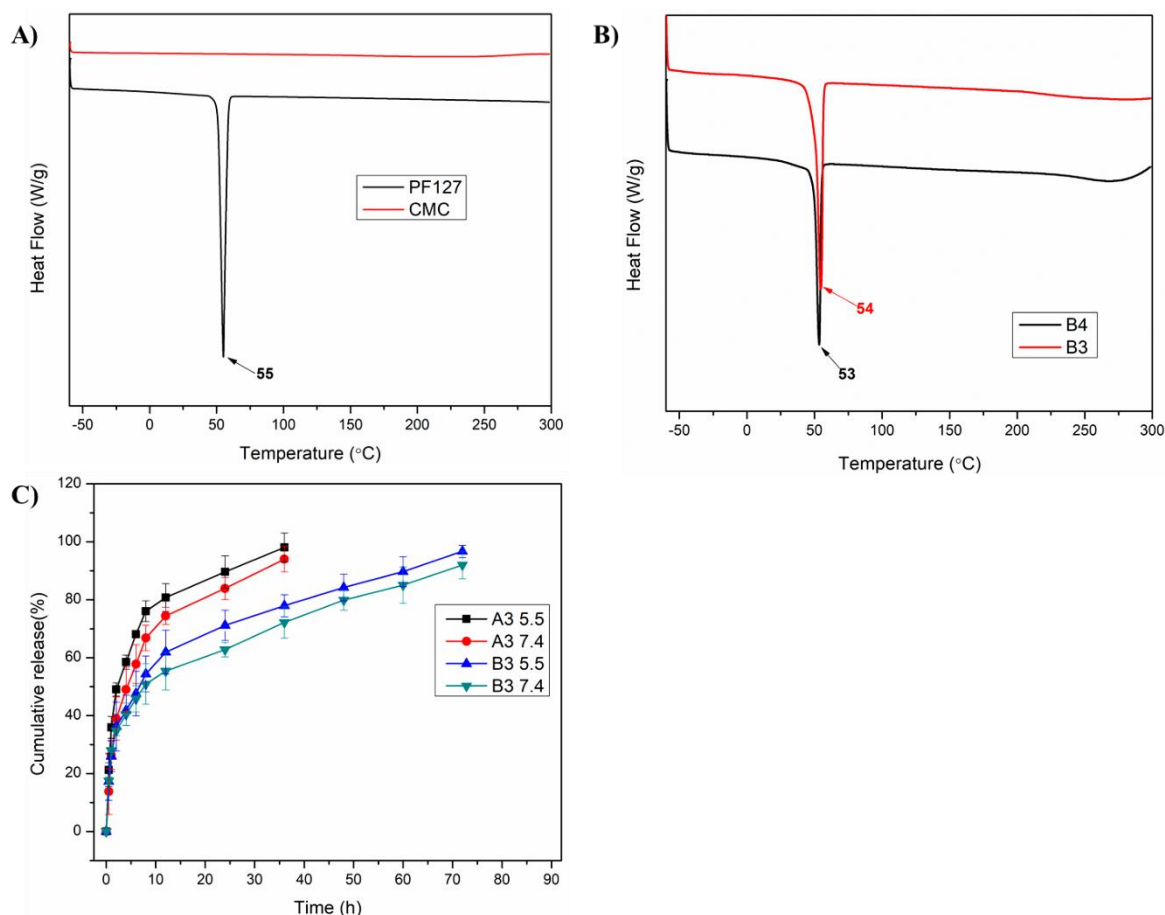


**Figure 5.4** A) DSC thermograms of CMC and PF127, B) DSC thermograms of B3 and B4 NPs, C) *In vitro* release profile of Eu.

### 5.3.3 Conjugation of Cet to NPs

An established chemical coupling reaction using EDC/sulfo NHS was performed to conjugate Cet to CMC NPs (B3 and B4). The carboxyl groups ( $-\text{COOH}$ ) of the CMC were available for crosslinking with the amino groups ( $-\text{NH}$ ) of the Cet to form a stable amide bond<sup>29</sup>. At acidic pH, the carboxyl groups of CMC NPs are activated by water-soluble crosslinker EDC forming O-acylisourea intermediate and the reverse reaction

was prevented by Sulfo NHS. This intermediate reacted with the amino group available on Cet to form an amide bond<sup>10,11</sup>. The complexation of Cet onto NPs was confirmed by the BCA assay, which estimates the protein concentration by estimation of colorimetric absorbance at 550 nm. After optimization of the reaction, we could achieve 42% conjugation efficiency which is in accordance with the reported literature<sup>40</sup>.

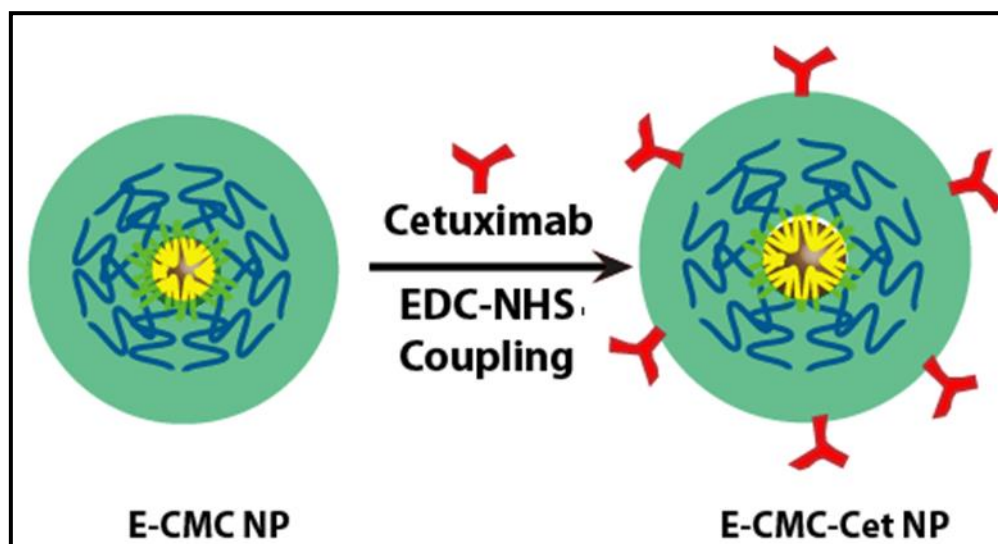


**Figure 5.5** Graphical representation of Cet conjugation to NPs.

### 5.3.4 Hemolysis assay

Hemolysis assay is demonstrated to validate the biocompatibility of biomaterial or polymer. According to the ASTM standards (E2524-08), hemolysis for the test samples above 5% indicates toxicity to the RBCs<sup>49</sup>. Likewise, the test samples NPs were assessed for their biocompatibility in human blood at a concentration of 0.5 and 1 mg/mL. The % of hemolysis was calculated from equation 2, considering 100% lysis in DI water and 0% lysis in PBS. In Figure 5.6A histogram, CMC and PF127 displayed less than 5% hemolysis hence, they can be termed as non-hemolytic material, and after the formation of NPs (B3 and B4), the material maintained its hemocompatibility. In the case of blank (B4) and Eu loaded (B3) NPs, even at a higher concentration of 1 mg/mL, the observed hemolysis was  $1.87 \pm 0.45$  and  $1.73 \pm 0.35\%$  respectively. The hemocompatibility of the NPs could be attributed to the hydrophilicity of CMC which

decreased the interaction with RBCs, therefore the extent of lysis was insignificant<sup>50</sup>. Further, Eu has been established as a non-hemolytic compound by various studies, according to the reports at a concentration of 2 mg/mL it induces only 4.4% hemolysis<sup>51,52,53</sup>. In line with these findings, we consider that the developed NPs are biocompatible and can be used as a potential nanocarrier for cancer therapy.

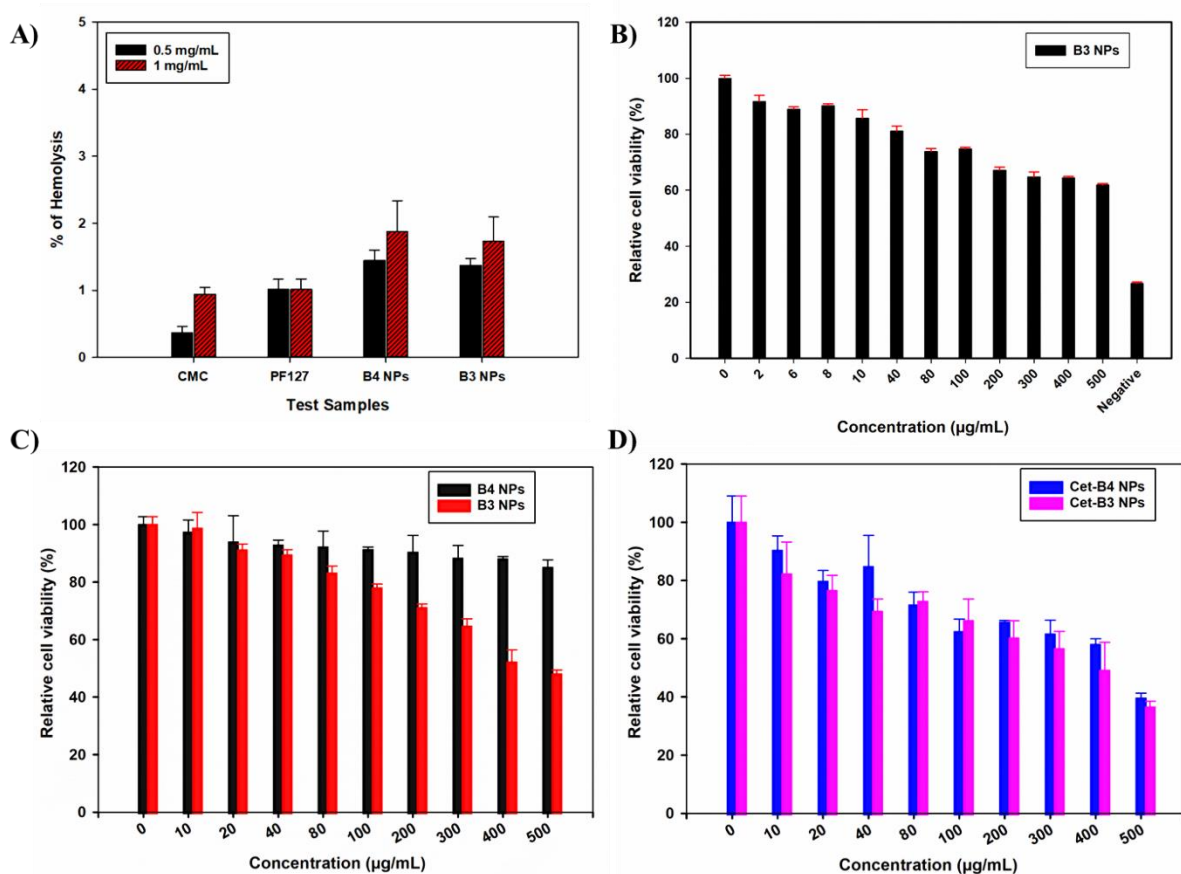


**Figure 5.6** **A)** % of Hemolysis on exposure to pristine polymers (CMC and PF127) and their blank (B4) and Eu loaded (B3) NPs, **B)** Cell viability of L929 cells treated by B3 NPs for 48 h. **C)** Cell viability of A549 cells treated by B3 and B4 NPs for 24 h. **D)** Cell viability of A549 cells treated by Cet conjugated B3 and B4 NPs for 24 h.

### 5.3.5 Cell studies

**Cytotoxicity assay:** The cytotoxicity of blank and Eu loaded NPs was determined by the MTT assay. The cytotoxic effects of Eu loaded B3 NPs were investigated in fibroblast L929 and lung cancer A549 cell lines. DMSO solubilized the formazan

crystals formed after the addition of the MTT reagent which indicated cellular respiratory activity. As shown in Figure 5.6B, B3 NPs exhibited no cellular toxicity towards L929 cells for up to 48 h of incubation with varying concentrations. The relative cell viability was above 60% even at the higher concentration of NPs at 500  $\mu\text{g/mL}$ . Thus, demonstrating the non-cytotoxic nature of the Eu loaded NPs and establishing them as promising drug delivery vehicle. The cytotoxic ability of B3 and B4 NPs was investigated in lung cancer cell lines, A549 for 24 h. From the histogram, as shown in Figure 5.6C, the Eu loaded B3 NPs recorded a decrease in cell viability as a function of Eu dose concentration. The concentration of the NPs was varied from 0  $\mu\text{g/mL}$  to 500  $\mu\text{g/mL}$ , and the  $\text{IC}_{50}$  (the dose inducing 50% cell inhibition) value noted for NPs in the cell line was around 400  $\mu\text{g/mL}$ . In the case of blank NPs (B4), we noticed no cytotoxicity even at higher concentrations of NPs. The conjugation of Cet to the NPs proved to be effective in inhibiting the A549 cancer cell line. The anti-cancer activity of Cet is well documented and as observed in Figure 5.6D, the NPs are exhibiting cytotoxicity on conjugation with Cet<sup>54,55,56</sup>. Further, Cet conjugated B3 NPs demonstrated higher toxicity towards A549 cells due to the combination of Eu and Cet. These results proved the competence of NPs as biocompatible and non-toxic DDS to deliver Eu at a controlled rate over an extended period.

***In vitro cellular uptake:*** The cellular uptake of B3 and B4 NPs with and without Cet was studied in EGFR+ve lung cancer cells A549 by incubating them with the samples in the media at 37 °C for 2.5 h, and later analyzed using epifluorescence microscopy. The nuclei of cells were stained with DAPI, and rhodamine B emitted red fluorescence. In the cells treated with NPs at 200  $\mu\text{g/mL}$ , it was observed that the red fluorescence of rhodamine B was located in the cytoplasmic region of cells treated with Cet-NPs compared to NPs without Cet (Figure 5.7). This observation leads to an inference that the Cet conjugated NPs were taken up by the cells via the receptor-mediated endocytosis pathway and were located in the intracellular compartment (endosomes and lysosomes), which is supported by the reported literature<sup>10,57</sup>. Thus, the microscopic images indicated the advantage of attaching targeting moiety (Cet) on NPs in their cellular internalization.

---



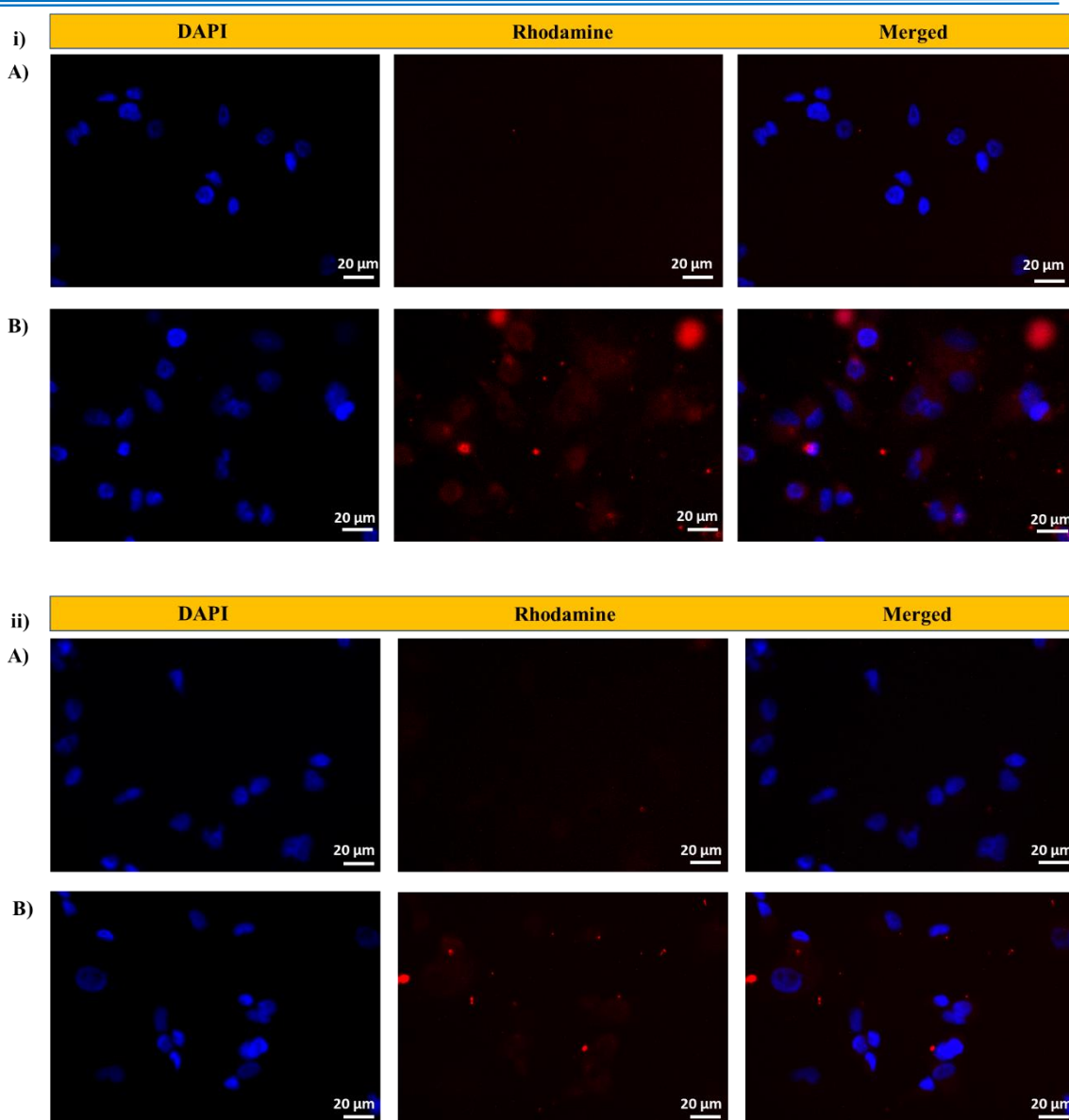


**Figure 5.7** Fluorescent images of A549 cells treated (for 2.5 h) with 200 μg/mL of **i)** **A)** B4 NPs without Cet, **B)** B4 NPs with Cet. **ii)** **A)** B3 NPs without Cet, **B)** B3 NPs with Cet. The right panels show the merged image of the nucleus stained with DAPI (blue), and NPs fluorescence red because of Rhodamine B staining. Scale bar corresponds to 20 μm.

#### 5.4 Conclusions

Active targeting of anti-cancer drugs or bioactive molecules *via* NDDS is a promising approach to circumvent their off-target effects during cancer therapy. In this chapter,

we have reported a Cet conjugated NDDS developed from biodegradable polymers like CMC and PF127 for targeted delivery of anti-cancer phytochemical Eu. Emulsion-ionic gelation technique was used to develop nano-sized NPs which exhibited high Eu encapsulation efficiency. These NPs were characterized by different techniques to confirm their physicochemical properties and they displayed sustained release at 5.5 and 7.4 pH up to 72 h. The NPs were non-toxic to the fibroblast cells L929 and demonstrated toxicity towards the cancer cell line, A549. The cellular uptake of the targeted NPs was analyzed qualitatively by fluorescent microscopy and showed enhanced uptake by EGFR over-expressing cancer cell line, A549. The above findings concluded that Cet conjugated NPs exhibit better selectivity for targeting cancer cells and contributed to the enhanced cytotoxicity. Among the various formulations studied, B3 composition was more preferable as NDDS, as the physicochemical properties and drug release studies were more favorable. Hence, the Eu loaded Cet-CMC NPs can be used as a potential NDDS to target EGFR overexpressing cancer cells.

## 5.5 References

- (1) Chari, R. V. J. Targeted delivery of chemotherapeutics: tumor-activated prodrug therapy. *Advanced drug delivery reviews* **1998**, 31 (1-2), 89-104.
- (2) Cavallaro, U. G. O.; Christofori, G. Multitasking in tumor progression: signaling functions of cell adhesion molecules. *Annals of the New York Academy of Sciences* **2004**, 1014 (1), 58-66.
- (3) Mendelsohn, J. The epidermal growth factor receptor as a target for cancer therapy. *Endocrine-related cancer* **2001**, 8 (1), 3-9.
- (4) Bianco, R.; Gelardi, T.; Damiano, V.; Ciardiello, F.; Tortora, G. Rational bases for the development of EGFR inhibitors for cancer treatment. *The international journal of biochemistry & cell biology* **2007**, 39 (7-8), 1416-1431.
- (5) Master, A. M.; Sen Gupta, A. EGF receptor-targeted nanocarriers for enhanced cancer treatment. *Nanomedicine* **2012**, 7 (12), 1895-1906.
- (6) Sakai, K.; Mori, S.; Kawamoto, T.; Taniguchi, S.; Kobori, O.; Morioka, Y.; Kuroki, T.; Kano, K. Expression of epidermal growth factor receptors on normal human gastric

epithelia and gastric carcinomas. *Journal of the National Cancer Institute* **1986**, 77 (5), 1047-1052.

(7) Rocha-Lima, C. M.; Soares, H. P.; Raez, L. E.; Singal, R. EGFR targeting of solid tumors. *Cancer control* **2007**, 14 (3), 295-304.

(8) Noh, T.; Kook, Y. H.; Park, C.; Youn, H.; Kim, H.; Oh, E. T.; Choi, E. K.; Park, H. J.; Kim, C. Block copolymer micelles conjugated with anti-EGFR antibody for targeted delivery of anticancer drug. *Journal of Polymer Science Part A: Polymer Chemistry* **2008**, 46 (22), 7321-7331.

(9) Liu, P.; Li, Z.; Zhu, M.; Sun, Y.; Li, Y.; Wang, H.; Duan, Y. Preparation of EGFR monoclonal antibody conjugated nanoparticles and targeting to hepatocellular carcinoma. *Journal of Materials Science: Materials in Medicine* **2010**, 21 (2), 551-556.

(10) Maya, S.; Kumar, L. G.; Sarmiento, B.; Rejinold, N. S.; Menon, D.; Nair, S. V.; Jayakumar, R. Cetuximab conjugated O-carboxymethyl chitosan nanoparticles for targeting EGFR overexpressing cancer cells. *Carbohydrate polymers* **2013**, 93 (2), 661-669.

(11) Deepagan, V. G.; Sarmiento, B.; Menon, D.; Nascimento, A.; Jayasree, A.; Sreeranganathan, M.; Koyakutty, M.; Nair, S. V.; Rangasamy, J. In vitro targeted imaging and delivery of camptothecin using cetuximab-conjugated multifunctional PLGA-ZnS nanoparticles. *Nanomedicine* **2012**, 7 (4), 507-519.

(12) Yogalakshmi, B.; Viswanathan, P.; Anuradha, C. V. Investigation of antioxidant, anti-inflammatory and DNA-protective properties of eugenol in thioacetamide-induced liver injury in rats. *Toxicology* **2010**, 268 (3), 204-212.

(13) Devi, K. P.; Nisha, S. A.; Sakthivel, R.; Pandian, S. K. Eugenol (an essential oil of clove) acts as an antibacterial agent against *Salmonella typhi* by disrupting the cellular membrane. *Journal of ethnopharmacology* **2010**, 130 (1), 107-115.

(14) Zheng, G.-Q.; Kenney, P. M.; Lam, L. K. T. Sesquiterpenes from clove (*Eugenia caryophyllata*) as potential anticarcinogenic agents. *Journal of natural products* **1992**, 55 (7), 999-1003.

(15) Jaganathan, S. K.; Mazumdar, A.; Mondhe, D.; Mandal, M. Apoptotic effect of eugenol in human colon cancer cell lines. *Cell biology international* **2011**, 35 (6), 607-615.

(16) Choi, M.-J.; Soottitantawat, A.; Nuchuchua, O.; Min, S.-G.; Ruktanonchai, U. Physical and light oxidative properties of eugenol encapsulated by molecular inclusion and emulsion–diffusion method. *Food Research International* **2009**, 42 (1), 148-156.

- (17) Garg, A.; Singh, S. Enhancement in antifungal activity of eugenol in immunosuppressed rats through lipid nanocarriers. *Colloids and Surfaces B: Biointerfaces* **2011**, 87 (2), 280-288.
- (18) Maurer, N.; Fenske, D. B.; Cullis, P. R. Developments in liposomal drug delivery systems. *Expert opinion on biological therapy* **2001**, 1 (6), 923-947.
- (19) Mourtzinou, I.; Kalogeropoulos, N.; Papadakis, S. E.; Konstantinou, K.; Karathanos, V. T. Encapsulation of nutraceutical monoterpenes in  $\beta$ -cyclodextrin and modified starch. *Journal of food science* **2008**, 73 (1), S89-S94.
- (20) Ernsting, M. J.; Foltz, W. D.; Undzys, E.; Tagami, T.; Li, S.-D. Tumor-targeted drug delivery using MR-contrasted docetaxel-carboxymethylcellulose nanoparticles. *Biomaterials* **2012**, 33 (15), 3931-3941.
- (21) Zhu, K.; Ye, T.; Liu, J.; Peng, Z.; Xu, S.; Lei, J.; Deng, H.; Li, B. Nanogels fabricated by lysozyme and sodium carboxymethyl cellulose for 5-fluorouracil controlled release. *International journal of pharmaceutics* **2013**, 441 (1-2), 721-727.
- (22) Ernsting, M. J.; Tang, W.-L.; MacCallum, N. W.; Li, S.-D. Preclinical pharmacokinetic, biodistribution, and anti-cancer efficacy studies of a docetaxel-carboxymethylcellulose nanoparticle in mouse models. *Biomaterials* **2012**, 33 (5), 1445-1454.
- (23) Ernsting, M. J.; Tang, W.-L.; MacCallum, N.; Li, S.-D. Synthetic modification of carboxymethylcellulose and use thereof to prepare a nanoparticle forming conjugate of docetaxel for enhanced cytotoxicity against cancer cells. *Bioconjugate chemistry* **2011**, 22 (12), 2474-2486.
- (24) Qian, H.; Wang, X.; Yuan, K.; Xie, C.; Wu, W.; Jiang, X.; Hu, L. Delivery of doxorubicin in vitro and in vivo using bio-reductive cellulose nanogels. *Biomaterials science* **2014**, 2 (2), 220-232.
- (25) Manaspon, C.; Viravaidya-Pasuwat, K.; Pimpha, N. Preparation of folate-conjugated pluronic F127/chitosan core-shell nanoparticles encapsulating doxorubicin for breast cancer treatment. *Journal of Nanomaterials* **2012**, 2012.
- (26) Torchilin, V. P. Structure and design of polymeric surfactant-based drug delivery systems. *Journal of controlled release* **2001**, 73 (2-3), 137-172.
- (27) Wagh, V. T.; Jagtap, V. A.; Shaikh, T. J.; Nandedkar, S. Y. Formulation and Evaluation of Glimepiride Solid Dispersion Tablets for Their Solubility Enhancement. *Journal of Advanced Scientific Research* **2012**, 3 (4).
- (28) Nguyen, D. T.; Dinh, V. T.; Dang, L. H.; Nguyen, D. N.; Giang, B. L.; Nguyen, C. T.; Nguyen, T. B. T.; Thu, L. V.; Tran, N. Q. Dual interactions of amphiphilic gelatin
-

copolymer and nanocurcumin improving the delivery efficiency of the nanogels. *Polymers* **2019**, *11* (5), 814.

(29) Kocbek, P.; Obermajer, N.; Cegnar, M.; Kos, J.; Kristl, J. Targeting cancer cells using PLGA nanoparticles surface modified with monoclonal antibody. *Journal of controlled release* **2007**, *120* (1-2), 18-26.

(30) Woranuch, S.; Yoksan, R. Eugenol-loaded chitosan nanoparticles: I. Thermal stability improvement of eugenol through encapsulation. *Carbohydrate polymers* **2013**, *96* (2), 578-585.

(31) Keawchaon, L.; Yoksan, R. Preparation, characterization and in vitro release study of carvacrol-loaded chitosan nanoparticles. *Colloids and surfaces B: Biointerfaces* **2011**, *84* (1), 163-171.

(32) Leitner, S.; Grijalvo, S.; Solans, C.; Eritja, R.; García-Celma, M. J.; Calderó, G. Ethylcellulose nanoparticles as a new “in vitro” transfection tool for antisense oligonucleotide delivery. *Carbohydrate polymers* **2020**, *229*, 115451.

(33) Singam, A.; Killi, N.; Patel, P. R.; Gundloori, R. V. N. PEGylated ethyl cellulose micelles as a nanocarrier for drug delivery. *RSC Advances* **2021**, *11* (49), 30532-30543.

(34) Song, Y.; Chen, L. Effect of net surface charge on physical properties of the cellulose nanoparticles and their efficacy for oral protein delivery. *Carbohydrate polymers* **2015**, *121*, 10-17.

(35) Butun, S.; Ince, F. G.; Erdugan, H.; Sahiner, N. One-step fabrication of biocompatible carboxymethyl cellulose polymeric particles for drug delivery systems. *Carbohydrate polymers* **2011**, *86* (2), 636-643.

(36) Liang, H.; Huang, Q.; Zhou, B.; He, L.; Lin, L.; An, Y.; Li, Y.; Liu, S.; Chen, Y.; Li, B. Self-assembled zein–sodium carboxymethyl cellulose nanoparticles as an effective drug carrier and transporter. *Journal of Materials Chemistry B* **2015**, *3* (16), 3242-3253.

(37) Karolewicz, B.; Górniak, A.; Owczarek, A.; Żurawska-Płaksej, E.; Piwowar, A.; Pluta, J. Thermal, spectroscopic, and dissolution studies of ketoconazole–Pluronic F127 system. *Journal of Thermal Analysis and Calorimetry* **2014**, *115* (3), 2487-2493.

(38) Shaikh, S.; Ray, D.; Aswal, V. K.; Sharma, R. K. Incorporation of lamotrigine drug in the PEO–PPO–PEO triblock copolymer (pluronic F127) micelles: Effect of hydrophilic polymers. *Journal of Surfactants and Detergents* **2017**, *20* (3), 695-706.

(39) Pramod, K.; Suneesh, C. V.; Shanavas, S.; Ansari, S. H.; Ali, J. Unveiling the compatibility of eugenol with formulation excipients by systematic drug–excipient compatibility studies. *Journal of Analytical Science and Technology* **2015**, *6* (1), 1-14.

---

- (40) Maya, S.; Sarmiento, B.; Lakshmanan, V.-K.; Menon, D.; Jayakumar, R. Actively targeted cetuximab conjugated  $\gamma$ -poly (glutamic acid)-docetaxel nanomedicines for epidermal growth factor receptor over expressing colon cancer cells. *Journal of biomedical nanotechnology* **2014**, *10* (8), 1416-1428.
- (41) da Silva, J. B.; Dos Santos, R. S.; da Silva, M. B.; Braga, G.; Cook, M. T.; Bruschi, M. L. Interaction between mucoadhesive cellulose derivatives and Pluronic F127: Investigation on the micelle structure and mucoadhesive performance. *Materials Science and Engineering: C* **2021**, *119*, 111643.
- (42) Djekic, L.; Čalija, B.; Medarević, Đ. Gelation behavior, drug solubilization capacity and release kinetics of poloxamer 407 aqueous solutions: The combined effect of copolymer, cosolvent and hydrophobic drug. *Journal of Molecular Liquids* **2020**, *303*, 112639.
- (43) Kurdtabar, M.; Heris, S. S.; Dezfulian, M. Characterization of a Multi-responsive Magnetic Graphene Oxide Nanocomposite Hydrogel and Its Application for DOX Delivery. *Chinese J. Polym. Sci* **2021**.
- (44) Li, W.; Sun, B.; Wu, P. Study on hydrogen bonds of carboxymethyl cellulose sodium film with two-dimensional correlation infrared spectroscopy. *Carbohydrate polymers* **2009**, *78* (3), 454-461.
- (45) Monteiro, O. S.; Souza, A. G.; Soledade, L. E. B.; Queiroz, N.; Souza, A. L.; Mouchrek Filho, V. E.; Vasconcelos, A. F. F. Chemical evaluation and thermal analysis of the essential oil from the fruits of the vegetable species *Pimenta dioica* Lindl. *Journal of Thermal Analysis and Calorimetry* **2011**, *106* (2), 595-600.
- (46) Agustinisari, I.; Mulia, K.; Nasikin, M. The effect of eugenol and chitosan concentration on the encapsulation of eugenol using whey protein–maltodextrin conjugates. *Applied Sciences* **2020**, *10* (9), 3205.
- (47) Cai, X.; Luan, Y.; Dong, Q.; Shao, W.; Li, Z.; Zhao, Z. Sustained release of 5-fluorouracil by incorporation into sodium carboxymethylcellulose sub-micron fibers. *International journal of pharmaceutics* **2011**, *419* (1-2), 240-246.
- (48) Liang, H.; He, L.; Zhou, B.; Li, B.; Li, J. Folate-functionalized assembly of low density lipoprotein/sodium carboxymethyl cellulose nanoparticles for targeted delivery. *Colloids and Surfaces B: Biointerfaces* **2017**, *156*, 19-28.
- (49) Choi, J.; Reipa, V.; Hitchins, V. M.; Goering, P. L.; Malinauskas, R. A. Physicochemical characterization and in V itro hemolysis evaluation of silver nanoparticles. *Toxicological Sciences* **2011**, *123* (1), 133-143.
- (50) Jhong, J.-F.; Venault, A.; Hou, C.-C.; Chen, S.-H.; Wei, T.-C.; Zheng, J.; Huang, J.; Chang, Y. Surface zwitterionization of expanded poly (tetrafluoroethylene)
-

membranes via atmospheric plasma-induced polymerization for enhanced skin wound healing. *ACS applied materials & interfaces* **2013**, 5 (14), 6732-6742.

(51) He, M.; Du, M.; Fan, M.; Bian, Z. In vitro activity of eugenol against *Candida albicans* biofilms. *Mycopathologia* **2007**, 163 (3), 137-143.

(52) Dubey, K.; Anand, B. G.; Shekhawat, D. S.; Kar, K. Eugenol prevents amyloid formation of proteins and inhibits amyloid-induced hemolysis. *Scientific reports* **2017**, 7 (1), 1-11.

(53) Hemaiswarya, S.; Doble, M. Synergistic interaction of eugenol with antibiotics against Gram negative bacteria. *Phytomedicine* **2009**, 16 (11), 997-1005.

(54) Chen, C. F.; Lu, C. C.; Chiang, J. H.; Chiu, H. Y.; Yang, J. S.; Lee, C. Y.; Way, T. D.; Huang, H. J. Synergistic inhibitory effects of cetuximab and curcumin on human cisplatin-resistant oral cancer CAR cells through intrinsic apoptotic process. *Oncology letters* **2018**, 16 (5), 6323-6330.

(55) Kim, J. S.; Kim, J. E.; Kim, K.; Lee, J.; Park, J. O.; Lim, H. Y.; Park, Y. S.; Kang, W. K.; Kim, S. T. The impact of cetuximab plus AKT-or mTOR-inhibitor in a patient-derived colon cancer cell model with wild-type RAS and PIK3CA mutation. *Journal of Cancer* **2017**, 8 (14), 2713.

(56) Hsu, Y.-F.; Ajona, D.; Corrales, L.; Lopez-Picazo, J. M.; Gurrpide, A.; Montuenga, L. M.; Pio, R. Complement activation mediates cetuximab inhibition of non-small cell lung cancer tumor growth in vivo. *Molecular cancer* **2010**, 9 (1), 1-8.

(57) Bareford, L. M.; Swaan, P. W. Endocytic mechanisms for targeted drug delivery. *Advanced drug delivery reviews* **2007**, 59 (8), 748-758.



---

# *Chapter 6*

---

Conclusions and Future Prospects





---

## 6.1 Conclusions and future prospects

The work reported in this thesis constitutes the use of biodegradable and biocompatible polymers for the development of NDDS to deliver anti-cancer bioactive molecules. It summarizes the application of biodegradable polymers like PEGylated EC, chitosan, Eudragit, CMC in the fabrication of drug carriers in the form of nano-systems. These NDDS can deliver chemotherapeutic drugs, phytochemicals (possessing anti-cancer properties), and gene silencing nucleic acids. As anticipated, encapsulation of these bioactive molecules in a polymeric system enhanced their therapeutic potential. Further, we have designed smart polymers which are sensitive to pH changes and accordingly released the drugs with precision at specific locations in the body. The size of these NDDS plays an important role in the passive targeting of the anti-cancer bioactive molecules to tumor sites. Also, the nanosized DDS has a high surface area to volume ratio which is amenable to modifications via functional groups. Accordingly, the functional groups on the polymeric NPs were utilized to anchor targeting moieties by immobilization. This surface decorated NDDS has an application in the active targeting of cargo to cancer cells. The comprehensive findings of these studies are discussed in the successive passages.

In the first chapter, an elaborate literature survey is reviewed on biodegradable polymers, NDDS like NPs, and PMs, their design, development, properties, and applications specifically for anti-cancer drug delivery. Various characterization techniques like SEM, TEM, DLS, etc for studying the physical properties of NDDS were briefly explained. The second chapter explains the scope and objectives of the thesis work.

The third chapter disclosed the application of EC, a derivative of cellulose in drug delivery. Natural polymers and their derivatives like EC possess renewability, biocompatibility, and low immunogenicity; therefore, they are being studied for the development of bulk/nanoformulations. With this knowledge, EC was grafted with mPEG<sub>2000</sub> to develop EC-PEG graft copolymer. The grafting was confirmed by <sup>1</sup>H and <sup>13</sup>C NMR, along with FTIR spectra. Further, this copolymer demonstrated a very low CMC (critical micellar concentration) to self-assemble into nano-micelles in the

---

aqueous medium. A model anti-cancer drug DOX (doxorubicin) was successfully loaded in these micelles to study their drug delivery ability. The micelles showed faster drug release properties at 5.5 pH (tumor) as compared to the pH 7.4 (physiological) hence, they are considered suitable for cancer therapy. The micelles were characterized by various analytical tools to understand their physicochemical properties. The micelles were ~ 100 nm, which was confirmed by TEM analysis. The FTIR and DSC studies suggested the presence of DOX in an amorphous state in the polymer matrix. To understand the biocompatibility and cytotoxicity of the DOX-loaded micelles, MTT and hemolysis assay were performed and the results confirmed blood compatibility and non-toxicity. The cellular uptake study of DOX-loaded micelles in MDA-MB 231 cancer cells illustrated their entry and release of DOX within the cells, thus establishing their potential as a nanocarrier for cancer therapy. Based on these studies, we concluded that the developed material could be studied further *via in vivo* studies to understand its potential as a controlled DDS to treat cancer.

In the fourth chapter, we have investigated the application of pH-sensitive biodegradable polymers for the delivery of curcumin and Ephb4 shRNA for combinatorial colon cancer therapy. Curcumin a phytochemical derived from turmeric has anti-proliferative properties useful for anti-cancer therapy but it suffers from poor bioavailability under acidic conditions of pH 1.2 (gut). To overcome such shortcomings and deliver it to the desired region, (the colonic region) it was coated with chitosan and Eudragit S100. In addition, a gene silencing Ephb4 shRNA was complexed to these NPs and later coated with Eudragit as it is stable at 1.2 pH, therefore, protecting the system from degradation in the gut. The NPs were characterized by various physicochemical methods and were observed to be around 200 nm, zeta potential measurements and FTIR results confirmed the layer by layer coating of polymer. The thermal study (DSC), demonstrated the presence of curcumin in disordered crystalline nature, thereby increasing its solubility. *In vitro*, drug release experiments confirmed the encapsulation of curcumin as the release of curcumin at gut pH (1.2) was negligible and showed a significant release at colonic pH (7.4). The *in vitro* cell studies like MTT and cellular uptake validated the cytotoxic and cellular

---

translocation properties of the NPs. Accordingly, these results led to the translation of this NDDS to *in vivo* colon cancer mouse models. From the above studies, we accomplish that the NDDS was successful in extending the life expectancy. Finally, we conclude that the combinatorial approach involving RNA interference and curcumin-based NDDS is a promising alliance for next-generation cancer therapeutics. Therefore, the developed NDDS can be investigated in large animal models before being considered for clinical trial and regulatory studies.

In the fifth chapter, we reported the design and development of eugenol-loaded CMC NPs conjugated with cetuximab. Like curcumin, eugenol is also a phytochemical with lots of therapeutic properties along with anti-cancer properties, but it suffers from sensitivity to air, light, low bioavailability. Therefore, it was entrapped in a biodegradable polymeric matrix of CMC with the aid of surfactant, pluronic F127 to develop NPs. EGFR receptors are over-expressed in cancer cells, therefore designing NPs with specificity can provide active targeting for ideal cancer therapy. Further, cetuximab (Cet) a monoclonal antibody specific to epithelial growth factor receptor (EGFR) was conjugated to the NPs via EDC/sulfo NHS coupling. The conjugation of Cet to the NPs was confirmed by the BCA assay. The NPs were characterized by different techniques that confirmed the presence of the drug within the polymeric matrix and were observed to ~100 nm, which was confirmed by HRTEM analysis. The *in vitro* drug release recorded sustained release of eugenol at cancer pH (5.5) and physiological pH (7.4). The MTT and hemolysis assays established the NPs to be non-toxic and biocompatible. The cellular uptake of NPs with and without Cet was investigated in A549 lung cancer cell lines that overexpress EGFR. The observations from the uptake experiments indicated better localization of Cet-NPs compared to NPs, thus expounding the advantage of the active targeting in cancer therapy. This work can be further carried out *in vivo* to consolidate the findings of the *in vitro* experiments of targeted NDDS to understand their potential for enhanced cancer therapy.

---

---

**ABSTRACT**

-----  
**Name of the Student:** Amarnath Singam    **Registration No.:** 10BB14A26041

**Faculty of Study:** Biological Sciences    **Year of Submission:** 2022

**CSIR Lab:** NCL, Pune    **Name of the Supervisor:** Dr. GVN Rathna

**Title of the Thesis:** Studies on Development of Polymeric Nano-systems for Delivery of Anti-cancer Bioactive Molecules  
-----

This thesis focuses on the design and development of nano-drug delivery systems (NDDS) from biocompatible polymers for cancer therapy. We have explored NDDS for the delivery of anti-cancer drugs and bioactive molecules. All the NDDS developed in this research work were characterized by various physicochemical methods and their efficacy was studied by *in vitro* cell studies. **Chapter 1** of this thesis gives an overview of the prior art and progress in the field of NDDS especially, polymer-based NDDS, and their applications in cancer therapy. **Chapter 2** investigates the objectives and scope of the work carried out in this thesis. **Chapter 3** discloses the modification of ethyl cellulose by PEG grafting and the development of this grafted copolymer as nano micelles for drug delivery applications, herein we chose a model anti-cancer drug, doxorubicin. **Chapter 4** presents a novel combinatorial therapeutic system of curcumin and Ephb4 shRNA complexed in pH-sensitive polymers (chitosan and Eudragit S100) and developed as nanoencapsulates for colon cancer therapy. **Chapter 5** demonstrates the potential of active targeting NDDS, here we conjugated epithelial growth factor receptor (EGFR) specific monoclonal antibody Cetuximab to carboxymethyl cellulose nanoparticles loaded with anti-cancer phytochemical eugenol. **Chapter 6** summarizes the overall work done in the present thesis and recommends the scope of the research for their application in drug delivery. It also elucidates the prospects of the NDDS in treating cancers and overcoming the shortcomings of the current therapies.

### **List of Publications Emanating from the Thesis Work**

1. **Amarnath Singam**, Naresh Killi, Pratiksh kumar Patel and Rathna Venkata Naga Gundloori. "PEGylated ethyl cellulose micelles as nanocarrier for drug delivery." RSC Advances, **2021**, 11, 30532
2. Aviral Kumar#, **Amarnath Singam**#, Guruprasadh Swaminathan, Naresh Killi, Naveen Kumar Tangudu, Jedy Jose, Rathna Gundloori VN, Lekha Dinesh Kumar. "Combinatorial therapy using RNAi and curcumin nano-architectures regress tumors in breast and colon cancer models." RSC Nanoscale, **2021**, (DOI: 10.1039/d1nr04411g) (# equal contribution)
3. Rathna VN Gundloori, **Amarnath Singam** and Naresh Killi. "Nanobased Intravenous and Transdermal Drug Delivery Systems." Book Chapter in "Applications of targeted nano drugs and delivery systems: nanoscience and nanotechnology in drug delivery." Elsevier, **2018**
4. **Amarnath Singam** and Rathna VN Gundloori. "Cetuximab conjugated eugenol loaded carboxymethyl cellulose nanoparticles for active targeting anti-cancer therapy" (*Manuscript under preparation*)

### **List of Publications Non-Emanating from the Thesis Work**

1. Naresh Killi, Runali Arjun Dhakare, **Amarnath Singam**, Metta Lokanadham, Harshavardhan Chitikeshi, and Rathna Venkata Naga Gundloori, "Design and fabrication of mechanically strong nano-matrices of linseed oil based polyesteramide blends." MedChemComm, **2016**, 7, 2299-2308
2. Pratikshkumar R. Patel, **Amarnath Singam**, Gundloori Rathna, "Blend of bioactive oil-based polyesteramide as magnetic nanofiber mat for efficient cancer therapy" (Under revision with Elsevier, JDDST)
3. Pratikshkumar R. Patel, **Amarnath Singam**, Naresh Killi, Arun Iyer\*, Rathna Venkata Naga Gundloori\*, "3, 4- difluorobenzylidene curcumin immobilized in nanomaterial to control bacterial infection" (Manuscript ready for submission)

**List of Poster presentations and Conferences attended**

1. Presented poster in ICONSAT, Pune, February 2016, on “Nanocurcumin encapsulates for anti-cancer therapy.”
2. Presented poster in MACRO, Thiruvananthapuram, January 2017, on “Active Targeting of Nano-curcumin Encapsulates for Cancer Therapy.”
3. Presented poster in Science Day Celebration - 2017 held at CSIR-National Chemical Laboratory, Pune.
4. Presented poster in APA, Delhi, November 2017, on “Development of biocompatible disc-shaped ethyl cellulose nanoparticles for drug delivery.”
5. Presented poster in APA, Goa, October 2019, on “A Novel Combinatorial Approach of Curcumin Nanoencapsulates with Cited 1 shRNA against Colorectal Cancer”


 Cite this: *RSC Adv.*, 2021, **11**, 30532

# PEGylated ethyl cellulose micelles as a nanocarrier for drug delivery†

 Amarnath Singam,<sup>ab</sup> Naresh Killi,<sup>ab</sup> Pratikshkumar R. Patel<sup>ab</sup>  
 and Rathna V. N. Gundloori<sup>\*ab</sup>

Natural polymers provide a better alternative to synthetic polymers in the domain of drug delivery systems (DDSs) because of their renewability, biocompatibility, and low immunogenicity; therefore, they are being studied for the development of bulk/nanoformulations. Likewise, current methods for engineering natural polymers into micelles are in their infancy, and in-depth studies are required using natural polymers as controlled DDSs. Accordingly, in our present study, a new micellar DDS was synthesized using ethyl cellulose (EC) grafted with polyethylene glycol (PEG); it was characterized, its properties, cell toxicity, and hemocompatibility were evaluated, and its drug release kinetics were demonstrated using doxorubicin (DOX) as a model drug. Briefly, EC was grafted with PEG to form the amphiphilic copolymers EC-PEG1 and EC-PEG2 with varying PEG concentrations, and nano-micelles were prepared with and without the drug (DOX) *via* a dialysis method; the critical micelle concentrations (CMCs) were recorded to be 0.03 mg mL<sup>-1</sup> and 0.00193 mg mL<sup>-1</sup> for EC-PEG1 and EC-PEG2, respectively. The physicochemical properties of the respective nano-micelles were evaluated *via* various characterization techniques. The morphologies of the nano-micelles were analyzed *via* transmission electron microscopy (TEM), and the average size of the nano-micelles was recorded to be ~80 nm. *In vitro*, drug release studies were done for 48 h, where 100% DOX release was recorded at pH 5.5 and 52% DOX release was recorded at pH 7.4 from the micelles. In addition, cytotoxicity studies suggested that DOX-loaded micelles were potent in killing MDA-MB-231 and MCF-7 cancer cells, and the blank micelles were non-toxic toward cancerous and normal cells. A cellular uptake study *via* fluorescence microscopy indicated the internalization of DOX-loaded micelles by cancer cells, delivering the DOX into the cellular compartments. Based on these studies, we concluded that the developed material should be studied further *via in vivo* studies to understand its potential as a controlled DDS to treat cancer.

 Received 1st June 2021  
 Accepted 30th July 2021

DOI: 10.1039/d1ra04242d

[rsc.li/rsc-advances](http://rsc.li/rsc-advances)

## 1. Introduction

Amphiphilic polymers have been explored as micelles for several decades and they have been extensively studied for various applications.<sup>1</sup> In pharmaceuticals, polymeric micelles (PMs) gained attention as DDSs because of their nanosize and their ability to solubilize hydrophobic molecules and shield them until the molecules are used. *In vivo* studies documented that these micelles have higher drug loading capacities and enhanced stability in comparison to other nanosystems like liposomes, nanoparticles, and dendrimers.<sup>2,3</sup> They demonstrate prolonged circulation times in the bloodstream, avoiding rapid clearance by the renal system and reticuloendothelial system (RES).<sup>4</sup> Micelles in an aqueous medium have an exposed hydrophilic corona,

which is responsible for the protection of these systems from the RES; it also enhances the permeability of PMs and regulates the pharmacokinetic behavior. In addition, the inner hydrophobic domain supports and stabilizes hydrophobic drugs, allowing slow and sustained release.<sup>2</sup> It has been well documented that nanosized PMs can extravasate and penetrate tumors and their extracellular matrix due to the loosely formed blood vessels and sluggish blood flow, thus generating the enhanced permeability and retention (EPR) effect.<sup>5,6</sup> As a result, PMs become accumulated and deliver drugs at a controlled rate for a sustainable period, thereby decreasing drug resistance and increasing the effectiveness of therapy. Accordingly, anti-cancer formulations like Genexol-PM® and Nanoxel® have been developed and approved by the FDA for human treatment. In line with these studies, advanced PM formulations (*e.g.*, NK105, NK911, and NC-6004) are being studied, and some are in the clinical trial stage for anti-cancer therapy.<sup>7</sup>

Generally, the designed PMs use synthetic block co-polymers and triblock copolymers and are extensively being studied for drug delivery applications.<sup>1</sup> However, synthetic PMs are less

<sup>a</sup>Polymer Science and Engineering, CSIR-National Chemical Laboratory, Homi Bhabha Road, Pune-411008, Maharashtra, India. E-mail: [rv.gundloori@ncl.res.in](mailto:rv.gundloori@ncl.res.in)

<sup>b</sup>Academy of Scientific and Innovative Research (AcSIR), Ghaziabad-201002, Uttar Pradesh, India

† Electronic supplementary information (ESI) available. See DOI: 10.1039/d1ra04242d



compatible with human anatomy, showing high immunogenicity, as their interactions with human cells are less favorable. Further, to produce these PMs, complex protocols are involved, and the cost of manufacture is exorbitant; therefore, the application of these materials is unattainable for a wide range of the population. Currently, PM formulations designed from natural and renewable polymers are attracting much attention, because they are highly biocompatible with low immunogenicity. With proteins and polysaccharides being an integral part of humans, they are well tolerated and, further, developing these materials as nanoassemblies may not be expensive, as the design protocols would be less expensive and the materials are easily available from renewable resources and are safe to use. Accordingly, micelles are being investigated based on proteins (albumin, gelatin, zein, *etc.*) and polysaccharides (hyaluronic acid, chitosan, pullulan, dextran, alginate, xyloglucan, inulin, *etc.*) using functional modification to attain self-assembled nanocarriers.<sup>8</sup>

Polysaccharide-based DDSs are reported to form nano-micelles at very low concentrations in an aqueous medium, demonstrating the ability to enter cells and improve the drug pharmacokinetics, and providing a platform for sustained and controlled drug release.<sup>8</sup> Ethyl cellulose (EC), a derivative of polysaccharide cellulose, is being explored for use in the fields of cosmetics, food additives, adhesives, and medicine owing to its chemically inert nature, stability, sustained drug release abilities, and good biocompatibility.<sup>9,10</sup> In a report by Balzus *et al.*, EC displayed extended-release behavior in comparison to polymers like Eudragit RS 100 and other lipids.<sup>11</sup> However, there are very few reports about the application of EC in drug delivery systems, other than in oral and topical administrations. Nevertheless, S. Leitner *et al.* reported the development of EC nanoparticles as a new transfection tool for antisense oligonucleotide delivery.<sup>12</sup> The hydrophobic nature of EC has benefits in terms of sustained release for oral administration; however, its hydrophobicity is a hurdle preventing its use in parenteral administration, as its hydrophobicity activates the macrophages of the immune system. To overcome this, the structure of EC needs to be modified without sacrificing its desirable properties. Therefore, the synthesis of EC-grafted polymers has attracted significant attention in recent years. For instance, Yuan *et al.* reported the synthesis, characterization, and *in vitro* degradation properties of EC-graft-poly( $\epsilon$ -caprolactone)-block-poly(L-lactide) copolymers obtained *via* sequential ring-opening polymerization.<sup>13</sup> One of the best choices for drug delivery pharmaceuticals is FDA-approved PEG because of its tunable properties and well-established safety profile in terms of biocompatibility and non-immunogenicity. Several polymers with different properties have been PEGylated to prolong their blood circulation times, shield them from the immune system, and allow them to complete their target function.<sup>14</sup> For example, the PEGylation of cellulose or its derivatives has been explored to improve the dispersibility and colloidal stability. For instance, Lasseguette grafted PEG with micro-fibrillated cellulose *via* EDC-coupling.<sup>15</sup> T. Kald us *et al.* reported the PEGylation of TEMPO-oxidized cellulose and studied its colloidal stability.<sup>16</sup> EC is a well-established material for oral delivery; however, there are few reports on the use of EC for systemic applications due to its drawbacks, as explained above. As the properties of EC are favorable for drug

delivery, its potential application in invasive delivery has been explored *via* addressing its incompatibility and immunogenicity through grafting with PEG. For example, Huang *et al.* synthesized thermosensitive micelles from an amphiphilic graft copolymer of EC-poly(PEG methyl methacrylate), EC-PMMA, for systemic drug delivery applications.<sup>17</sup> In their studies, they designed and developed EC-PMMA in the form of nano self-assemblies and characterized the thermosensitive behavior. However, a detailed study of EC-PMMA nano-assemblies for drug delivery and cytotoxicity and hemocompatibility studies have not been reported to support their potential for systemic applications. In accordance with these studies, we aimed to develop EC-PEG nano-micelles *via* a simple method, to evaluate their physicochemical properties, and to carry out *in vitro* studies, such as cytotoxicity, drug delivery, cell interaction, and hemolysis studies, so as to understand their potential for systemic applications. We have chosen doxorubicin (DOX) as a model drug for loading EC-PEG micelles for anti-cancer therapy in the form of a CDDS. DOX is a potent anti-cancer drug used in chemotherapy to treat solid tumors, lymphomas, soft tissue sarcomas, *etc.* However, its application at higher doses is limited because of its side effects, like cardiotoxicity, and its role in the development of tumor cell resistance.<sup>18</sup> To mitigate these limitations, we designed amphiphilic copolymer-based micelles.

In this study, EC was converted to carboxylated EC (CEC) *via* TEMPO-mediated oxidation and this was subsequently grafted with mPEG<sub>(2000)</sub> *via* *N,N'*-dicyclohexylcarbodiimide (DCC) coupling. mPEG-grafted EC (EC-PEG) was developed in the form of micelles in an aqueous medium and loaded with hydrophobic DOX. The release pattern of the drug showed a sustained release profile. The *in vitro* effectivity of the system was also investigated toward the breast cancer cell lines MDA-MB-231 and MCF-7. Herein, the use of EC in the form of micelles as a DDS to deliver DOX is reported for the first time.

## 2. Experimental methods

### 2.1 Materials

Ethyl cellulose (ethoxy content: 44–51%, 18–24 mPa s) was procured from S.D. Fine Chemicals, India. Doxorubicin HCl (hydrochloride) and 4-dimethylaminopyridine (DMAP) were obtained from Himedia Laboratories, India. Poly(ethylene glycol) methyl ether ( $M_w$ : 2000; mPEG) and (2,2,6,6-tetramethylpiperidin-1-yl)oxidanyl (TEMPO) were procured from Aldrich, USA. *N,N'*-Dicyclohexylcarbodiimide (DCC) was procured from Spectrochem Pvt. Ltd, India. DMEM (Dulbecco's modified Eagle's medium), MEM (minimal essential medium), and MTT (3-(4,5-dimethylthiazol-2-yl)-2,5-diphenyltetrazolium bromide) were purchased from Invitrogen, India. All solvents and salts were of analytical grade and used without any further purification. Cell lines were procured from the National Centre for Cell Science (NCCS) Pune.

### 2.2 Synthesis and characterization of the EC-PEG graft polymer

**2.2.1 TEMPO-mediated oxidation of EC.** The oxidation of the hydroxy groups of EC ( $-CH_2OH$ ) was done according to





a reported literature method by J. Araki *et al.*,<sup>19</sup> as shown in Fig. 1. Briefly, TEMPO (0.4 g) and sodium bromide (4 g) were added to 400 mL of an aqueous suspension of EC (10 mg mL<sup>-1</sup>, 4 g), and this was stirred at room temperature (RT) for 15 min. The oxidation was initiated *via* the addition of 60 mL of NaClO (sodium hypochlorite) solution, where the concentration of NaClO was maintained at 25 wt% with respect to EC (1.25 g of NaClO for 5 g of EC). The solution pH was maintained between 10 and 11 while stirring at RT for 4 h. After 4 h, NaCl (30 g) was added to the reaction mixture and the EC suspension was precipitated. The product was filtered through a pore-fritted glass filter and washed with 0.5–1.0 M NaCl. The product was dispersed in NaCl of the same concentration and centrifuged at 12 000 rpm for 30 min at 25 °C. This washing procedure was repeated 3 times to remove unreacted NaClO. The EC sodium salt was converted to the free acid form *via* washing it twice with 0.1 N HCl. The obtained product was dialyzed against deionized water for 3 days with frequent water changes. The colloidal carboxylic EC obtained was dried, quantified, and characterized to confirm the product (yield: 2.32 g, 58%).

**2.2.2 Determination of the carboxylate charge density of EC.** The carboxylate charge density of EC after the oxidation reaction was estimated *via* the conductometric titration method. Briefly, TEMPO-oxidized EC (240 mg) was dispersed in 30 mL of de-ionized (DI) water. This dispersion was stirred and sonicated for 30 min in a bath sonicator (Bio-Technics, India) and left standing overnight. Later, 10 mL of the dispersion was added to 80 mL of DI water. Subsequently, 50  $\mu$ L of concentrated HCl was added to the carboxylated EC (CEC) dispersion and this was titrated against 0.5 M NaOH. The conductivity of

the solution was measured (Orion Star, Thermo Scientific Conductometer, India) upon each addition of 20  $\mu$ L of 0.5 M NaOH to the CEC-HCl dispersion. The degree of carboxylated EC was estimated *via* plotting a graph of the conductivity of the CEC-HCl dispersion against the volume of NaOH.

**2.2.3 PEGylation of carboxylated EC (CEC).** mPEG ( $M_w$  2000) was grafted to CEC using DCC reagent and the catalyst DMAP. For example, in a two-necked RB flask, CEC [400 mg, (0.33 mmol (calculated using the titration eqn (S1)))] was dispersed in 10 mL of dry tetrahydrofuran (THF) and stirred for 45 min under a N<sub>2</sub> atmosphere at RT. A solution of DCC (0.99 mmol) and DMAP (0.165 mmol) prepared in dry THF was added to the CEC solution and stirred for 2 h at RT. Later, to the solution mixture, mPEG (0.33 mmol) dissolved in 5 mL of dry THF was added dropwise using a syringe. Following this, the reaction mixture was stirred under a nitrogen atmosphere at 40 °C for 48 h. After 48 h, the reaction was stopped and the solution was filtered through Whatman's filter paper to collect the filtrate. This filtrate was concentrated using a rotary evaporator at 50 °C and then precipitated in diethyl ether. The diethyl ether was evaporated and the precipitate was dispersed in DI water and dialyzed (10 kDa cut-off) against DI water for 48 h to remove the unreacted mPEG and reagents, obtaining an EC to PEG ratio of 1 : 1. Similarly, in another set of reactions, mPEG (0.66 mmol) was reacted with EC following the same procedure and reaction conditions to obtain an EC to PEG ratio of 1 : 2. The final EC-PEG compounds (1 : 1 and 1 : 2), labeled EC-PEG1 and EC-PEG2, respectively, were characterized *via* <sup>1</sup>H NMR, <sup>13</sup>C NMR, and FTIR studies. The yield of this reaction was 320 mg (80%).

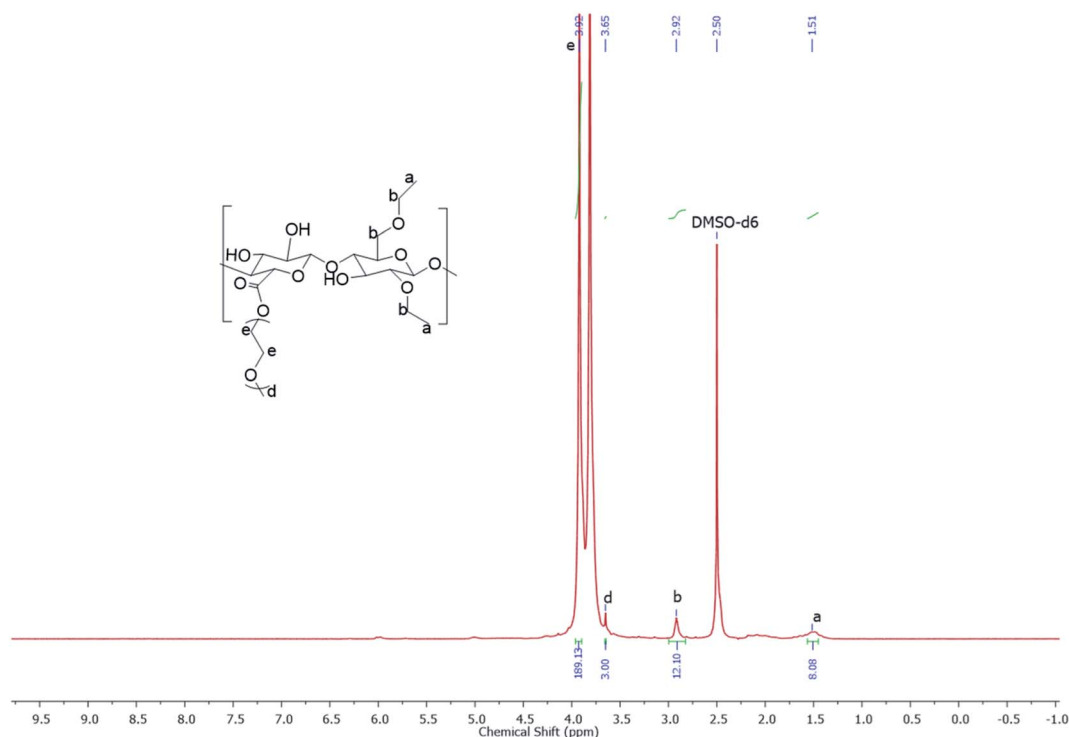


Fig. 1 The <sup>1</sup>H NMR spectrum of EC-PEG1 recorded using a Bruker AV-200 NMR spectrometer operating at a frequency of 200 MHz with DMSO-d<sub>6</sub> as the solvent.



### 2.2.4 Critical micellar concentration (CMC) of EC-PEG.

Following a protocol reported by J. Chen *et al.*,<sup>20</sup> the CMCs of EC-PEG1 and EC-PEG2 were determined. The hydrophobic probe pyrene was used for estimating the CMCs of the respective EC-PEG materials in water *via* fluorescence spectroscopy. A total of 25  $\mu\text{L}$  of pyrene in acetone solvent ( $20 \mu\text{g mL}^{-1}$ ) was added to individual 5 mL vials, and the acetone was allowed to evaporate to obtain dry pyrene. To these respective vials, 5 mL of an aqueous solution of EC-PEG copolymer was added, with varying concentrations from 0.00025 to 0.09  $\text{mg mL}^{-1}$ . The final concentration of pyrene in each sample solution was 0.1  $\mu\text{g mL}^{-1}$ . The excitation spectra (300–360 nm) of the solutions were recorded at an emission wavelength of 395 nm. The ratios of the peak intensity at 338 nm to the intensity at 334 nm ( $I_{338}/I_{334}$ ) of the excitation spectra were recorded and plotted as a function of the polymer concentration ( $\log C$  ( $\text{mg mL}^{-1}$ )).

### 2.3 Preparation and characterization of micelles

**2.3.1 Preparation of EC-PEG micelles.** The dialysis method was used for fabricating micelles of EC-PEG (1 : 1 and 1 : 2). Briefly, EC-PEG1 (20 mg) was dissolved in 1 mL of DMF, and 10 mL of PBS buffer (pH 7.4) was added dropwise while sonicating at a 20% amplitude (Vibracell, VCX 500, USA). Later this solution was dialyzed against DI water for 24 h using a dialysis membrane with a 10 kDa cut-off to obtain micelles. These micelles were lyophilized to obtain dry powder, which was used for characterization. In a similar fashion, EC-PEG2 micelles were also prepared and characterized.

**2.3.2 Preparation of DOX-loaded EC-PEG micelles.** EC-PEG micelles loaded with DOX were prepared at 0.1% (w/v) following the described procedure. Briefly, DOX (1 mg) was dissolved in 1 mL of DMF, 1.5 eq. of triethylamine was added, and the mixture was stirred at RT. Later, 20 mg of EC-PEG1 was added to this DOX solution and this was stirred for 1 h while maintaining RT conditions. To this, PBS buffer (10 mL) was added dropwise under sonication at a 20% amplitude. Further, this solution was dialyzed against DI water for 24 h using a membrane with a 10 kDa cut-off. After dialysis, the obtained DOX-loaded micelles were lyophilized to give DOX-EC-PEG1 powder, which was red in color. The same protocol was followed to obtain DOX-loaded micelles of EC-PEG2. The developed formulations are shown

in Table 1. The micelles with and without DOX were characterized *via* various physicochemical characterization methods.

### 2.4 Characterizations

**2.4.1 NMR spectroscopy.**  $^1\text{H}$  NMR spectra for the characterization of mPEG and EC-PEG were recorded using a Bruker AV-200 NMR spectrometer operating at a  $^1\text{H}$  frequency of 200 MHz.  $^1\text{H}$  spectra of all compounds were recorded in DMSO- $d_6$  (concentration of polymer = 50  $\text{mg mL}^{-1}$ ). The samples were homogenized before recording the NMR spectra. Similarly,  $^{13}\text{C}$  NMR spectra of mPEG and EC-PEG were also recorded using a Bruker AV-500 NMR spectrometer operating at a  $^{13}\text{C}$  frequency of 125 MHz.

### 2.5 Physicochemical characterization of the micelles

The size distribution, hydrodynamic diameter, and charge density data for blank and DOX-loaded micelles were determined *via* DLS (90 Plus Brookhaven Instruments Corp, PALS zeta potential analyzer, USA). The morphologies of the micelles were investigated *via* TEM (FEI Tecnai TF20, 200 kV FEG high-resolution transmission electron microscope, USA). For TEM analysis, samples were diluted ( $5\times$ ) in Millipore water, stained with 1% (w/v) uranyl acetate dye, and drop-cast on a copper grid mesh.

The drug loading efficiency and content percentages were determined using a UV-vis spectrophotometer (UV 1601 PC UV spectrophotometer, Shimadzu, Japan). As an example, 1.5 mg of DOX-loaded micelles were dissolved in 1 mL of DMF and filtered, and the DOX content was estimated using the standard DOX calibration curve recorded at 480 nm. The drug loading efficiency and loading content percentages were calculated using the following equations:

$$\text{Drug-loading efficiency (\%)} = \frac{\text{wt of loaded DOX}}{\text{wt of fed DOX}} \times 100 \quad (1)$$

$$\text{Drug-loading content (\%)} = \frac{\text{wt of loaded DOX}}{\text{wt of DOX-loaded polymer}} \times 100 \quad (2)$$

Table 1 Formulations and their characteristics

Batch	EC-PEG1% (w/v)	DOX% (w/v)	Hydrodynamic diameter (nm)	PDI	Drug-loading efficiency (%)	Drug-loading content (%)
B1	2	—	153.5	0.293	—	—
B2	2	0.1	204.9	0.122	36.73	1.73
B3	2	0.15	257.7	0.297	52.73	4.11
Batch	EC-PEG2% (w/v)	DOX% (w/v)	Hydrodynamic diameter (nm)	PDI	Drug-loading efficiency (%)	Drug-loading content (%)
B4	2	—	249.9	0.191	—	—
B5	2	0.1	338.6	0.180	32.93	1.55
B6	2	0.15	350.5	0.357	52.51	3.66



FTIR spectroscopy analysis was conducted on DOX, bare polymers (EC and mPEG), grafted copolymers (EC-PEG1 and EC-PEG2), and DOX-loaded micelles (batches 3 and 6) to confirm the grafting of mPEG with EC and the functional interactions with DOX. For FTIR, samples (2–3 mg) were ground with anhydrous potassium bromide, KBr, (97 mg) to form a pellet, which was used for analysis (PerkinElmer spectrometer I, FT-IR diffuse reflectance (DRIFT) mode, USA). The scans were recorded from 400  $\text{cm}^{-1}$  to 4000  $\text{cm}^{-1}$  with an average of 10 scans per sample.

Thermal analysis was carried out using DSC (Model Q100 DSC, TA instruments, Newcastle, DE, USA) to investigate the thermal properties of EC in its pristine form, after grafting, and after DOX loading (batches 3 and 6). The samples were crimped in aluminum pans and the thermal properties were analyzed in cycles. In the first heating cycle, the temperature was ramped from  $-70\text{ }^{\circ}\text{C}$  to  $100\text{ }^{\circ}\text{C}$  at a rate of  $10\text{ }^{\circ}\text{C min}^{-1}$ . The sample was then cooled to  $-70\text{ }^{\circ}\text{C}$  in the 2nd cycle at a rate of  $10\text{ }^{\circ}\text{C min}^{-1}$ , and in the third heating cycle, the temperature was ramped from  $-70\text{ }^{\circ}\text{C}$  to  $100\text{ }^{\circ}\text{C}$  at a rate of  $10\text{ }^{\circ}\text{C min}^{-1}$ . The entire experiment was done under nitrogen gas ( $50\text{ mL min}^{-1}$ ). An empty aluminum pan was used as a reference pan.

**2.5.1 In vitro DOX release.** The release of DOX from the micelles was studied *via* dispersing 5 mg of DOX-loaded micelles (B3 and B6) in 10 mL of buffer and enclosing them in a dialysis membrane tube ( $M_w$  cut-off: 12 kDa). This dialysis bag was kept in 20 mL of phosphate buffer (100 mM, pH 7.4) and incubated at  $37\text{ }^{\circ}\text{C}$  in a shaker bath (Julabo SW23) at 100 rpm. At regular intervals of time, 1 mL was withdrawn from the buffer and 1 mL of fresh buffer was added to maintain the sink conditions. The withdrawn buffer was analyzed for the amount of DOX released using a UV-vis spectrophotometer at 480 nm. Similarly, release studies were performed in phosphate buffer at pH 5.5.

**2.5.2 Hemolysis assays.** To study the biocompatibility of the developed graft polymer toward RBCs (red blood cells), hemolysis assays were conducted. Briefly, blood was collected in tubes containing EDTA from healthy volunteers at the National Chemical Laboratory, Pune, India. The RBCs were separated from the whole blood by density gradient centrifugation. As an example, 5 mL of whole blood was added slowly to 5 mL of PBS and centrifuged at 2000 rpm for 30 min. The supernatant, which was devoid of RBCs, was discarded and the pellet was washed thrice with PBS and centrifuged again for 30 min at 2000 rpm. Later, the cells were dispersed in PBS to prepare a 2% (v/v) stock dispersion. Further, 2 mL of this stock dispersion was dispensed in 2 mL vials in duplicate, and test samples, such as EC, CEC, B1, B3, B4, and B6, at concentrations of  $0.5\text{ mg mL}^{-1}$  and  $1\text{ mg mL}^{-1}$  were added to the respective vials. Respective controls, like a RBC suspension in PBS (negative) and a RBC suspension in DI water (positive), were prepared. All respective test samples and controls were incubated at  $37\text{ }^{\circ}\text{C}$  for 2 h under gentle shaking every 30 min to re-suspend precipitated RBCs. After the incubation period, the suspensions were centrifuged at 1500g for 10 min at RT. The obtained supernatant was dispensed in a 96-well plate, and the hemoglobin (Hb) release was obtained spectrophotometrically using a microtiter plate

reader at 540 nm (Multiskan Ex, (51118170 (200–240 V) Thermo Scientific, Finland)). Considering 100% cell lysis in DI water and 0% lysis in PBS, the hemolysis percentages for test samples were calculated using the following equation.

$$\text{Hemolysis (\%)} = \frac{\text{abs. test} - \text{abs. negative control}}{\text{abs. positive control} - \text{abs. negative control}} \times 100 \quad (3)$$

## 2.6 Cell studies

The fibroblast cell line L929 and breast cancer cell line MDA-MB-231 were maintained in DMEM supplemented with 10% FBS under standard conditions at  $37\text{ }^{\circ}\text{C}$  in a humidified  $\text{CO}_2$  incubator. Under similar incubation conditions, the breast cancer cell line MCF-7 was also cultured in MEM supplemented with 10% FBS. Cells were routinely grown as monolayer cultures in a  $25\text{ cm}^2$  flask and passaged once a week using trypsin/EDTA at 80% confluence.

**2.6.1 Cytotoxicity assays.** Blank micelles, B1, and B4 were investigated for their cellular toxicity toward L929 fibroblast cells *via* MTT assays. A confluent flask of L929 cells was trypsinized to harvest cells, which were further seeded in a 96-well plate at 10 000 cells per well. The plate was incubated at  $37\text{ }^{\circ}\text{C}$  under a 5%  $\text{CO}_2$  humidified atmosphere for 16 h to allow cells to attach and form a monolayer. Later, the media from the wells was flicked off, and B1 and B4 micelles were added, respectively. Stock concentrations of micelles at  $1\text{ mg mL}^{-1}$  were prepared in serum-free media. From these, a series of concentrations ranging from 0 to  $400\text{ }\mu\text{g mL}^{-1}$  was added to the respective wells, which were incubated for 48 h. Post incubation, the media was removed from the wells and MTT solution prepared in DMEM-FBS medium was added to the wells. Following this, the plate was incubated in the dark at  $37\text{ }^{\circ}\text{C}$  in a humidified  $\text{CO}_2$  incubator for 4 h. Finally, the MTT media in the wells was replaced with 100  $\mu\text{L}$  of DMSO and the plate was read at 550 nm using a plate reader (Multiskan Ex, (51118170 (200–240 V) Thermo Scientific, Finland)). Cells grown in wells devoid of any test sample were considered as a positive control and cells incubated in media with 30% DMSO (v/v) were the negative control. The relative cell viabilities were calculated *via* comparing the absorbance read from test samples to the positive control  $[(\text{abs. sample}/\text{abs. positive control}) \times 100]$ . Data are presented as average  $\pm$  SD ( $n = 3$ ). The cytotoxicity of B1 and B4 micelles was also evaluated toward MDA-MB-231 cells *via* this assay using the same parameters. Similarly, the MTT assay was also carried out for DOX-loaded micelles (B3 and B6) in MDA-MB-231 and MCF-7 cells for 72 h.

**2.6.2 In vitro cellular uptake.** The uptake of the B3 and B6 micelles was studied in MDA-MB-231 cells.  $5 \times 10^4$  cells were seeded on sterile 12 mm round coverslips placed in a 24 well plate, and these were incubated for 24 h at  $37\text{ }^{\circ}\text{C}$  under a 5%  $\text{CO}_2$  atmosphere. After incubation, the media were aspirated from the wells followed by washing thrice with PBS. Free DOX at a concentration of  $4\text{ }\mu\text{g mL}^{-1}$  and DOX-loaded micelles (B3 and B6) at  $100\text{ }\mu\text{g mL}^{-1}$  containing an equivalent amount of DOX (calculated based on the loading efficiency) were dispersed in



serum-free media and incubated for 4 and 8 h separately. Later, the cells were washed thrice with PBS and fixed *via* adding 300  $\mu\text{L}$  of 4% paraformaldehyde and incubating for 15 min at RT. After the fixing step, the cells were washed extensively with PBS and incubated with Alexa Fluor 488 phalloidin (60 nM) for 30 min in the dark to colorize the actin filaments, so as to allow the identification of the cytoplasm and cell boundaries. The nuclei were stained with DAPI (300 nM) for 15 min in the dark, which was washed off with PBS. Finally, the coverslips were mounted on a clean slide with the application of mounting media (Fluoroshield). Excess mounting media was dabbed off with tissue, and the cells were visualized using an epifluorescence microscope (Carl Zeiss, model: Axio Observer Z1, oil-emersion objective, 63 $\times$ ). The nuclei stained with DAPI were observed under the blue channel, the cytoskeletons stained with Alexa Fluor 488 under the green channel, and DOX under the red channel.

### 3. Results and discussion

EC, a natural polymer derivative, was grafted covalently with mPEG to develop an amphiphilic copolymer that assembles into micellar structures in an aqueous medium. The EC core of the micellar architecture was used for loading the anti-cancer drug DOX. The purpose of the mPEG graft on the outer layer is to protect the drug carrier from being recognized by the immune system and to prolong the micelle circulation time in the blood for effective therapy.

#### 3.1 TEMPO-mediated oxidation and the determination of the carboxylate charge density on EC

TEMPO-mediated oxidation has been explored over the last few decades for the conversion of polysaccharide alcoholic hydroxyls to carboxyls under aqueous alkaline conditions.<sup>21</sup> It is a highly selective reaction and oxidizes only the primary hydroxyl group at carbon (C-6) on the EC backbone. TEMPO, in combination with NaBr and NaClO, efficiently converts the hydroxyl groups to carboxylates *via* aldehydes. Under alkaline conditions, the selectivity of TEMPO is further enhanced; hence, the oxidation of EC was performed at pH 10–11.<sup>22–24</sup> The degree of substitution of primary hydroxyl groups of EC with carboxylate groups after TEMPO oxidation was calculated *via* conductometric titration, as described in the ESI.† From the graph in Fig. S2 and eqn (S1),† the density of EC carboxylate groups was calculated to be 625  $\text{mmol kg}^{-1}$ . It was observed that with an increase in the volume of NaClO, the degree of carboxylation was increased, which is similar to the reported literature.<sup>19</sup> The concentration of NaClO was optimized at 25% relative to the dry weight of EC to obtain a carboxylate content of  $\sim 600 \text{ mmol kg}^{-1}$  in EC. The reproducible yield of this reaction was 58%. The carboxylate groups are available for further modification with mPEG so as to increase the hydrophilicity of EC.

#### 3.2 PEGylation of carboxylated EC (CEC)

After the confirmation of the oxidation of EC based on conductometric titration, the product, CEC, was used for

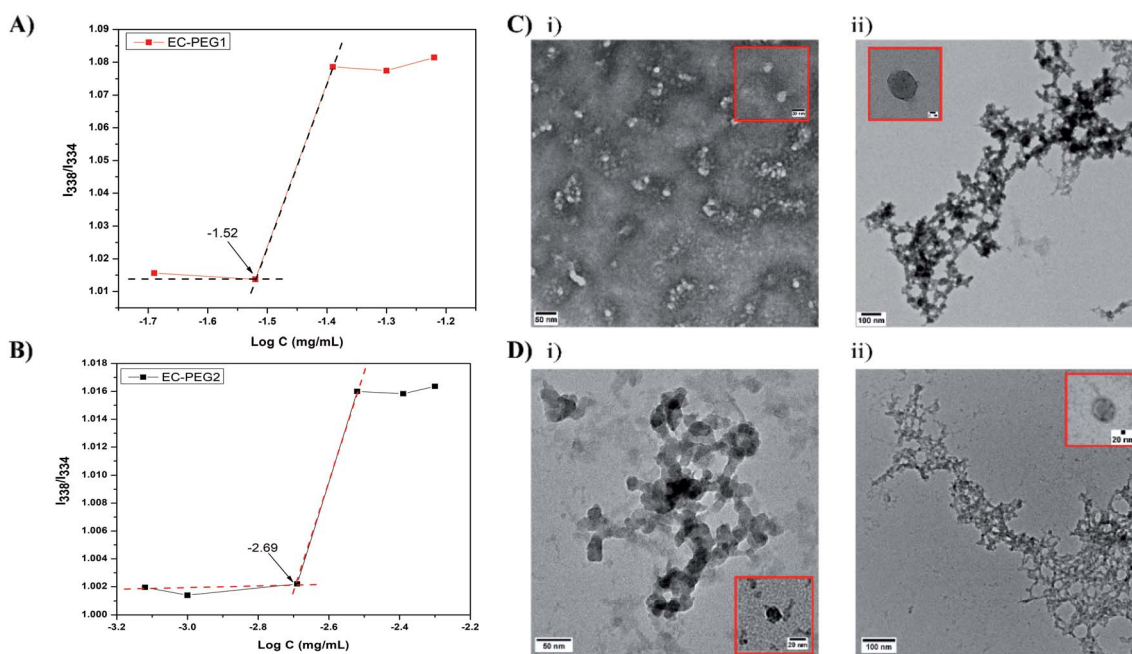


Fig. 2 (A) The critical micelle concentration (CMC) of EC-PEG1 derived from a plot of the  $I_{338}/I_{334}$  ratio vs. the copolymer concentration. (B) The CMC of EC-PEG2 derived from a plot of the  $I_{338}/I_{334}$  ratio vs. the copolymer concentration. (C) (i) A TEM image of B1 micelles (scale bar: 50 nm) and (ii) a TEM image of B3 micelles (scale bar: 100 nm). (D) (i) A TEM image of B4 micelles (scale bar: 50 nm) and (ii) a TEM image of B6 micelles (scale bar: 100 nm).



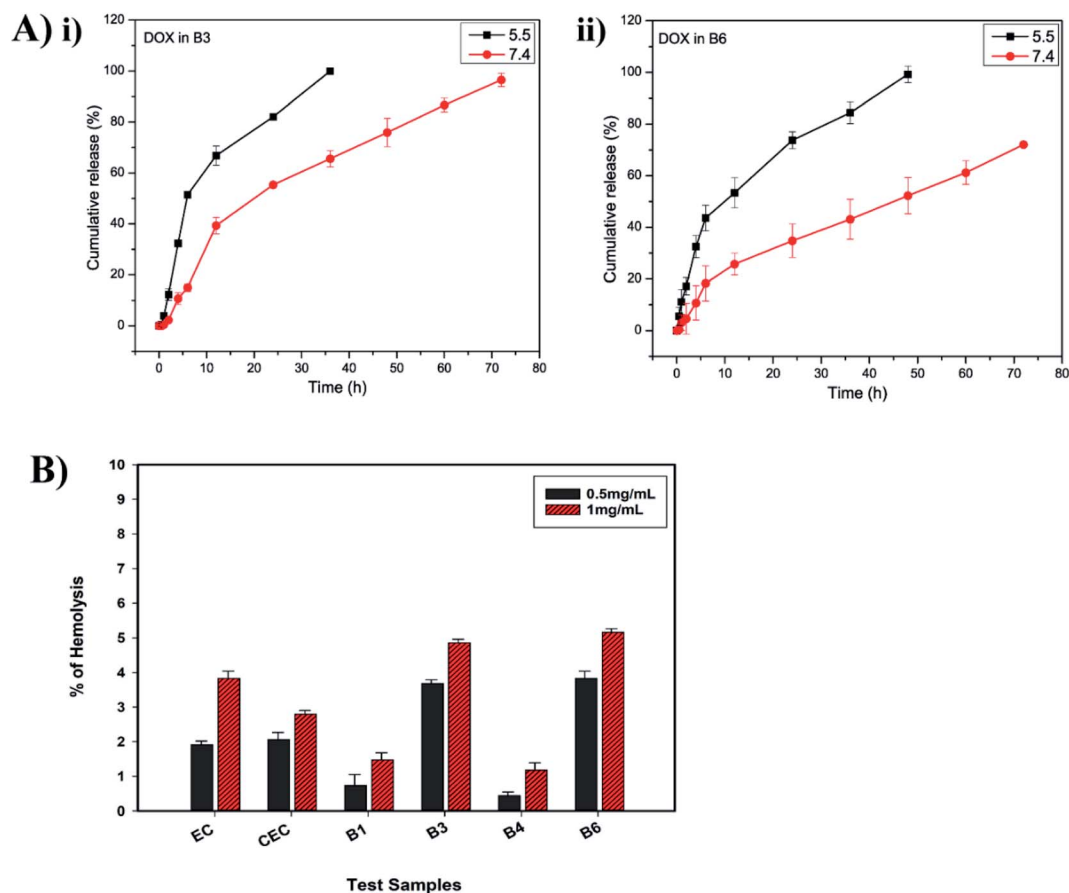


Fig. 3 (A) (i) DOX release from B3 micelles in PBS at pH 5.5 and 7.4 over 72 h; and (ii) DOX release from B6 micelles in PBS at pH 5.5 and 7.4 over 72 h. (B) Hemolysis percentages upon exposure to test samples: EC, CEC, and B1, B3, B4, and B6 micelles.

synthesizing graft copolymers of EC-PEG *via* esterification. The reaction was carried out in THF; the carboxylic acid of CEC was deprotonated *via* DMAP, and DCC was nucleophilically added to give the intermediate O-acylisourea, a good leaving group. The hydroxyl groups of mPEG were nucleophilically reacted with this intermediate to form the desired ester bond between the carboxyl group of CEC and the hydroxyl group of mPEG.<sup>25</sup> Along with the grafted copolymer, the side product dicyclohexyl urea (DCU) was obtained, which was removed during the filtration steps. The grafting of mPEG onto CEC was performed with 1 and 2 equivalents, and the products were labeled as EC-PEG1 and EC-PEG2, respectively. The final products were dialyzed against DI water to remove unreacted mPEG and reagents, and the products were finally confirmed *via* <sup>1</sup>H NMR and <sup>13</sup>C NMR spectroscopy analysis (see the ESI†) in DMSO-d<sub>6</sub>. The yield of this reaction was optimized to 80%. Fig. 1 shows the <sup>1</sup>H NMR spectrum (DMSO-d<sub>6</sub>) of the EC-PEG1 copolymer with the following peaks (ppm):  $\delta$  3.92 (–OCH<sub>2</sub>CH<sub>2</sub>O–),  $\delta$  3.65 (CH<sub>3</sub>–OCH<sub>2</sub>CH<sub>2</sub>OH),  $\delta$  1.51 (–CH<sub>2</sub>CH<sub>3</sub> of ethyl groups), and  $\delta$  2.92 (CH<sub>3</sub>CH<sub>2</sub>OCH–, CH<sub>3</sub>CH<sub>2</sub>OCH<sub>2</sub>CH). Integration of the peaks corresponding to the terminal methyl (–CH<sub>3</sub>) of mPEG at 3.65 ppm and the methylene (–CH<sub>2</sub>CH<sub>2</sub>–) group of ethylene glycol at 3.92 ppm suggests 46 repeating units, corresponding to mPEG<sub>2000</sub>. From the reported literature,<sup>25–29</sup> in the <sup>1</sup>H NMR

spectrum of ethyl cellulose (EC), the protons of the EC backbone appear between 3.4 and 4.5 ppm. The peaks of mPEG also appear in a similar region, which resulted in the merging of the peaks of protons of EC with the protons of mPEG.

The CMC is an important factor deciding the micelle formation capacity of any amphiphilic polymer. To determine the CMCs of the developed graft copolymers of EC-PEG, the well-documented method of fluorometry was used with the hydrophobic probe pyrene. The excitation spectra of the probes with increasing concentrations of polymer were monitored at an emission wavelength of 395 nm. Fig. 2A and B shows the  $I_{338}/I_{334}$  intensity ratios plotted against the log of concentration, varying from 0.00025 mg mL<sup>–1</sup> to 0.09 mg mL<sup>–1</sup>. The CMC value was taken from the intersection point of the tangent to the curve at high concentrations with a horizontal line passing through the point at low concentrations. From the graphs, the CMCs of EC-PEG1 (Fig. 2A) and EC-PEG2 (Fig. 2B) were observed to be 0.03 mg mL<sup>–1</sup> and 0.00193 mg mL<sup>–1</sup>, respectively. Therefore, with an increase in the amount of mPEG grafting to EC, the CMC value dropped. This suggested that in an aqueous medium, EC-PEG2 formed micelles at a much lower concentration compared to EC-PEG1. The grafting of 2 equivalents of mPEG to EC made the molecules more amphiphilic compared to 1 equivalent of mPEG. This observation was similar to that



reported in the literature by Chen *et al.*, where a polymer modified with PEG with a  $M_w$  of 5000 had a lower CMC value than that modified with PEG with a  $M_w$  of 2000.<sup>20</sup> A lower CMC value signifies the ability of a polymer to maintain a stable micellar structure under diluted conditions, like in the bloodstream.<sup>30</sup>

### 3.3 The preparation and physicochemical characterization of micelles

Table 1 shows the various formulations of EC-PEG with and without DOX at various concentrations, which were abbreviated as B1, B2, B3, B4, B5, and B6. Micelles of EC-PEG (B1 and B4) were prepared *via* dissolving the polymer in DMF and dialyzing these against DI water. Similarly, DOX-loaded micelles were also fabricated *via* dissolving the copolymer along with DOX in DMF and dialyzing against DI water. Fig. 2C and D shows the morphologies and size distributions of the prepared micelles, which were analyzed *via* DLS and TEM. From the DLS measurements, as shown in Table 1, it was seen that the sizes (B1 = 153.5 and B4 = 249.9 nm) of the micelles increased with the addition of DOX; this confirmed the interaction and entrapment of DOX within the hydrophobic cores of the micelles. TEM images of blank and DOX-loaded micelles shown in Fig. 2C and D present average micelle sizes below 150 nm, which are lower than the mean diameters measured *via* the DLS method. It should be noted that the mean diameters of the micelles determined *via* the DLS method depend on the size of the biggest micelle. Further, DLS measures the hydrodynamic diameters of solvated micelles whereas TEM measures dried micelles.<sup>12</sup> The PEG chains in the outer domains of the micelles are hydrophilic and hold water molecules, which is reflected in the DLS measurements; hence, formulations with a higher content of grafted mPEG (B4, B5, and B6) are larger in size. All these formulations possessed net negative charge on their surfaces (−15 mV to −42 mV), which was due to the OH<sup>−</sup> groups on the PEG chains of the micelles. The formulations prepared from EC-PEG2 had slightly more negative charge than the formulations prepared from EC-PEG1, which could be explained due to the additional mPEG grafting. The drug-loading efficiency was determined *via* UV-vis spectrophotometric analysis, and the obtained values are shown in Table 1. The formulations with higher drug-loading efficiencies, namely B3 and B6 (52.73% and 52.51%, respectively), were chosen for further studies.

The functional group interactions relating to the polymers and their formulations in the form of micelles were characterized *via* FTIR spectroscopy. The FTIR spectrum of EC (Fig. S7A†) showed characteristic peaks at 3485 cm<sup>−1</sup>, due to O–H stretching, and at 2974 cm<sup>−1</sup>, 2872 cm<sup>−1</sup>, and 1376 cm<sup>−1</sup>, due to C–H stretching and bending. The peak noticed at 1060 cm<sup>−1</sup> corresponds to C–O–C groups, while the one at 1120 cm<sup>−1</sup> is particular to C–C stretching.<sup>31</sup> Bare mPEG showed a broad absorption peak from terminal O–H that appeared at around 3421 cm<sup>−1</sup>. Characteristic C–H bending bands were observed at 2880 cm<sup>−1</sup>, 1475 cm<sup>−1</sup>, 948 cm<sup>−1</sup>, and 842 cm<sup>−1</sup>. The peaks that were visible at 1150 cm<sup>−1</sup> and 1060 cm<sup>−1</sup> were due to the ether

Table 2 The thermal properties of pure polymers and micelles with DOX

Chemical composition name	Glass transition temperature ( $T_g$ ) (°C)	Crystallization temperature ( $T_c$ ) (°C)	Melting temperature ( $T_m$ ) (°C)
EC	115	—	233
mPEG	−66	29	56
CEC	116	—	233
B1	−24	24	53, 176
B4	−29	21	53, 176
B3	−29	25	53, 176
B6	−26	24	53, 175

linkage of the C–O–C groups (Fig. S7A†).<sup>32–34</sup> The spectrum of EC-PEG1, as shown in Fig. S7B,† showed peaks at 3465 cm<sup>−1</sup>, 2972 cm<sup>−1</sup>, and 2879 cm<sup>−1</sup>, which represented both EC and mPEG, and characteristic peaks in the fingerprint region of mPEG at 1112 cm<sup>−1</sup>, 948 cm<sup>−1</sup>, and 842 cm<sup>−1</sup> are evident<sup>32</sup>. A peak at 1745 cm<sup>−1</sup> was observed due to the formation of ester C=O bonds between CEC and mPEG. Further, similar peaks were observed in the EC-PEG2 spectrum (Fig. S7B†) at 3465 cm<sup>−1</sup>, 2972 cm<sup>−1</sup>, 2879 cm<sup>−1</sup>, 1745 cm<sup>−1</sup>, 1112 cm<sup>−1</sup>, 948 cm<sup>−1</sup>, and 842 cm<sup>−1</sup>. The FTIR spectrum of DOX (Fig. S7A†) possessed characteristic peaks from N–H stretching at 3527 cm<sup>−1</sup>, carbonyl C=O at 1730 cm<sup>−1</sup>, aromatic C=C stretching at 1620 cm<sup>−1</sup>, aromatic C–H stretching at 2930 cm<sup>−1</sup>, and O–H stretching at 3334 cm<sup>−1</sup>.<sup>35,36</sup> The FTIR spectra of the DOX-EC-PEG micelles B3 and B6 are shown in Fig. S7C.† The spectra displayed a broad peak at 3464 cm<sup>−1</sup> due to N–H and O–H functional groups being present in the compositions (B3 and B6). C–H stretching peaks present in the EC and mPEG spectra were observed at 2880 cm<sup>−1</sup> and 2974 cm<sup>−1</sup>. A broad peak at 1740 cm<sup>−1</sup> was attributed to the characteristic C=O groups of DOX and CEC. The sharp peak from C–C stretching at 1120 cm<sup>−1</sup>, which is characteristic of EC, was also observed; the C–O–C peak at 1060 cm<sup>−1</sup> of mPEG merged with this sharp broad peak. The characteristic C–H bending peaks of mPEG at 948 cm<sup>−1</sup> and 842 cm<sup>−1</sup> were also observed in the B3 and B6 spectra. Observations from the FTIR spectra of B3 and B6 suggested that the prepared micelles were a combination of the copolymer EC-PEG with DOX. Moreover, the peaks of DOX merged with the copolymer EC-PEG due to their interactions and the good distribution in the micelles.

The thermal properties of the pure polymers (EC, mPEG, and CEC) and formulations with (B3 and B6) and without (B1 and B4) DOX are shown in Table 2 and Fig. S8.† The glass transition temperature ( $T_g$ ) of pure EC was recorded to be 115 °C with a melting temperature ( $T_m$ ) of 233 °C. Similarly, CEC showed  $T_g$  and  $T_m$  values of 116 °C and 233 °C, respectively. Further, the  $T_g$ , crystallization temperature ( $T_c$ ), and  $T_m$  values of mPEG were −66 °C, 29 °C, and 56 °C, respectively. The thermogram of B4 showed  $T_g$ ,  $T_c$ , and  $T_m$  values of −29 °C, 21 °C, and 53/176 °C, respectively, which indicated the semi-crystalline nature of EC-PEG. Further, the  $T_g$  value of EC was greatly changed after grafting mPEG to CEC. These results suggested that the grafting



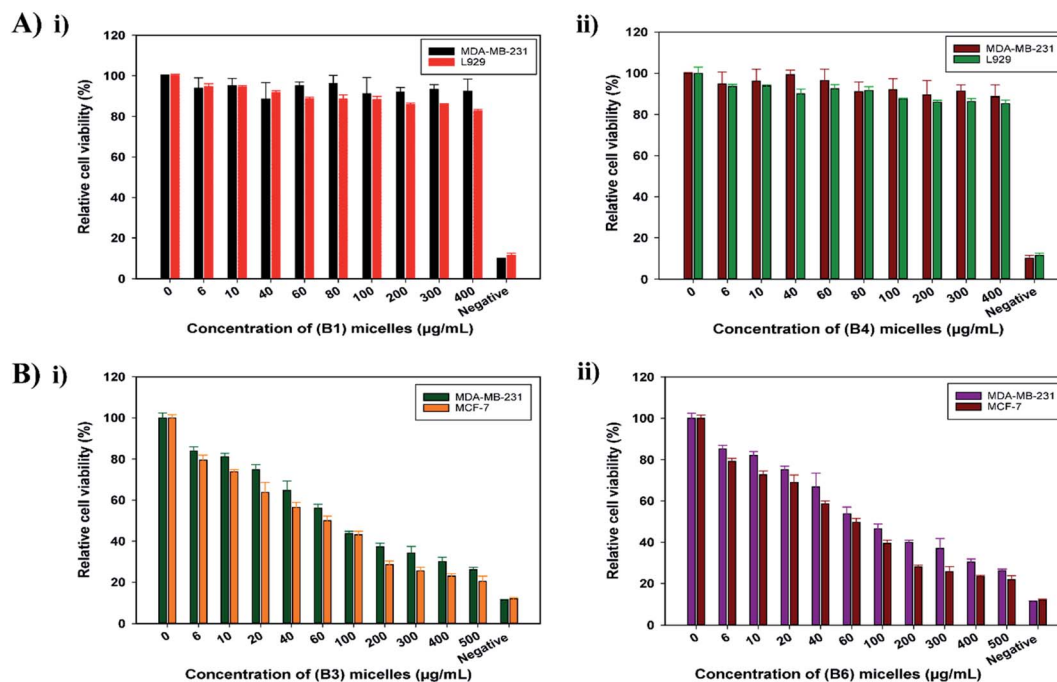


Fig. 4 (A) (i) Cytotoxic effects toward MDA-MB-231 and L929 cells treated with B1 micelles for 48 h; and (ii) cytotoxic effects toward MDA-MB-231 and L929 cells treated with B4 micelles for 48 h. (B) (i) Cytotoxic effects toward MDA-MB-231 and MCF-7 cells treated with B3 micelles for 72 h; and (ii) cytotoxic effects toward MDA-MB-231 and MCF-7 cells treated with B6 micelles for 72 h.

of PEG to CEC was done successfully. The thermal properties of the B6 micelles were recorded, where the  $T_g$ ,  $T_c$ , and  $T_m$  values were  $-26$  °C,  $24$  °C, and  $53/175$  °C, respectively. The changes in  $T_g$  and  $T_c$  indicated the loading of DOX into the micelles. According to the reported literature,<sup>37</sup> DOX has a  $T_m$  value of  $218$  °C. The  $T_m$  value of DOX was greatly changed based on the thermograms of the DOX-loaded micelles B3 and B6, which indicated that the drug was molecularly dispersed and bound to the polymers.<sup>14</sup> This also suggests the improved solubility of crystalline DOX in an aqueous medium when it is entrapped in a polymeric system.

**3.3.1 In vitro DOX release.** The release of DOX from EC-PEG micelles (B3 and B6) was studied for 72 h *via* a dialysis method at  $37$  °C using phosphate buffer at pH 5.5 and 7.4, respectively. The release of DOX was faster at pH 5.5 compared to the release of DOX at pH 7.4 because the ester bonds formed between CEC and mPEG were susceptible to the acidic pH.<sup>38,39</sup> Fig. 3A shows the release profiles of DOX at different pH values from B3. At pH 5.5, the B3 micelles recorded 100% release of DOX within 35 h and at pH 7.4, 96% DOX release was recorded within 72 h. The release of DOX from B6 micelles was slow at both pH values compared to that from the B3 micelles. For instance, 99% DOX release was recorded at pH 5.5 within 48 h and 72% DOX release was recorded at pH 7.4 within 72 h. This trend of slow release from B6 micelles compared to from B3 micelles suggested that increased mPEG grafting increased the molecular weight of the copolymer, thus the rate of release was slowed.<sup>40</sup> Overall, the sustained release of DOX can be attributed to the encapsulating properties of EC and hydrophobic interactions between DOX and EC.<sup>30,41</sup> The pH-dependent release

from the micelles can be utilized to deliver DOX at tumor pH, because the tumor extracellular environment is slightly acidic (pH 6.8) and, after endocytosis by cancer cells, the pH of lysosomes/endosomes is also acidic (pH 5.5); there is also minimized release of DOX at normal tissue pH (pH 7.4).<sup>42–44</sup>

**3.3.2 Hemolysis assays.** Hemolysis assays are used to validate the biocompatibility of a biomaterial or polymer. According to ASTM standards (E2524-08), hemolysis for a test sample of above 5% indicates toxicity toward RBCs.<sup>45</sup> The test samples EC, CEC, B1, B3, B4, and B6 were assessed for their biocompatibility in human blood at concentrations of 0.5 and 1 mg mL<sup>-1</sup>. The hemolysis percentages were calculated *via* eqn (3), considering 100% lysis in DI water and 0% lysis in PBS. As seen in the histogram shown in Fig. 3B, EC displayed less than 5% hemolysis, hence it can be termed a non-hemolytic material, and after modification and the formation of micelles (B1, B3, B4, and B6), the material maintained its hemocompatibility. As observed, CEC had slightly better hemocompatibility than EC, which could be due to the addition of negatively charged carboxylic groups. In the cases of B1 and B4, even at a higher concentration of 1 mg mL<sup>-1</sup>, the observed hemolysis% values were  $1.47 \pm 0.2$  and  $1.17 \pm 0.2$ , respectively. The improved hemocompatibility of the micelles in comparison to EC and CEC can be attributed to the mPEG grafting.<sup>46</sup> These results confirm the advantages of the PEGylation of polymers; upon mPEG grafting, the ability of the test materials to induce RBC lysis decreased significantly. In B3 and B6, at 0.5 mg mL<sup>-1</sup>, the observed hemolysis% values were  $3.68 \pm 0.1$  and  $3.82 \pm 0.2$ , respectively, which are within the permissible limit of 5%, whereas at 1 mg mL<sup>-1</sup>, hemolysis is close to 5%. The toxicity to



RBCs in the presence of B3 and B6 samples at higher concentrations was due to DOX. DOX is known to enter RBCs and cause swelling and lysis *via* building up the osmotic pressure.<sup>47</sup> As per the report by Shuai *et al.*,<sup>48</sup> free DOX induces 11% hemolysis at  $200 \mu\text{g mL}^{-1}$ , but when loaded into micelles its toxicity is largely diminished. The reason for the lower hemotoxicity of DOX in EC-PEG micelles in comparison to that reported for free DOX is the entrapment of DOX in the hydrophobic core, thus reducing the amount of DOX available on the surface for interactions with RBCs. As mentioned earlier, the hydrophilic mPEG chains formed a protective cover and, therefore, the RBCs were inhibited from being lysed. In line with these findings, we consider that the developed copolymer EC-PEG is biocompatible and can be used as a potential nanocarrier for DD.

### 3.4 Cell studies

**3.4.1 Cytotoxicity assays.** The cytotoxic effects of blank and DOX-loaded EC-PEG micelles were determined *via* MTT assays. The cytotoxic effects of B1 and B4 micelles were investigated toward fibroblast L929 and breast cancer MDA-MB-231 cell lines. DMSO was used to solubilize the formazan crystals formed after the addition of the MTT reagent, which indicated cellular respiratory activity. As shown in Fig. 4, B1 (Fig. 4A(i)) and B4 (Fig. 4A(ii)) micelles exhibited no cellular cytotoxicity for up to 48 h of incubation at varying concentrations. The relative cell viability was above 80% even at the highest micelle concentration of  $400 \mu\text{g mL}^{-1}$ . Thus, this demonstrated the non-cytotoxic nature of the mPEG-grafted EC micelles and established them as a promising drug-delivery vehicle. The cytotoxic effects of B3 and B6 micelles were investigated toward

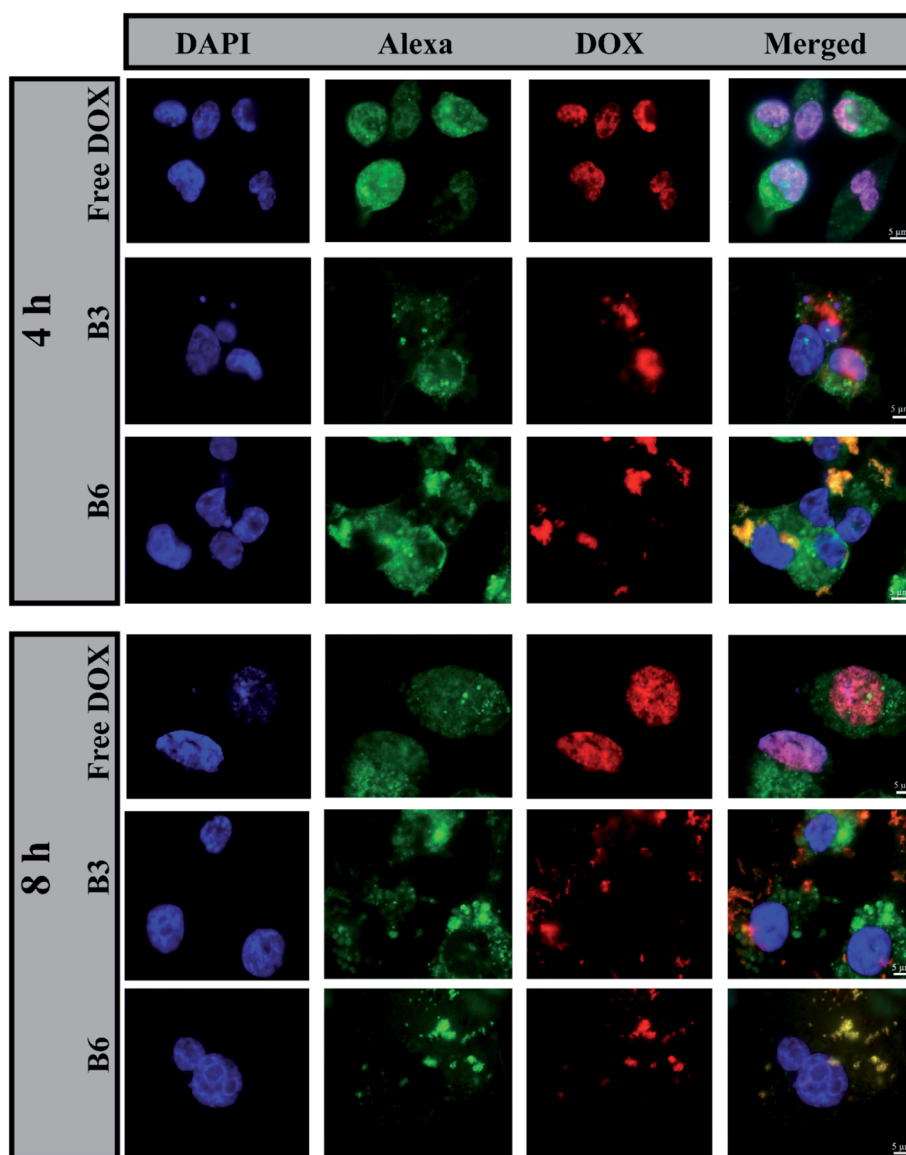


Fig. 5 Fluorescence images of MDA-MB-231 cells treated with free DOX, B3 micelles, or B6 micelles for 4 h and 8 h. The right panels show merged images of nuclei stained with DAPI (blue), F-actin stained with Alexa Fluor 488 phalloidin (green), and DOX fluorescence (red). The scale bars correspond to  $5 \mu\text{m}$ .





the breast cancer cell lines MDA-MB-231 and MCF-7 for 72 h. From the histogram, as shown in Fig. 4B, the DOX-loaded micelles B3 (Fig. 4B(i)) and B6 (Fig. 4B(ii)) showed a decrease in cell viability as a function of the DOX dose concentration. The concentration of micelles was varied from 0  $\mu\text{g mL}^{-1}$  to 500  $\mu\text{g mL}^{-1}$  and the  $\text{IC}_{50}$  (the dose inducing 50% cell inhibition) values noted for B3 and B6 toward both cell lines were  $\sim 100 \mu\text{g mL}^{-1}$ . These results proved that EC-PEG micelles are a biocompatible and non-toxic DDS for delivering DOX at a controlled rate over an extended period of time.

**3.4.2 In vitro cellular uptake.** The cellular uptake of free DOX and DOX-EC-PEG (B3 and B6) micelles was studied in breast cancer cells MDA-MB-231 *via* incubating them with the samples in media at 37 °C for 4 h and 8 h, respectively; later, analysis was conducted *via* epifluorescence microscopy. The nuclei of cells were stained with DAPI, the actin filaments of the cytoskeleton were stained with Alexa Fluor 488 phalloidin, and DOX emitted red fluorescence. In cells treated with free DOX, as shown in Fig. 5, it was observed that DOX was exclusively present in the nuclei. This can be explained based on the fact that DOX can be readily transported into cells *via* the mechanism of passive diffusion, which is energy independent, where it binds to DNA in the nuclei *via* intercalation.<sup>49,50</sup> In cells treated with B3 and B6 micelles at 100  $\mu\text{g mL}^{-1}$ , it was observed that the red fluorescence of DOX was located in the cytoplasm and nuclear region (Fig. 5, B3 and B6 rows). This observation leads to the inference that the DOX-loaded micelles were taken up by the cells *via* an endocytosis pathway and were located in the intracellular compartment (endosomes and lysosomes), which is supported by the reported literature.<sup>42,51</sup>

## 4. Conclusions

In this study, we synthesized a new amphiphilic copolymer *via* grafting PEG to EC. The developed copolymer was self-assembled into micelles in an aqueous system *via* a dialysis method, and the micelle properties were confirmed *via* DLS, TEM, and fluorescence spectroscopy studies; the CMCs of the copolymers EC-PEG1 and EC-PEG2 were recorded to be 0.03 mg  $\text{mL}^{-1}$  and 0.00193 g  $\text{mL}^{-1}$ , respectively. The sizes of the DOX-encapsulated EC-PEG nano-micelles were larger than the size of the blank micelles, which was confirmed *via* DLS. The DOX-loaded micelles demonstrated faster release at an acidic pH of 5.5, whereas slow DOX release was observed at physiological pH of 7.4. Hemolysis assay and MTT assay studies confirmed that the micelles were biocompatible and non-toxic toward normal cells. Further, the DOX-loaded micelles showed toxicity toward the cancerous cells MDA-MB-231 and MCF-7, and fluorescence microscopy images showed the internalization of the DOX-loaded micelles in MDA-MB-231 cells. According to the above observations, we concluded that the developed micelles can be used as a potential DDS for cancer therapy. In the future scope of this work, the micelles could be tailored with various targeting moieties to achieve site-specific targeted delivery.

## Conflicts of interest

There are no conflicts to declare.

## Acknowledgements

The authors are grateful to the funding agencies CSIR (MLP034726, CSC0302, CSC0134) and DBT-SRF, New Delhi. The authors also are thankful to Dr Neha Tiwari and Mr Prashant Yadav for support in designing the synthesis scheme and for input relating to NMR evaluations.

## References

- 1 D. Hwang, J. D. Ramsey and A. V. Kabanov, *Adv. Drug Delivery Rev.*, 2020, **156**, 80–118.
- 2 J. Gong, M. Chen, Y. Zheng, S. Wang and Y. Wang, *J. Controlled Release*, 2012, **159**, 312–323.
- 3 Z. Ahmad, A. Shah, M. Siddiq and H.-B. Kraatz, *RSC Adv.*, 2014, **4**, 17028–17038.
- 4 H. Cabral and K. Kataoka, *J. Controlled Release*, 2014, **190**, 465–476.
- 5 J. Fang, H. Nakamura and H. Maeda, *Adv. Drug Deliv. Rev.*, 2011, **63**, 136–151.
- 6 S. Wilhelm, A. J. Tavares, Q. Dai, S. Ohta, J. Audet, H. F. Dvorak and W. C. W. Chan, *Nat. Rev. Mater.*, 2016, **1**, 1–12.
- 7 S. Biswas, P. Kumari, P. M. Lakhani and B. Ghosh, *Eur. J. Pharm. Sci.*, 2016, **83**, 184–202.
- 8 S. Sabra, M. Abdelmoneem, M. Abdelwakil, M. T. Mabrouk, D. Anwar, R. Mohamed, S. Khattab, A. Bekhit, K. Elkhodairy and M. Freag, *Curr. Pharmaceut. Des.*, 2017, **23**, 5213–5229.
- 9 X. Su, Z. Yang, K. B. Tan, J. Chen, J. Huang and Q. Li, *Carbohydr. Polym.*, 2020, **241**, 116259.
- 10 S. Muschert, F. Siepman, B. Leclercq, B. Carlin and J. Siepman, *J. Controlled Release*, 2009, **135**, 71–79.
- 11 B. Balzus, M. Colombo, F. F. Sahle, G. Zoubari, S. Staufienbiel and R. Bodmeier, *Int. J. Pharm.*, 2016, **513**, 247–254.
- 12 S. Leitner, S. Grijalvo, C. Solans, R. Eritja, M. J. García-Celma and G. Calderó, *Carbohydr. Polym.*, 2020, **229**, 115451.
- 13 W. Yuan, J. Yuan, F. Zhang and X. Xie, *Biomacromolecules*, 2007, **8**, 1101–1108.
- 14 R. Gref, A. Domb, P. Quellec, T. Blunk, R. H. Müller, J. M. Verbavatz and R. Langer, *Adv. Drug Deliv. Rev.*, 2012, **64**, 316–326.
- 15 E. Lasseguette, *Cellulose*, 2008, **15**, 571–580.
- 16 T. Kaldéus, M. Nordenström, A. Carlmark, L. Wågberg and E. Malmström, *Carbohydr. Polym.*, 2018, **181**, 871–878.
- 17 D. Shen and Y. Huang, *Polymer*, 2004, **45**, 7091–7097.
- 18 Q. Zhao, B. Han, Z. Wang, C. Gao, C. Peng and J. Shen, *Nanomedicine*, 2007, **3**, 63–74.
- 19 J. Araki, M. Wada and S. Kuga, *Langmuir*, 2001, **17**, 21–27.
- 20 J. Chen, X. Qiu, J. Ouyang, J. Kong, W. Zhong and M. M. Q. Xing, *Biomacromolecules*, 2011, **12**, 3601–3611.
- 21 M. Hirota, N. Tamura, T. Saito and A. Isogai, *Carbohydr. Polym.*, 2009, **78**, 330–335.
- 22 A. E. J. De Nooy, A. C. Besemer and H. Van Bekkum, *Recl. Trav. Chim. Pays-Bas*, 1994, **113**, 165–166.
- 23 B. Ding, Y. qing Ye, J. Cheng, K. Wang, J. Luo and B. Jiang, *Carbohydr. Res.*, 2008, **343**, 3112–3116.



- 24 A. Isogai, T. Saito and H. Fukuzumi, *Nanoscale*, 2011, **3**, 71–85.
- 25 T. Heinze, T. Liebert and A. Koschella, *Esterification of polysaccharides*, Springer Science & Business Media, 2006.
- 26 D. Shen, H. Yu and Y. Huang, *J. Polym. Sci., Part A: Polym. Chem.*, 2005, **43**, 4099–4108.
- 27 Y. Li, R. Liu, W. Liu, H. Kang, M. Wu and Y. Huang, *J. Polym. Sci., Part A: Polym. Chem.*, 2008, **46**, 6907–6915.
- 28 J. Zhu, X.-T. Dong, X.-L. Wang and Y.-Z. Wang, *Carbohydr. Polym.*, 2010, **80**, 350–359.
- 29 Y. Dong and K. J. Edgar, *Polym. Chem.*, 2015, **6**, 3816–3827.
- 30 S. Lv, Z. Tang, M. Li, J. Lin, W. Song, H. Liu, Y. Huang, Y. Zhang and X. Chen, *Biomaterials*, 2014, **35**, 6118–6129.
- 31 V. Suthar, A. Pratap and H. Raval, *Bull. Mater. Sci.*, 2000, **23**, 215–219.
- 32 Y. Li, R. Liu and Y. Huang, *J. Appl. Polym. Sci.*, 2008, **110**, 1797–1803.
- 33 P. Shoaefar, M. Abbasian and A. A. Entezami, *J. Polym. Res.*, 2007, **14**, 45–52.
- 34 H. Asadi, K. Rostamizadeh, D. Salari and M. Hamidi, *J. Microencapsulation*, 2011, **28**, 406–416.
- 35 D. Depan, J. Shah and R. D. K. Misra, *Mater. Sci. Eng., C*, 2011, **31**, 1305–1312.
- 36 A. Neacșu, *Thermochim. Acta*, 2018, **661**, 51–58.
- 37 D. Missirlis, R. Kawamura, N. Tirelli and J. A. Hubbell, *Eur. J. Pharm. Sci.*, 2006, **29**, 120–129.
- 38 K. Rostamizadeh, M. Manafi, H. Nosrati, H. K. Manjili and H. Danafar, *New J. Chem.*, 2018, **42**, 5937–5945.
- 39 T. D. Carrillo-Castillo, J. S. Castro-Carmona, A. Luna-Velasco and E. A. Zaragoza-Contreras, *e-Polym.*, 2020, **20**, 624–635.
- 40 Y.-Z. Du, Q. Weng, H. Yuan and F.-Q. Hu, *ACS Nano*, 2010, **4**, 6894–6902.
- 41 K. Wasilewska and K. Winnicka, *Materials*, 2019, **12**, 3386.
- 42 S. Lv, M. Li, Z. Tang, W. Song, H. Sun, H. Liu and X. Chen, *Acta Biomater.*, 2013, **9**, 9330–9342.
- 43 Z. Wang, X. Deng, J. Ding, W. Zhou, X. Zheng and G. Tang, *Int. J. Pharm.*, 2018, **535**, 253–260.
- 44 C. R. Justus, L. Dong and L. V. Yang, *Front. Physiol.*, 2013, **4**, 354.
- 45 J. Choi, V. Reipa, V. M. Hitchins, P. L. Goering and R. A. Malinauskas, *Toxicol. Sci.*, 2011, **123**, 133–143.
- 46 S. V. Lale, A. Kumar, F. Naz, A. C. Bharti and V. Koul, *Polym. Chem.*, 2015, **6**, 2115–2132.
- 47 D. Lu, J. Liang, Y. Fan, Z. Gu and X. Zhang, *Adv. Eng. Mater.*, 2010, **12**, B496–B503.
- 48 X. Shuai, H. Ai, N. Nasongkla, S. Kim and J. Gao, *J. Controlled Release*, 2004, **98**, 415–426.
- 49 Y. Cao, Y. Gu, H. Ma, J. Bai, L. Liu, P. Zhao and H. He, *Int. J. Biol. Macromol.*, 2010, **46**, 245–249.
- 50 H. Wang, Y. Zhao, Y. Wu, Y.-l. Hu, K. Nan, G. Nie and H. Chen, *Biomaterials*, 2011, **32**, 8281–8290.
- 51 H. C. Arora, M. P. Jensen, Y. Yuan, A. Wu, S. Vogt, T. Paunesku and G. E. Woloschak, *Cancer Res.*, 2012, **72**, 769–778.





Cite this: DOI: 10.1039/d1nr04411g

## Combinatorial therapy using RNAi and curcumin nano-architectures regresses tumors in breast and colon cancer models†

Aviral Kumar,<sup>†</sup> Amarnath Singam,<sup>‡</sup> Guruprasadh Swaminathan,<sup>a</sup> Naresh Killi,<sup>§</sup> Naveen Kumar Tangudu,<sup>§</sup> Jedy Jose,<sup>a</sup> Rathna Gundloori VN<sup>†</sup> and Lekha Dinesh Kumar<sup>†\*</sup>

Cancer is a debilitating disease and one of the leading causes of death in the world. In spite of the current clinical management being dependent on applying robust pathological variables and well-defined therapeutic strategies, there is an imminent need for novel and targeted therapies with least side effects. RNA interference (RNAi) has gained attention due to its precise potential for targeting multiple genes involved in cancer progression. Nanoparticles with their enhanced permeability and retention (EPR) effect have been found to overcome the limitations of RNAi-based therapies. With their high transportation capacity, nano-carriers can target RNAi molecules to tumor tissues and protect them from enzymatic degradation. Accumulating evidence has shown that tyrosine kinase *Ephb4* is overexpressed in various cancers. Therefore, we report here the development and pre-clinical validation of curcumin-chitosan-loaded: eudragit-coated nanocomposites conjugated with *Ephb4* shRNA as a feasible bio-drug to suppress breast and colon cancers. The proposed bio-drug is non-toxic and bio-compatible with a higher uptake efficiency and through our experimental results we have demonstrated the effective site-specific delivery of this biodrug and the successful silencing of their respective target genes *in vivo* in autochthonous knockout models of breast and colon cancer. While mammary tumors showed a considerable decrease in size, oral administration of the biodrug conjugate to *Apc* knockout colon models prolonged the animal survival period by six months. Hence, this study has provided empirical proof that the combinatorial approach involving RNA interference and nanotechnology is a promising alliance for next-generation cancer therapeutics.

Received 7th July 2021,  
 Accepted 12th November 2021

DOI: 10.1039/d1nr04411g

rsc.li/nanoscale

### 1. Introduction

Cancer, a sequential process of genetic alterations, is counted as the most menacing health-related problem worldwide. According to the GLOBOCAN, cancer-related mortality surged to 10 million deaths, with 19.3 million new incidences reported in 2020.<sup>1</sup> Although different treatment modalities are present for cancer, most of them are associated with debilitating side effects and lower patient survival.<sup>2</sup> The inherent limitations of existing therapeutic strategies, along with current treatment impediments, accentuate the need for more specific and targeted alternative therapies.<sup>3–5</sup> With the advent of next-

generation technologies and high-throughput analysis, innovative and personalized biological anticancer treatment is expected to find its way from bench to bedside.<sup>6–9</sup> RNA interference (RNAi), a post-transcriptional gene silencing phenomenon, is gaining immense clinical attention regarding its usage as a potential weapon against solid tumors.<sup>10</sup> RNAi could target multiple genes in different pathways that are involved in tumor progression, making them more effective with no side effects.<sup>11</sup> Most of the existing chemotherapeutic agents are directed towards tyrosine kinases to suppress cancer.<sup>12</sup> One of the significant tyrosine kinase receptors overexpressed in various cancers is the *Ephb4* receptor, which is associated with tumor angiogenesis, growth, and metastasis.<sup>13–16</sup> In the present study, we aimed at silencing this *Ephb4* receptor using the RNAi approach in different cancer models to assess its effect in tumor suppression.

The lack of safe and effective delivery methods for RNAi molecules remains the primary challenge that prevents the full utilization of the potential of RNAi-based therapy in biological systems.<sup>17,18</sup> A plethora of literature demystifies the promising potential of nanoparticles in delivering RNA-based therapeutics

<sup>a</sup>Cancer Biology, CSIR-Centre for Cellular and Molecular Biology, (CCMB) Uppal Road, Hyderabad, 500007 Telangana, India. E-mail: lekha@ccmb.res.in

<sup>b</sup>Polymer Science and Engineering Division, CSIR-National Chemical Laboratory, Pune, 411008 Maharashtra, India. E-mail: rv.gundloori@ncl.res.in

<sup>c</sup>Academy of Scientific and Innovative Research (AcSIR), Ghaziabad, 201002 Uttar Pradesh, India

† Electronic supplementary information (ESI) available. See DOI: 10.1039/d1nr04411g

‡ These authors contributed equally to this work.

§ These authors contributed equally to this work.

because of their surface modifications, site targeted delivery, enhanced permeability and retention effect, and accumulation at pharmacological levels.<sup>19–23</sup> To this end, we designed a combinatorial approach of using nano-curcumin to encapsulate Ephb4 shRNA along with other bioactive agents such as chitosan and eudragit for enhanced targeting and uptake by the cancerous cells at the tumor site. As well documented, curcumin, a bioactive spice from *Curcuma longa*, has been used since a long time to treat various chronic diseases, including cancers.<sup>24</sup> Curcumin possesses potent anticarcinogenic, anti-inflammatory, and antioxidant properties making it one of the best-studied nutraceuticals for cancer therapeutics.<sup>25–27</sup> However, its poor water solubility and bioavailability prevent its use as an ideal therapeutic molecule and recently, various investigations have fabricated different types of nano-formulations using curcumin with increased pharmacokinetics and bioavailability.<sup>28,29</sup> For the complexation of nucleic acids in RNAi delivery of the nano-curcumin structures, polymers forming complexes with these molecules *via* multivalent interactions are preferred.<sup>30</sup> Chitosan is a biodegradable, non-toxic, and well-researched mucoadhesive polymer obtained from natural sources like shells of crustaceans can be used as a cationic biopolymer.<sup>31</sup> Furthermore, targeting the nano-RNAi complexes in the colon through the oral route requires bypassing the formulation from the harsh conditions of the stomach.<sup>32–34</sup> Eudragit S-100, an anionic pH-sensitive polymer, has been used as a protective coating to protect the drugs from degradation in the stomach and the subsequent release of the therapeutic molecules in the colon region where the pH is 7.5, low alkaline to neutral.<sup>35–38</sup>

With this background, the present investigation conceptualized a nano-RNAi based approach by using Ephb4 shRNA conjugated to curcumin–chitosan and encapsulated by the Eudragit S-100 nanoarchitecture to specifically silence the overexpressed oncogenic Ephb4 mRNA in the double knockout autochthonous *Bra2/p53*<sup>−/−</sup> breast and *Apc*<sup>−/−</sup> colon cancer murine models. Our results demonstrated that the nano-RNAi biodrug formulation efficiently regresses the tumors by effective knockdown of target genes with a concomitant increase in survivability. Although various studies have explored the combinatorial effects of nanoparticles with small oligos, this is the first report of a combinatorial drug, bringing together the synergistic effect of a natural compound (curcumin) with gene silencing using shRNA in solid tumors. Our work combines the effectiveness of curcumin, the golden nutraceutical well known for its anti-cancer and anti-inflammatory properties, and the RNA interference approach for a site-specific and effective therapeutic outcome in two different tumor murine models. Hence, this pre-clinical study delineates a promising approach for using non-synthetic nanomaterials with RNA interference in biological systems for cancer therapeutics.

## 2. Materials and methods

### 2.1 Materials

Chitosan (190–310 kDa) was procured from Sigma-Aldrich, USA. Eudragit S-100 was a gift sample from Evonik Industries,

Germany. Crystalline curcumin was procured from S. D. Fine, India. Calcium chloride and cyanine 7.5 NHS ester dye were procured from Spectrochem, India and Lumiprobe, USA, respectively. FBS (fetal bovine serum), DMEM (Dulbecco's modified Eagle's medium), MTT (3-(4,5-dimethylthiazol-2-yl)-2,5-diphenyltetrazolium bromide) were purchased from Invitrogen, USA. L929, HCT116, and MCF-7 cell lines were obtained from the cell repository of the National Centre for Cell Science (NCCS), India. Primary and secondary antibodies were purchased from Abcam, UK. Immunohistochemistry kits were procured from the DAKO Envision system, USA. The solvents and reagents of analytical grade were obtained from a local vendor. The liver function test (LFT) and renal function test (RFT) kits were purchased from Coral Clinical Systems, India.

### 2.2 Experimental methods

**2.2.1 Preparation of fluorescent nanoencapsulate of curcumin–chitosan (CU–CS).** Curcumin (CU) (1 g per 100 mL) was dispersed in 60% ethanol and subjected to sonication by an ultra-probe sonicator (VCX 500, Vibra-Cell, Sonics, USA) at 40% amplitude for 1 h with a sonication time of 5 seconds in an ice bath. After sonication, cyanine 7.5 NHS dye (10  $\mu\text{g mL}^{-1}$ ) was dissolved in DMSO and was added to the dispersed CU solution. The solution mixture was stirred for 30 min at ambient temperature. Furthermore, the respective 1 and 2 wt% of chitosan (CS) solutions of pH 5.0 were prepared in 2% (v/v) acetic acid solution by stirring for 6 h. Equal volumes of CS and CU-cyanine-7.5 NHS dye dispersion were added slowly drop wise under high-speed stirring to make a CU–CS suspension. The CU nanoparticle concentration was fixed at 1 wt%, and the CS concentration was varied to attain various formulations. To crosslink, the individual formulations were electrosprayed vertically in 100 mL of calcium chloride (5 wt%) solution using an electrospinning unit (ESPIN Nano, PECO, India). The parameters for electrospraying were optimized at a voltage of 24 kV with a flow rate of 0.5 mL h<sup>−1</sup>. The distance between the tip of the needle and the collector was maintained at a distance of 15 cm. The electrosprayed dispersion was centrifuged at 16 000 rpm for 24 min at 12 °C to pelletize the NPs. The obtained pellet was dispersed in 20 mL of deionized water (DI) and washed twice, followed by repeated centrifugations. Furthermore, the pellet of the NPs was dried by lyophilization and characterized to analyze the Ephb4–shRNA (plasmid DNA) complexation and eudragit S-100 (ES) coating.

**2.2.2 Entrapment and loading efficiency.** The entrapment and loading efficiency of NPs were calculated according to the reported literature.<sup>30,33</sup> Briefly, 2 mg of 1 : 1 ratio of CU–CS NPs was dispersed in 2 mL of methanol by sonication for 2 min. The resulting dispersion was centrifuged at 16 500 rpm for 35 min at 12 °C and collected from the supernatant. The untrapped CU concentration present in the supernatant was calculated using a standard calibration curve of CU at  $\lambda_{\text{max}}$  of 423 nm, which was analyzed using a UV-vis spectrophotometer (UV 1601PC UV spectrophotometer, Shimadzu, Japan). The percent of entrapment efficiency (EE) was estimated using eqn

(1). The percent of loading efficiency was estimated using eqn (2). Similarly, the percent of entrapment and loading efficiency were calculated for other formulations.

$$\%EE = \frac{(\text{wt. of CU used} - \text{wt. of untrapped CU})}{\text{wt. of CU used}} \times 100 \quad (1)$$

$$\%LE = \frac{\text{entraped CU in NPs}}{\text{wt. of NPs}} \times 100 \quad (2)$$

**2.2.3 Complexation of shRNA to CU-CS NPs.** Complexes of Ephb4-shRNA with the respective ratios of CU-CS NPs were formed with two different weight ratios, 25:0.8 and 25:1.0 [(CU-CS) and shRNA]. The respective NPs with different ratios of Ephb4-shRNA were heated separately for 12 min at 55 °C and then the solutions were mixed and vortexed for 30 seconds to obtain the respective complexes of CU-CS-shRNA NPs. The respective complexed NPs were loaded into the wells of an agarose gel (1 wt%) and complexation was confirmed by agarose gel retardation assay.

**2.2.4 Eudragit S-100 coated NPs.** CU-CS-shRNA NPs were coated with ES using 1 wt% ES solution of pH 5, which was prepared using a solvent mixture of ethanol and acetone in a 2:1 ratio. From this solution, 200 µL was added dropwise to the dispersion of 800 µL of CU-CS-shRNA NPs to form ES coated CU-CS-shRNA (CU-CS-shRNA-ES) NPs.

**2.2.5 In vitro CU release studies.** The drug release studies for the developed formulations were performed by the direct dispersion method in different buffers, HCl-KCl (hydrochloric acid-potassium chloride 0.1 M, pH 1.2), and PBS (phosphate buffered solution, 0.1 M, pH 6.8), and PBS (phosphate buffered solution, 0.1 M, pH 7.4).<sup>39</sup> The release of CU from CU-CS NPs and CU-CS-ES NPs was determined according to the reported protocol.<sup>34</sup> For example, 5 mg of the respective lyophilized NPs were dispersed separately in 20 mL of different buffers as mentioned above. A duplicate set of 1 mL each was aliquoted from the above respective dispersions. Release kinetics was monitored at 37 °C in a water bath shaker (50 rpm) for a period of 4 h in the buffer of pH 1.2. Similarly, the release studies were done in the respective buffers of pH 6.8 and 7.4 for up to 72 h. After the designated time intervals, the sample tubes were taken out and centrifuged at 1200 rpm for 3 min to collect the pellet of released CU. Later, the collected CU pellet was dissolved in 1 mL of methanol and the amount of CU was quantified by a UV-Vis spectrophotometer (UV 1601PC UV spectrophotometer, Shimadzu, Japan) at a wavelength of 423 nm.

**2.2.6 Characterization of NPs.** The zeta potential and particle size distribution of CU NP, CU-CS NPs, CU-CS-shRNA NPs, and CU-CS-shRNA-ES NPs were analyzed using a 90 Plus Brookhaven Instruments Corp, PALS zeta potential analyzer, USA. The morphological characterization of CU-CS-shRNA-ES NPs was done using an ESEM (Quanta 200 3D, FEI, USA). The lyophilized NPs were dispersed and diluted (10×) in Millipore water to form a suspension that was later cast on a silicon wafer and sputter-coated with gold for ESEM analysis.

Similarly, NP dispersions were prepared, drop cast on a copper grid, and stained with 1 wt% uranyl acetate dye for transmission electron microscope (TEM) analysis (FEI Tecnai TF20 200 kV FEG high-resolution Transmission Electron Microscope, USA). Pure polymers, curcumin encapsulates and polymeric interactions with CU were analyzed by FTIR (PerkinElmer spectrometer I, FT-IR diffused reflectance (DRIFT) mode, USA). The spectra recorded were in the range of 400 to 4000 cm<sup>-1</sup> with an average of 10 scans per sample. The thermal behaviors of pure polymers (CS and ES), CU, and NPs (CU-CS and CU-CS-ES) were recorded using a differential scanning calorimetry (DSC) instrument (Model Q10 DSC, TA instrument, USA). Respective samples of ~5 mg were used for recording the thermograms. Each sample was crimped in an aluminum pan and placed in the sample chamber of a DSC that was equilibrated to -80 °C for 2 min and exposed to the heating and cooling cycles. In the first cycle, the sample was heated to 200 °C at a rate of 10 °C min<sup>-1</sup>. In the second cycle, the sample was quenched to -80 °C at a rate of 100 °C min<sup>-1</sup>. In the third cycle, the sample was heated from 0 to 200 °C at a rate of 10 °C min<sup>-1</sup>. The DSC studies were done under a dry nitrogen atmosphere at a purging rate of 50 mL min<sup>-1</sup>.

**2.2.7 In vitro studies.** The mouse fibroblast L929 cell line was grown as monolayer cultures under standard cell culture conditions in a DMEM media supplemented with 10% FBS, incubated at 37 °C, and humidified under a 5% CO<sub>2</sub> atmosphere and used as a control. Similarly, human colorectal carcinoma HCT116 and breast adenocarcinoma cell line MCF-7 were cultured in DMEM and MEM media, respectively. The respective media were supplemented with 10% FBS, and incubated while maintaining similar conditions.

**2.2.8 MTT assay.** The cytotoxicity assay, MTT for CU-CS-Ephb4 shRNA-ES NPs was done in HCT116 and MCF-7 cell lines for 48 h. Briefly, a confluent flask of cells was harvested by trypsinization and to each well of a 96 well plate, 100 µL of cell suspension (~10 000 cells) was introduced. The plate was incubated at 37 °C under a 5% CO<sub>2</sub> humidified atmosphere for 16 h to allow the cells to attach and form a monolayer. Thereafter, the media from the wells was flicked off and NPs were added. The NPs dispersed in serum-free media at 1 mg mL<sup>-1</sup> stock concentration were sterilized for 30 min under UV light and different concentrations ranging from 2 µg mL<sup>-1</sup> to 500 µg mL<sup>-1</sup> were added. These cells were incubated at 37 °C in 5% CO<sub>2</sub> conditions for 48 h and then the media from the wells was replaced with an MTT reagent. After 4 h of the incubation period, the media was siphoned off and 100 µL of DMSO was added to the wells to solubilize formazan crystals to develop color and the readings were recorded at 550 nm using a UV plate reader (Multiskan, Thermo Scientific, Finland).

**2.2.9 Cellular uptake studies.** The cellular uptake behavior of the NPs was evaluated in L929 fibroblast cells using fluorescence microscopy. For instance, L929 fibroblast cells were seeded on the top of glass coverslips in a 24 well plate and incubated for 24 h at 37 °C under a 5% CO<sub>2</sub> atmosphere. After incubation, the media was aspirated from the wells and was washed thrice with phosphate buffer (PBS). CU alone, CU-CS

NPs, and CU-CS-ES NPs were added to the individual wells at different concentrations and incubated for 3 h at 37 °C. Later, the media was aspirated off, the cells were washed with PBS, 300  $\mu\text{L}$  of 4% paraformaldehyde was added to the respective wells and incubated for 15 min at ambient temperature to fix the cells. Then, the paraformaldehyde was washed off using PBS along with 0.1% (v/v) Triton X-100 wash for 8 min and then stained with a DAPI-PBS (1  $\mu\text{g mL}^{-1}$ ) solution for 5 min. Subsequently, the coverslips were washed with a PBS solution and placed on a clean glass slide with mounting media (Fluoroshield). Excess media was wiped off with tissue and the cells were observed using an epi-fluorescence microscope (Carl Zeiss, Model: Axio Observer.Z1, Oil immersion objective, 60 $\times$ ). The nuclei of the cells were observed using the blue filter of DAPI and CU being fluorescent was visualized using the green filter of FITC (535–600 nm).

**2.2.10 Hemolytic assay.** To examine the hemolytic capacity of the developed nanocarrier *i.e.*, CU-CS-shRNA, the hemolytic assay was performed on fresh rodent red blood cells (RBCs). A 2% v/v suspension of RBCs was prepared. Then dispersions of CU-CS-Ephb4 shRNA-ES NPs of concentrations 0, 2, 4, 6, 8, 20, 40, 60, 80, 100, 150, 200, 300, 400, and 500  $\mu\text{g mL}^{-1}$  were incubated with the suspension of RBCs at 37 °C for 1 h. The positive and negative controls were Milli-Q water (100% hemolysis) and normal saline (0% hemolysis), respectively. After 1 h of incubation at room temperature, nanoparticles treated RBCs were spun at 4000 rpm at 4 °C for 10 min and the supernatant was separated. The absorbance was measured at 540 nm using a Microplate Reader (Thermo Scientific, USA). The percent hemolysis was calculated as follows:

$$\text{Hemolysis[\%]} = \frac{\text{Abs. sample} - \text{Abs. negative control}}{\text{Abs. positive control} - \text{Abs. negative control}} \times 100$$

**2.2.11 *In vivo* studies.** All experiments were performed at the Centre for Cellular and Molecular Biology (CCMB), Hyderabad in compliance with the relevant guidelines of 'The Committee for the Purpose of Control and Supervision of Experiments on Animals' (CPCSEA), Government of India. All animal studies were conducted by following the strict ethical guidelines stipulated by institutional guidelines and as per the approval of the Institutional Animal Ethical Committee (IAEC) (project no. IAEC 03/2019). To analyze the biodistribution of orally delivered nanoparticles in mice, *in vivo* multispectral imaging was performed. Wild type mice (C57BL/6J) ( $n = 3$ ) were treated for 15 days with NPs conjugated with the cyanine 7.5 NHS ester dye, where the first image was taken after the mice were humanely anesthetized using isoflurane after 6 hours of treatment and visualized under a multispectral imager. Two different animal knockout models were used in the study to assess the drug's efficacy against solid tumors. For evaluating the therapeutic potential of the biodrug in breast cancer murine models, conditional *Brca2/p53* knockout under control of Blg-cre transgene was used ESI Table S1.† This model develops tumors on any of the five pairs of mammary after 6–15 months of birth. Mice developing 0.5  $\text{m}^3$  mammary

tumors were selected for different cohorts which included shRNA+ NPs, scr control (scrambled shRNA + NPs), shRNA + lipofectamine, NPs only, and untreated (only induction and no treatment). Intratumoral injections of 10  $\mu\text{g}$  of Ephb4 shRNA (in pGFP-V-RS vector) complexed with 250  $\mu\text{g}$  of nanoparticles (CU-CS; in a volume of 50  $\mu\text{L}$ ) were given to the treated cohorts along with the respective controls. The mice were given the drugs equally and the tumor sizes were measured every day and selected for survival and other data analyses.

The inducible Apc knockout colon murine models (*AhCre-ErT Apcf1/fl*) develop the crypt progenitor phenotype in the intestine upon induction with  $\beta$ -naphthoflavone, and tamoxifen, demonstrating a progressive knockout, causing mortality of the animal within 8–10 days. To assess the efficacy of the formulated biodrug against colorectal cancer, CU-CS-Ephb4 shRNA-ES NPs were orally administered to Apc knockout models. The mice subjects were divided into five different cohorts of five mice each and were given the following treatments. The cohorts included those treated with shRNA+ NPs (treatment), scr control (scrambled shRNA + NPs), Ephb4 shRNA + lipofectamine, control (NPs only) and untreated (only induction and no treatment). Six to eight-week-old mice were selected for the study and were given intraperitoneal injections comprising 80  $\text{mg kg}^{-1}$  of  $\beta$ -naphthoflavone and tamoxifen (dissolved together in corn oil 10  $\text{mg mL}^{-1}$  each) once daily for 5 days to induce the recombination of the targeted alleles (knockout). The Apc knockout induced mice were treated with a daily oral dose of 50  $\mu\text{g}$  of Ephb4 shRNA (in pGFP-V-RS vector)-encoding plasmid DNA complexed to 1.25  $\text{mg}$  of NPs (in a total volume of 250  $\mu\text{L}$ ) from day 1 of induction until the end time point at which the mice survived. After treatment, the animals were sacrificed as per the ethical guidelines after 180 days by cardiac perfusion (using 4% paraformaldehyde) and tissue collection was performed. The tissues harvested were preserved accordingly for all downstream experiments. The intestines were specifically cleaned in running tap water and 1 $\times$  PBS, opened up, and fixed in methacarn for 48 h. The intestines were then made into a gut roll and preserved in 10% formalin and after the processing was sectioned with 4  $\mu\text{m}$  thickness.

**2.2.12 LFT/RFT studies.** The mice subjects (C57BL/6J) were divided into two different cohorts, namely control and treatment for the liver function test (LFT) and renal function test (RFT). The control group was treated with a buffer and the treatment cohort received 1  $\text{mg mL}^{-1}$  concentration of the drug (CU-CS-shRNA-ES NPs) for 2 weeks in a subchronic study. After treatment, the mice were sacrificed as per ethical guidelines and the blood was harvested in vacutainers. The whole blood was allowed to clot for about 15–30 minutes followed by centrifugation at 1500g for 15 minutes at 4 °C in a refrigerated centrifuge and the serum was isolated for the assessment. For LFT, the determinations of albumin, total bilirubin, alkaline phosphatase, SGOT, and SGPT were performed and for RFT, urea and creatinine were measured. Each particular test was performed using the mentioned concentrations and ratios as per the manufacturer's instructions. The time, temperature of incubation, and the filter wavelength were accurately followed.

The results were analyzed, and the corresponding values were plotted as graphs using GraphPad Prism 9.0.

**2.2.13 Immunohistochemistry.** The sections were deparaffinized in xylene followed by gradient washes of ethanol and rehydration. Heat-induced antigen retrieval was performed by boiling the slides in two different buffers, 10 mM sodium citrate buffer of pH 6.0 for  $\beta$ -catenin and Nf- $\kappa$ B and 10 mM Tris base and 1 mM EDTA of pH 9.0 for c-Myc, each for 30 min at 100 °C. The slides were then brought to room temperature before washing with 1 $\times$  TBS. The slides were blocked using 10% BSA in 1 $\times$  TBS for 2 h at room temperature. They were then incubated with primary antibodies  $\beta$ -catenin, Nf- $\kappa$ B, and c-Myc, and Ephb4 all at 1 : 100 dilutions at 4 °C overnight in a humid chamber. The next day, the slides were washed three times with 1 $\times$  TBST (0.1% Triton-X) for 15 min each and were blocked with 3% H<sub>2</sub>O<sub>2</sub> in methanol for 30 min to quench the endogenous peroxidase activity of the sections. The slides were washed first with water and then with TBS and were incubated with anti-rabbit HRP conjugated secondary IgG (Abcam ab97051) for 1.5 h at room temperature in a humid chamber. After incubation, the slides were again washed thrice with 1 $\times$  TBST for 15 min each and diaminobenzidine (DAKO) was used (1 min for  $\beta$ -catenin and Nf- $\kappa$ B and 45 seconds for c-Myc) as a chromogenic agent for color development. After water wash, the slides were counterstained with Gill's Hematoxylin Mod III and were mounted. Negative controls of IHCs were prepared for each set of sections by replacing the primary antibody with TBS. The results were analyzed, and corresponding values were plotted as graphs using GraphPad Prism 9.0

### 3. Results and discussion

#### 3.1 Synthesis and characterization of curcumin–chitosan nanoparticles

Hydrophobic curcumin (CU) was sized down to nano-CU by sonication. The CU nanoparticles, being negatively charged, interact with positively charged polymers.<sup>40</sup> The desolvation approach is usually used for the encapsulation of CU with polymers. However, following this method, the yield of the NPs was low. Therefore, several alternative methods were tried for the fabrication of the nanoparticles. Electrospraying is one of the simple and powerful methods that is being used for the production of NPs with high yields and reproducibility.<sup>41</sup> Accordingly, the electrospraying method was successfully employed for fabricating the nanoparticulate system and the nanoparticles were obtained in sufficient quantities.

The morphology of the fabricated NPs was examined by ESEM and TEM. The size, shape, and distribution of the formulated CU–CS and CU–CS–shRNA–ES NPs were in the range of 100–200 and 110–230 nm diameter, respectively, with a distorted spherical to square morphology as shown in Fig. 1A(i–iii). Coatings of polymers on CU nanoparticles were observed in TEM images, where coating with ES changed the surface morphology of CU with a thickness of the polymer coating between 20–30 nm. Nanoencapsulation of negatively charged

CU was carried out using the individual polymer, chitosan (CS), followed by Eudragit S-100 (ES). The charge of the CU particles before and after coating with polymers was confirmed by zeta ( $\zeta$ ) potential measurements. CU possessed a net negative charge of  $-24.78$  mV, which upon interaction with a cationic polymer, CS ( $+29.1$  mV), yielded positively charged particles of  $+51.52$  mV. The increase in the positive charge was attributed due to the crosslinking of NPs with Ca<sup>++</sup> ions. With an increase in the ratio of CS, the positive charge of the NPs increased in a concentration-dependent manner. ESI Table S2† shows the different formulations and their PDI with varying concentrations of CS. With the progress of Ephb4, shRNA plasmid conjugation, the net positive charge on NPs decreased to  $24.83$  mV. This complex formation of CU–CS–shRNA NPs was aided by the positively charged amine groups of CS. Furthermore, the complexed NPs recorded a decrease in net positive charge when coated with anionic ES [Fig. 1A(iv)]. While different ratios of CU–CS NPs were formulated and checked for their charge and shRNA plasmid retention, based on the suitability, the 1 : 2 ratio of CU–CS NPs was selected for pre-clinical evaluation. Furthermore, the gel retardation assay was used to validate the conjugation of the Ephb4 shRNA plasmid to the CU–CS NP system. Two different ratios of NPs to Ephb4 shRNA plasmid were prepared (25 : 0.8 and 25 : 1.0) and were tested for their electrophoretic mobility in 1% of agarose gel. It was observed that the control lane containing free nucleic acids migrated down the gel without hindrance, while the lane with the Ephb4 conjugated NPs did not show the migration. Additionally, the 25 : 0.8 ratio exhibited better conjugation efficiency than the 25 : 1.0 ratio (ESI Fig. S1-A†).

#### 3.2 FTIR spectra and differential scanning calorimetric analysis

The nanoparticulate system consisted of the respective components CU, CS, and ES possessing the characteristic functional groups and their sequential additions were confirmed by FTIR. The individual peaks of the respective components were first observed to understand the functional changes before and after the fabrication of NPs. In the CU spectrum, characteristic peaks such as the phenolic O–H peak were observed at  $3500$  cm<sup>-1</sup>, the carboxylic C=O stretching at  $1628$  cm<sup>-1</sup>, the C=C stretching at  $1512$  cm<sup>-1</sup> and the C–H stretching at  $1430$  cm<sup>-1</sup> (ESI Fig. S1-B†).<sup>42</sup> For the CS spectrum, a characteristic broad peak at  $3450$  cm<sup>-1</sup> was observed due to the merging of the N–H and O–H functional groups. Other characteristic peaks included the C–H stretching peak at  $2961$  cm<sup>-1</sup> and  $2921$  cm<sup>-1</sup>, the carboxylic C=O peak at  $1655$  cm<sup>-1</sup>, and the bending peak for N–H at  $1590$  cm<sup>-1</sup>.<sup>43</sup> In the ES spectrum, the characteristic broad O–H absorption band at  $3100$ – $3500$  cm<sup>-1</sup> was noticed along with C–H stretching vibrations at  $2998$  and  $2954$  cm<sup>-1</sup>, C=O stretching at  $1730$  cm<sup>-1</sup>, and C–O–C stretching vibration at  $1150$  cm<sup>-1</sup>.<sup>37</sup> The IR spectrum of CU–CS exhibited the C=C peaks of curcumin at  $1512$  cm<sup>-1</sup> and  $1430$  cm<sup>-1</sup>, the downshift of the C=O peak from  $1655$  cm<sup>-1</sup> to  $1635$  cm<sup>-1</sup> and the N–H peak of CS merged into this C=O peak, which suggested the strong interaction of CU with CS (ESI Fig. S1-C†). The IR spectrum of CU–

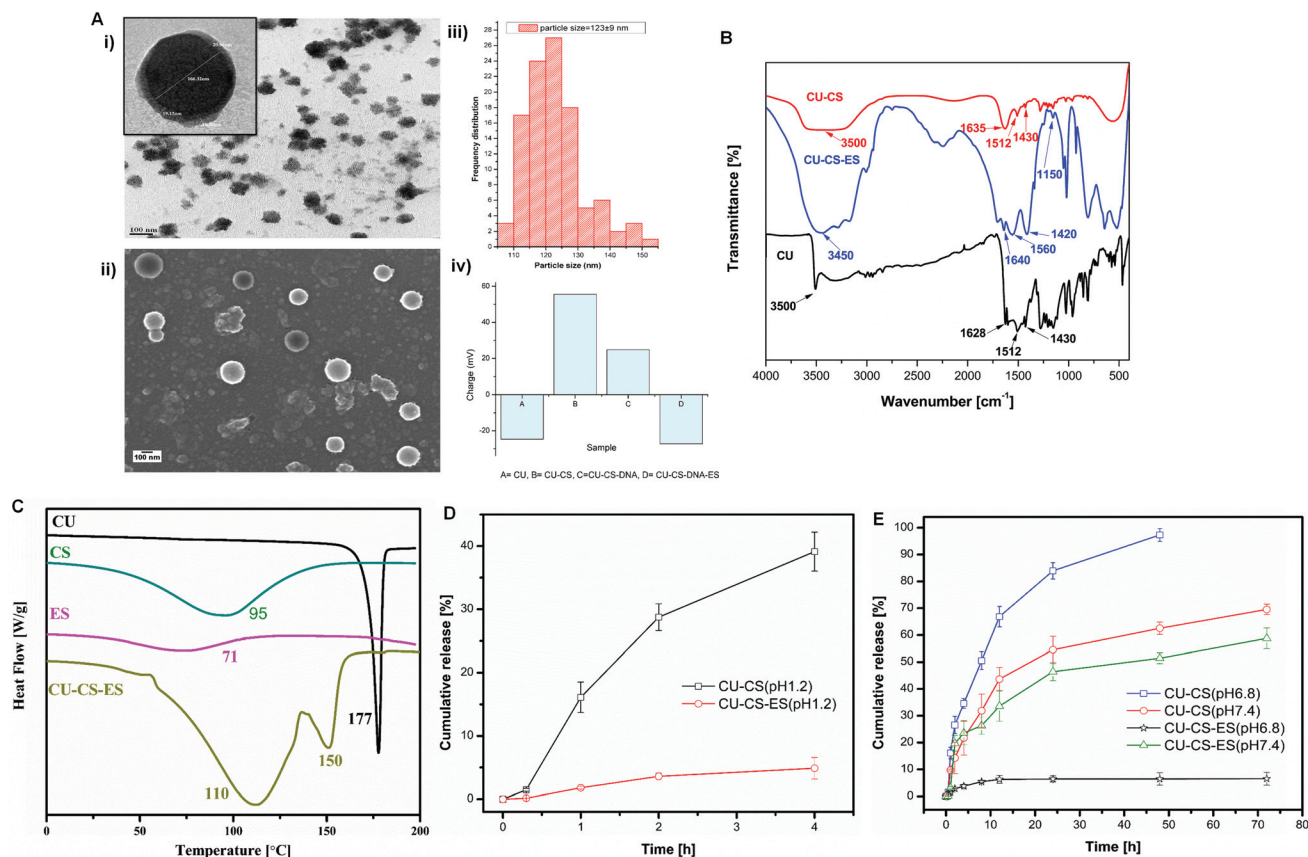


**Fig. 1** Characterization of CU-CS-ES nanoparticles. (A) i. TEM image and analysis of CU-CS-Eph4 shRNA-ES, ii. SEM image of CU-CS-Eph4 shRNA-ES, iii. frequency distribution graph of CU-CS-Eph4 shRNA-ES nanoparticles (median size 123 + 9 nm), and iv. Zeta potential measurements of different nanoparticle formulations after each coating. (B) The FTIR spectra of bare CU, CU coated with CS (CU-CS), and CU coated with CS and ES (CU-CS-ES), (C) differential scanning calorimetric analysis using bare CU, CS, and ES with CU-CS-ES nanoparticles, (D) Cumulative CU release at 1.2 pH from CU-CS and CU-CS-ES, and (E) Cumulative curcumin release at 6.8 and 7.4 pH from CU-CS and CU-CS-ES.

CS-ES reported the changed peak at 1640 cm<sup>-1</sup>, which could be attributed to the formation of a carboxylate bond between the -NH<sup>+</sup> groups of CS and the COO<sup>-</sup> groups of ES which are as per the earlier literature (ESI Fig. S1-D<sup>†</sup>).<sup>44</sup> These findings confirmed the encapsulation of CU-CS NPs with ES (Fig. 1B and ESI Table S3<sup>†</sup>).

To understand the coating strength of ES on the CU-CS NP system, thermal analysis by DSC was performed for CU, CS and ES, and CU-CS-ES NPs as shown in Fig. 1C. The glass transition temperature ( $T_g$ ) was observed at 95 °C for CS and 71 °C for ES, which was in accordance with the reported literature.<sup>37,45</sup> Likewise, a sharp endothermic peak due to the melting temperature ( $T_m$ ) for CU was observed at 177 °C. For CU-CS-ES NPs, two broad endothermic peaks were observed at 110 °C and 150 °C. The  $T_m$  of CU decreased because of the interactions between the CS and CU. The crosslinking of CU-CS with CaCl<sub>2</sub> resulted in a shift of the endothermic peak ( $T_g$ ) from 95 °C to 110 °C which could be attributed to an increase in the rigidity of the nanoparticle system. As reported in the earlier studies, the shift in the peak of CU to a lower temperature indicated the disordered crystalline phase in the final preparation.<sup>46</sup> Finally, we could conclude that the shifting and

broadening of the CU peak supported and validated the encapsulation of CU by CS and ES polymers.

### 3.3 Entrapment efficiency and drug release studies

The entrapment and loading efficiency of CU was determined using eqn (1) and (2) as outlined in the Experimental section. The CU-CS-NPs were sonicated, centrifuged and the untrapped CU was extracted into methanol and quantified using a calibration curve recorded at  $\lambda_{max}$  423. Later, the percent of CU concentration was estimated using eqn (1). The entrapment efficiency for different compositions of CU-CS (1:1 and 1:2) was 76.67 and 68.21%, respectively. The loading efficiency was calculated using eqn (2), which was 38.3 and 22.85% for the respective compositions, 1CU-1CS and 1CU-2CS. We observed that with the increase in chitosan concentration, the entrapment and loading efficiency of CU were reduced, which could be attributed to the hindrance of CU entrapment as a result of an increase in the viscosity of CS solution.

The CU-CS NPs coated with and without ES were studied for their release of CU at three different pH values (1.2, 6.8 and 7.4) to mimic the different conditions that exist in the alimentary/gastrointestinal canal. The physiological pH of the stomach is 1.2



(acidic) whereas the pH of the gut ranges from 6.8 to 7.5. Different pH values chosen helped in understanding the ability of the conjugated bio-drug to reach the targeted site without degradation. It was observed that at 1.2 pH after 4 h of release studies, the amount of CU released from the nanoparticle system without ES coating was 39%, which is considered as burst release, whereas the NPs of CU-CS-ES recorded only ~5% CU release. This decrease in the quantity of CU release is expected to be due to the ES coating as a result of the protonation of the COO<sup>-</sup> groups of ES which enabled the protection of chitosan from degradation at the acidic pH of 1.2. CU release at pH 7.4 for NPs of CU-CS and CU-CS-ES after 8 h of release, was 32% and 26%, respectively (Fig. 1D), which indicated a sustained release mechanism. Furthermore, a continuation of CU release for 72 h at the same pH recorded 70 and 59% from CU-CS and CU-CS-ES, respectively. At this pH, the carboxyl groups of ES were ionized leading to the dissolution of ES thereby exposing CS coated CU NPs.<sup>35,47</sup> At 6.8 pH (Fig. 1E), the entire CU was released from CU-CS complex alone within 48 h, whereas the release was only 7% was released from CU-CS-ES, even after 72 h of release. The diffusion of CU and swelling of chitosan at pH 6.8 resulted in high CU release from CU-CS, while the stability of ES at pH 6.8 did not lead to any CU release from CU-CS-ES NPs.

### 3.4 Cell cytotoxicity studies

To demonstrate the cytotoxic effects of the biodrug (CU-CS-Ephb4 shRNA-ES) was assessed through MTT assay in normal L929, colon cancer HCT116 and breast cancer MCF-7 cell lines exposed for 48 h. MTT reagent solubilized the formazan crystals which indicated cellular respiratory activity in live cells. The viability of L929, HCT116 and MCF-7 cells after incubation with varying concentrations of NPs are shown in Fig. 2A. The CU-based NPs were observed to inhibit the proliferation of both cancer cell lines in a concentration-dependent manner as compared with the controls. We observed the highest toxicity in cancer cell lines (HCT116 and MCF-7) where the cell viability was reduced by more than 50%. Furthermore, there was no toxicity observed in normal L929 cell lines, demonstrating its specificity against only the cancer cell lines. Thus, the results clearly indicate that the developed CU-CS-Ephb4 shRNA-ES biodrug is potent in reducing colon and breast cancer cell proliferation *in vitro*.

### 3.5 Cellular uptake studies

The cellular uptake and intracellular trafficking of free CU NPs and CU based NPs (CU-CS and CU-CS-ES NPs) formulations were investigated in L929 fibroblast cells at a concentration of 50  $\mu\text{g mL}^{-1}$  for CU loaded NPs and 11  $\mu\text{g mL}^{-1}$  for CU NPs (calculated from the loading %). The NPs and free CU were incubated for 3 h with the cells for assessing their internalization. Nuclei were visualized by DAPI and intrinsic green fluorescence from CU was detected using FITC filter. Control cells that were not exposed to CU did not display any fluorescence. As seen in Fig. 2B, after 3 h incubation, CU appeared to enter the cells and green fluorescence was observed in the cytoplasmic region of the cells. Moreover, the positive charge on CS is reported to be beneficial in interacting with the cells

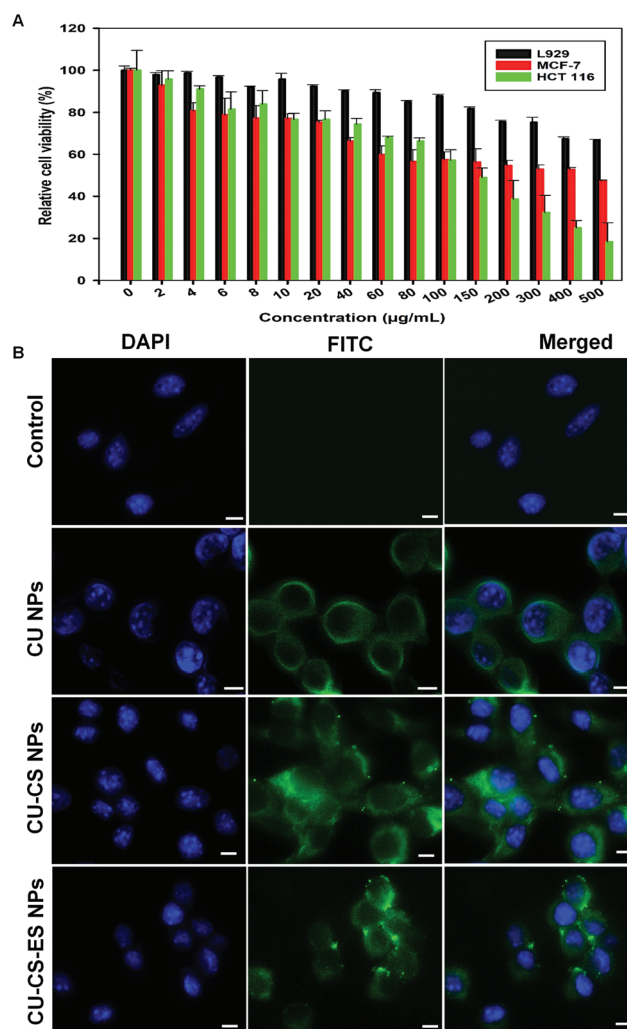


**Fig. 2** *In vitro* cellular studies of CU-CS-Ephb4 shRNA-ES nanoparticles. (A) Cell viability assay results of HCT116 and MCF-7 (cancer cell lines) with L929 cells (control) after 48 h of CU-CS-Ephb4 shRNA-ES treatment.  $n = 3$ , error bars: mean + SD;  $p < 0.005$ . (B) Cellular uptake assay representing the L929 cells after 3 h involving CU, CU-CS, and CU-CS-ES with each 50  $\mu\text{g mL}^{-1}$ . Scale bar: 5  $\mu\text{m}$ .

having an intrinsic negative charge and is able to loosen the tight junction of cells to facilitate the uptake of the particles.<sup>48</sup> This also suggested that after the pH-responsive release of ES, the CU-CS-Ephb4 shRNA had a better cellular uptake, thus increasing the efficacy of the biodrug.

### 3.6 *In vivo* toxicity and biodistribution

A major concern of all bio drugs in translational research is their potential toxicity *in vivo* and as a result, it is imperative to cautiously evaluate the biodistribution and toxicity profiles of our polymeric nanocomposites *in vivo* before validating their therapeutic efficacy.<sup>49</sup> We speculated that for the oral delivery, the ES coating around the CU-CS-shRNA nanocomposites will protect them from the harsh conditions of the stomach and deliver them effectively in the colon. To this end, we performed *in vivo* multispectral imaging in C57BL/6J healthy mice after

oral gavage of CU-CS-Ephb4 shRNA NPs conjugated with cyanine 7.5 NHS ester far red dye. Live imaging tracked the presence of the NPs at 810 nm  $\lambda_{em}$  which was localized basically in the gut region after 24 h of oral administration as compared with the control (Fig. 3A). Moreover, ex vivo multispectral imaging revealed that the distribution of NPs after 24 hrs were localized all along the intestinal tract, with higher doses in the regions of small intestines, colon, liver and kidney. Notably, the presence of NPs was not observed in the gall bladder, spleen, heart, lungs and pancreas (ESI-Supplementary Fig. S5†). The *in vivo* toxicity of CU-CS-ES polymeric nanocomposites conjugated with Ephb4 shRNA plasmid were investigated in C57BL/6J healthy mice for a period of 14 days in a sub-chronic study. Mice were administered with the bio-conjugated drug orally at a

dose of 1 mg ml<sup>-1</sup> BW, and their behavior (*i.e.*, exploratory activity, eating, sleeping, and neurological symptoms) was carefully monitored. We tested the safety of this drug in the circulatory system using hemolytic assay in murine systems. The hemolysis brought about by altered concentrations of the polymeric nanocomposites was measured after incubating the drug with a 2% v/v suspension of red blood cells (Fig. 3B). A concentration of 100  $\mu\text{g ml}^{-1}$  induced maximum hemolysis among all the concentrations of nanoparticles. Likewise, histological examinations using hematoxylin and eosin staining revealed that major organs like the brain, heart, lungs, stomach, liver, spleen, and kidneys were not exposed to toxicity and there was no inflammation after oral administration of the bioformulation when compared with controls (Fig. 3C). Moreover, second-

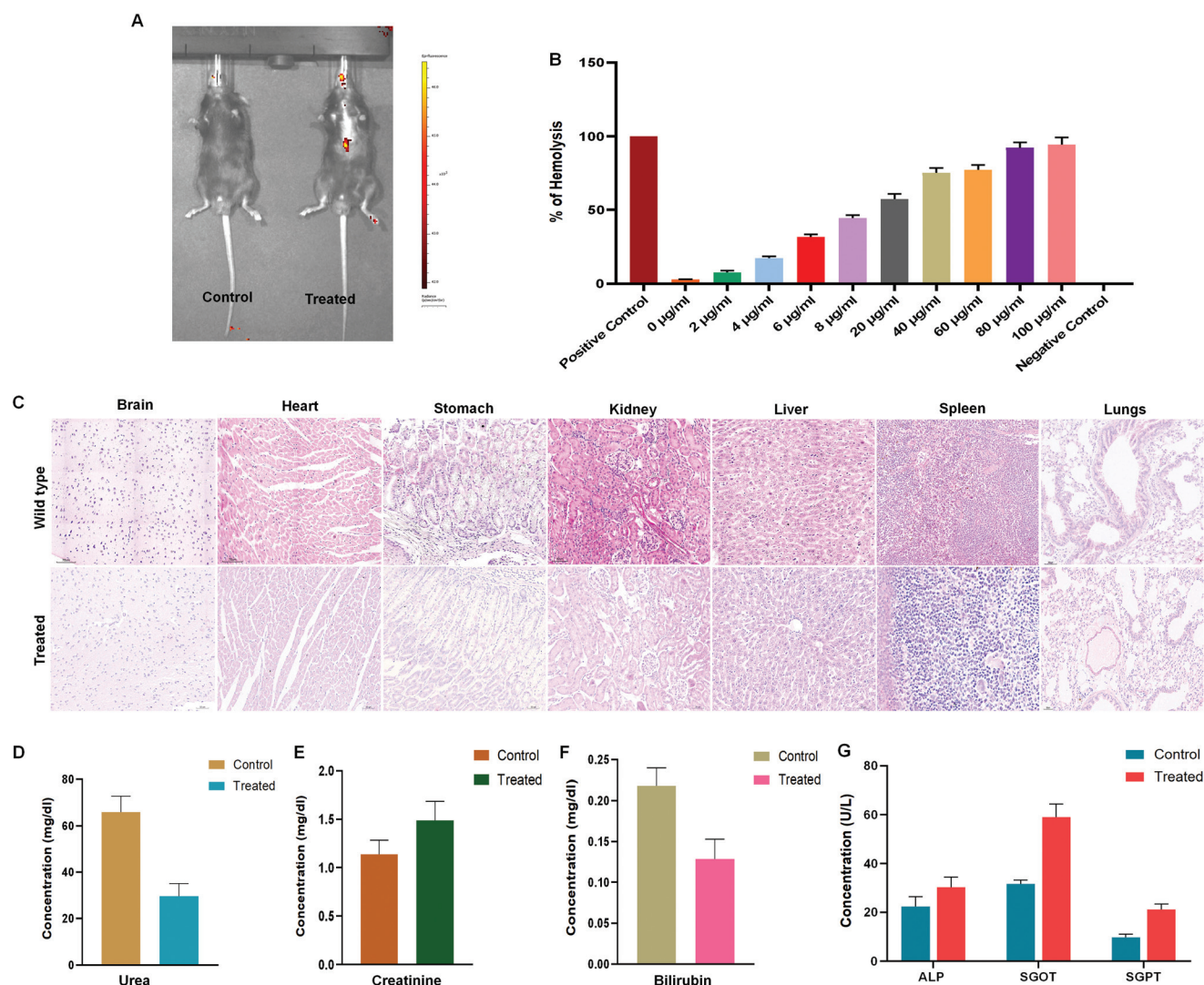


**Fig. 3** *In vivo* biodistribution and toxicity of nanoparticles in C57BL/6J mice models. (A) *In vivo* multispectral image of the CU-CS-Ephb4 shRNA-ES NPs conjugated with cyanine 7.5 NHS ester far-red dye in two different mice models (control and treated) at 810 nm  $\lambda_{em}$ . (B) quantitative analysis of % hemolysis induced by the CU-CS-Ephb4 shRNA NPs in murine systems at various concentrations. Error bars, mean + SD;  $p < 0.05$ . (C) histological studies of the nanoparticle in two different mice models (control and treated) post treatment. Hematoxylin and eosin staining of different organs (the brain, heart, stomach, kidneys, lungs, liver, and spleen) depicting no inflammation and unchanged morphology. Images were taken at  $\times 20$  magnification, quantitative indirect assessment of renal functions (D) Urea, (E) Creatinine, and hepatic functions like (F) Bilirubin, (G) ALP, SGOT, and SGPT were estimated through colorimetric tests in control and treated mice cohorts.

ary assessment of the liver and kidney functions by means of indirect colorimetric tests like LFT and RFT assays exhibited no noticeable changes in all the parameters of the biodrug in the treated cohorts when compared with the controls. The concentrations of urea, creatinine, alkaline phosphatase, ALT, SGPT, and SGOT were well within the reference levels in both groups (Fig. 3D–G). The toxicological results obtained after the oral administration of this bioformulation to healthy mice were satisfactory as they were not detrimental. These results suggested that the bioformulations tested in the present investigation were not only safe but also bio-compatible in the murine system. The results also suggest that these bio-formulations could be exploited in humans after careful pre-clinical clinical trials.

### 3.7 Suppression of autochthonous *Brca2/p53* knockout breast cancer models

Solid autochthonous tumors are relatively distinct from xenograft models for most treatment regimens and often pose challenges due to their inherent nature of origin and the associated complications with delivery to necrotic tumor cores<sup>50</sup> (Fig. 4A). The ability of Ephb4 shRNA to suppress tumors was tested *in vivo* by encapsulating with CU–CS–ES nanocomposites in an established transgenic Blg-cre *Brca2/p53* double knockout murine breast cancer model where the mice develop mammary tumors naturally between 6 and 15 months of age (ESI Fig. S2-A, and S3†). It is well documented in humans that the inheritance of mutations in the susceptibility

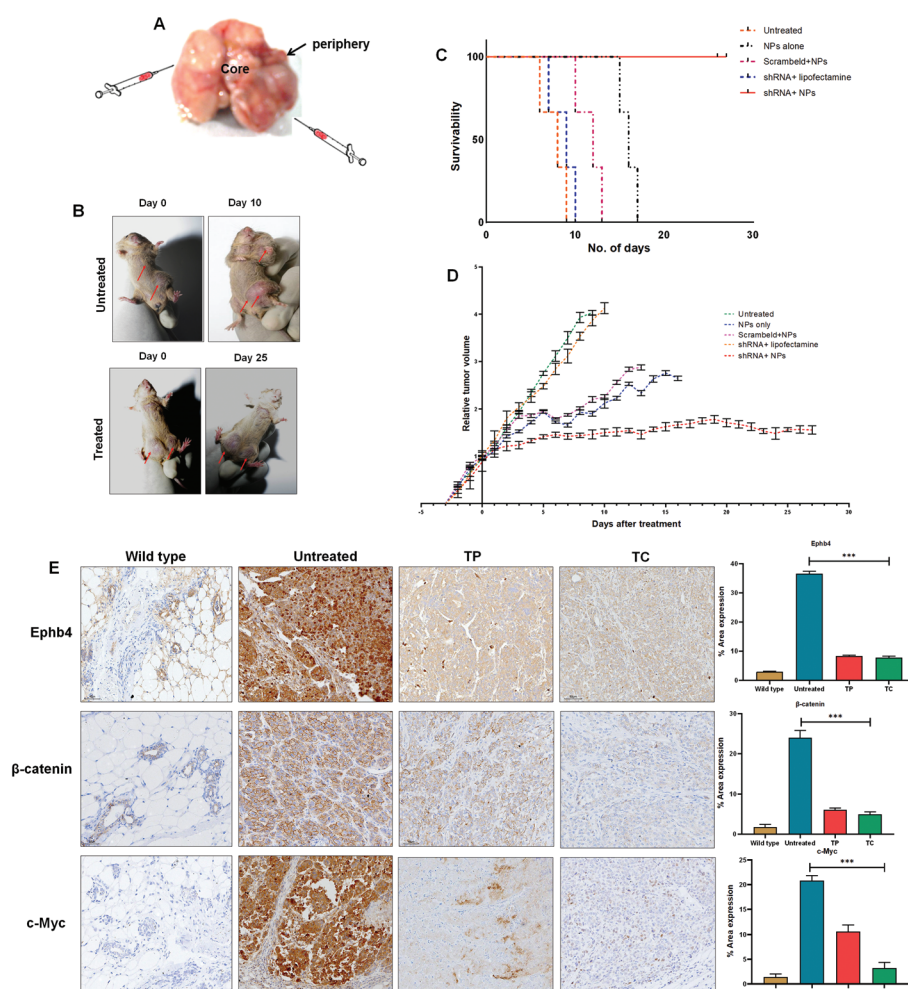


**Fig. 4** Tumor arrest and regression in the autochthonous BRCA2/p53 knockout breast cancer models. (A) A schematic diagram of the mammary tumor, constituting a tumor necrotic core (TC) and where the intratumoral injections are given at the tumor periphery (TP), (B) an example of mammary tumor growth arrest in conditional BRCA2/p53 knockout mouse model upon treatment with CU–CS–Ephb4 shRNA–ES NPs, wherein the untreated mice show aggressive tumor growth in 10 days but treated mice depict tumor arrest even after 25 days. (C) Kaplan–Meier survival plots demonstrating the extension of the lifetime of the treated cohorts (shRNA + NPs) to 27 days compared to that of the control cohorts. (D) The tumor retardation curve indicates a tumor growth arrest with a prolonged survival of 27 days in CU–CS–Ephb4 shRNA–ES NPs treated cohorts compared to other treated cohorts (scrambled shRNA + NPs, shRNA alone, NPs alone, and induced but untreated mice (control)). (E) Immunohistochemistry of Ephb4, β-catenin, and c-Myc in wild type, untreated, and treated cohort sections demonstrating a decrease in the target genes as compared to the controls both in the tumor periphery (TP) and tumor core (TC). Images were developed in  $\times 20$  magnification. Quantification of the area of degradation through the Image J software. Error bars, mean + SD; \*\*\* $p < 0.001$ .

genes such as BRCA1 and BRCA2 increases the risk of developing breast cancer. The somatic loss of BRCA2 and p53 in mice models mimics human cancers and induces mammary tumors naturally between 6 months to one year of age in any/all of the five mammary glands making it one of the best models akin to human breast cancer.<sup>11,51–53</sup> Since it is an autochthonous tumor, regression is a difficult process compared to xenograft models. To assess the efficacy of this biodrug in solid tumors, intratumoral injections of the biodrug along with appropriate controls were administered directly to tumor periphery in different cohorts (Ephb4 shRNA + NPs, along with controls like untreated, NPs alone, scrambled control + NPs, and Ephb4 shRNA + lipofectamine). Tumors treated with the biodrug showed a marked arrest and subsequent decrease of tumor size compared with different controls (Fig. 4B). Moreover, biodrug treated cohorts exhibited an increased median survival response of 35–40 days when compared with the various controls where the mice survived only for 10–15 days. Interestingly, CU nanoparticles demonstrated median survival of 15–20 days, which was higher than the other controls, as CU has been well established for its potent anti-inflammatory and anti-cancerous attributes (Fig. 4C and D). Immunohistochemical analysis of core tumor sections revealed a significant reduction in the expression levels of the Ephb4 protein in the treated cohorts that resulted in the suppression of tumor growth and therefore increased survival rates. The reduction of Ephb4 levels in the tumor core proved beyond doubt that the administered drug from the tumor periphery has penetrated to the core to bring about the suppression and subsequent repression of tumor size. Accumulating evidence has linked the deregulation of the Wnt pathway as a major causative factor in most cancers including breast cancer. Aberrant Wnt signaling results in the translocation of oncogene  $\beta$ -catenin from the cytoplasm to the nucleus which results in the activation of transcription of many downstream oncogenes like *c-Myc*, *CD44*, *LFY* etc.<sup>54</sup> The re-localization of  $\beta$ -catenin from the nucleus to the cytoplasm was observed in the biodrug treated cohort, indicating a return to a non-Wnt-deregulated state for this group which was almost similar to the wild-type. Studies over the past decades have established oncogene *c-Myc* to be highly overexpressed in all cancers.<sup>55,56</sup> Here in the current study, treatment with the biodrug CU-CS-Ephb4 shRNA-ES NPs resulted in a concomitant decrease in the expression levels of the oncogene *c-Myc* in the treatment groups when compared with untreated control (Fig. 4E). This implicated that the biodrug not only helped in regressing the tumor size but also in increasing the survival of the transgenic mice by effectively knocking down the downstream activated genes. On-site delivery of the Ephb4 shRNA plasmid straight into the mammary tumor periphery enabled targeting of the necrotic tumor core, aiding in the effective knockdown of Ephb4, thus enabling the arrest of tumor growth and the subsequent regression of tumor volume over a period of time. This simultaneous suppression and regression of tumor burden within a short time span indicated the dual action of the biodrug involving the anti-inflammatory attributes of curcumin along with

the gene silencing of Ephb4 by RNA interference. Thus, this study reiterates the use of combinatorial therapy involving RNA interference and nanotechnology for combating cancer.

### 3.8 Effective reversal of intestinal tumorigenesis in Apc knockout murine models

The Wnt pathway is involved in orchestrating the development and maintenance of the niche in the intestines.<sup>57</sup> Adenomatous polyposis coli (*Apc*), a tumor suppressor gene in the Wnt pathway, is the main component of the destruction complex that phosphorylates the oncogene  $\beta$ -catenin for degradation. Mutations of the adenomatous polyposis coli gene predispose individuals to familial adenomatous polyposis (FAP) syndrome. Similarly, *Apc* knockout colon cancer models ( $Cre^+Apc^{fl/fl}$ ) develop altered crypt/villus architecture that mimics human colon cancer and die between one week to 10 days, thus making this robust model ideal for drug testing compared to other existing models. Moreover, in the *Apc* inducible knockout model, the deletion of the *Apc* gene results in the unphosphorylated  $\beta$ -catenin getting translocated from the cytoplasm to nucleus. This results in the activation of downstream genes like *c-Myc*, *CD44*, etc. that consequently affects the development of an aggressive *c-Myc* dependent crypt progenitor phenotype across the intestine. This results in the formation of early tumor lesions leading to the death of the animals within 7 to 10 days (ESI Fig. S2-B, and S4†).<sup>11</sup> In order to assess the therapeutic potential of our multimodal nanosystem, we administered the biodrug orally to target the gut in *Apc* knockout murine models in an attempt to suppress and reverse the Wnt induced deregulated state. The biodrug formulation (CU-CS-ES-Ephb4 shRNA) was orally administered to a cohort of three mice each, along with appropriate controls (untreated, scrambled control, and Ephb4 shRNA + lipofectamine). Although the CU NPs exhibited median survival between 35 to 40 days, the combinatorial approach using RNA interference and CU NPs had a high median survival of 180 days when compared with the controls having median survival in the range of 10–15 days (Fig. 5A). Morphological evaluation by hematoxylin and eosin (H&E) staining revealed a return of the crypt structures that were nearly akin to wild type in the treatment cohorts when compared with the untreated sections where the villi appeared to be fused with the crypts exhibiting a crypt progenitor type state (ESI Fig. S6-A†). Immunohistochemical analysis throughout the treatment reflected a reduced expression of Ephb4 levels indicating a successful shutdown of the Ephb4 by the biodrug. The altered crypt progenitor type was no longer identifiable thus bringing about the normal morphology of the crypt–villus axis indicating a reversal of intestinal tumorigenesis. Moreover,  $\beta$ -catenin was re-localized from the nucleus to the cytoplasm during the treatment, indicating a return to a non-Wnt-deregulated state (ESI Fig. S6-B†). Increasing experimental evidence have well established the oncogenic role of *c-Myc* in colorectal carcinoma.<sup>58</sup> Here, treatment with Ephb4 shRNA conjugated CU-CS nanocomposites resulted not only in decreasing the level of Ephb4 proteins but also decreased the expression levels of

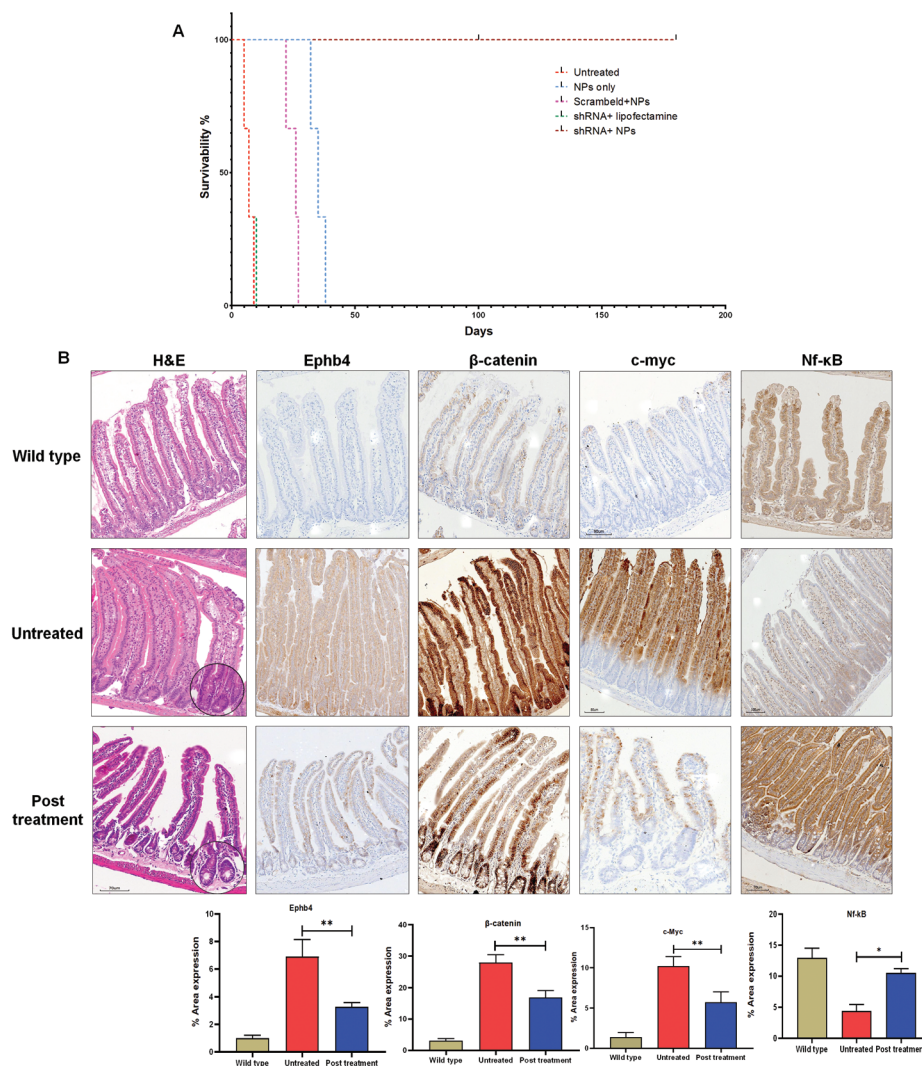


**Fig. 5** Suppression of intestinal tumorigenesis in *AhCre-ErT Apcfl/fl* murine models. (A) Survival curve of mice treated with CU-CS-Ephb4 shRNA-ES NPs with different treatment controls (scrambled shRNA + NPs, shRNA alone, NPs alone and induced but untreated mice (control)) indicating a prolonged survival of 180 days in the nano-RNAi treatment group as compared to respective controls. (B) Hematoxylin and eosin staining of gut sections from the *Apc*-deficient mice treated with CU-CS-Ephb4 shRNA-ES NPs compared with other controls. Immunohistochemical results show the site-specific knockdown of target genes like Ephb4,  $\beta$ -catenin, c-Myc, and Nf- $\kappa$ B in the treated cohorts as compared to the respective controls. The images were developed in  $\times 20$  magnification. Quantification of the area of degradation through the Image J software. Error bars, mean  $\pm$  SD.

oncoprotein c-Myc in the test groups compared to untreated controls. Thus, the Ephb receptor tyrosine kinase controls Wnt signaling through its target genes that are active in cell compartmentalization along the crypt axis. Hence, the shutdown of Ephb4 might have resulted in reduced expression of Wnt target genes like  $\beta$ -catenin and c-Myc stimulating the intestine cell niche to return to a near normal state. Nf- $\kappa$ B, a known transcription factor, is responsible for regulating various immune responses and acute inflammation in normal physiological processes.<sup>59,60</sup> The treatment resulted in increased Nf- $\kappa$ B expression in the treated cohorts which mimicked the wild type state potentiating a strong survival response (Fig. 5B). This prolonged survival due to tumor regression is an indication of the synergistic action of the shutdown of upregulated Wnt genes by RNAi as well as the tumor suppressive action of

the curcumin nanoparticles. These results substantiate the importance of recognizing shRNA molecules as more stable compared to siRNA to bring about efficient and consistent gene silencing and also reveal the role of nanotechnology not only as a carrier molecule but also as a therapeutic molecule as well. These findings advocated the high pharmacological potential and synergistic effect of this combinatorial biodrug in suppressing and abrogating the intestinal tumorigenesis and helped in returning it to a near wild type state.

## 4. Conclusion

The emergence of gene-based therapies in the clinical realm has enabled the use of nucleic acids in therapeutic

approaches, opening infinite possibilities for the treatment of a wide range of genetic, innate, and acquired diseases, including cancers. Nano-formulations, with their unique characteristics, have been positively established as competent carriers for delivering RNAi molecules. In addition, it has been suggested that the shRNA-based approach could be better than siRNA-based RNAi approach as shRNAs is known to be more stable compared to siRNAs which are degraded rapidly under *in vivo* conditions. Also, it has been opined that natural therapeutic compounds as carrier molecules enable biocompatible, nontoxic, targeted delivery with prolonged survival. To this end, we have demonstrated the development and applicability of a combinatorial approach involving the nano-RNAi biodrug formulation for successful site-specific delivery in both breast and colon cancer knockout mice models. In the current study, we have used nanoformulations of curcumin (CU), a well-known anticancer nutraceutical agent, with chitosan (CS) for an enhanced permeation effect. The CU-CS NPs were conjugated with Eph4 shRNA and then coated with Eudragit S-100 for specific delivery to the site of action. Our study showed that the nano-RNAi biodrug was stable, biocompatible and non-toxic, and possessed pH-specific attributes. Moreover, the uptake in the colon models was found to be efficient, with the distribution of NPs localized mostly to the intestinal tract. The efficient and site-specific knockdown of Eph4 resulted in attenuated tumor growth leading to increased survival in both mice models. Oral delivery of this bio-formulation permitted the drug to be precisely delivered to the tumor micro-environment, therein, guarding it against degradation under harsh conditions of the stomach. Though the NPs alone cohorts showed the animals survived up to 37 days, the Apc-deficient mice treated with the combination (NPs and Eph4 shRNA) showed a remarkable survival of more than 6 months as compared to controls where the median survival was 10 days, thus affirming the synergistic effect and potential of this bio-formulation for efficient colon cancer treatment. The administration of this biodrug in mammary models led to the suppression and regression of the tumorigenic state. To the best of our knowledge, we are the first to demonstrate the combination of curcumin nanoparticles with RNA interference in a pre-clinical setting for cancer therapeutics. Our bio-drug formulation, a combination of RNAi and nanotechnology, illustrated the high therapeutic efficacy with biocompatibility and no toxicity of our novel nano-based formulation in two different solid tumor models of breast and colon. Thus, this demonstration of a proof of concept has paved the way for a promising alliance of RNA interference and nanotechnology as next-generation cancer therapeutics.

## CRedit authorship contribution statement

Aviral Kumar: Methodology, Investigation, Validation, Visualization, Writing – Original Draft, Writing – Review & Editing, Amarnath Singam: Methodology, Investigation, Formal

analysis, Writing – Original Draft, Validation, Visualization, Guruprasadh Swaminathan: Methodology, Investigation, Writing – Original Draft, Writing – Review & Editing, Visualization, Naresh Killi and Naveen Kumar Tangudu: Investigation, Formal analysis, Jedy Jose: Resources, Rathna Gundloori VN: Conceptualization, Funding acquisition, Project administration, Supervision, Writing – Review & Editing, Lekha Dinesh Kumar: Conceptualization, Funding acquisition, Project administration, Supervision, Writing – Review & Editing.

## Conflicts of interest

The authors declare that they have no known competing financial interests or personal relationships that could have appeared to influence the work reported in this paper.

## Acknowledgements

Lekha Dinesh Kumar was supported by CSIR-CCMB funds. Rathna Gundloori VN was supported by CSIR-CSC0302 and 0134 funds. Aviral Kumar was supported by a fellowship from the Ministry of Education (MOE), Government of India. Amarnath Singam was supported by a DBT-SRF fellowship, New Delhi, India. Naresh Killi was supported by a CSIR-SRF fellowship, New Delhi, India. Naveen Kumar Tangudu's present affiliation is Department of Pharmacology and Chemical Biology, UPMC Hillman Cancer Center, University of Pittsburgh, USA. The Graphical Abstract was created using BioRender.com. The authors are grateful to Mr Pratiksh Kumar Patel for his help in recording the thermograms of the nanoparticles. The authors acknowledge Ms Khushboo Kourani for her help in *in vivo* drug trials. The authors are extremely thankful to Prof. Alan Clarke, Cardiff University for his kind gift of *Brca2/p53* and *Apc* knockout models. The authors acknowledge Mr T. Avinash Raj for his help in sectioning of tissue samples and Dr V. Dinesh Kumar for critical evaluation and help in editing the manuscript.

## Notes and references

- 1 H. Sung, J. Ferlay, R. L. Siegel, M. Laversanne, I. Soerjomataram, A. Jemal and F. Bray, *CA Cancer J. Clin.*, 2021, **71**, 209–249.
- 2 A. Kumar, A. Golani and L. D. Kumar, *Front. Biosci., Landmark Ed.*, 2020, **25**, 979–1010.
- 3 S. Chakraborty, A. Kumar, M. M. Faheem, A. Katoch, A. Kumar, V. L. Jamwal, D. Nayak, A. Golani, R. U. Rasool, S. M. Ahmad, J. Jose, R. Kumar, S. G. Gandhi, L. Dinesh Kumar and A. Goswami, *Cell Death Dis.*, 2019, **10**, 467.
- 4 N. Gegechkori, L. Haines and J. J. Lin, *Med. Clin. North Am.*, 2017, **101**, 1053–1073.
- 5 A. Katoch, D. Nayak, M. M. Faheem, A. Kumar, P. K. Sahu, A. P. Gupta, L. D. Kumar and A. Goswami, *Cell Death Discovery*, 2021, **7**, 25.

- 6 A. Rawoof, G. Swaminathan, S. Tiwari, R. A. Nair and L. Dinesh Kumar, *Database*, 2020, **2020**.
- 7 K. Rishabh, S. Khadilkar, A. Kumar, I. Kalra, A. P. Kumar and A. B. Kunnumakkara, *Int. J. Mol. Sci.*, 2021, **22**(5), 2561.
- 8 M. D. Kumar, A. Dravid, A. Kumar and D. Sen, *Cancer Gene Ther.*, 2016, **23**, 115–124.
- 9 G. Swaminathan, A. Shigna, A. Kumar, V. V. Byroju, V. R. Durgempudi and L. Dinesh Kumar, *Front. Nanotechnol.*, 2021, **3**, 42.
- 10 P. Wang, Y. Zhou and A. M. Richards, *Theranostics*, 2021, **11**, 8771–8796.
- 11 N. K. Tangudu, V. K. Verma, T. D. Clemons, S. S. Beevi, T. Hay, G. Mahidhara, M. Raja, R. A. Nair, L. E. Alexander, A. B. Patel, J. Jose, N. M. Smith, B. Zdyrko, A. Bourdoncle, I. Luzinov, K. S. Iyer, A. R. Clarke and L. Dinesh Kumar, *Mol. Cancer Ther.*, 2015, **14**, 1259–1269.
- 12 J. Chen, *Adv. Cancer Res.*, 2012, **114**, 1–20.
- 13 X. Huang, Y. Yamada, H. Kidoya, H. Naito, Y. Nagahama, L. Kong, S. Y. Katoh, W. L. Li, M. Ueno and N. Takakura, *Cancer Res.*, 2007, **67**, 9800–9808.
- 14 S. A. Stephenson, S. Slomka, E. L. Douglas, P. J. Hewett and J. E. Hardingham, *BMC Mol. Biol.*, 2001, **2**, 15.
- 15 G. Xia, S. R. Kumar, R. Masood, S. Zhu, R. Reddy, V. Krasnoperov, D. I. Quinn, S. M. Henshall, R. L. Sutherland, J. K. Pinski, S. Daneshmand, M. Buscarini, J. P. Stein, C. Zhong, D. Broek, P. Roy-Burman and P. S. Gill, *Cancer Res.*, 2005, **65**, 4623–4632.
- 16 N. Y. Yang, P. Lopez-Bergami, J. S. Goydos, D. Yip, A. M. Walker, E. B. Pasquale and I. M. Ethell, *Pigm. Cell Melanoma Res.*, 2010, **23**, 684–687.
- 17 D. Hattab, A. M. Gazzali and A. Bakhtiar, *Pharmaceutics*, 2021, **13**(7), 1009.
- 18 D. Li, C. Gao, M. Kuang, M. Xu, B. Wang, Y. Luo, L. Teng and J. Xie, *Molecules*, 2021, **26**(8), 2380.
- 19 J. Conde, C. Bao, Y. Tan, D. Cui, E. R. Edelman, H. S. Azevedo, H. J. Byrne, N. Artzi and F. Tian, *Adv. Funct. Mater.*, 2015, **25**, 4183–4194.
- 20 J. Conde, F. Tian, Y. Hernandez, C. Bao, P. V. Baptista, D. Cui, T. Stoeger and J. M. de la Fuente, *Nanoscale*, 2015, **7**, 9083–9091.
- 21 D. Cui, C. Zhang, B. Liu, Y. Shu, T. Du, D. Shu, K. Wang, F. Dai, Y. Liu, C. Li, F. Pan, Y. Yang, J. Ni, H. Li, B. Brand-Saber and P. Guo, *Sci. Rep.*, 2015, **5**, 10726.
- 22 B. Liu, W. Cao, G. Qiao, S. Yao, S. Pan, L. Wang, C. Yue, L. Ma, Y. Liu and D. Cui, *Acta Biomater.*, 2019, **99**, 307–319.
- 23 X. Sun, Y. Chen, H. Zhao, G. Qiao, M. Liu, C. Zhang, D. Cui and L. Ma, *Drug Delivery*, 2018, **25**, 1718–1727.
- 24 A. Kumar, C. Harsha, D. Parama, S. Girisa, U. D. Daimary, X. Mao and A. B. Kunnumakkara, *Phytother. Res.*, 2021.
- 25 B. B. Aggarwal and B. Sung, *Trends Pharmacol. Sci.*, 2009, **30**, 85–94.
- 26 A. Duvoix, R. Blasius, S. Delhalle, M. Schneckeburger, F. Morceau, E. Henry, M. Dicato and M. Diederich, *Cancer Lett.*, 2005, **223**, 181–190.
- 27 S. Girisa, A. Kumar, V. Rana, D. Parama, U. D. Daimary, S. Warnakulasuriya, A. P. Kumar and A. B. Kunnumakkara, *ACS Pharmacol. Transl. Sci.*, 2021, **4**, 647–665.
- 28 P. Anand, A. B. Kunnumakkara, R. A. Newman and B. B. Aggarwal, *Mol. Pharm.*, 2007, **4**, 807–818.
- 29 A. B. Kunnumakkara, C. Harsha, K. Banik, R. Vikkurthi, B. L. Sailo, D. Bordoloi, S. C. Gupta and B. B. Aggarwal, *Expert Opin. Drug Metab. Toxicol.*, 2019, **15**, 705–733.
- 30 S. B. Sun, P. Liu, F. M. Shao and Q. L. Miao, *Int. J. Clin. Exp. Med.*, 2015, **8**, 19670–19681.
- 31 A. Narmani and S. M. Jafari, *Carbohydr. Polym.*, 2021, **272**, 118464.
- 32 N. Wathoni, A. N. Nguyen, A. Rusdin, A. K. Umar, A. F. A. Mohammed, K. Motoyama, I. M. Joni and M. Muchtaridi, *Drug Des., Dev. Ther.*, 2020, **14**, 4387–4405.
- 33 N. Chishti, S. Jagwani, D. Dhamecha, S. Jalalpure and M. H. Dehghan, *Medicina*, 2019, **55**(6), 294.
- 34 D. Hales, L. R. Tefas, I. Tomuța, C. Moldovan, D. Gulei, R. Munteanu and A. Porfire, *Pharmaceutics*, 2020, **12**(11), 1027.
- 35 R. Khatik, R. Mishra, A. Verma, P. Dwivedi, V. Kumar, V. Gupta, S. K. Paliwal, P. R. Mishra and A. K. Dwivedi, *J. Nanopart. Res.*, 2013, **15**, 1–15.
- 36 A. K. Philip and B. Philip, *Oman Med. J.*, 2010, **25**, 79–87.
- 37 M. Vlachou, S. Kikionis, A. Siamidi, S. Kyriakou, A. Tsotinis, E. Ioannou and V. Roussis, *Pharmaceutics*, 2019, **11**(9), 480.
- 38 T. Yoshida, T. C. Lai, G. S. Kwon and K. Sako, *Expert Opin. Drug Delivery*, 2013, **10**, 1497–1513.
- 39 S. D'Souza, *Adv. Pharm.*, 2014, **2014**.
- 40 D. Fu, H. Okimoto, C. W. Lee, T. Takenobu, Y. Iwasa, H. Kataura and L. J. Li, *Adv. Mater.*, 2010, **22**, 4867–4871.
- 41 R. Sridhar and S. Ramakrishna, *Biomater.*, 2013, **3**(3), e24281.
- 42 C. J. Pan Ch, J. J. Tang, Y. J. Weng, J. Wang and N. Huang, *J. Controlled Release*, 2006, **116**(1), 42–49.
- 43 M. Fernandes Queiroz, K. R. T. Melo, D. A. Sabry, G. L. Sasaki and H. A. O. Rocha, *Mar. Drugs*, 2014, **13**(1), 141–158.
- 44 M. L. Lorenzo-Lamosa, C. Remunan-Lopez, J. L. Vila-Jato and M. J. Alonso, *J. Controlled Release*, 1998, **52**, 109–118.
- 45 R. S. Nair, A. Morris, N. Billa and C. O. Leong, *AAPS PharmSciTech*, 2019, **20**, 69.
- 46 R. Sabra, N. Billa and C. J. Roberts, *React. Funct. Polym.*, 2018, **123**, 54–60.
- 47 A. Popat, S. Karmakar, S. Jambhrunkar, C. Xu and C. Yu, *Colloids Surf., B*, 2014, **117**, 520–527.
- 48 D. Vllasaliu, R. Exposito-Harris, A. Heras, L. Casettari, M. Garnett, L. Illum and S. Stolnik, *Int. J. Pharm.*, 2010, **400**, 183–193.
- 49 X. Li, L. Wang, Y. Fan, Q. Feng and F.-z. Cui, *J. Nanomater.*, 2012, **2012**, 548389.
- 50 H. Maeda and M. Khatami, *Clin. Transl. Med.*, 2018, **7**, 11.
- 51 R. Hakem, J. L. de la Pompa and T. W. Mak, *J. Mammary Gland Biol. Neoplasia*, 1998, **3**, 431–445.

- 52 C.-X. Deng and S. G. Brodie, *Semin. Cancer Biol.*, 2001, **11**, 387–394.
- 53 X. Liu, H. Holstege, H. van der Gulden, M. Treur-Mulder, J. Zevenhoven, A. Velds, R. M. Kerkhoven, M. H. van Vliet, L. F. A. Wessels, J. L. Peterse, A. Berns and J. Jonkers, *Proc. Natl. Acad. Sci. U. S. A.*, 2007, **104**, 12111–12116.
- 54 S. Zhang, Y. Li, Y. Wu, K. Shi, L. Bing and J. Hao, *Anat. Rec.*, 2012, **295**, 2104–2113.
- 55 C. Gao, G. Xiao and J. Hu, *Cell Biosci.*, 2014, **4**, 13.
- 56 S. P. Monga, P. Pediaditakis, K. Mule, D. B. Stolz and G. K. Michalopoulos, *Hepatology*, 2001, **33**, 1098–1109.
- 57 D. J. Flanagan, C. R. Austin, E. Vincan and T. J. Phesse, *Genes*, 2018, **9**(4), 178.
- 58 C. V. Dang, *Cell*, 2012, **149**, 22–35.
- 59 J. L. Teo and M. Kahn, *Adv. Drug Delivery Rev.*, 2010, **62**, 1149–1155.
- 60 A. Vallée, Y. Lecarpentier and J. N. Vallée, *Cells*, 2019, **8**(7), 726.